Technical Report
TR-19-08
June 2019

CIEMAT studies within POSKBAR project

Bentonite expansion, sedimentation and erosion in artificial fractures

Ursula Alonso
Tiziana Missana
Miguel García Gutiérrez
Jesús Morejón
Manuel Mingarro
Ana María Fernández

SVENSK KÄRNBRÄNSLEHANTERING AB

SWEDISH NUCLEAR FUEL
AND WASTE MANAGEMENT CO

Box 3091, SE-169 03 Solna
Phone +46 8 459 84 00
skb.se

SVENSK KÄRNBRÄNSLEHANTERING

ISSN 1404-0344
SKB TR-19-08
ID 1703221
June 2019

CIEMAT studies within POSKBAR project

Bentonite expansion, sedimentation and erosion in artificial fractures

Ursula Alonso, Tiziana Missana, Miguel García Gutiérrez, Jesús Morejón, Manuel Mingarro, Ana María Fernández

CIEMAT (Spain)

Keywords: Bentonite, Erosion, Expansion, Sedimentation, Fracture, Water chemistry, Accessory minerals, Colloid.

Abstract

Erosion of the bentonite barrier in a high-level radioactive waste repository is important, because the clay mass loss may compromise its performance. In addition, colloid particles formed upon clay erosion may contribute to radionuclide transport.

The erosion behaviour of compacted bentonite was experimentally studied in artificial fractures under different physico-chemical conditions. Experiments were carried out both in smooth and rough fractures with an experimental set-up specifically designed to evaluate: 1. Bentonite expansion in horizontal fractures, 2. Sedimentation in sloped fractures and 3. Erosion promoted by water flow.

In all erosion experiments, carried out with different bentonites in fractures with apertures lower than 1 mm, clay expansion in the fracture stopped at a certain time.

Studies carried out with natural and calcium-rich clays, in smooth and rough sloped fractures, revealed that, under the experimental conditions analysed, sedimentation along fracture slope is not appreciated when fracture aperture was thinner than 0.4 mm.

The contribution of accessory minerals and soluble salts to clay erosion processes was analysed in detail. Previous studies hypothesized that accessory minerals accumulate at the edge of the expanded clay, hindering further expansion. The erosion behaviour of a raw smectite was compared to that of two different clay fractions: the first one where soluble salts were removed and the second where accessory mineral and soluble salts were eliminated. An outer region with enriched minerals was not appreciated in any case. In fact, results suggested that the smectite particles themselves act as a filter, hindering further clay expansion.

Erosion experiments carried out under water flow conditions, with low flow velocities (10^{-8} to 10^{-6} $m \cdot s^{-1}$, indicated that particle mobilisation is very limited, since eluted clay fraction was always lower than a 0.02 % of the clay mass initially installed.

Overall results showed the primary relevance of water chemistry established at the equilibrium on erosion processes.

Sammanfattning

Erosion av bentonitbarriären i ett förvar för högaktivt radioaktivt avfall är en viktig process, eftersom massförlust genom erosion kan äventyra barriärens funktion. Dessutom kan de kolloidpartiklar som bildas av leran genom erosion bidra till radionuklidtransport.

Erosionsbeteendet hos kompakterad bentonit har studerats experimentellt i konstgjorda sprickor under olika fysikalisk-kemiska betingelser. Experiment genomfördes både i släta och ojämna sprickor med en experimentell uppsättning speciellt utformad för att utvärdera: 1. Bentonit-expansion i horisontella sprickor, 2. Sedimentation i sluttande sprickor och 3. Erosion som funktion av vattenflöde.

I alla erosionsexperiment, utförda med olika bentoniter i sprickor med aperturer lägre än 1 mm, avstannar expansionen efter en viss tid.

Studier utförda med naturliga och kalciumrika leror, i släta och ojämna sluttande sprickor, visade, att under de analyserade experimentella förhållandena, förekom ingen sedimentation längs lutningen när sprickaperturen var mindre än 0,4 mm.

Effekten av accessoriska mineral och lättlösliga salter på erosionsprocessen analyserades i detalj. I tidigare studier har det antagits att accessoriska mineral ackumuleras vid fronten av den expanderade leran, vilket i sin tur förhindrar ytterligare expansion. Erosionsbeteendet hos en naturlig smektit jämfördes med den hos två olika preparerade lerfraktioner: i den första hade lättlösliga salter avlägsnats och i den andra där både accessoriska mineral och lättlösliga salter avlägsnats. En yttre region med anrikade mineral kunde inte identifieras i något fall. I själva verket antydde resultaten att smektit-partiklarna själva fungerar som ett filter, vilket hindrar ytterligare expansion.

Erosionsexperiment utförda under förhållanden med vattenflöde och med låga flödeshastigheter (10^{-8} till 10^{-6} m · s^{-1}) indikerade att frigörelsen av partiklar är mycket begränsad, eftersom den eluerade lerfraktionen alltid var lägre än a 0,02 % av lermassan som ursprungligen installerades. Generellt visar resultaten att erosionsprocessen primärt beror på den vattenkemi som etableras vid jämvikt.

Contents

1 Introduction

Compacted bentonite is an engineered barrier included in high-level radioactive waste (HLRW) repository designs to isolate the waste (Pusch 2008, Sellin and Leupin 2013). Bentonite is selected for being a clay with adequate properties to overall contribute to repository safety. In particular, bentonites with high smectite content are considered the most appropriated, because they develop high swelling pressure, provide low hydraulic conductivity and hinder radionuclide migration (Kaufhold and Dohrmann 2016, Sellin and Leupin 2013).

Amongst the processes that may compromise the bentonite barrier performance, erosion and colloid formation are considered of concern (Missana et al. 2011, Sellin and Leupin 2013). Bentonite erosion would cause mass loss that directly affects the barrier integrity. In addition, eroded particles of colloidal nature (diameter < 1 μm) may contribute to radionuclide transport (Missana et al. 2008, Schaefer et al. 2012).

Bentonite erosion is defined as the removal of surface material and its transportation by a natural agent, in this context flowing water, which promote chemical and mechanical weathering.

Clay erosion has been extensively studied in other fields analysing, for example, soil resistance to water irrigation (Grissinger 1966), conclusions can be somehow transferred to a repository case. However, the particular characteristics of a bentonite barrier in a HLRW repository, where the clay is compacted at high density and confined by the repository host rock, may have consequences on erosion process.

Different studies have been previously devoted to assess the magnitude of bentonite erosion and to identify the mechanisms and geochemical conditions that favour it (Albarran et al. 2014, Alonso et al. 2006, 2018, Baik et al. 2007, Bessho and Degueldre 2009, Birgersson et al. 2009, Degueldre and Benedicto 2012, García-García et al. 2009, Kaufhold and Dohrmann 2008, Liu and Neretnieks 2006, Missana et al. 2003, 2011, Pusch 1999, Reid et al. 2015, Rinderknecht 2017, Schatz et al. 2013, Schatz and Akhanoba 2016, Seher et al. 2009).

In a HLRW repository, the groundwater coming from the host rock fractures will hydrate the clay, clay swelling will be favoured (Norrish 1954) and its extrusion will be promoted in available pore spaces and micro-fractures. If a local hydraulic gradient does not exist, diffusion will be the driving force for particle releases (Kallay et al. 1987) and clay dispersion is considered as the primary process inducing particle detachment in water (Birgersson et al. 2011, García-García et al. 2009, Hedström et al. 2016, Kaufhold and Dohrmann 2008, Luckham and Rossi 1999, Norrish 1954, Pertsov 2005, Pusch 1999). In fact, the mass of dispersed colloids was considered the first important parameter to assess clay erodibility (Missana et al. 2018a).

Bentonite erosion and clay dispersion may be different under compacted and confined conditions because, the interlayer space is in the nanometre scale, affecting the electrical interactions (overlapping of electrical double layers). Moreover, the high ion concentration of the clay porewater (Bradbury and Baeyens 2009, Fernández et al. 2004, Karnland et al. 2011, Wersin et al. 2016), and the presence of soluble salts in clay inventory (Fernández et al. 2017) may affect the water conditions at equilibrium, especially at high solid to liquid ratios.

It is well accepted that groundwater with low ionic strength and low content of divalent cations promotes peptisation (de-flocculation) and favour the separation of individual smectite layers, giving to the clay/water system a sol character and favouring spontaneous colloid formation, influenced by the water chemical conditions (Birgersson et al. 2011, Hedström et al. 2011, 2016). On the contrary, in groundwaters whose ionic strength is above the minimum concentration to cause flocculation, smectite forms a gel inhibiting particles release and restricting colloid stability (Luckham and Rossi 1999, Missana et al. 2003, 2018b) and therefore their mobility.

Mechanical forces, like those produced by advective water flow, may additionally favour clay erosion and particle detachment, being dependant on the water chemistry, flow rates and fracture conditions (Birgersson et al. 2009, Missana et al. 2011, Pusch 1999, Schatz et al. 2013).

Theoretical models have been developed to describe particle detachment by diffusion (Kallay et al. 1987) or swelling and detachment promoted by advective flow (Liu and Neretnieks 2006, Liu 2010, Liu et al. 2009, Neretnieks et al. 2009). These models sometimes apply to simplified systems: flat surfaces, Na-homoionic clays and low ionic strength groundwater.

However, uncertainties are still associated to bentonite erosion, under real repository conditions, preventing the precise quantification and assessment of erosion and colloid formation at the bentonite/ host rock interface.

The aim of this study was to analyse which physico-chemical factors are playing a major role in bentonite erosion within fractures, under compacted and confined conditions. Experimental conditions were selected to evaluate aspects not previously analysed (Alonso et al. 2018, Missana et al. 2018a, Schatz et al. 2013, Schatz and Akhanoba 2016).

Amongst the main processes evaluated, the following aspects can be highlighted:

1. Clay expansion behaviour in smooth narrow fractures (with apertures lower than 1 mm), because previous erosion studies in artificial fractures were mainly carried out in 1 mm fracture apertures (Schatz et al. 2013, Schatz and Akhanoba 2016).
2. Sedimentation behaviour of different clays (Na-rich and Ca-rich bentonites) in smooth fractures with narrow apertures and rough fractures, since uncertainties still exist (Neretnieks et al. 2017).
3. Role of accessory minerals, naturally present in the clay, on erosion process. In previous erosion studies it was hypothesized that the accessory minerals may be clogging the thinner fracture apertures hindering erosion (Richards 2010, Richards and Neretnieks 2010).
4. Relevance of water chemistry at equilibrium on erosion process, which was concluded by the comparison of experiments carried out under dispersed conditions (Missana et al. 2018a) and under compacted and confined conditions, with a different set-up (Alonso et al. 2018).

Expansion, sedimentation, and erosion induced by water flow will be analysed both in smooth and rough fractures. An experimental set-up, already used formerly in EC-BELBAR project, was selected.

Experiments were mainly carried out accounting for experimental conditions considered favourable for erosion: Na-clay, 1.4 $g \cdot cm^{-3}$ compaction density and low ionic strength water (1 mM) (Albarran et al. 2014, Missana et al. 2003, 2011, Alonso et al. 2018).

2 Objectives

The main objective of the erosion tests was to experimentally analyse bentonite expansion, sedimentation and erosion within well-defined artificial fractures under different experimental conditions. The pursued objectives can be divided within the following eight specific tasks.

Expansion

Task 1. To analyse the **expansion rate** of **smectites** using **horizontal (0°) smooth fractures** with different fixed apertures (< 1 mm) and considering different water chemical conditions (NaCl 10^{-3} M and concentration above critical coagulation concentration, CCC).

Task 2. To analyse **expansion and erosion** of **other 2:1 clays** (e.g. saponite) using **horizontal (0°) smooth fractures** with fixed apertures.

Task 3. To analyse the **role of accessory minerals** on **expansion rate** of **smectites**, using **horizontal (0°) smooth fractures** with fixed apertures, by comparing the expansion behaviour of:

- Raw sodium-rich bentonite.
- Smectite without soluble salts.
- Smectite without accessory minerals and without soluble salts.

Sedimentation

Task 4. To evaluate the **sedimentation behaviour** of **sodium-rich smectites** in **sloping (0° to 90°) smooth fractures** with different fixed apertures, filled with NaCl 10^{-3} M.

Task 5. To evaluate the **sedimentation behaviour** of **calcium-rich smectites** in **sloping (0° to 90°) smooth fractures** with different fixed apertures, filled with NaCl 10^{-3} M.

Task 6. To study **sedimentation behaviour** in **sloping (0° to 90°) fractures with different roughness** with:

- Raw bentonite.
- Sodium-rich smectite.
- Calcium-rich smectite.

Erosion promoted by flow

Task 7. To analyse bentonite **erosion** rates promoted **by flow**, with **sodium-rich smectites**, using **horizontal (0°) smooth fractures**, with different fixed apertures.

Task 8. To analyse bentonite **erosion** rates promoted **by flow**, with **sodium-rich smectites**, using **horizontal (0°) rough fractures**.

In all cases, flow conditions were applied after previous expansion in the fracture during 30 days under stagnant conditions (Task 1 or Task 2).

3 Experimental set-up

Clay erosion experiments were carried out in a custom-designed artificial fracture. The basic outline of the experimental set-up is shown in Figure 3-1. The fracture surface can be either smooth or rough.

The fracture can be positioned at different angles, to carry out experiments with different slope (angle, Θ) and different tests can be carried out.

These artificial fractures were already successfully used within a former project devoted to bentonite erosion (Schatz et al. 2015). Equivalent set-up was used in previous erosion tests (Schatz et al. 2013, Schatz and Akhanoba 2016).

3.1 Smooth fractures

The *smooth fracture* was made up by two square flat plates of methacrylate (20 cm x 20 cm) with a central drilled cylinder where a compacted clay pellet (diameter 19 mm and 10 mm height) can be placed. The methacrylate plates can be conveniently separated, so that different fracture apertures were analysed: 0.1, 0.2, 0.4, 1 and 1.7 mm. The methacrylate sheets are sealed and the final fracture is a square, with a length of 17 cm.

The fracture can be positioned at different slopes (Θ). The slopes analysed were horizontal (0°), sloping (45°) and vertical (90°).

The initial aim was to analyse erosion processes within *narrow fractures* (apertures < 0.4 mm) which were not previously analysed. Some experiments were planned considering wider apertures (1 and 1.7 mm) to facilitate the comparison with previous expansion tests performed by B+Tech (Schatz et al. 2013, Schatz and Akhanoba 2016) which were mainly carried out within 1 mm apertures and also to approach the higher volumes of rough fractures (Table 3-1).

According to their dimensions, the fractures have different volume and the values are indicated in Table 3-1.

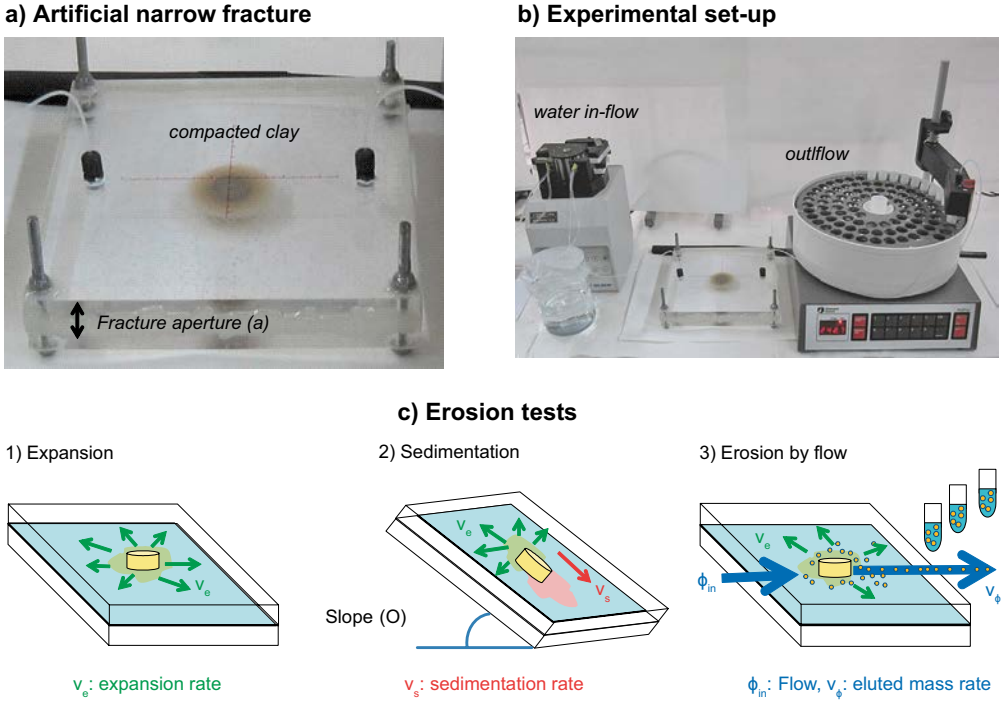

Figure 3-1. *a). Experimental set-up, b). Artificial fracture, c). Scheme of experimental tests: 1). Expansion 2). Sedimentation and 3). Erosion by flow.*

3.2 Rough fractures

Experiments within *rough fractures* were planned to elucidate wall friction effects on clay erosion. The rough fractures were made with square methacrylate plates (20 cm x 20 cm) with a well-defined roughness pattern (Figure 3-2). The fracture dimension was 17 cm x 17 cm, as well as in the smooth case. The pellet dimensions were the same in all experiments (diameter 19 mm and 10 mm height).

To account for different roughness experiments were conducted considering: a) two flat surfaces (*smooth fracture*); b) one rough surface (*Roughness 1*) and c) two rough surfaces (*Roughness 2*). Figure 3-3 shows a sketch of fracture sections with the different roughness analysed.

In rough fractures, the aperture is not homogenous and the comparison with different experiments may be done considering the fracture volumes (Table 3-1). The volume of fractures with *Roughness 1* is equivalent to that of the smooth fracture with 1 mm aperture and that of fracture with *Roughness 2* is equivalent to that of the smooth fracture with the widest aperture (1.7 mm).

Table 3-1. Fracture volumes (in mL and m^3) according to fracture dimensions and characteristics.

Fracture aperture	Fracture volume (mL)	Fracture volume (m^3)
0.1 mm	2.9	2.9×10^{-6}
0.2 mm	5.8	5.8×10^{-6}
0.4 mm	11.6	1.2×10^{-5}
1.0 mm	28.9	2.9×10^{-5}
1.7 mm	49.1	4.9×10^{-5}
Roughness 1	30	3×10^{-5}
Roughness 2	50	5×10^{-5}

Figure 3-2. *Photography of a rough fracture, including a methacrylate plate with well-defined rough pattern (clay pellet dimeter is 19 mm).*

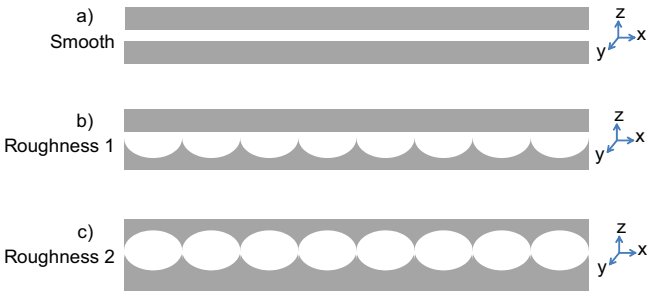

Figure 3-3. *Schematic section of fractures with different roughness: a). Smooth, b). Roughness 1 (with one rough surface) and c). Roughness 2 (two rough surfaces).*

3.3 Clay materials

3.3.1 Raw clays

Most experiments were carried out with a commercial Na-exchanged montmorillonite (Nanocor®) from China. Some experiments were carried out with raw natural bentonites (Wyoming MX-80 and Ibeco) and with a natural Mg-saponite (MCA-C).

- ***Nanocor®*** is a commercial Na-exchanged and purified montmorillonite from China with a 98 % smectite content, used as reference material in the recent EC-BELBAR project (http:/www.skb.e/belbar/).
- ***Wyoming MX-80*** is a Na-rich bentonite from Wyoming (USA) produced by Am. Coll. Co (Müller-Vonmoss and Kahr 1983) with high smectite content (89 %).
- ***Ibeco*** is a Ca–Mg bentonite (sample Ibeco RWC 16) from Milos island in Greece, mined by Silver & Baryte Mining Company S.A (Koch 2002, 2008) with 90 % smectite content.
- ***MCA-C*** is a Mg saponite, from Cerro del Aguila, Spain (Cuevas et al. 1993, Pusch et al. 1996).

Clay samples were used *as received* and they were previously deeply characterised (Fernández et al. 2017). Table 3-2 presents the mineralogical composition of selected clays determined by X-Ray diffraction (XRD) analyses (Fernández et al. 2017). Table 3-3 includes the main clay characteristics: smectite content (Sm. in wt %), Na^+ and Ca^{2+} and Mg^{2+} content in exchange positions and initial clay water content (w.c. in %). Other structural features that allow smectite classification, such as clay mineral layer charge, charge distribution between tetrahedral and octahedral sheets, cation distribution within the octahedral sheet and inside the interlayer, can be found in Fernández et al. (2017). Obtained physico-chemical and mineralogical parameters measured were comparable to those reported in the literature, *i.e.* for MX-80 or Ibeco (Karnland 2010).

Selected clay minerals are 2:1 phyllosilicates of the smectite group. Smectite is a planar hydrous phyllosilicate, with a layered structure, where two tetrahedral (τ) sheets sandwich an octahedral (O) sheet (TOT structure type 2:1). Selected clays are di-octahedral smectites, except for the MCA-C saponite which is tri-octahedral.

Under experimental conditions analysed, where the solid to liquid ratio is high, the natural presence of soluble salts is relevant because their dissolution will establish a chemical equilibrium determinant for erosion process (Alonso et al. 2018).

Table 3-4 presents the anion inventory (Cl^- and SO_4^{2-} content in mmol·100 g^{-1} of clay), measured for studied clays (Fernández et al. 2017). According to the major anions measured, dissolution of halite (NaCl), gypsum ($CaSO_4 \cdot 2H_2O$) and also calcite ($CaCO_3$) is expected.

It should be noted that Nanocor® clay is a commercial purified bentonite which has high anion content in the salt inventory, especially of sulphates, probably coming from the industrial treatment used to homoionise the clay. But also, the salt inventory of MX-80 bentonite is higher than that of other smectites being studied in the frame of radioactive waste repositories (Alonso et al. 2018).

Table 3-2. Mineralogical composition of selected clays according to DRX analyses (Fernández et al. 2017).

Minerals/Clay	MX-80	Ibeco	MCA-C
Phyllosilicates (%)	89.0	91.1	85.0
Quartz (%)	5.1	0.4	4.0
K-feldspars (%)	2.0	0.1	3.0
Plagioclase (%)	2.0	0.6	7.0
Calcite		5.0	1.0
Pyrite		0.8	
Dolomite		2.0	
Cristobalite	1.9	0.0	
Siderite		0.1	

Table 3-3. Main characteristics of selected clays: clay type, smectite content (wt %), Na^+ and Ca^{2+} and Mg^{2+} content in exchange positions (Fernández et al. 2017) and initial water content (w.c. in %).

Clay	Type T:O	Smectite (wt %)	Exch. Na^+ (%)	Exch. (Ca^{2+} + Mg^{2+}) (%)	w.c. (%)
Nanocor®	2:1 Na-smectite	98	93.45	2.51	10.57
MX-80	2:1 Na-smectite	89	68.32	26.27	9.39
Ibeco	2:1 Ca–Mg smectite	88	26.30	68.97	12.90
MCA-C	2:1 Mg-saponite	78	4.16	87.95	8.89

Table 3-4. Anion inventory measured in selected clays (Fernández et al. 2017).

Clay	Cl^- (mmol·100 g^{-1})	SO_4^{2-} (mmol·100 g^{-1})
Nanocor®	4.40	10.68
MX-80	1.36	3.26
Ibeco	1.82	1.35
MCA-C (saponite)	1.56	0.09

The dispersion and maximum colloid releases form powdered clays was analysed in Missana et al. (2018b). Their erosion behaviour was analysed with a different set-up, under compacted and confined conditions in Alonso et al. (2018).

3.3.2 Homoionic clays

Sodium and calcium homoionic fractions of Wyoming MX-80 were prepared in the laboratory (respectively named Na-MX-80 and Ca-MX-80) following a standard procedure (Missana et al. 2008).

To exchange the clay, it was washed three times with the Na or Ca electrolyte (1 M $NaClO_4$ or $Ca(ClO_4)_2$), that were selected considering that ClO_4 is not present in the clay. Then, the clay was washed several times with deionised water (DW), and later with a mixture of DW and ethanol, until the electrical conductivity of the suspension was lower than 100 $\mu S \cdot cm^{-1}$.

Afterwards, the exchanged clays were dried in the oven (40 °C). The dry clay was powdered in an agate mortar and sieved (< 63 μm). In the homoionisation procedure the soluble salts are removed.

3.3.3 Salt-free MX-80

Salt-free MX-80 was obtained from raw MX-80 by successive washings and centrifugation steps with a mixture of deionised water and ethanol, until final conductivity was lower than 100 $\mu S \cdot cm^{-1}$. Once this conductivity was reached, the clay samples were air dried and homogenised by grinding and sieving (< 63 mm). The main physico-chemical and structural characteristics of the salt-free clay fraction were evaluated with the same procedure, later used for post-mortem analyses (Section 3.7.3).

3.3.4 Minerals&salt-free MX-80

Minerals&salt-free MX-80 clay fraction was obtained by sedimentation procedure. Both the largest accessory mineral particles (> 2 mm) and the soluble salts were removed. After that, the clay was air dried, homogenised by grinding and sieving (< 63 mm) and was characterised following the same procedure used for post-mortem analyses (Section 3.7.3).

3.4 Clay pellets preparation

Compacted clay pellets were prepared from powdered material at ambient conditions. Prior to compaction, clay was pre-hydrated by adding the necessary water solution (the same used in each erosion test) to achieve complete clay saturation. After that, the hydrated clay was compacted at 1.4 $g \cdot cm^{-3}$ in cylindrical pellets with a diameter of 19 mm and 10 mm height.

The same pellet dimensions were used in all experiments but clay masses slightly varied depending on clay initial water content (see Table 3-3). The clay surface exposed to hydration in the fracture depends on the fracture aperture (Table 3-1) and is determinant for erosion process (Alonso et al. 2018).

3.5 Water solutions

The reference water solution was NaCl of analytical grade (Merck). Main experiments were carried out at an ionic strength of 10^{-3} M, considered as favourable for erosion for its low ionic strength and absence of divalent cations. Some experiments were carried out at higher ionic strengths (10^{-2} and 10^{-1} M) which are conditions that hinder erosion (Missana et al. 2011, Alonso et al. 2018) and restrict particle stability (Missana et al. 2018a).

The water volumes in each experiments depended on the fracture volume (Table 3-1). Relevant chemical parameters like pH, electric conductivity (E.C.), ionic strength and ion concentration, were measured at the beginning and at the end of each erosion experiment, as below described in Section 3.7.1.

As reference, the initial pH and electric conductivity of NaCl at different ionic strength is indicated in Table 3-5.

Table 3-5. Initial water solutions: pH and electric conductivity (E.C.).

Solution	Initial pH	Initial E.C. ($\mu S \cdot cm^{-1}$)
NaCl 10^{-3} M	6.5	100 ± 5
NaCl 10^{-2} M	6.5	1 000 ± 50
NaCl 10^{-1} M	6.5	10 000 ± 500

3.6 Tests protocol

Three types of bentonite erosion tests were conducted in the artificial fractures.

1. Expansion test.
2. Sedimentation test.
3. Erosion by flow test.

The basic outline of each type of test is sketched in Figure 3-1. All experiments were conducted under atmospheric conditions and at room temperature. Each type of test is below described.

3.6.1 Expansion tests

Figure 3-4 presents a photograph of three expansion tests carried out in horizontal fractures.

In expansion tests, compacted clay at selected density and pre-hydrated with selected solution (Section 3.4), is placed at horizontal slope (0°). At the beginning of the test, the fracture is carefully filled with a syringe with selected water solution and the clay is allowed to freely expand/extrude within the fracture, under stagnant conditions.

During expansion, photographs were periodically taken for 30 days (Figure 3-5), with and without a graded transparent sheet to facilitate the measurements of expansion distances.

In the photos, the radial expansion was measured, from the clay pellet surface, along four radial directions (r_A, r_B, r_C and r_D) as sketched in Figure 3-5c.

When the radial increase was homogenous, the value provided as *expansion distance* (in cm) is the average value of these four measured radial lengths.

In those cases where sedimentation was observed along some fracture direction, the average expansion distance is calculated excluding the direction where clay deposition was detected.

At the end of the experiment, the clay fraction extruded in the fracture and the equilibrium water were sampled and analysed, as below described in Section 3.7 (post-mortem analyses).

In expansion tests, the following variables were analysed:

Fracture aperture effect on clay expansion

Expansion test were carried out in horizontal fractures (slope 0°) with different apertures (0.1, 0.2, 0.4 1 mm and 1.7 mm).

Water ionic strength effect on clay expansion

Expansion tests were carried out with Nanocor® and MX-80 clays, as prior step to erosion by flow tests. Additional expansion tests were carried out with Nanocor® clay, with NaCl at different ionic strengths (10^{-3}, 10^{-2} and 10^{-1} M).

Clay type effect on clay expansion

Expansion behaviour of Ibeco bentonite and MCA-C saponite was compared to that of Na-rich bentonites (MX-80 and Nanocor®).

Figure 3-4. *Example of expansion tests carried out in artificial smooth fractures placed at horizontal slope.*

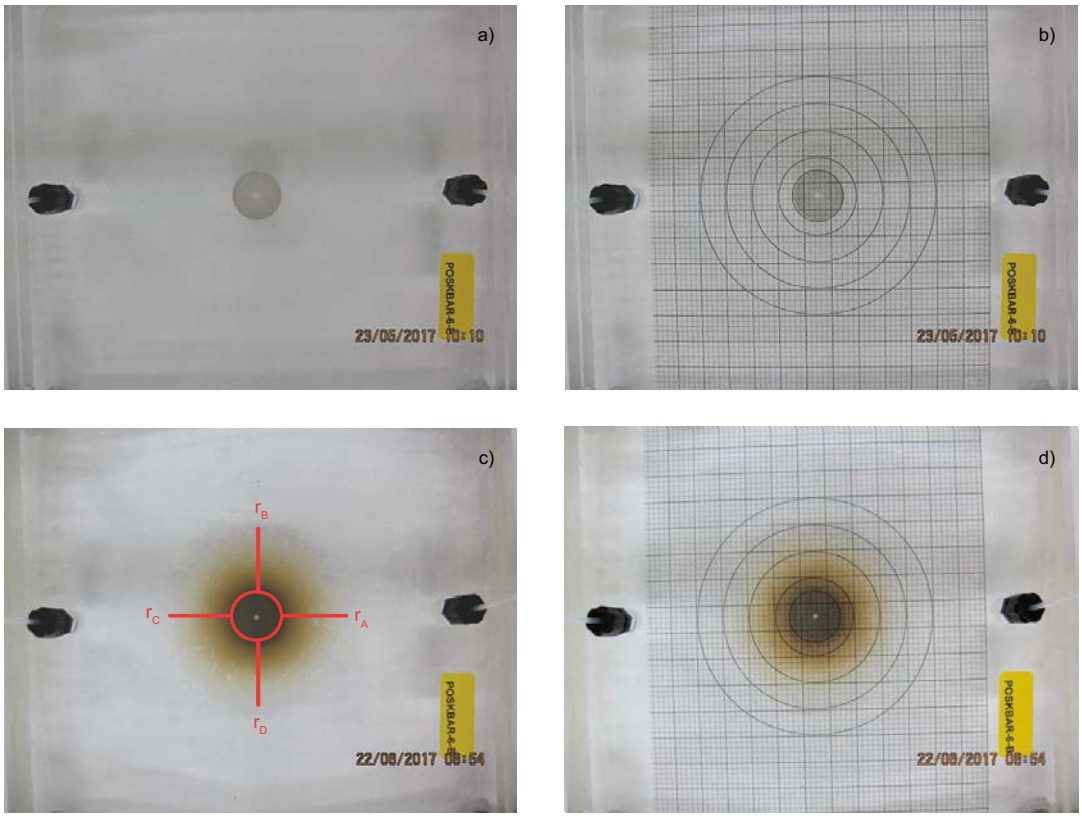

Figure 3-5. *Example of periodical photographs taken to erosion tests, with and without a graduated sheet of mm scale at: (a–b) beginning of test; (c–d) end of test. Four radial distances from the pellet surface were measured (r_A, r_B, r_C, r_D) to determine the average expansion distance, as shown in (c).*

Role of accessory minerals and soluble salts on clay expansion

The role of accessory minerals and of the chemical equilibrium imposed by the dissolution of soluble salts naturally present in bentonites on erosion was analysed.

To do so, we compared the expansion behaviour of:

1. *Raw MX-80:* natural bentonite with high smectite content.
2. S*alt-free MX-80: w*ashed MX-80 bentonite without soluble minerals.
3. M*inerals&salt-free MX-80:* purified MX-80 bentonite where both the accessory minerals and the soluble salts were removed.

These experiments were all carried in smooth fractures with 0.2 mm aperture, placed at horizontal slope (0°) and with NaCl 10^{-3} M.

The experiments were done in triplicate (Tests 50, 51 and 55, A, B and C, in Table 4-2) to have sufficient clay mass to carry out complete post-mortem mineralogical and compositional analyses (described in Section 3.7.3).

3.6.2 Sedimentation tests

In sedimentation tests, compacted clay at selected density, previously hydrated, is placed in the centre of the fracture. The fracture apertures analysed were 0.1, 0.2, 0.4 and 1 mm.

With an appropriate support, the fracture can be placed as well at different slopes (Θ): horizontal (0°), sloping (45°) and vertical (90°).

Figure 3-6 shows two photographs of sedimentation tests carried out in vertical (90°) and sloping (45°) fractures.

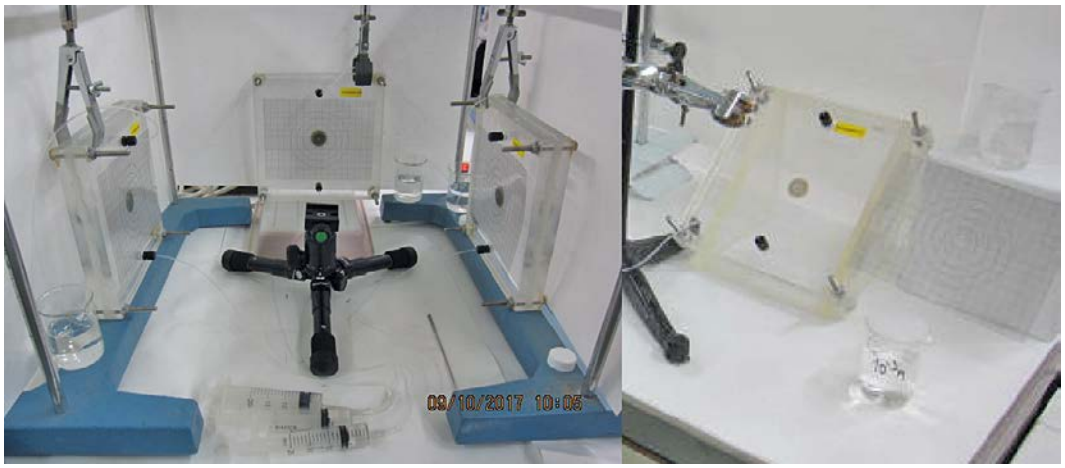

Figure 3-6. *Photographs of sedimentation tests carried out at: (left) 90° slope and (right) 45° slope.*

To carry out the sedimentation test, the fracture is filled with selected water solution (NaCl 10^{-3} M) and the clay is allowed to freely expand within the fracture – and to sediment – under stagnant conditions.

Again, the tests lasted 30 days and photographs were continuously taken (at least 6 photos/day during first expansion period).

At the end of the experiment, the clay fraction extruded in the fracture – or deposited – was sampled, and the equilibrium water was analysed, as below described in Section 3.7.

3.6.3 Erosion by flow tests

The aim of erosion by flow tests was to evaluate if a low water flow promotes the mobilisation of the clay particles which had previously extruded in the fracture. To do so, water flow conditions were always applied after the expansion period of 30 days. This is a very important feature to be considered when comparing to other erosion studies (Schatz and Akhanoba 2016) where the flow conditions were applied from the beginning and there was no previous period of free-expansion in the fracture.

A test protocol equivalent to that of the benchmark test carried out within the EC-BELBAR project (Schatz et al. 2015) was followed.

Flow experiments were all carried out in horizontal fractures (slope 0°) with commercial Nanocor® and with raw MX-80 clay. Flow experiments were carried out in rough and smooth fractures with different fracture apertures (0.1, 0.2 and 0.4 mm).

Once expansion test was finished, water flow was provided to the fracture by a peristaltic pump at selected flow rate (ϕ_{in}), as can be seen in the set-up image (Figure 3-1). At the output, a fraction collector is placed to sample eluted water at selected times and volumes. Eluted volumes were fixed for all experiments to around 2 mL/day, and flow velocities (ϕ_{in}) ranged between 10^{-7} to 10^{-6} m·s^{-1}, depending on the fracture aperture.

Eluted water samples were analysed by Photon Correlation Spectrometry (PCS) to determine both the eluted mass and the average particle size.

Photon Correlation spectrometry (PCS) analyses

Photon Correlation Spectrometry (PCS) technique (Holthoff et al. 1996) was selected to evaluate the concentration of eroded particles in water and their average hydrodynamic diameter.

PCS measurements were carried out with a Zetasizer NanoS Malvern equipment with a He–Ne laser source of λ = 633 nm and detection at 173°, at particle concentrations higher than 0.5 mg·L^{-1}.

In PCS analyses, particle concentration can be determined with appropriate calibration curves (Ledin et al. 1993), obtained with laboratory prepared colloids of the same clay and under the same chemical conditions (Missana et al. 2011).

To obtain the colloidal fraction, for calibration purposes, bentonites are dispersed in NaCl 10^{-3} M and afterwards centrifuged (at 600 g during 20 minutes) to extract the colloidal fraction (particles with diameters < 1 μm). The colloid concentration was determined by gravimetric measurements.

Figure 3-7 presents an example of calibration curve (PCS counts *vs* particle concentration, in $mg \cdot L^{-1}$) carried out with laboratory-prepared Nanocor colloids, suspended in NaCl 10^{-3} M.

PCS analyses additionally provided measurement of average particle diameter, a very relevant parameter to predict stability and migration behaviour of eroded particles. The average hydrodynamic diameter of particles from 2 nm to 3 mm can be determined. The errors of size measurements are obtained by the standard deviation of at least five measurements.

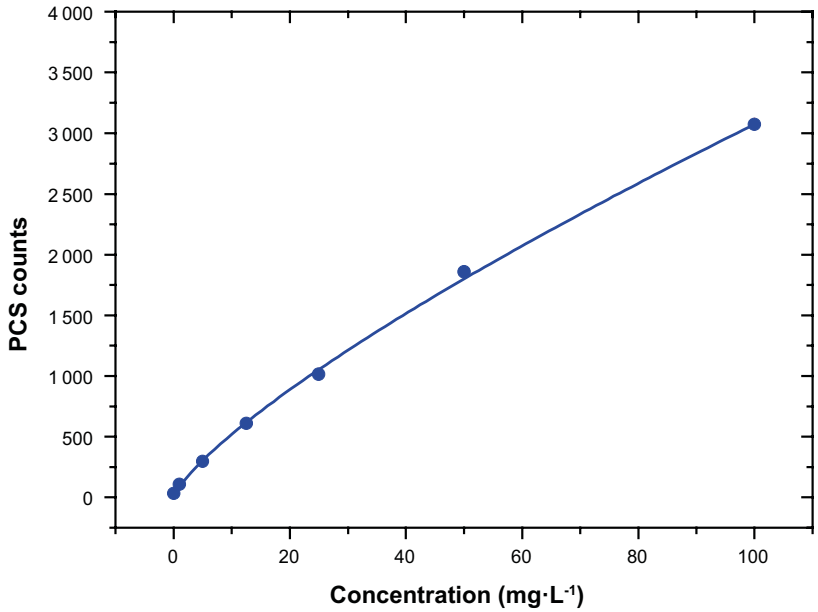

Figure 3-7. *Example of calibration curve, PCS counts vs particle concentration, carried out with laboratory prepared Nanocor® colloids in NaCl 10^{-3} M.*

3.7 Post-mortem analyses

Post-mortem analyses were always carried out after 30 days, at the end of expansion and sedimentation tests. In the erosion by flow experiments, post-mortem analyses were not carried out after the expansion period, but after the flow experiment (i.e. after 60 days).

Both the equilibrium water and the clay fraction eroded in the fracture were sampled and analysed.

3.7.1 Water chemistry in the fracture at equilibrium

At the end of the experiments, the water inside the fractures was carefully sampled with a syringe, prior to dismantling the artificial fracture, through the same tube used to initially fill-in the fracture (Figure 3-1a).

The water was weighed to verify that the final volume was in agreement to the experimental conditions of the test (fracture aperture, roughness, etc in Table 3-1) and also to verify that there was no water leak during the experiment.

In all experiments, the initial electrolyte is NaCl, but soluble salts present in clays (Table 3-4) and cation exchange reactions, provide characteristic equilibrium conditions for each material. The pH and electric conductivities (E.C.) of equilibrium water was checked at the end of all experiments. To facilitate comparison, the initial pH and E.C. of initial NaCl electrolytes are indicated in Table 3-5.

In some experiments complete chemical analyses were carried out on the final waters, to analyse chemical changes (major and trace elements) promoted by the presence of bentonite.

Major and trace cations were analysed by Inductively Coupled Plasma Atomic Emission Spectrometer (Varian 735ES, AA240 FS). Sodium and potassium were determined by Atomic Absorption Spectrometry using a Agilent AA 240 FS spectrometer. Anions were analysed by ion chromatography (DIONEX ICS-2000).

The mass and size of released particles present in the liquid phase (in mg) were analysed by PCS, as above described for the analyses of water eluted samples, in Section 3.6.3.

Geochemical calculations were carried out considering the clays salt inventories, with the Geochemist's Workbench® (v. 8.0) code.

3.7.2 Eroded mass

Post-mortem analyses were carried out to analyse the clay expanded in the fracture, as shown in Figure 3-8 and Figure 3-9.

At the end of each experiment, the water in the fracture was removed with care with a syringe for further analyses. Afterwards the fracture was dismantled and the methacrylate sheets that made up the artificial fracture were separated and dried at 60°C in an oven, to facilitate clay sampling.

Once dried, both the (final) clay pellet and the clay fraction expanded in the fracture (*expanded clay*) were sampled and weighed.

Eroded mass is reported as the difference in weigh between the final and initial pellets (in g, and in %, in relation to the initial mass installed). This measurement has the lowest associated error. However, the *eroded mass* includes up to four different fractions, depending on the test, which are separately evaluated:

1. *Expanded clay* in the fracture (all tests) is directly sampled from the pellet surface and weighed, after drying the methacrylate sheets. Measured quantities were not specifically indicated in the results, because due to the low masses that are sometimes sampled, they have big uncertainties.
2. *Suspended clay* in the water phase (all tests), which is determined by PCS analyses, carried out in the water extracted in the fracture.
3. *Deposited clay* at the bottom of the fracture (only in sedimentation tests in sloped fractures). This fraction is difficult to sample and errors are high.
4. *Eluted fraction* (only in erosion by flow tests), which is determined by PCS analyses on each sample (Section 3.6.3).

It has to be noted that *eroded masses* should be taken with care, and the values cannot be directly extrapolated. The calculated percentages depend on the installed mass, which is around 4 grams under experimental conditions. But actually, previous studies indicated that it is the clay area exposed to hydration which determines the extrusion, and not the total mass installed. This means that if compaction density and the area exposed were the same, equivalent expansion would be measured with different clay amounts.

In some tests, specifically in those experiments devoted to analyse the role of accessory minerals and soluble salts on erosion, the *expanded clay* was sampled in different rings, radially from the pellet surface, as indicated in Figure 3-9. The sampled rings cover the following distances from the pellet surface of (I) 0–0.5 cm, (II) 0.5–1.5 cm, (III) 1.5–2.5 cm and (IV) < 2.5 cm. The clay sampled in each region is weighed and separately analysed.

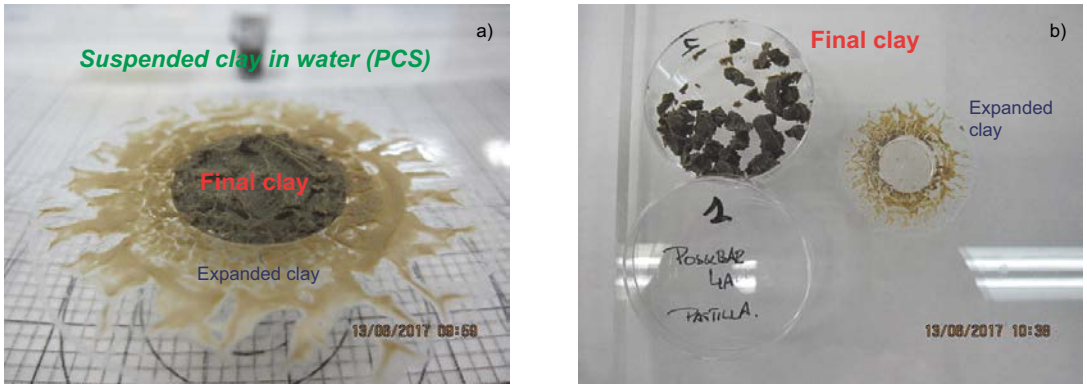

Figure 3-8. *Photographs of post-mortem procedure. The final pellet mass and the expanded clay are separated for weighing. The water in the fracture is sampled with a syringe for further chemical analyses and to evaluate the mass of suspended particles (by PCS analyses).*

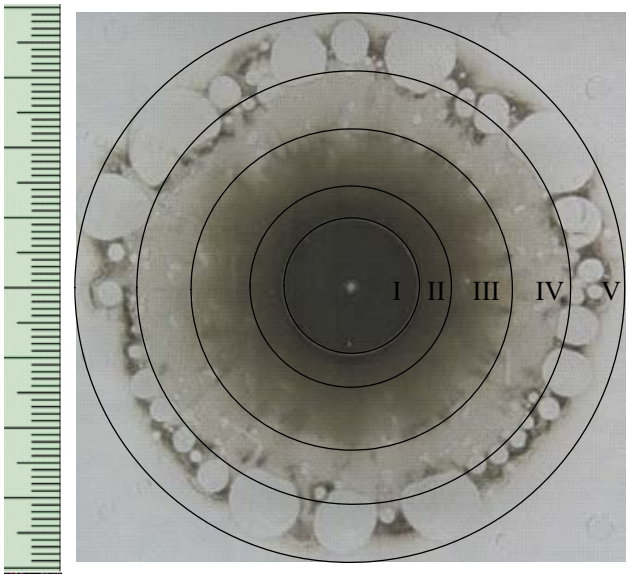

Figure 3-9. *Scheme of post-mortem radial sampling of expanded clay in the fracture. This detailed sampling was only carried out on tests devoted to analyse the role of accessory minerals (in the picture Test 51C). Pellet diameter is 1.9 cm.*

3.7.3 Mineralogical and physico-chemical characterisation of expanded clay

In-depth characterisation of expanded clay fraction was carried out on selected experiments, mainly devoted to analyse the role of accessory minerals and soluble salts, naturally present in the clay, on erosion processes. The following analyses were carried, to identify changes in mineralogy or differences in the smectite structure.

X-Ray diffraction (XRD)

XRD patterns were obtained from dry powders to identify the mineralogical species present in the samples. The powders were obtained by grinding the samples in a RETSCH RM 100 agate mortar to a size of less than 63 μm.

XRD analyses were carried out with a Philips X'Pert - PRO MPD diffractometer, equipped with a Cu–Ka anode at 45 kV and 40 mA, with a fixed divergence slit (0.1245° size) Scientific X´celerator detector. Measurements were carried out from 2° to 70° 2θ, with a step size 0.017° 2θ, and a scan rate of 50 s per step. The XRD database used for mineral identification was the Power Diffraction File from the International Center for Diffraction Data (ICDD).

Fourier Transform Infrared (FTIR) spectroscopy

FTIR spectroscopy was applied to complement XRD mineralogical analyses. FTIR spectra were obtained in the middle-IR region (4 000–400 cm^{-1}) with a Nicolet 6700 with a DTGS KBr detector (resolution 4 cm^{-1}, 32 scans) on KBr-pressed discs in transmission technique, in an atmosphere continuously purged from water and atmospheric CO_2.

Powdered air-dried clay samples (2 mg) were dispersed in 200 mg of KBr and pressed to a clear disc. The pressed samples were analysed at room temperature, after heating in an oven overnight at 110 °C. The spectra were examined in the OH stretching region (3 400–3 800 cm^{-1}) and the region below 1 200 cm^{-1}, where intense Si–O absorptions and OH bending bands are present.

Thermal Analysis (TG/DSC)

Simultaneous Thermogravimetry and Differential Scanning Calorimetry (TG/DSC) analyses were performed with a Setaram Setsys Evolution 16 equipment at a heating rate of 10 °C·min^{-1} and under a dynamic argon atmosphere (20 mL·min^{-1}) at temperatures between 20 °C and 1 100 °C (Mackenzie 1957).

Total cation Exchange Capacity (CEC)

Cation exchange capacity (CEC) of clay samples was determined with copper triethylenetetramine (Cu-Trien or $[Cu(trien)]^{2+}$ solution following the method described in (Ammann et al. 2005).

Clay samples (200 mg) were placed in 60 mL centrifuge tubes with 25 mL of deionized water and dispersed by ultrasonic treatment for 5 min. Then, 10 mL of 0.01 M $[Cu(trien)]^{2+}$ were added and allowed to react by end-over-end shaking for 1 hour. After this procedure, a complete exchange of the $[Cu(trien)]^{2+}$ complex with the exchangeable cations is guaranteed. Afterwards, the suspensions were centrifuged (15 500 rpm for 20 min) to separate the solid and liquid phase.

The supernatant (3 mL) was sampled and filtered through 0.45 μm pore size syringe filter and transferred to glass cuvettes to measure their concentration. The $[Cu(trien)]^{2+}$ concentration was evaluated through the measurement of their absorbance by using a UV-VIS spectrophotometer (Lambda EZ 210, Perkin Elmer) at 578 nm wavelength. The analyses were performed in duplicate and concentrations were determined with calibration curves carried out with known $[Cu(trien)]^{2+}$ concentrations. The standard deviation of the measurement is ± 2 meq·100 g^{-1}.

Cation Exchange Population

Cation exchange population was determined by using Cs as index cation (Sawhney 1970). Cs acts as a high selective cation to displace all exchangeable cations from the clay minerals if its concentration is sufficiently high. Solid samples were equilibrated inside a JACOMEX glove box (< 1 ppm O_2) at 1:4 solid to liquid ratio (0.25 $kg \cdot L^{-1}$) with 0.5 M $CsNO_3$ at pH 8.2. After phase separation by centrifugation (outside the glove box), the supernatant solutions were filtered through 0.45 μm pore size syringe filter (inside the anoxic glove box), and the concentration of the major cations was analysed. Sodium and calcium results were corrected considering their natural content as soluble salts.

Granulometry analyses

Granulometry analyses were performed to analyse the particle size distribution in the solid fraction. About 1–2 grams of sample were mixed with in water and the wet slurry was well dispersed in an ultrasonic bath prior to analysis. A Microtrac X100 equipment, which use scattered light from a laser beam, was used. An optical detector measures size distribution of particles in the range between 0.021 to 704 μm.

4 List of tests and experimental conditions

Table 4-1 lists erosion tests carried out and experimental conditions. In the test reference, #A denotes one single test, and #B or #C notation refers to replica tests.

The corresponding task, according to the objectives described in Section 2 is indicated, as well as the ype of test, bentonite, fracture conditions (smooth, Roughness 1 or Roughness 2), slope and fracture aperture.

In the rough fractures, the fracture aperture is averaged to that of an equivalent smooth fracture with the same fracture volume (V). The initial water solution was in all experiments NaCl and the ionic strength (in M) is indicated.

The last column indicates if water flow is applied and, in case, the water velocity.

Table 4-1. (Part I of II) Erosion tests and experimental conditions analysed.

Test reference	Task	Type of test	Bentonite (1.4 g·cm^{-3})	Fracture	Aperture (mm)	Fracture Slope	NaCl I (M)	Water velocity (m·s^{-1})
Test 1A	#T4	Sedimentation	Nanocor®	smooth	0.2	0°	10^{-3}	no
Test 2A	#T4	Sedimentation	Nanocor®	smooth	0.2	45°	10^{-3}	no
Test 3A	#T4	Sedimentation	Nanocor®	smooth	0.2	90°	10^{-3}	no
Test 4A; 4B	#T1	Expansion	Nanocor®	smooth	0.1	0°	10^{-3}	no
5A; 5B	#T7	Flow	Nanocor®	smooth	0.1	0°	10^{-3}	10^{-6}
Test 6A; 6B	#T1	Expansion	Nanocor®	smooth	0.2	0°	10^{-3}	no
7A; 7B	#T7	Flow	Nanocor®	smooth	0.2	0°	10^{-3}	10^{-6}
Test 8A; 8B	#T1	Expansion	Nanocor®	smooth	0.4	0°	10^{-3}	no
9A; 9B	#T7	Flow	Nanocor®	smooth	0.4	0°	10^{-3}	10^{-6}
Test 10A	#T1	Expansion	MX-80	smooth	0.1	0°	10^{-3}	no
11A	#T7	Flow	MX-80	smooth	0.1	0°	10^{-3}	10^{-6}
Test 12A	#T1	Expansion	MX-80	smooth	0.2	0°	10^{-3}	no
13A	#T7	Flow	MX-80	smooth	0.2	0°	10^{-3}	10^{-6}
Test 14A	#T1	Expansion	MX-80	smooth	0.4	0°	10^{-3}	no
15A	#T7	Flow	MX-80	smooth	0.4	0°	10^{-3}	10^{-6}
Test 16A	#T4	Sedimentation	MX-80	smooth	0.2	0°	10^{-3}	no
Test 17A	#T4	Sedimentation	MX-80	smooth	0.2	45°	10^{-3}	no
Test 18A	#T4	Sedimentation	MX-80	smooth	0.2	90°	10^{-3}	no
Test 19A	#T1	Expansion	Nanocor®	smooth	0.2	0°	10^{-2}	no
Test 20A	#T1	Expansion	Nanocor®	smooth	0.2	0°	10^{-1}	no
Test 21A	#T2	Expansion	MCA-C clay	smooth	0.2	0°	10^{-3}	no
Test 22A	#T2	Expansion	Ibeco clay	smooth	0.2	0°	10^{-3}	no
Test 23A	#T5	Sedimentation	Ca-MX-80	smooth	0.1	90°	10^{-3}	no
Test 24A	#T5	Sedimentation	Ca-MX-80	smooth	0.2	90°	10^{-3}	no
Test 25A	#T5	Sedimentation	Ca-MX-80	smooth	0.4	90°	10^{-3}	no
Test 26A	#T4	Sedimentation	Nanocor®	smooth	0.2	45°	10^{-2}	no
Test 27A	#T4	Sedimentation	Nanocor®	smooth	0.2	45°	10^{-1}	no
Test 28A	#T4	Sedimentation	Nanocor®	smooth	0.2	45°	10^{-3}	no

Table 4-2. (Part II of II) Erosion tests and experimental conditions analysed. *The aperture indicated for rough fractures is calculated considering an equivalent smooth fracture with the same volume (V).

Test reference	Task	Type of test	Bentonite (1.4 g·cm^{-3})	Fracture	Aperture* (mm)	Fracture Slope	NaCl l (M)	Water velocity (m·s^{-1})
Test 29A	#T1	Expansion	Nanocor®	smooth	0.1	0°	10^{-3}	no
30A	#T7	Flow	Nanocor®	smooth	0.1	0°	10^{-3}	10^{-6}
Test 31A	#T6	Expansion	Nanocor®	Roughness 1	V (1 mm)	0°	10^{-3}	no
32A	#T8	Flow	Nanocor®	Roughness 1	V (1 mm)	0°	10^{-3}	10^{-6}
Test 33A	#T6	Expansion	Nanocor®	Roughness 2	V (1.7 mm)	0°	10^{-3}	no
34A	#T8	Flow	Nanocor®	Roughness 2	V (1.7 mm)	0°	10^{-3}	10^{-6}
Test 35A	#T1	Expansion	MX-80	smooth	0.2	0°	10^{-3}	no
36A	#T7	Flow	MX-80	smooth	0.2	0°	10^{-3}	10^{-6}
Test 37A	#T6	Expansion	MX-80	Roughness 1	V (1 mm)	0°	10^{-3}	no
38A	#T1	Flow	MX-80	Roughness 1	V (1 mm)	0°	10^{-3}	10^{-6}
Test 39A	#T6	Expansion	MX-80	Roughness 2	V (1.7 mm)	0°	10^{-3}	no
40A	#T8	Flow	MX-80	Roughness 2	V (1.7 mm)	0°	10^{-3}	10^{-6}
Test 41A	#T6	Sedimentation	MX-80	Roughness 1	V (1 mm)	0°	10^{-3}	no
Test 42A	#T6	Sedimentation	MX-80	Roughness 1	V (1 mm)	45°	10^{-3}	no
Test 43A	#T6	Sedimentation	MX-80	Roughness 1	V (1 mm)	90°	10^{-3}	no
Test 44A	#T6	Sedimentation	Na-MX-80	Roughness 1	V (1 mm)	0°	10^{-3}	no
Test 45A	#T6	Sedimentation	Na-MX-80	Roughness 1	V (1 mm)	45°	10^{-3}	no
Test 46A	#T6	Sedimentation	Na-MX-80	Roughness 1	V (1 mm)	90°	10^{-3}	no
Test 47A	#T6	Sedimentation	Ca-MX-80	Roughness 1	V (1 mm)	0°	10^{-3}	no
Test 48A	#T6	Sedimentation	Ca-MX-80	Roughness 1	V (1 mm)	45°	10^{-3}	no
Test 49A	#T6	Sedimentation	Ca-MX-80	Roughness 1	V (1 mm)	90°	10^{-3}	no
Test 50A, B, C	#T3	Expansion	MX-80	smooth	0.2	0°	10^{-3}	no
Test 51 A, B, C	#T3	Expansion	Minerals&salt-free MX-80	smooth	0.2	0°	10^{-3}	no
Test 52A	#T4	Sedimentation	Nanocor®	smooth	1	0°	10^{-3}	no
Test 53A	#T4	Sedimentation	Nanocor®	smooth	1	45°	10^{-3}	no
Test 54A	#T4	Sedimentation	Nanocor®	smooth	1	90°	10^{-3}	no
Test 55A, B, C	#T3	Expansion	Salt-free MX-80	smooth	0.2	0°	10^{-3}	no
Test 56A	#T1	Expansion	Nanocor®	smooth	1.7	0°	10^{-3}	no
Test 57A	#T1	Expansion	MX-80	smooth	1.7	0°	10^{-3}	no

5 Results

Periodical photographs were taken to all expansion and sedimentation tests, at different times (in days, d) which allow following the evolution of clay expansion in the fractures from initial conditions (0 d) and up to 30 days (30 d).

Appendix 1 presents selected photographs for each erosion tests carried out, tests are ordered by number, as in Table 4-1. The number in the left upper side of the picture is the photograph number, to facilitate identification, if required. Additional photographs were taken at intermediate times.

On these periodical photographs it was clearly appreciated that, in all conditions analysed, clay extruded in the fractures. As sketched in Figure 3-5, extruded distances were measured in four axial directions, from the pellet surface, as a function of time. When homogenous radial extrusion was identified, the distances in the fracture are presented as the average value of the four radial lengths measured on perpendicular axis.

In erosion tests carried out under flow conditions, there was an initial expansion period during 30 days, which was analysed as an individual expansion test. However, post-mortem analyses, and therefore eroded mass evaluation was carried out at the end of the flow period (after 60 days).

Main results are below described and compared. From here after, results are presented grouped by type of test, expansion, sedimentation or erosion by flow and by the main variable analysed: aperture, slope, clay type, ionic strength or roughness. All results are separately discussed in Section 6.

Table 5-1 presents the initial clay masses, weighed and dry, the clay water content (w.c. in %) and the final pellet dry mass. As mentioned, the *eroded mass* was determined by the difference in weigh between the final and the initial clay pellet masses. In most of experiments this eroded mass only corresponds to the clay mass extruded in the fracture. However, in sedimentation and flow experiments, deposited and/or eluted fractions are also included in the total *eroded mass*. When measured, the deposited and eluted mass fractions were separately indicated in the table.

In most of the cases, reported masses are the result of a single test. Therefore, measurement errors basically depend on the sampling procedure and on the availability of more or less clay amount. When sufficient clay amounts were sampled, the associated errors are generally lower than 5 % but, when the amount to be sampled is small (tens of mg) the uncertainties are greater.

As mentioned in the experimental section, the remaining water in the fracture was sampled at the end of the experiments, and the measured chemical conditions (pH and conductivity) are listed in Table 5-3 and Table 5-4. It is noteworthy that, in all cases, measured conductivities were higher than that of the initial water, what suggests that erosion behaviour will be highly influenced by the clay/water interactions establishing the final chemical conditions. Complete chemical analyses were carried out in selected tests.

Table 5-1. (Part I of II) Mass results in erosion tests: Initial and final pellet masses, clay water content (w.c. in %), eroded mass (g and %), deposited and eluted masses.

Tests reference	Pellet initial weighed mass (g)	w.c. (%)	Pellet initial dry mass (g)	Pellet final dry mass (g)	Eroded (g)	Deposited mass (g)	Eluted mass (g)	Eroded (%)
Test 1A	4.43	10.57	3.9617	3.2480	0.7137	0	-	18.0
Test 2A	4.43	10.57	3.9617	3.0548	0.9069	0	-	22.9
Test 3A	4.43	10.57	3.9617	3.3909	0.5708	0	-	14.4
Test 4A, 4B	4.43	10.57	3.9617			0		
5A, 5B				3.6238	0.3379	0	6.2×10^{-4}	8.5
Test 6A, 6B	4.43	10.57	3.9617			0		
7A, 7B				3.2480	0.7137	0	6.0×10^{-3}	18.0
Test 8A, 8B	4.43	10.57	3.9617			0		
9A, 9B				3.0310	0.9307	0	9.9×10^{-3}	23.5
Test 10A	4.39	9.39	3.9778			0		
11A				3.9573	0.0205	0	2.0×10^{-4}	0.5
Test 12A	4.39	9.39	3.9778			0		
13A				3.9116	0.0662	0	5.0×10^{-4}	1.7
Test 14A	4.39	9.39	3.9778			0		
15A				3.8078	0.1700	0	5.0×10^{-3}	4.3
Test 16A	4.39	9.39	3.9778	3.9116	0.0662	0	-	1.7
Test 17A	4.39	9.39	3.9778	3.8936	0.0842	0	-	2.1
Test 18A	4.39	9.39	3.9778	3.9000	0.0778	0	-	2.0
Test 19A	4.43	10.57	3.9617	3.5678	0.3939	0	-	9.9
Test 20A	4.43	10.57	3.9617	3.6929	0.2688	0	-	6.8
Test 21A	4.37	8.89	3.9815	3.7008	0.2807	0	-	7.1
Test 22A	4.53	12.90	3.9456	3.9185	0.0271	0	-	0.7
Test 23A	4.5	12.15	3.9533	3.7454	0.2079	0	-	5.3
Test 24A	4.5	12.15	3.9533	3.6463	0.3070	0	-	7.8
Test 25A	4.5	12.15	3.9533	3.7150	0.2383	0	-	6.0
Test 26A	4.43	10.57	3.9617	3.5453	0.4164	0	-	10.5
Test 27A	4.43	10.57	3.9617	3.6364	0.3253	0	-	8.2

Table 5-2. (Part II of II) Mass results in erosion tests: Initial and final pellet masses, clay water content (w.c. in %), eroded mass (g and %), deposited mass and eluted masses.

Tests reference	Pellet initial weighed mass (g)	w.c. (%)	Pellet initial dry mass (g)	Pellet final dry mass (g)	Eroded (g)	Deposited mass (g)	Eluted mass (g)	Eroded (%)
Test 29A	4.43	10.57	3.9617			0		
30A				3.3199	0.6418	0	6.2×10^{-4}	16.2
Test 31A	4.43	10.57	3.9617			0		
32A				2.7108	1.2509	0	4.5×10^{-4}	31.6
Test 33A	4.43	10.57	3.9617			0		
34A				2.9910	0.9707	0	1.5×10^{-3}	24.5
Test 35A	4.39	9.39	3.9778			0		
36A				3.8620	0.1138	0	1.3×10^{-4}	2.9
Test 37A	4.39	9.39	3.9778			0		
38A				3.2849	0.6929	0	1.18×10^{-3}	17.4
Test 39A	4.39	9.39	3.9778			0		
40A	4.39	9.39	3.9778	3.5716	0.4062	0	3.8×10^{-4}	10.2
Test 41A	4.39	9.39	3.9778	3.5205	0.4573	0		11.5
Test 42A	4.39	9.39	3.9778	3.4601	0.5177	0.2715		13.0
Test 43A	4.39	9.39	3.9778	3.2801	0.6977	0.0570		17.5
Test 44A	4.17	3.95	4.0053	2.4861	1.5192	0		37.9
Test 45A	4.17	3.95	4.0053	2.4673	1.5380	0.1255		38.4
Test 46A	4.17	3.95	4.0053	2.3551	1.6502	0.1369		41.2
Test 47A	4.5	11.95	3.9623	3.9558	0.0065	0		0.2
Test 48A	4.5	11.95	3.9623	3.8120	0.1503	0		3.8
Test 49A	4.5	11.95	3.9623	3.8204	0.1419	0		3.6
Test 50A, B, C	4.39	9.39	3.9778	3.9067	0.0711	0		1.8
Test 51A, B, C	4.39	9.39	3.9588	3.3205	0.6383	0		16.1
Test 52A	4.43	10.57	3.9617	2.8343	1.1274	0		28.5
Test 53A	4.43	10.57	3.9617	2.5429	1.4188	0.1350		35.8
Test 54A	4.43	10.57	3.9617	2.3611	1.6006	0.2780		40.4
Test 55A, B, C	4.4717	11.47	3.9645	3.6663	0.2982	0		7.5
Test 56A	4.43	10.57	3.9617	2.2983	1.1274	0		42.0
Test 57A	4.39	9.39	3.9778	2.5429	1.4188	0		35.8

Table 5-3. (Part I of II) Final pH and electrical conductivity (E.C. in µS·cm^{-1}) of equilibrium water at the end of experiments. n.d. no data.

Tests reference	Clay	Fracture aperture (mm)	pH	E.C. (µS·cm^{-1})
Test 1A	Nanocor®	0.2	7.93	4150
Test 2A	Nanocor®	0.2	8.03	4570
Test 3A	Nanocor®	0.2	n.d	n.d
Tests 4A and 5A	Nanocor®	0.1	8.55	6260
Tests 6B and 7B	Nanocor®	0.2	n.d	n.d
Tests 8B and 9B	Nanocor®	0.4	7.16	1315
Tests 10A and 11A	MX-80	0.1	7.21	542
Tests 12A and 13A	MX-80	0.2	7.04	218
Tests 14A and 15A	MX-80	0.4	6.85	230
Test 16A	MX-80	0.2	8.29	2360
Test 17A	MX-80	0.2	8.36	2230
Test 18A	MX-80	0.2	7.96	2600
Test 19A	Nanocor®	0.2	7.37	2230
Test 20A	Nanocor®	0.2	7.60	18730
Test 21A	MCA-C	0.2	8.00	496
Test 22A	Ibeco	0.2	7.57	1692
Test 23A	Ca-MX-80	0.1	7.70	391
Test 24A	Ca-MX-80	0.2	7.52	370
Test 25A	Ca-MX-80	0.4	7.60	420
Test 26A	Nanocor®	0.2	7.81	5770
Test 27A	Nanocor®	0.2	7.88	15520
Test 28A	Nanocor®	0.2	8.03	4570

Table 5-4. (Part II of II) Final pH and electrical conductivity (E.C., in µS·cm^{-1}) of equilibrium water at the end of experiments. *The aperture indicated for rough fractures is that of an equivalent smooth fracture with the same volume (V). n.d. no data.

Reference	Clay	Fracture aperture*	pH	E.C. (µS·cm^{-1})
Tests 29A and 30A	Nanocor®	0.4 mm	7.23	1425
Tests 31A and 32A	Nanocor®	Rough 1 // 1 mm	8.13	1280
Tests 33A and 34A	Nanocor®	Rough 2 // 1.7 mm	n.d	n.d
Tests 35A and 36A	MX-80	0.4 mm	7.47	415
Tests 37A and 38A	MX-80	Rough 1 // 1 mm	8.53	598
Tests 39A and 40A	MX-80	Rough 2 // 1.7 mm	n.d	n.d
Test 41A	MX-80	Rough 1 // 1 mm	8.12	1317
Test 42A	MX-80	Rough 1 // 1 mm	7.82	1477
Test 43A	MX-80	Rough 1 // 1 mm	8.00	1570
Test 44A	Na-MX-80	Rough 1 // 1 mm	8.08	603
Test 45A	Na-MX-80	Rough 1 // 1 mm	7.76	742
Test 46A	Na-MX-80	Rough 1 // 1 mm	8.01	658
Test 47A	Ca-MX-80	Rough 1 // 1 mm	7.17	387
Test 48A	Ca-MX-80	Rough 1 // 1 mm	7.72	373
Test 49A	Ca-MX-80	Rough 1 // 1 mm	8.02	309
Test 50A	MX-80	0.2 mm	8.24	2005
Test 50B	MX-80	0.2 mm	8.21	2045
Test 50C	MX-80	0.2 mm	8.25	2220
Test 51A	Minerals&salt-free MX-80	0.2 mm	8.06	531
Test 51B	Minerals&salt-free MX-80	0.2 mm	8.11	518
Test 51C	Minerals&salt-free MX-80	0.2 mm	8.02	495
Test 52A	Nanocor®	1 mm	7.67	3170
Test 53A	Nanocor®	1 mm	7.72	3170
Test 54A	Nanocor®	1 mm	7.50	3040
Test 55A	Salt-free MX-80	0.2 mm	7.80	592
Test 55B	Salt-free MX-80	0.2 mm	7.60	557
Test 55C	Salt-free MX-80	0.2 mm	7.80	568
Test 56A	Nanocor®	1.7 mm	7.60	2960
Test 57A	MX-80	1.7 mm	7.79	1430

5.1 Expansion tests in smooth fractures at horizontal slope

5.1.1 Fracture aperture effect

The effect of fracture aperture on bentonite expansion was initially carried out in smooth narrow fractures placed at horizontal slope (0°) with different apertures considered as narrow: 0.1 mm, 0.2 mm and 0.4 mm. The expansion behaviour of Nanocor® (Tests 4B, 6B and 8A in Table 4-1) and MX-80 bentonite (Tests 10A, 12A and 14A) was compared.

Expansion experiments within wider fractures (1 mm and 1.7 mm) were also carried out in smooth fractures (Tests 52A, 55A and 56A) to reach comparable fracture volumes of those tests performed in rough fractures.

As can be seen in Appendix 1 (4B, 6B and 8A, pages 86–89; 10A, 12A and 14A, pages 91–93, 52A page 128, 55A page 131 and 57A page 135), in all cases, clay expansion in the fracture started once the fracture was filled with NaCl and the clay gradually extruded in the fracture. Experiments carried with Nanocor® clay exhibited an extrusion pattern fairly homogenous, with a radial geometry. However, in the case of MX-80 clay, extruded clay showed some fingering, most probably due to the fact the clay is coarser.

Figure 5-1 presents the average expansion distances, measured form the pellet surface, travelled by Nanocor® within smooth fractures, of different aperture. Figure 5-2 presents the results measured for MX-80 clay.

For both clays, clay expansion was lower within the fracture with thinner aperture (0.1 mm) but, however, extrusion distances measured within 0.2, 0.4 mm and 1 mm apertures were almost the same. When fracture aperture is increased up to 1.7 mm, clay extrusion was clearly favoured.

For fracture apertures lower than 1 mm, clay extrusion initially increased almost linearly with time, but after about 5 to 20 days, extrusion is stopped and a steady state is reached. Only in Test 56A, carried out with Nanocor® clay within 1.7 mm fracture aperture, clay extrusion was slowed down, but steady state was not fully reached. The experiment was stopped, to keep the time constant and to facilitate tests comparison. It is feasible that clay extrusion would be stopped as well at longer time, but it is something to be verified.

Nanocor® clay showed longer extrusion than MX-80 clay, but their behaviour was equivalent, with the only exception of test 10A, carried out with MX-80 bentonite showed a slightly different behaviour, most probably due to a later hydration. The amount of clay extruded in the fracture depended on the fracture aperture, and the higher the aperture the higher the eroded mass (Table 5-1), for both clays.

The longer expansion measured for Nanocor® can be due to the fact that it is Na-homoionised, while MX-80 is used “as received”. Higher erosion was as well measured, in other experimental configuration (Alonso et al. 2018) under confined and stagnant conditions. In that study, erosion results were related to clay smectite content (lower in MX-80 and almost 100 % in Nanocor®) and to some structural properties (*i.e* tetrahedral charge), which are slightly different in this clay.

Some tests were carried out in duplicate or triplicate to verify tests reproducibility.

Figure 5-3 presents the average expansion experienced by Nanocor® within 0.1, 0.2 and 0.4 mm fractures, in different replica tests. In Figure 5-3.a, the benchmark test carried out in the former EC-BELBAR project (Schatz et al. 2015) is included for comparison.

The extrusion distances measured in the three different tests carried out in the smaller aperture were equivalent, even in Test 4, in which a slight movement was provided trying to eliminate some bubbles, which can be appreciated in Appendix 1 (page 85). The two tests carried out within 0.2 mm fracture aperture showed slight differences (Appendix 1, pages 87–88), and it seems that the initial humidity of test 6A was lower and swelling and expansion was slightly delayed.

In general, measured average expansion distances were comparable and differences can be attributed to experimental uncertainties, such as slight changes in compaction density or ambient humidity. The replicates of tests indicate that the results are reproducible.

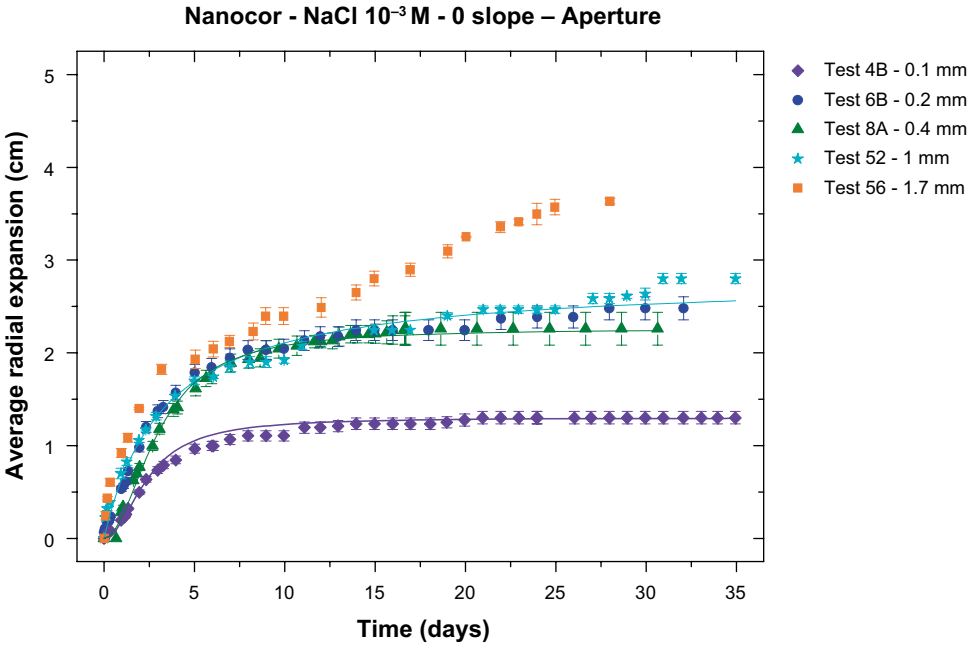

Figure 5-1. *Average radial expansion (in cm) of Nanocor® clay at 1.4 g·cm^{-3} within smooth fractures (apertures 0.1, 0.2, 0.4, 1 mm and 1.7 mm) filled with NaCl 10^{-3} M, placed at horizontal slope (0°). Lines are included to guide the eye.*

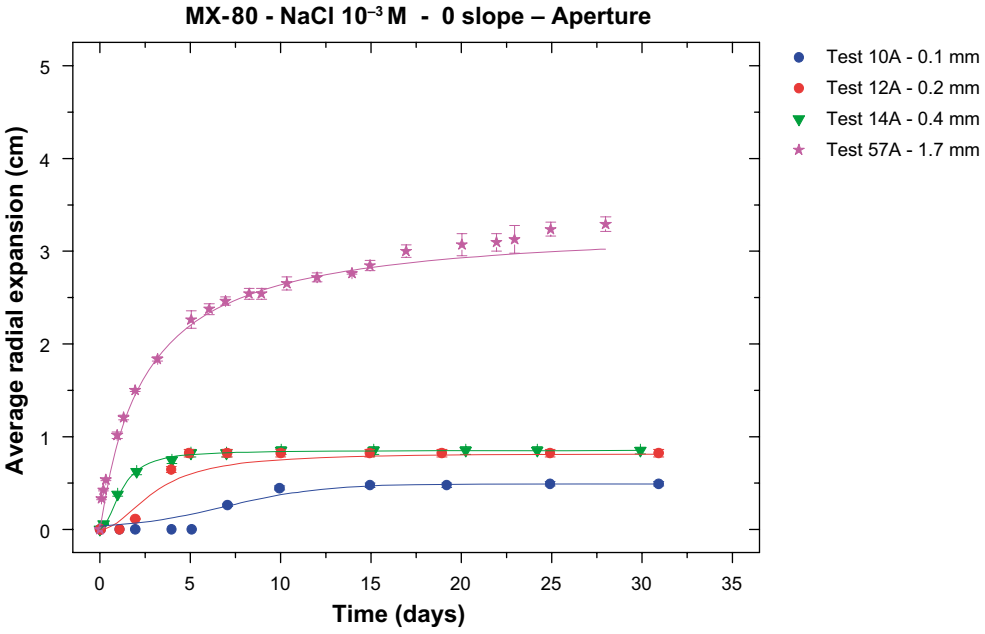

Figure 5-2. *Average radial expansion (in cm) of raw MX-80 clay at 1.4 g·cm^{-3} within smooth fractures (apertures 0.1, 0.2, 0.4 , 1 mm and 1.7 mm) filled with NaCl 10^{-3} M, placed at horizontal slope (0°). Lines are included to guide the eye.*

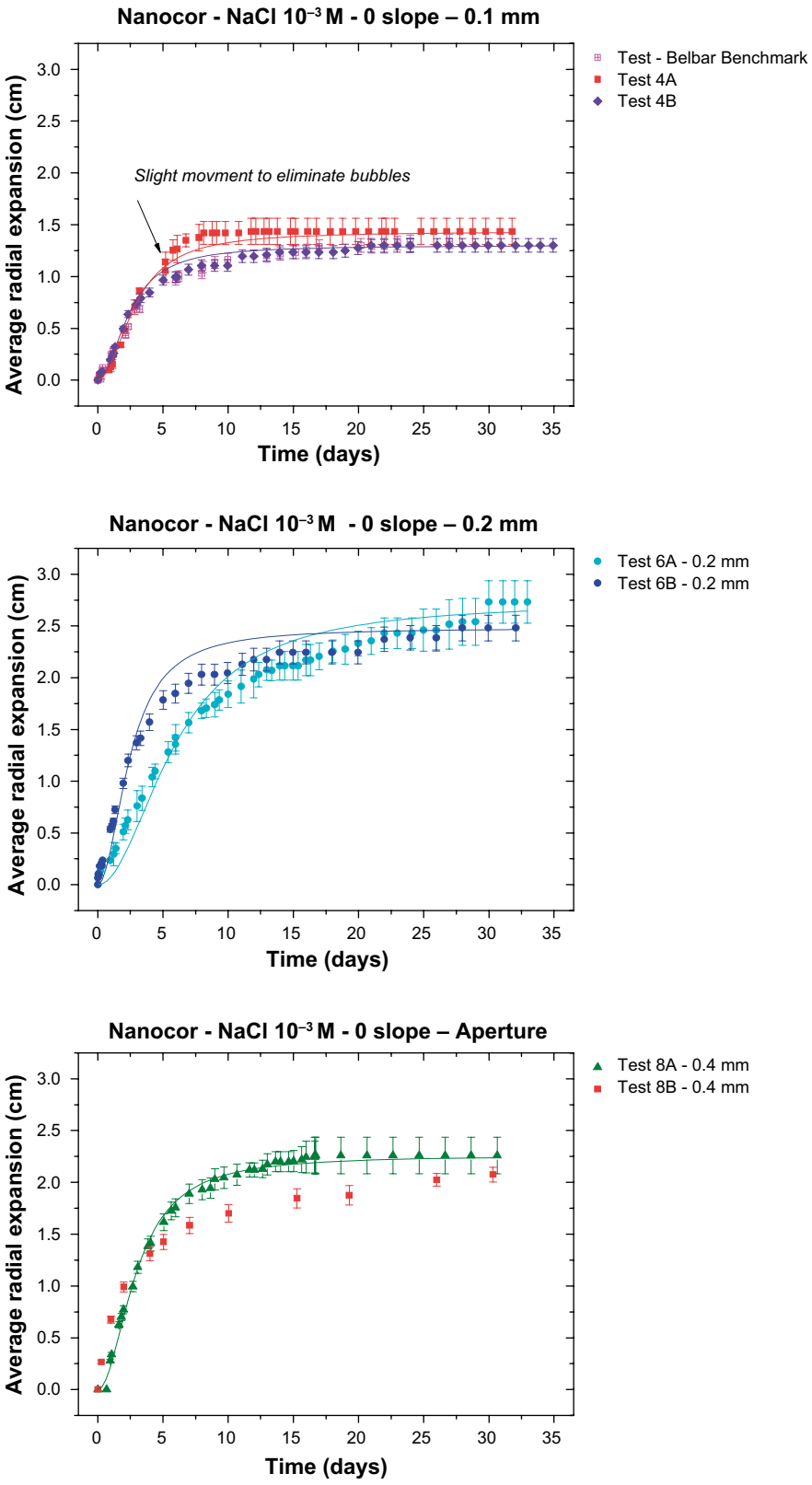

Figure 5-3. *Replica tests carried with Nanocor® at 1.4 g·cm^{-3} out in smooth fractures at 0° slope, filled with NaCl 10^{-3} M and with different apertures: (a) 0.1 mm, (b) 0.2 mm and (c) 0.4 mm.*

5.1.2 Ionic strength effect in smooth fractures at horizontal slope

Figure 5-4 presents the average radial expansion measured for Nanocor® clay in a 0.2 mm narrow fracture placed horizontally and filled with NaCl at different ionic strengths (10^{-3}, 10^{-2} and 10^{-1} M), tests respectively named 6B, 19A and 20 A (Table 4-1).

In the three tests, clay extrusion was homogenous and extrusion distances measured in different directions were comparable (Appendix 1, 6B (page 88), 19A (page 97) and 20 A (page 98). Clay extrusion rate initially increased almost linearly with time and after about 10 days, extrusion was stopped and a steady state was reached in all cases.

Clay expansion was higher at lower initial ionic strengths, but non-negligible extrusion distances are measured at highest ionic strength (10^{-1} M).

Eroded mass fraction was around an 18 % at 10^{-3} M, 10 % at 10^{-2} M and 6.8 % at 10^{-1} M. It is noticeable that the electrical conductivities measured at the end of all experiments (Table 5-3 and Table 5-4) were all rather high, but in any case clay expansion took place. This indicates that high ionic strength waters do not inhibit initial swelling, but most probably hinder further expansion.

5.1.3 Clay type effect in smooth fractures at horizontal slope

The extrusion behaviour of Nanocor®, MX-80, MCA-C saponite and Ibeco bentonite compared within a 0.2 mm horizontal fracture filled with NaCl at 10^{-3}: tests respectively named 6B, 12A, 19A, 21A and 22A. As can be seen in the corresponding photographs in Appendix 1 (6B page 88, 12A page 92, 19A page 97, 21A page 99 and 22A page 100), clay extrusion was always homogenous.

Figure 5-5 presents the average radial expansion measured for these clays. Expansion distances were equivalent for MX-80, MCA-C saponite and Ibeco bentonite, despite their different nature, but the expansion of Nanocor® was larger, probably because it is almost 100 % smectite and Na-homoionised. MX-80 is Na-rich clay as well, but Ibeco is a Ca–Mg, and its expansion should be in principle lower, considering the different nature.

Similar swelling pressures have been reported for MX-80 and Ibeco clay (around 1 MPa) (Karnland 2010), so that a relationship between swelling pressure and expanded masses can be expected.

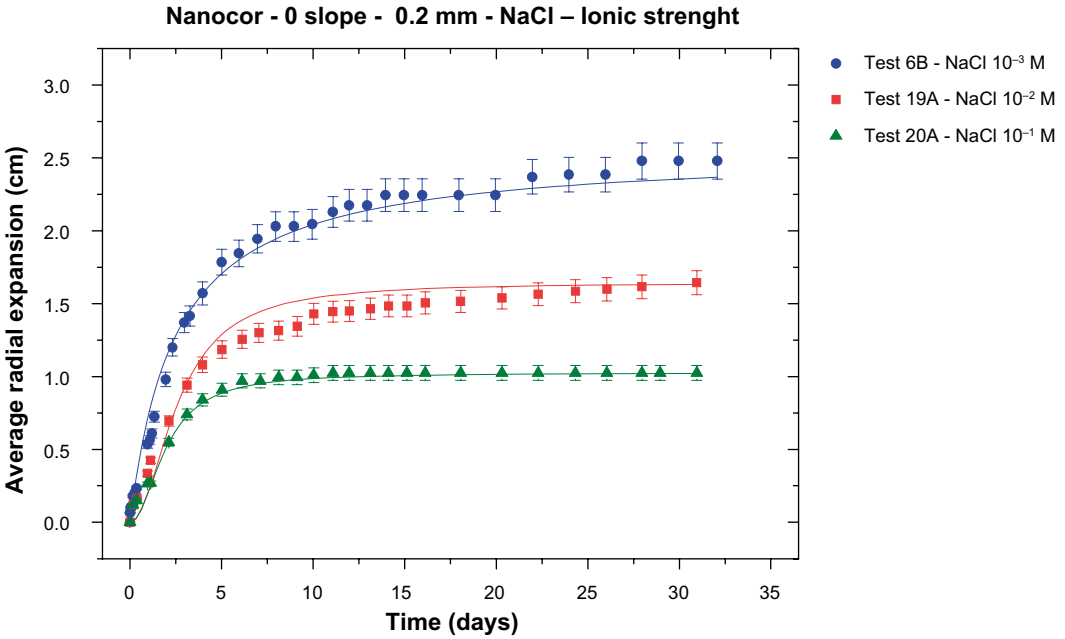

Figure 5-4. *Average radial expansion (in cm) of Nanocor® clay at 1.4 g·cm^{-3} within smooth artificial fractures of 0.2 mm aperture placed horizontally (slope 0°) and filled with NaCl at different ionic strength (10^{-3} M, 10^{-2} M and 10^{-1} M). Lines are included to guide the eye.*

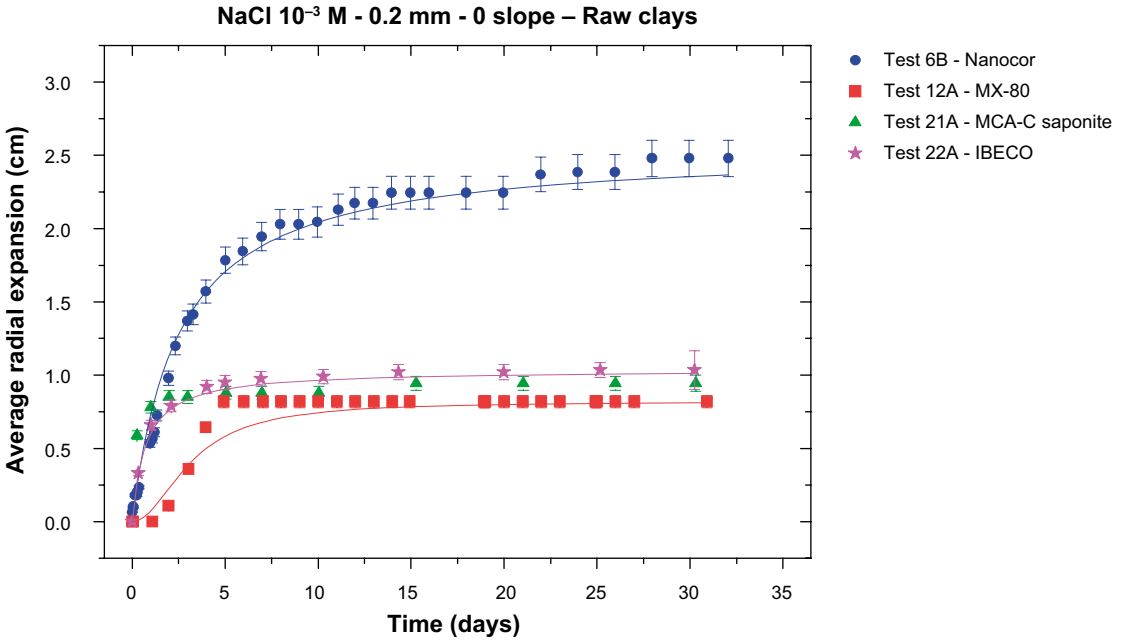

Figure 5-5. *Average radial expansion (in cm) of different clays, Nanocor®, MX-80, Ibeco and MCA-C, compacted at 1.4 g·cm^{-3}, within an 0.2 mm smooth fracture placed horizontally and filled with NaCl 10^{-3} M. Lines are included to guide the eye.*

5.2 Role of accessory minerals and soluble salts on clay expansion

A set of expansion tests was specifically devoted to analyse the role of accessory minerals and soluble salts, naturally present in the clays, on erosion process. These tests were done in triplicate to facilitate in-depth post-mortem analyses of the expanded region (Tests 50, 51 and 55 A, B and C in Table 4-2).

5.2.1 Mineralogical analyses of initial samples

Figure 5-6 presents the comparison of XRD patterns measured on raw MX-80, salt-free and minerals&salt-free MX-80 clay fractions.

As expected, the main mineral phases of the bulk or raw MX-80 bentonite, determined by XRD analyses, were smectite (Sm., 80 wt %), muscovite/illite (Mu. 2 wt %), quartz (Qz. 7 wt %), cristobalite (Cris. 4 wt %), K-feldspars (Fdls. 2 wt %), plagioclases (2 wt %), calcite (cc. 2 wt %) and gypsum (Gyp. 1 wt %).

According to XRD analyses carried out on salt-free and *minerals&salt-free* MX-80 clay fractions, the pre-treatment discarding accessory minerals avoided both the presence of larger minerals and of soluble salts (calcite and gypsum), but some accessory minerals such as quartz (probably colloidal), cristobalite and some type of feldspars are still observed.

Figure 5-7 presents the FTIR spectra obtained from the raw MX-80 and pre-treated clay fraction. Going into details, the FTIR spectra showed a band at 3 627 cm^{-1} which corresponds to the typical OH stretching region of structural hydroxyl groups of di-octahedral smectites, with Al-rich octahedral sheets. These are inner hydroxyl groups lying between the tetrahedral and octahedral sheets.

The broad band near 3 426 cm^{-1} is usually attributed to stretching H-O-H vibrations of adsorbed water, while the band at 1 642 cm^{-1} corresponds to the OH deformation or bending adsorption of water.

If the Si–O absorptions and OH bending bands in the 1 300–400 cm^{-1} range are examined, at around 1 030 cm^{-1}, a single broad complex Si–O stretching vibration band is seen, again typical of a di-octahedral smectite.

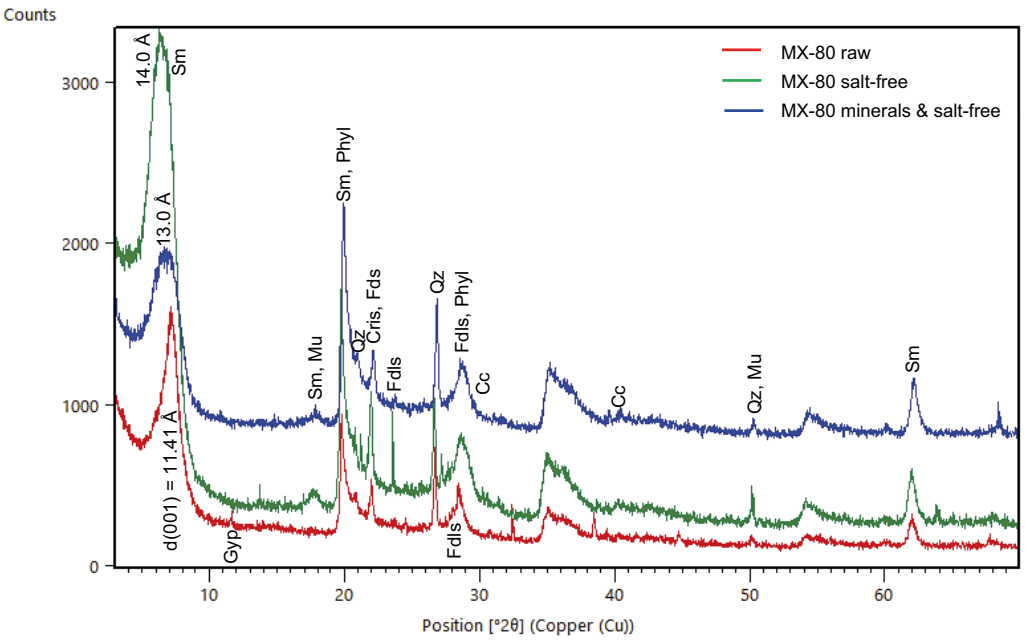

Figure 5-6. *Comparison of XRD patterns of the raw MX-80 bentonite and salt-free and minerals&salt-free MX-80 fractions.*

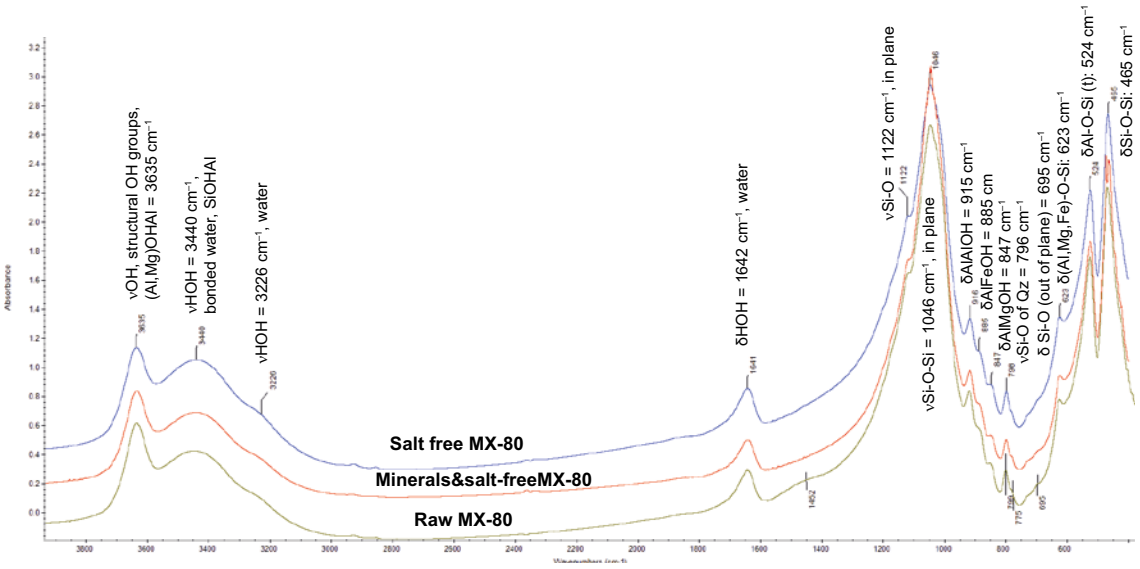

Figure 5-7. *FTIR spectra of the initial clayey materials: raw, salt-free and minerals&salt-free MX-80 samples.*

The occupancy of the octahedral sheet strongly influences the position of the OH bending bands, which arise from vibrations of the inner and surface OH groups. In these samples, the presence of peaks at 915 cm^{-1} (δAlAlOH), at 885 cm^{-1} (δAlFeOH),) and at 840 cm^{-1} (δAlMgOH) indicates a partial substitution of octahedral Al by Fe and Mg, again usual for di-octahedral smectites.

The adsorption band at 622 cm^{-1} can be attributed to an R-O-Si vibration (R = Al, Fe, Mg) and indicates a perpendicular vibration of the octahedral cations and their connection to the tetrahedral sheet. The bands at 524 cm^{-1} and 465 cm^{-1} correspond to Si–O–Al vibration of aluminium in the tetrahedral sheet and Si-O-Si bending vibrations, respectively. The weak band at 798 cm^{-1} or doublet (798 and 775 cm^{-1}) is caused by the Si–O stretching of quartz.

In the three cases, FTIR spectra are equivalent and the main typical bands of a di-octahedral smectite, and bands related to quartz presence are also identified. The main difference that can be extracted from the FTIR spectra measured for the raw and pre-treated samples is the presence of calcite (band at 1 452 cm^{-1}), which is no longer observed in the purified samples.

Figure 5-8 presents the TG-DSC curve measured for the raw MX-80 bentonite, which is typical of di-octahedral smectites, with most of the OH^- groups at cis-vacant positions (peak at 702 °C). The single dehydration peak at 123 °C in the raw MX-80 bentonite is characteristic of smectites with monovalent cations at exchange sites (in this case Na^+).

Figure 5-9 shows the TG-DSC comparison between raw MX-80 and salt-free and minerals&salt-free clay samples. The main difference that can be seen is that, in the treated samples, apart from the main peak at 120 °C, a shoulder between 166° and 186 °C is observed, which is usually related to divalent cations inside interlayer sites, what suggest that the treatment to extract soluble salts and accessory minerals favoured the incorporation of divalent cations, upon calcite dissolution.

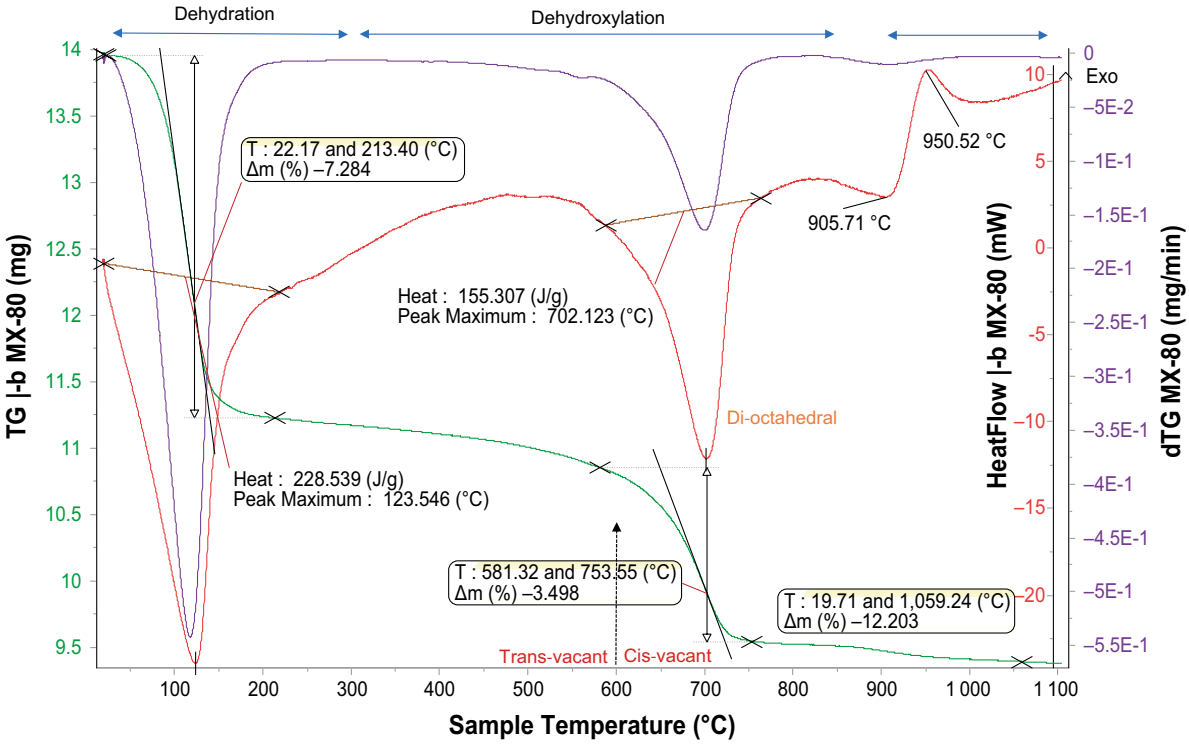

Figure 5-8. *TG-DTG-DSC curves from the raw MX-80 bentonite.*

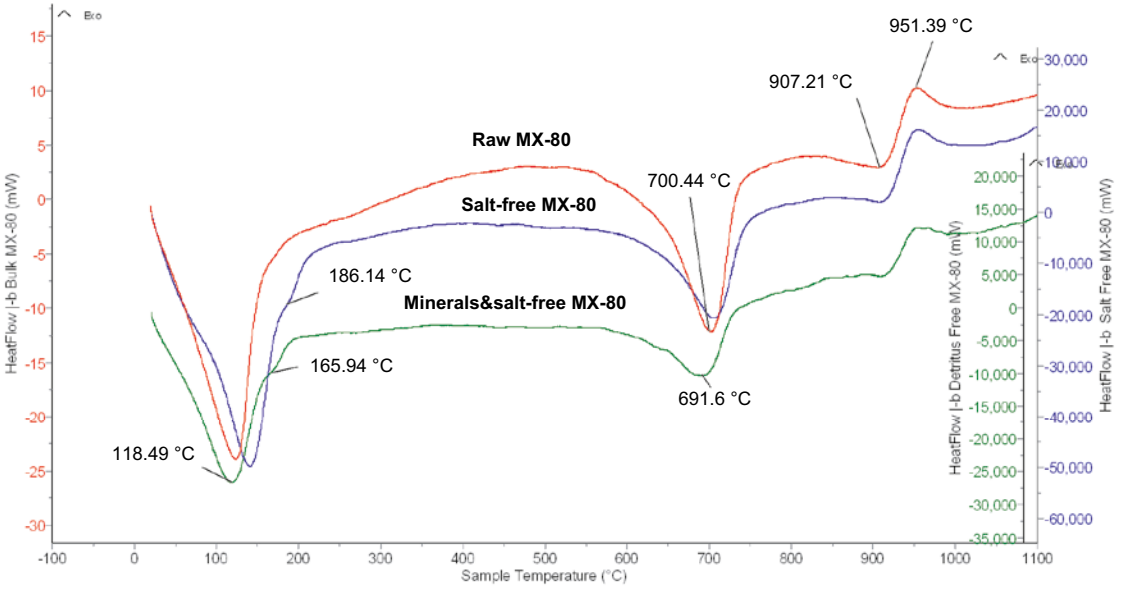

Figure 5-9. *Comparison of TG-DTG-DSC curves measured for raw MX-80 bentonite and pre-treated samples (salt-free and minerals&salt-free samples).*

Cation at interlayer sites and total cation exchange capacity (CEC) of raw, salt-free and minerals&salt-free MX-80 were measured (Table 5-5). In the three cases, the main cations at interlayer sites are sodium and calcium. It is interesting to note the increase of calcium content when the bentonite is treated (minerals&salt-free and salt-free) due to the dissolution of calcite and gypsum present in the raw sample. These analyses indicate that during the pre-treatment, the soluble minerals were dissolved, modifying the cation composition at interlayer sites, because divalent cations have higher selectivity to enter at interlayer sites. This was detected in the XRD patterns (Figure 5-6), since the 001 reflexion increased from 11.4 Å to 13–14 Å and, as mentioned, also in the TG-DSC curves (Figure 5-9).

Table 5-5. Cation presence at interlayer sites and total CEC of raw, salt-free and minerals&salt-free MX-80.

Clay material	Na	K	Mg	Ca	Sr	Ba	Sum cations	CEC*
Raw MX-80	58.49	4.18	6.86	15.63	0.44	0.01	85.61	83.6
Salt-free MX-80	37.39	1.43	8.74	33.79	0.51	0.12	81.97	78.9
Minerals&salt-free MX-80	42.39	1.71	7.47	31.85	0.53	0.04	84.00	76.0

* Determined by Cu-Trien complex.

5.2.2 Expansion tests of salt-free and minerals&salt-free MX-80 in smooth fractures

Figure 5-10 shows selected temporal images taken during expansion of *raw* MX-80, *salt-free* MX-80 and *minerals&salt-free* MX-80 clay fraction, in artificial smooth fractures filled with NaCl 10^{-3} M.

At first sight, the extrusion of raw MX-80 is different to that of salt free- or minerals&salt-free fractions.

The small black spots, appreciated in the figures corresponding to raw MX-80 are probably coarse accessory minerals. However, the extrusion patterns of the treated samples are very similar. At first sight, it is striking that the clay that shows an expansion pattern in which a darker outer ring can be appreciated, is that of the minerals&salt-free MX-80, in which most accessory minerals have been removed.

Figure 5-11 shows the average radial expansion (in cm) measured as a function of time for raw MX-80, salt-free MX-80 and minerals&salt-free MX-80. Results are presented in triplicate.

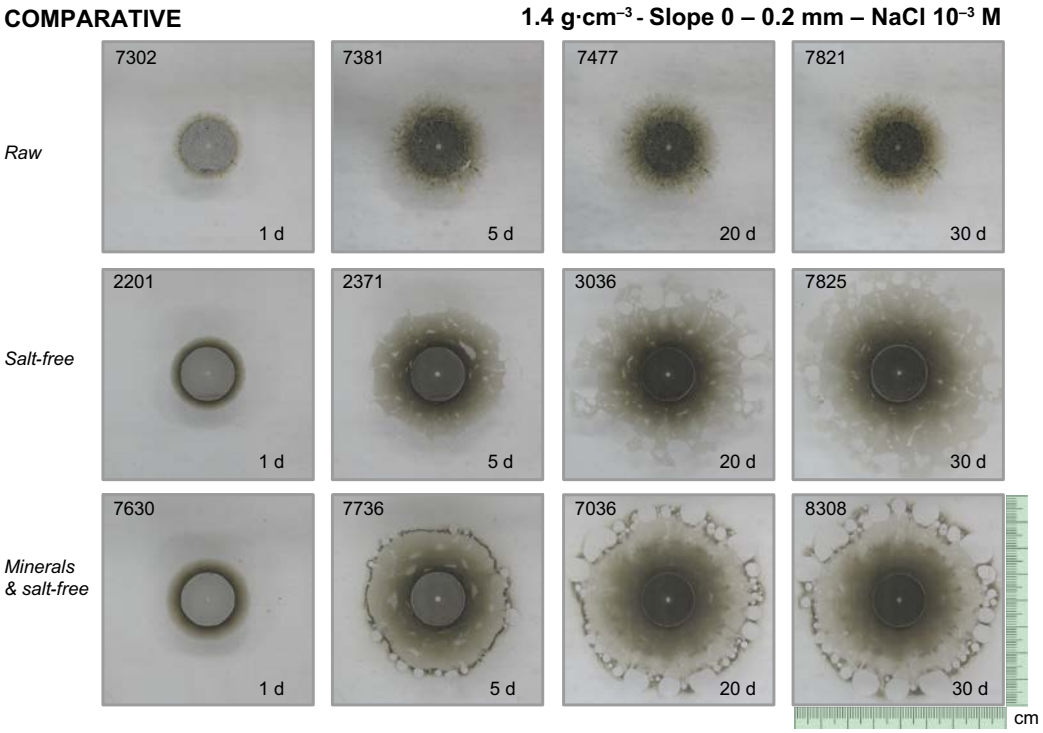

Figure 5-10. *Comparative expansion evolution of raw MX-80 clay, salt-free MX-80 and minerals&salt-free MX-80 in artificial smooth fractures of 0.2 mm aperture, placed at horizontal slope, filled with NaCl 10^{-3} M.*

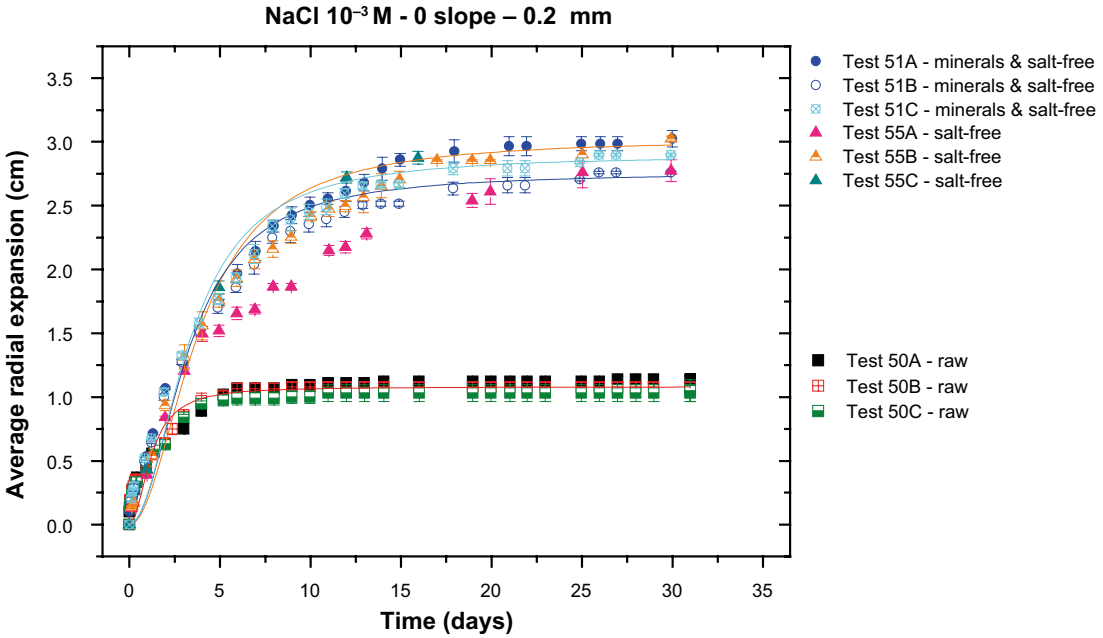

Figure 5-11. *Average radial expansion in cm) of raw MX-80, salt-free MX-80 and minerals&salt-free MX-80) compacted at 1.4 g·cm$^{-3,}$ within smooth artificial fractures of 0.2 mm aperture, placed horizontally (slope 0°) and filled with NaCl 10^{-3} M. Lines are included to guide the eye.*

First of all, the expansion of raw MX-80 in the smooth fracture is clearly more restricted (2 cm) than that of the salt-free or minerals-free fractions (expanded up to ≈ 3 cm). It is also noteworthy that the salt-free fraction experienced mostly the same expansion that the minerals&salt-free clay, in which both the accessory minerals and the soluble salts were removed. This indicates that accessory minerals are not responsible for slowing down clay expansion in the fractures (even though it is evident that, in a real case, coarse minerals would be efficiently filtered in small rock micro-fractures). Soluble salts seem to have greater effect restricting clay expansion than the accessory minerals.

5.2.3 Post mortem analysis

Water chemistry

Table 5-6 presents the chemical conditions of the equilibrium waters sampled in the tests carried out with raw MX-80, salt-free MX-80 and minerals&salt-free MX-80. Geochemical calculations were carried out considering MX-80 characteristics and the available anion inventory.

The chemical conditions exhibited by the equilibrium water measured in Test 50, indicate the preferential dissolution of Na-sulphates, what lead to an equilibrium water with high ionic strength. This is not applicable to the salt-free and minerals&salt-free MX-80 tests, because the soluble salts are in both cases removed, and in fact the equilibrium waters have lower ionic strengths but, in the tests carried out with "clean" MX-80 fractions, clay expansion reached as well a steady state. This is an interesting finding, because a major role was attributed to the high ionic strength conditions exhibited by the equilibrium waters measured in most tests (Table 5-3 and Table 5-4). High ionic strength conditions most probably affect the development of the expansion, but additional mechanisms hinder clay expansion in these cases.

Table 5-6. Chemistry of equilibrium water (filtered 0.2 mm).

Ion concentration (M)	Raw MX-80 Tests 50	Minerals&salt-free MX-80 Tests 51	Salt-free MX-80 Tests 55
Ca^{2+}	2.40×10^{-4}	2.02×10^{-5}	3.51×10^{-5}
Mg^{2+}	1.03×10^{-4}	1.61×10^{-5}	2.80×10^{-5}
Na^{+}	1.63×10^{-2}	3.70×10^{-3}	5.50×10^{-3}
K^{+}	2.56×10^{-4}	7.16×10^{-5}	7.32×10^{-5}
Al^{3+}	5.93×10^{-6}	-	-
HCO_3^{2-}	2.07×10^{-3}	1.69×10^{-3}	1.69×10^{-3}
SO_4^{2-}	6.99×10^{-3}	5.21×10^{-4}	6.25×10^{-4}
Cl^{-}	1.92×10^{-3}	1.38×10^{-3}	2.92×10^{-3}
Fe	$< 5 \times 10^{-9}$	4.30×10^{-6}	4.30×10^{-6}
pH	7.9	7.9	7.8
E.C. ($\mu S \cdot cm^{-1}$)	**1 580**	**390**	**590**
Ionic strength (M)	**2.36×10^{-2}**	**4.44×10^{-3}**	**4.63×10^{-3}**

Mineralogical analyses of expanded clay

Figure 5-12 presents the final state of test carried out with MX-80 and minerals&salt-free MX-80, to illustrate that the expanded clay was sampled in different rings. The clay amount on each ring was weigh and considered to calculate the expanded mass fraction.

The expanded mass recovered was higher from the minerals&salt-free fractions: 1.8 % from the raw clay, 7.5 % from salt-free and 16.1 % of the initial mass from minerals&salt-free MX-80. These differences can be attributed to their different nature, but also to their different water chemistry (Table 5-6).

To clarify observed differences, complete mineralogical measurements carried out on the extruded samples were compared to that of raw MX-80 bentonite and of the pre-treated fractions, as described in Section 3.7.2. It has to be noted that the quantity of clay sampled in all cases was limited.

Granulometry analyses were carried out to verify if the clay extruded in the fracture from MX-80, with and without accessory minerals, showed different particle size distributions at different distances. Results are expressed as relative amount measured for each size interval (Relative % Chan *vs* size). All essays were carried out within 0.2 mm aperture smooth fractures.

Figure 5-13 shows the particle distributions measured in expanded clay of Test 50A carried out with MX-80. The particle distributions measured at different distances from the pellet were quite similar, with particle sizes equitably distributed in size regions form clay particles (< 2 mm) to bigger minerals. No significant particle size increase is detected in the outer ring.

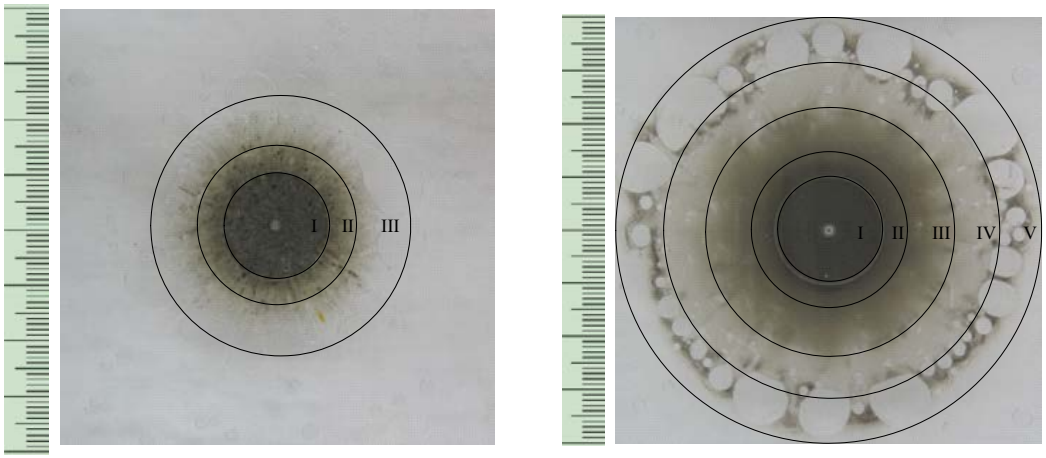

Figure 5-12. *Final state , after 30 days of expansion within artificial fracture placed horizontally (slope 0°) of fixed aperture (0.2 mm), filled with NaCl 10^{-3} M of (left) raw MX-80 and (right) Minerals&salt-free MX-80. The extruded clay was radially sampled in selected regions, as indicates in the figures.*

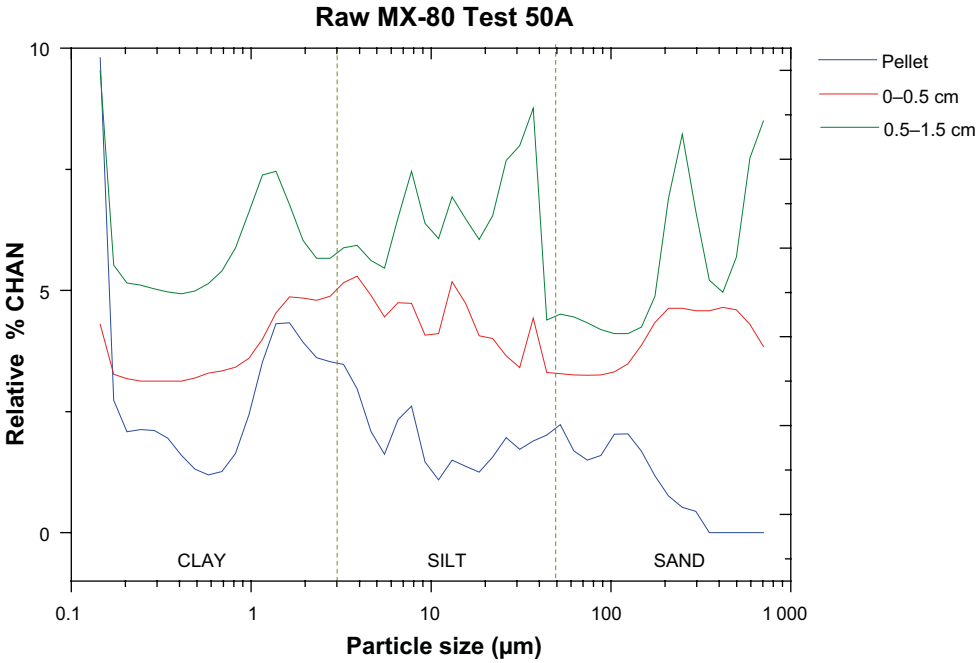

Figure 5-13. *Particle size distribution measured on the expanded clay form Test 50A carried out with raw MX-80, from the pellet to the out at different radial distances (0–0.5 cm and 0.5 to 1.5 cm).*

Table 5-7 presents the CEC analyses carried out on sampled fractions: values are generally higher in experiment carried out with raw MX-80 since, as mentioned before, previous characterisation of starting material revealed that due to soluble mineral dissolution, the cation composition at interlayer sites was slightly modified (Table 5-5). In any case, looking to CEC values measured in the expanded clay, not very big differences were measured at different distances from the pellet surface, suggesting that the percentage of smectite is basically maintained overall the expanded ring of each single test.

Table 5-7. Total CEC determined on sampled regions, by Cu-Trien method.

Experiment	Sample	CEC (meq·100 g^{-1})
Raw MX-80	Reference Raw MX-80	86.3
	Test 50C pellet	82.8
	Test 50C 0–0.5 mm	87.0
	Test 50C 0.5–1.5 mm	83.1
	Test 50C >1.5 mm	84.4
Salt-free MX-80	Reference Salt free MX-80	76.0
	Test 55B pellet	76.9
	Test 55B 0–0.5 mm	82.4
	Test 55B 0.5–1.5 mm	80.1
	Test 55B >1.5 mm	62.6*
Minerals&salt free MX-80	Test 51A pellet	78.0
	Test 51A 0–0.5 mm	80.0
	Test 51B 0.5–1.5 mm	80.5
	Test 51A 1.5–2.5	79.0

* Possible error in the determination due to low amount of sample available.

Figure 5-14a and b present measured particle distributions measured on the expanded clay from two replica tests carried out with *minerals&salt-free* MX-80 (Tests 51A and 51C). In these cases, the particle size distributed thorough the expanded ring mainly corresponds to smaller particles (clays), reasonable considering that the accessory minerals were previously removed. Only in the outer ring of Test 51A (Figure 5-14b) the presence of some larger mineral was detected, which may be some residual mineral or aggregated phase. The heterogeneity due to teh small quantity of sampled materila has be taken into account.

FTIR, TG-DSC and XRD analyses were carried out on the expanded clay of tests carried out with raw, salt-free and minerals&salt-free MX-80 clays. The aim of these analyses is to verify if a significant accumulation of accessory minerals is appreciated in the outer part of the expanded rings.In the case of raw MX-80, the analyses are presented for two different tests carried out within smooth fractures at two different apertures: 0.2 mm (Test 50C) and 1.7 mm (Test 56A). Results are respectively shown in Figure 5-15 (0.2 mm) and Figure 5-16 (1.7 mm). According to analyses the expanded ring, mainly composed by a di-octahedral montmorillonite, with Al, Mg and Fe at octahedral sites and it is homo-

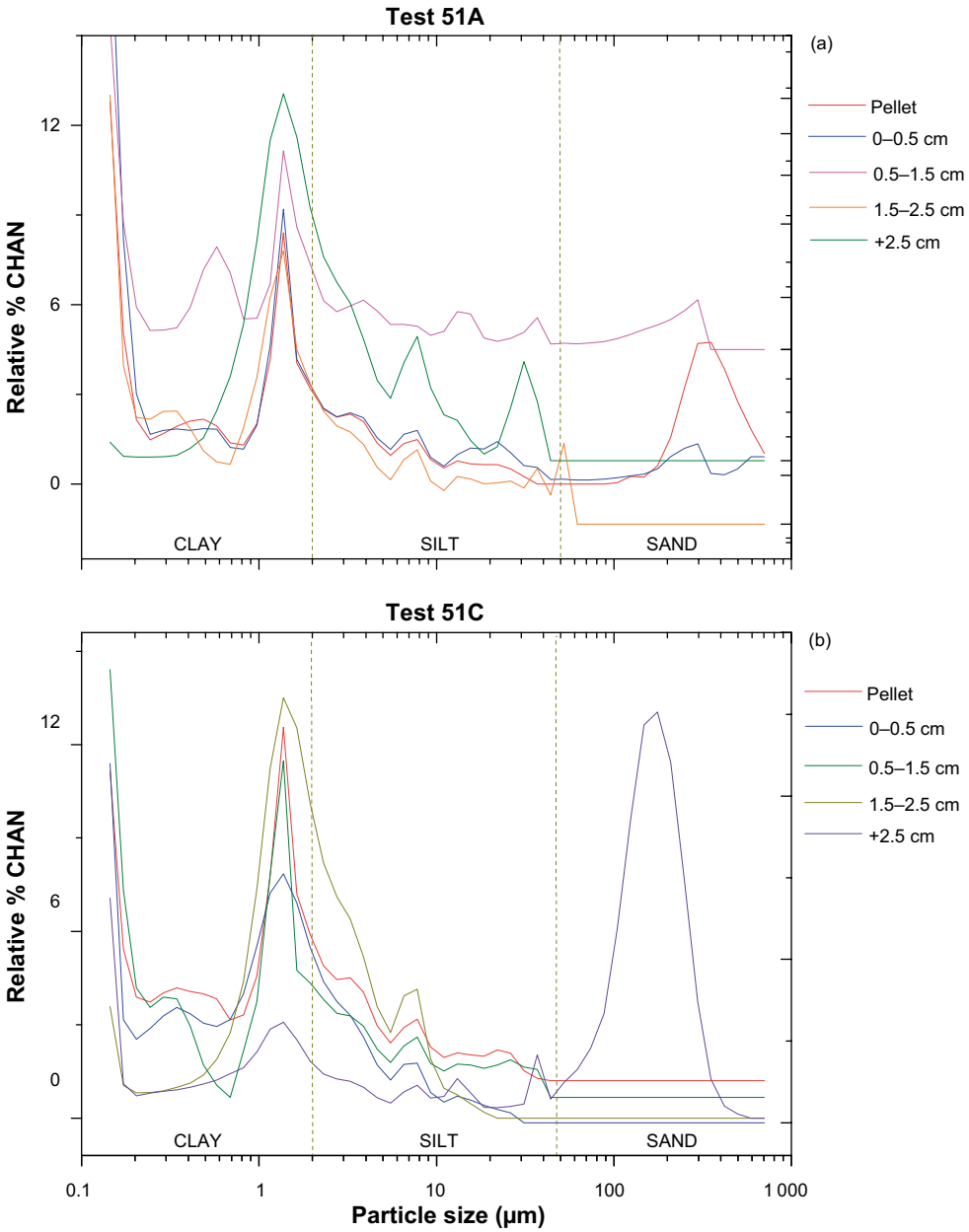

Figure 5-14. *Particle size distribution measured on the expanded clay from tow replica tests, carried out with minerasl&salt-free MX-80, from the pellet to the out at different radial distances (0–0.5 cm, 0.5 to 1.5 cm,1.5–2.5 cm and < 2.5 cm).*

geneously distributed from the pellet source and along. No significant mineralogical differences were neither observed on the extruded clay within different fracture apertures (0.2 mm compared to 1.7 mm), despite more amount of clay was extruded at wider aperture (36 % of expanded mass in 1.7 mm and 2 % in 0.2 mm, Table 5-2) and despite the equilibrium chemistry was different (Table 5-4).

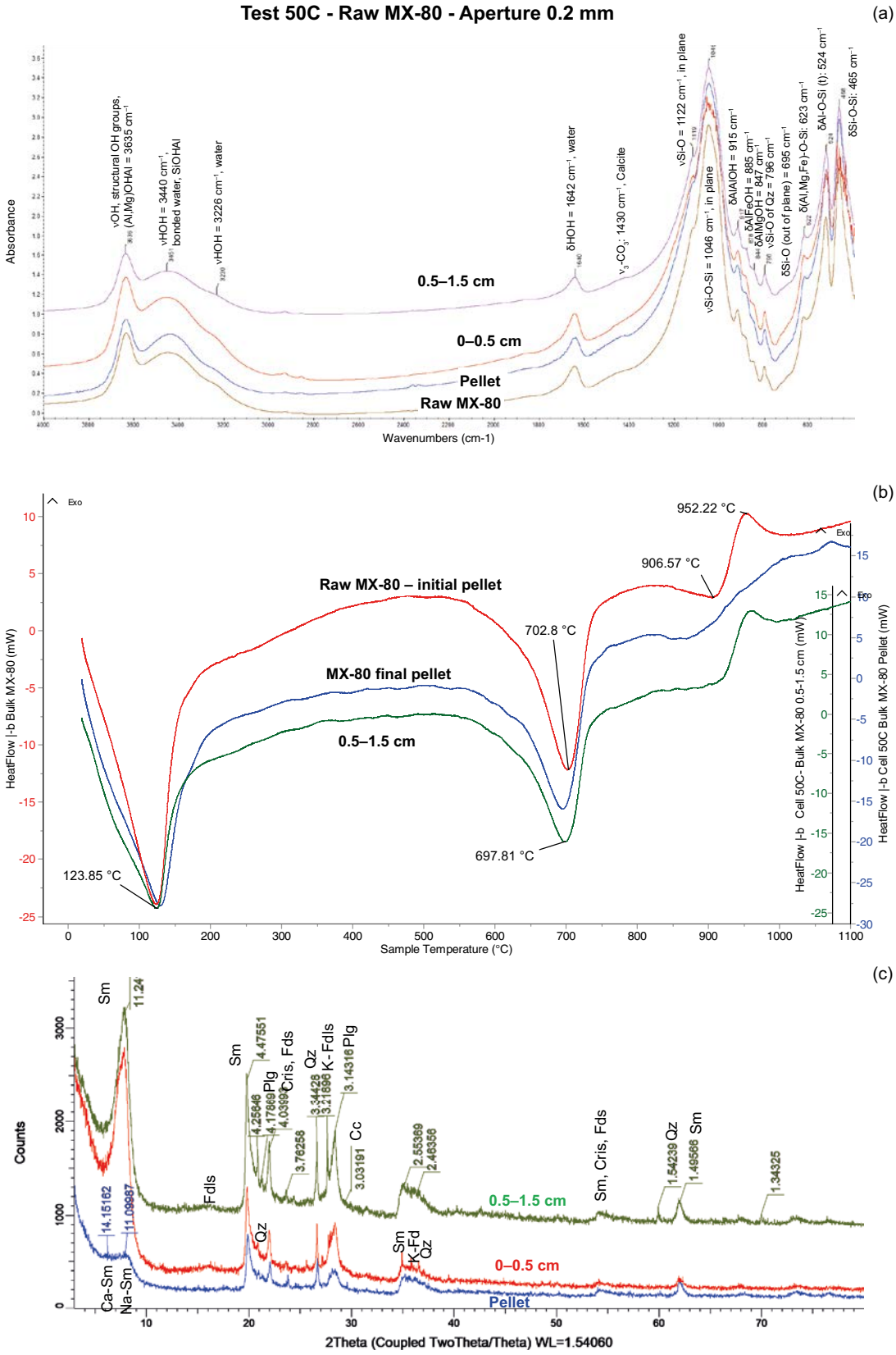

Figure 5-15. *Mineralogical analyses of expanded clay, at different distances, of Test 50C with raw MX-80 in smooth fracture of 0.2 mm aperture: a) FTIR spectra, b) TG/DSC curves, c) XRD patterns.*

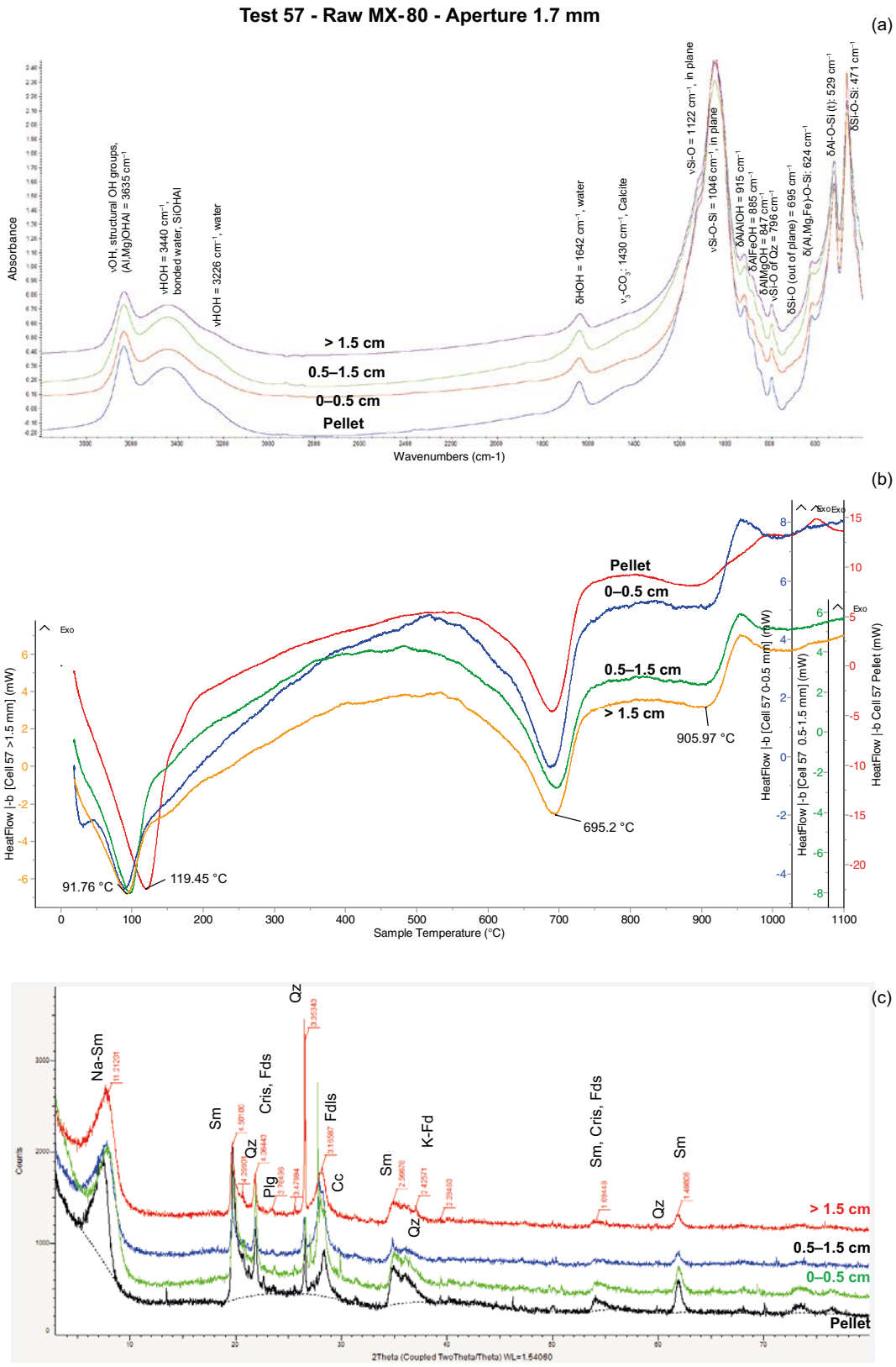

Figure 5-16. *Mineralogical analyses of expanded clay, at different distances, of Test 57A with raw MX-80 in smooth fracture of 1.7 mm aperture: (a) FTIR spectra, (b) TG/DSC curves, (c) XRD patterns.*

The measured FTIR spectra, TG/DSC curves and XRD patterns measured on the expanded clay sampled at different rings are respectively presented in Figure 5-15 (raw MX-80 0.2 mm aperture), Figure 5-16 (raw MX-80, 1.7 mm aperture), Figure 5-17 (salt-free MX-80, 0.2 mm aperture) and Figure 5-18 (minerals &salt-free MX-80).

The main characteristics that can be extracted form FTIR spectra, TG/DSC curves and XRD patterns were previously described for the starting materials (Section 5.2.1). For not describing again all analyses, focus was paid only on the main features. The characteristics of all spectra and curves obtained for each single test are basically the same than those observed for each corresponding starting material. Slight differences are sometimes appreciated, like for example in the tests carried out with salt-free material (Figure 5-17) zeolite presence was detected at 379 °C, at intermediate distance, but the general conclusion is not varied.

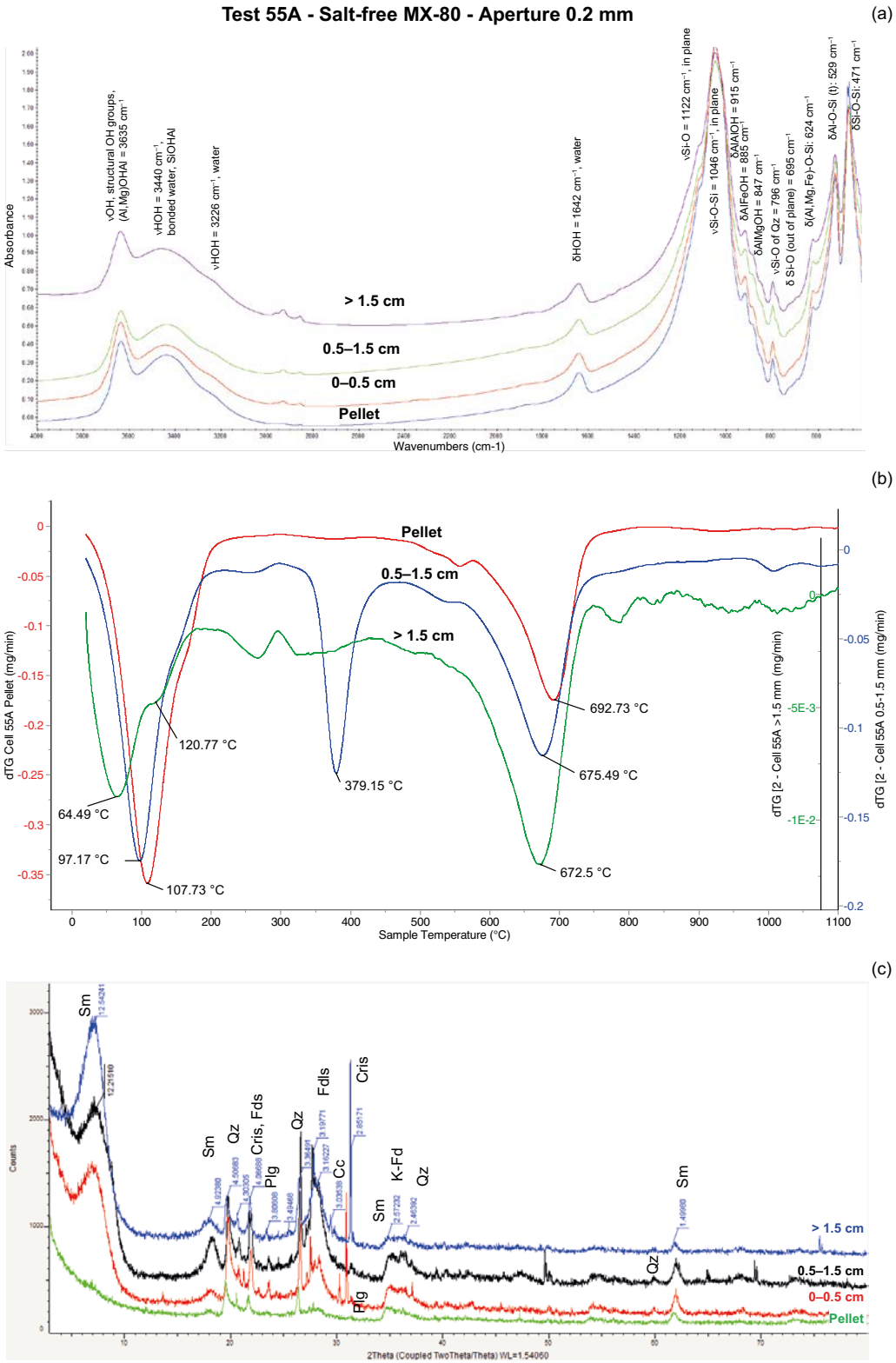

Figure 5-17. *Mineralogical analyses of expanded clay, at different distances, of Test 55A with salt-free MX-80 in smooth fracture of 0.2 mm aperture: a) FTIR spectra, b) TG/DSC curves, c) XRD patterns.*

Increased presence of accessory minerals was not preferentially appreciated in the outer ring of the expanded clay, in any case, since both accessory minerals and smectite were identified. The similarities of mineralogical analyses carried out at different distances indicate that the clay expands as a whole.

In fact, the darker outer region that was observed at sight in the experiment with minerals&salt-free clay Figure 5-10 was basically composed by smectite (Figure 5-18). Therefore, results indicate that the outer part of the extruded fraction the smectite particles themselves form a coherent filter, restricting further expansion.

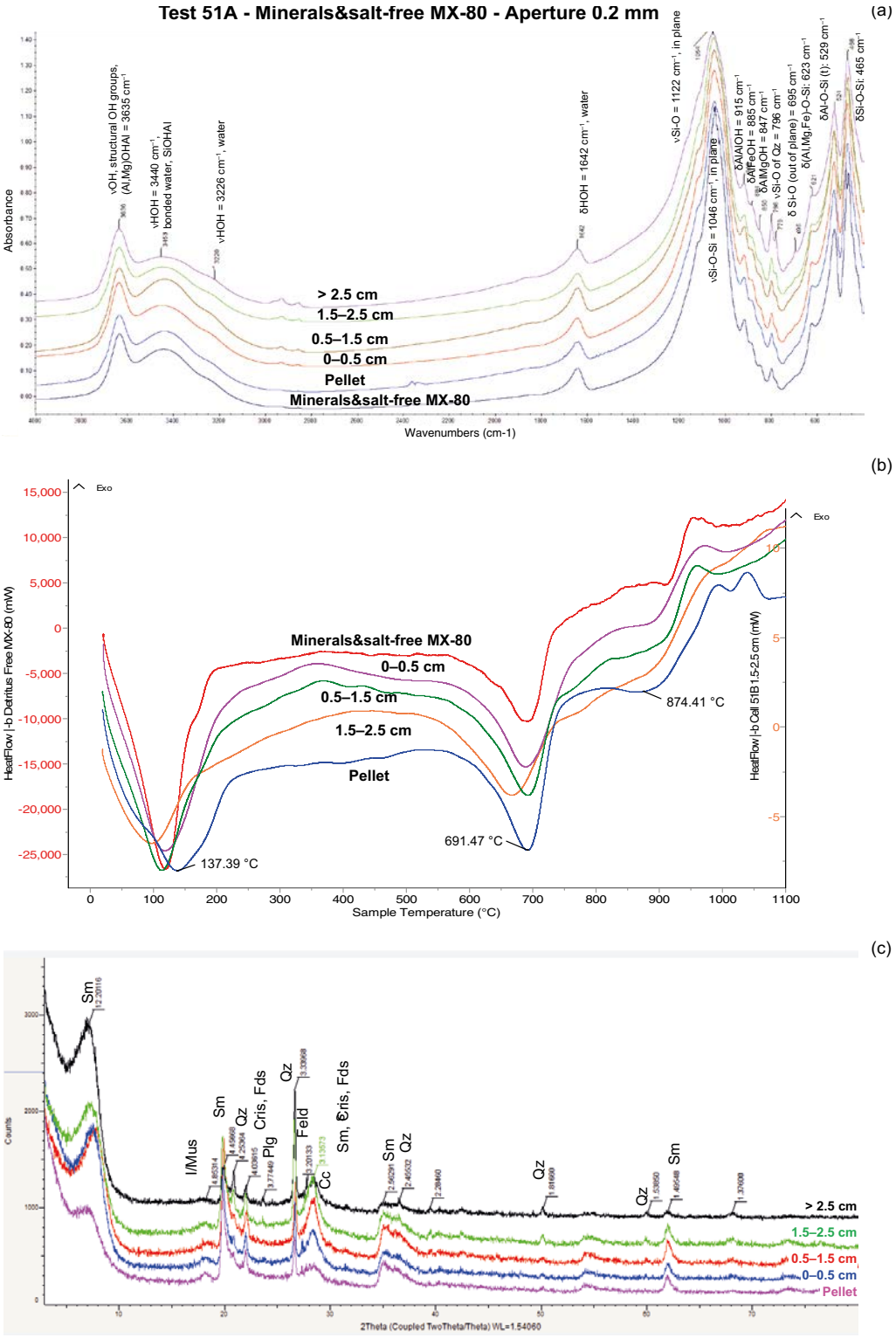

Figure 5-18. *Mineralogical analyses of expanded clay, at different distances, of Test 55A with salt-free MX-80 in smooth fracture of 0.2 mm aperture: a) FTIR spectra, b) TG/DSC curves, c) XRD patterns.*

5.3 Expansion tests in rough fractures at horizontal slope

5.3.1 Fracture dimensions

In Appendix 1, the extrusion evolution of Nanocor® and MX-80 clays within artificial fractures of different roughness (*Roughness 1* and *Roughness 2*) placed at horizontal slope (0°) can be examined. Test 31A (page 108) (and replica Test 41A, page 113) and Test 33A (page 109) corresponds to Nanocor® clay, while Tests 37A (page 111) and 39A (page 112) were those carried out with MX-80 clay. Fracture with type 1 roughness has one flat surface and one rough surface while in the fractures with type 2 roughness, both surfaces are rough (Figure 3-3). Expanded clay rings still presented a radial geometry but following the rough patterns and, in all cases, a steady state was reached.

As mentioned before, these rough surfaces have high fracture volumes (Table 3-1) and test comparison with smooth fractures must be done with equivalent volumes. The fracture with *Roughness 1* can be compared to an smooth fracture with 1 mm aperture (Test 52A), while the fracture with *Roughness 2* is comparable to an smooth fracture with 1.7 mm, where it was observed that expansion was clearly higher than that observed in narrow fractures (Figure 5-1 and Figure 5-2).

Figure 5-19 presents the average radial expansion experienced by Nanocor® within fractures with different roughness. Figure 5-20 shows the same expansion tests, but carried out with MX-80 clay. Again, the expansion of Nanocor® clay is enhanced compared to that of MX-80. For both clays, clay expanded longer within smooth fractures than within rough ones. In the case of Nanocor®, expansion was shorter in fractures with higher roughness and accordingly expanded masses were smaller: 24.5 % of the initial mass in the case of roughness 2, and 31.6 % within fractures with less roughness. However, in the case of MX-80, almost the same expansion distances and masses (≈ 10 %) where measured at the two roughness analysed. Nevertheless, once again, equilibrium chemistry may be playing a role, since measured E.C. in rough fractures were all in the range of 1 200–1 500 µS·cm^{-1}, not as high as those measured on fractures with smaller volumes (up to 6 000 µS·cm^{-1}), but still one order of magnitude higher than the initial values.

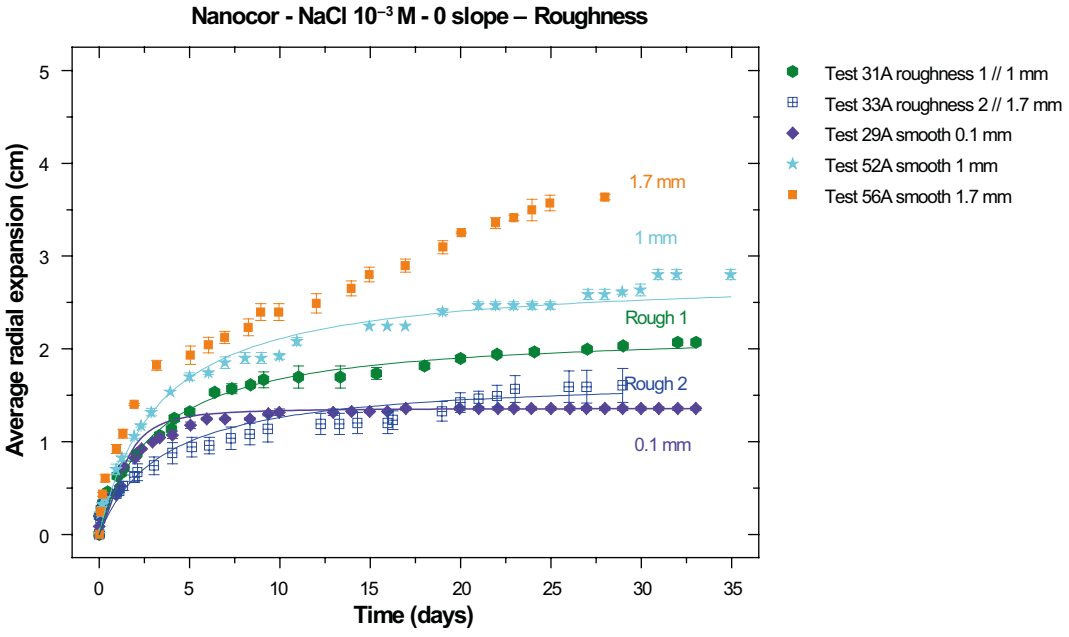

Figure 5-19. *Average radial expansion (in cm) of Nanocor® clay in fractures with different roughness (Roughness 1 and Roughness 2). The tests carried out in smooth fractures with equivalent fracture volumes are included for comparison. Fractures were placed horizontally (slope 0°) and filled with NaCl 10^{-3} M.*

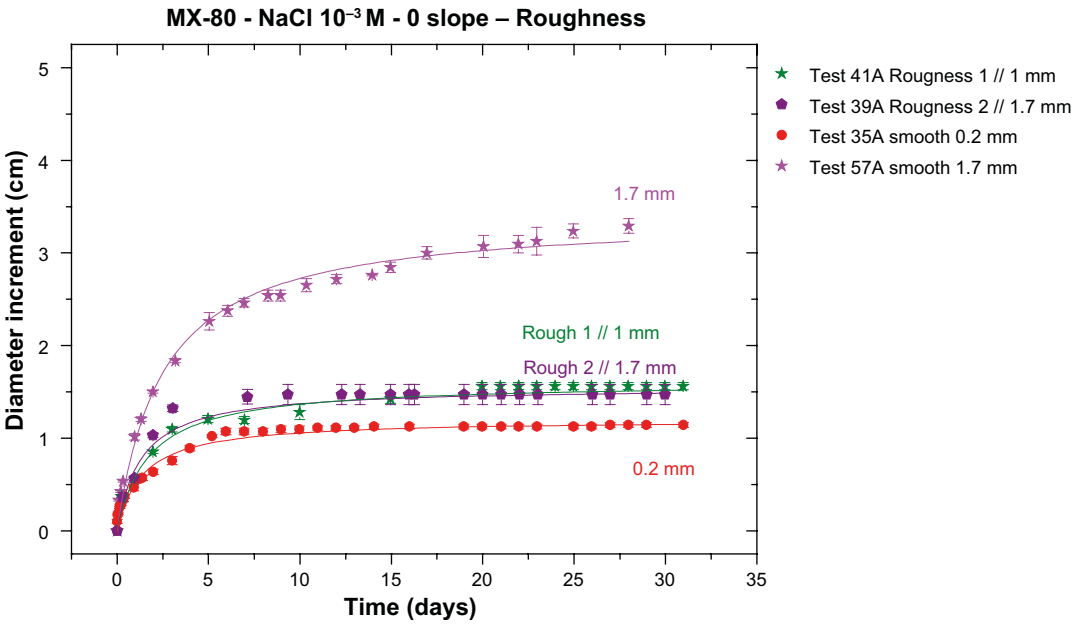

Figure 5-20. *Average radial expansion (in cm) of MX-80 clay in fractures with different roughness (Roughness 1 and Roughness 2). The tests carried out in smooth fractures with equivalent fracture volumes are included for comparison. Fractures were placed horizontally (slope 0°) and filled with NaCl 10^{-3} M.*

5.3.2 Clay type effect in rough fractures at horizontal slope

The expansion behaviour of raw MX-80 and of homoionic clay fractions (Na-MX-80 and Ca-MX-80) was analysed within rough fracture, placed at horizontal slope: Tests 41A, 44A and 47A.

Their expansion evolution can be followed in Appendix 1 (41A page 113, 44A page 116 and 47A page 119) and in Figure 5-22. The final state after 30 days of expansion is shown in Figure 5-22. The relevance of clay main exchange cation can be appreciated at sight. In all experiments clay extrusion was stopped as some time.

In all cases, and in spite of the fracture roughness, the pattern of extrusion continues to be radial and rather homogenous in all directions.

It is evident that the clay that undergoes the greatest extrusion in the fracture is the Na-homoionic MX-80, followed by raw MX-80. In general, the expansion of the Ca-rich clays is limited. In the same way, the expanded mass was higher with Na-MX-80 (37.9 %) than with raw MX-80 (11.5 %) or Ca-MX-80 (only a 0.2 %). Once again, their equilibrium chemistry is different. In the experiments with Na- or Ca-homoionic bentonites lower E.C. values were measured (respectively 387 and 603 $\mu S \cdot cm^{-1}$), because in the homoionisation procedure the soluble salts are removed, but the final water of the fracture with raw MX-80 had a final E.C of 1 317 $\mu S \cdot cm^{-1}$.

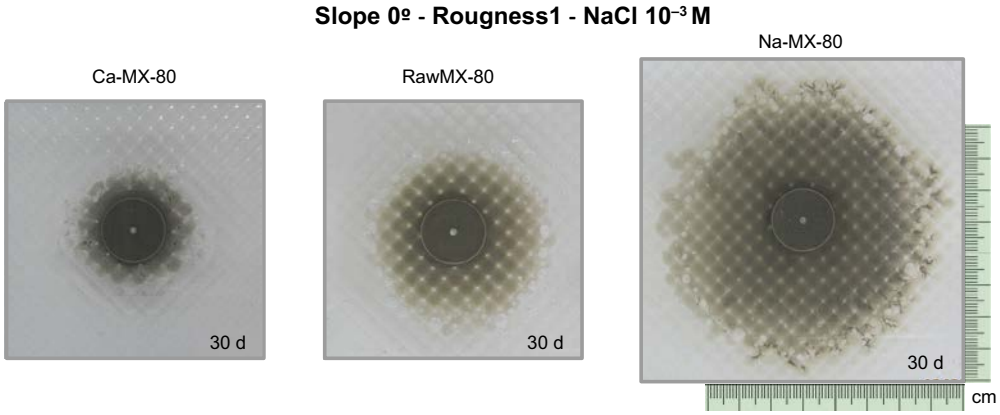

Figure 5-21. *Final state of Ca-MX-80, raw MX-80 and Na-MX-80 clays after 30 days expansion within a rough fracture placed at horizontal slope (0°).*

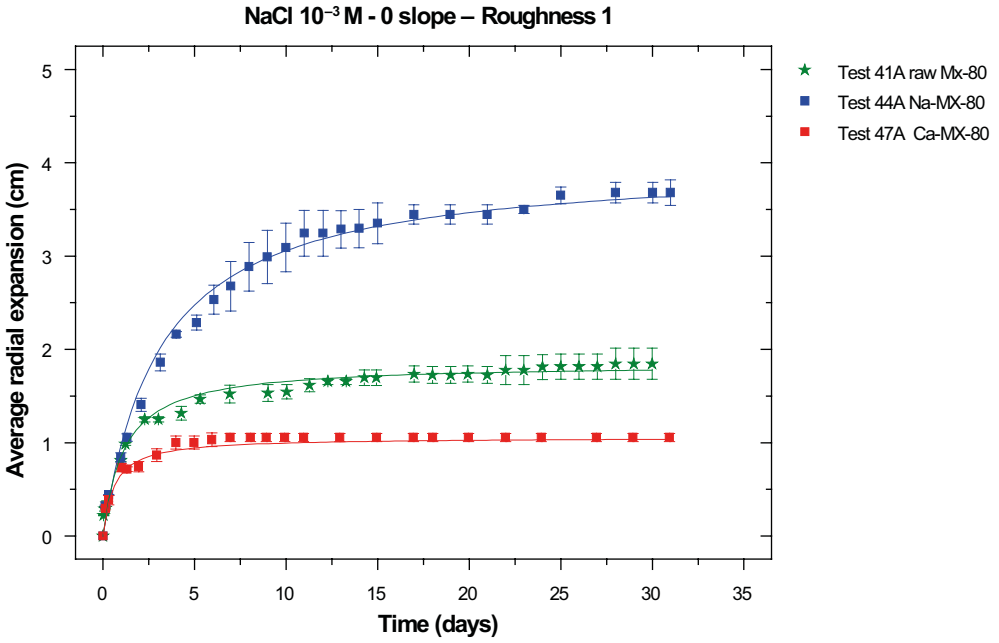

Figure 5-22. *Average radial expansion (in cm) of different clay fractions: raw MX-80, Na-MX-80 and Ca-MX-8, in fractures with roughness type 1.*

5.4 Sedimentation tests in smooth sloped fractures

5.4.1 Sedimentation tests on sloped smooth narrow fractures with 0.2 mm aperture

Six sedimentation tests were carried out in narrow fractures, placed at different slopes (0°, 45° and 90°) with Nanocor® (Tests 1A, 2A and 3A) and MX-80 clay (Tests 16A, 17A and 18A) at fixed aperture (0.2 mm) with NaCl 10^{-3} M.

Figure 5-23 presents the average radial expansion measured for Nanocor® clay, under the above-mentioned conditions and Figure 5-24 the images of the final states.

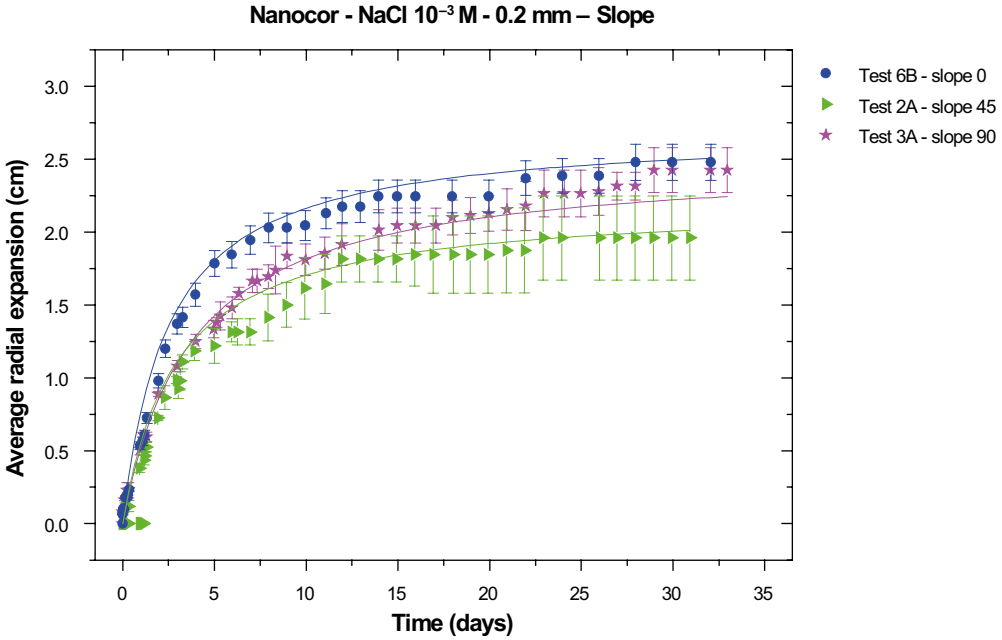

Figure 5-23. *Average radial expansion (in cm) measured for Nanocor® compacted at 1.4 g·cm^{-3}, within artificial fractures (0.2 mm) filled with NaCl 10^{-3} M, placed at different slope: 0°, 45° and 90°.*

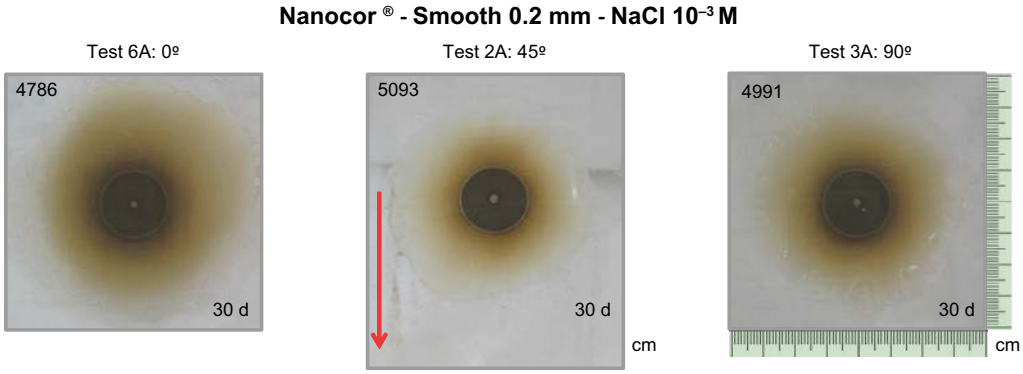

Figure 5-24. *Final diameter measured after 30 days for Nanocor® pellets 1.4 g·cm^{-3}, in fractures of 0.2 mm aperture filled with NaCl 10^{-3} M, placed horizontally (0°), at 45° or vertically (90° slope). Particle sedimentation was only observed at 45° slope (indicated by a red arrow).*

In the photographs presented in Appendix 1 (1A, 2A and 3A, pages 82–84; 16A, 17A and 18A, pages 94–96), it can be appreciated that, in spite of the fracture slope, clay extrusion was rather homogenous and values measured in different directions were not very different, not even at vertical slope.

With Nanocor® clay, only at 45° slope (Test 2A, page 83), higher clay sedimentation was measured along slope direction. In this test, after around 25 days of experiment some particle detachment was detected and the average values of average radial expansion presented larger errors (Figure 5-23). This test carried out at 45° slope showed at sight the "clearest" expansion ring.

The extruded distances were not very different at different slopes, and eroded mass was an 18 % (at 0°), 23 % at 45 ° and 14 % at 90 °, indicating the little influence of slope at this narrow aperture.

These results contrast with sedimentation experiments carried out by B+Tech (Schatz et al. 2013), where higher sedimentation along the slope direction was clearly evidenced. Our experiments were carried out at thinner fracture apertures, 0.2 mm, than B+Tech (1 mm), and smaller apertures may inhibit clay fall down.

Figure 5-25 presents the average radial expansion measured for MX-80 within an smooth narrow fracture (0.2 mm) placed at different slopes (0°, 45° and 90°), corresponding to sedimentation tests numbered 16A, 17a and 18A.

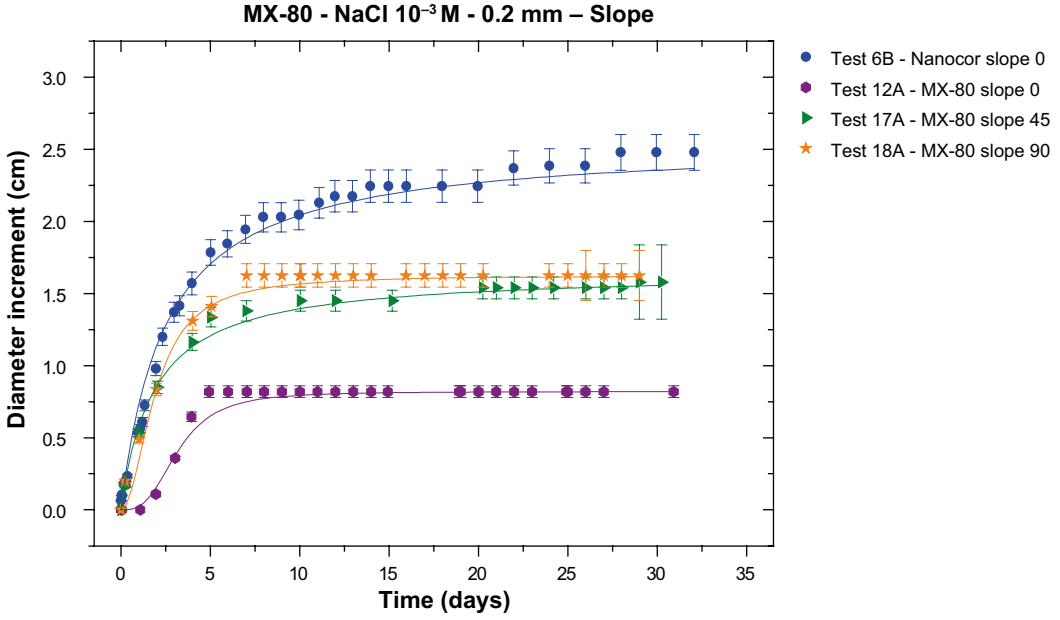

Figure 5-25. *Average radial expansion (in cm) measured for MX-80 compacted at 1.4 g·cm^{-3}, within smooth fractures (0.2 mm) filled with NaCl 10^{-3} M, placed at different slopes: 0°, 45° and 90°. Test with Nanocor® clay at 0° slope is also included.*

In Appendix 1 (16A, 17a and 18A, pages 94–96)., it can be seen that clay extrusion was fairly homogenous along all directions. Sedimentation tests carried out with MX-80 showed significant smaller distances than those with Nanocor®. In contrast to the Nanocor® tests (Figure 5-23), in this case, extrusion was lower at horizontal slope.

Post-mortem analyses revealed that eroded mass in sedimentation tests carried out with raw MX-80 was generally low, in all cases lower than a 2 % of the initial mass installed, indicating that sticking on wall fractures is significant. Again, values measured for MX-80 are lower than for Nanocor® (Table 5-1).

In Schatz and Akhanoba (2016), sedimentation experiments were carried out with Na-montmorillonite in fractures with wider apertures (1 mm) and sedimentation was observed. The fact that we do not observe particle sedimentation in narrower fractures can be therefore attributed to different experimental conditions.

Sedimentation tests are carried out with Nanocor® and MX-80 clays, and not with purified Na-montmorillonite. In general, when clays are homoionised in the lab, the soluble salts are removed, as well all the residues of salts used for homoionisation.

The fact that the clays are used "as received" induces chemical changes which are not negligible. Initial NaCl 10^{-3} M has a pH 6 and an electric conductivity around 100 µS·cm^{-1}. Final conditions were: 16A, pH 8.29, EC = 2.36 mS·cm^{-1}, 17A, pH 8.36 and EC = 2.23 mS·cm^{-1}, 18A: pH 7.96, EC = 2.60 mS·cm^{-1}.

Comparing the erosion results with different set-ups (Alonso et al. 2018, Missana et al. 2011) it is clear that the chemical conditions at equilibrium play a major role on erosion, especially at high solid to liquid ratios and under stagnant conditions.

5.4.2 Water ionic strength effect in smooth narrow fractures at 45° slope

Figure 5-26 presents three sedimentation tests carried out Nanocor® in narrow fractures, placed at 45° slope, with at fixed aperture (0.2 mm) filled with NaCl at different ionic strength: tests 2A, 26A and 27A.

Clay expansion in the fracture was higher at lower ionic strengths, as previously measured at horizontal slope (Figure 5-4). Again, non-negligible extrusion distances were measured at highest ionic strength (10^{-1} M). However, in this case, no very big differences are appreciated amongst different ionic strengths.

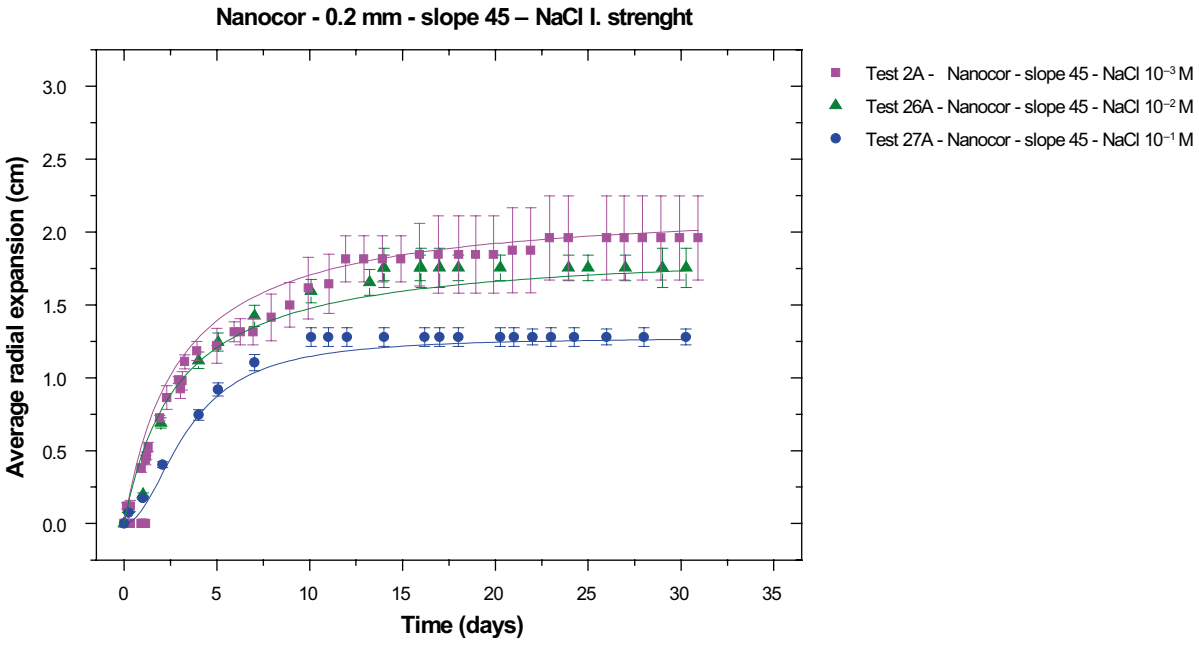

Figure 5-26. *Average radial expansion measured for Nanocor® compacted at 1.4 g·cm^{-3}, within smooth fractures with fixed aperture (0.2 mm), placed at 45° slope and filled with NaCl at different ionic strength: 10^{-3}, 10^{-2} and 10^{-1} M.*

In Appendix 1, the tests evolution can be seen (2A page 83, 26A and 27A, pages 104–105). In the experiment performed at lower ionic strength (Test 2A, page 83), la more extensive extrusion was measured along slope direction. And moreover, after 26 days of experiment, particle detachment and sedimentation streams were detected only in the test carried out at lower ionic strength (Test 2A), which was not detected at higher ionic strengths.

Eroded mass measured for Nanocor® at 45° slope was around 23 % at 10^{-3} M, 10 % at 10^{-2} M and 8.5 % at 10^{-1} M, fairly the same values measured at horizontal slope (Table 5-1), even though extrusion distances were smaller.

In these sedimentation tests carried out in narrow fractures, sedimentation streams were not appreciated. As indicated in the previous section, not only the narrow aperture (0.2 mm) but also the high ionic strength of the equilibrium water (Table 5-3) are restricting clay extrusion and sedimentation.

5.4.3 Sedimentation of Ca-clay in smooth narrow fractures at vertical slope

Three sedimentation tests were carried out at vertical slope (90°) with Ca-exchanged MX-80 in narrow fractures with different fracture apertures (0.1, 0.2 and 0.4 mm) with NaCl 10^{-3} M.

In the photographs of their expansion evolution (in Appendix 1, Tests 23A, 24A and 25A, pages 101–103) it is noticeable that clay expansion took place, despite the Ca-nature of the clay, and expansion pattern was again rather homogenous in the three cases.

It is noteworthy that in these tests carried out at vertical slope, clay sedimentation was not observed along slope direction (90°) and clay fall down was not detected, in contrast to previous sedimentation experiments carried out by B+Tech, where higher sedimentation along the slope direction was clearly evidenced, but within wider fracture apertures (1 mm) (Schatz et al. 2013).

Figure 5-27 shows the average radial expansion experienced by Ca-exchanged MX-80 within different fracture apertures. It can be seen that the values reached within 0.2 mm and 0.4 mm fracture apertures were the same but, unexpectedly; they were slightly higher at 0.1 mm aperture. In the figure, the expansion evolution experienced by Nanocor clay within 0.2 mm aperture, under the same conditions is plotted for comparison. It is evident that the extruded distances measured for Ca-MX-80 at vertical 90° slope were lower than those measured for raw MX-80, but not negligible. This may be caused by ionic exchange mechanism with Na electrolyte, which is diminishing the Ca content in the clay.

In these experiments, measured expanded mass was around 5 to 6 % of initial mass, for the three studied cases.

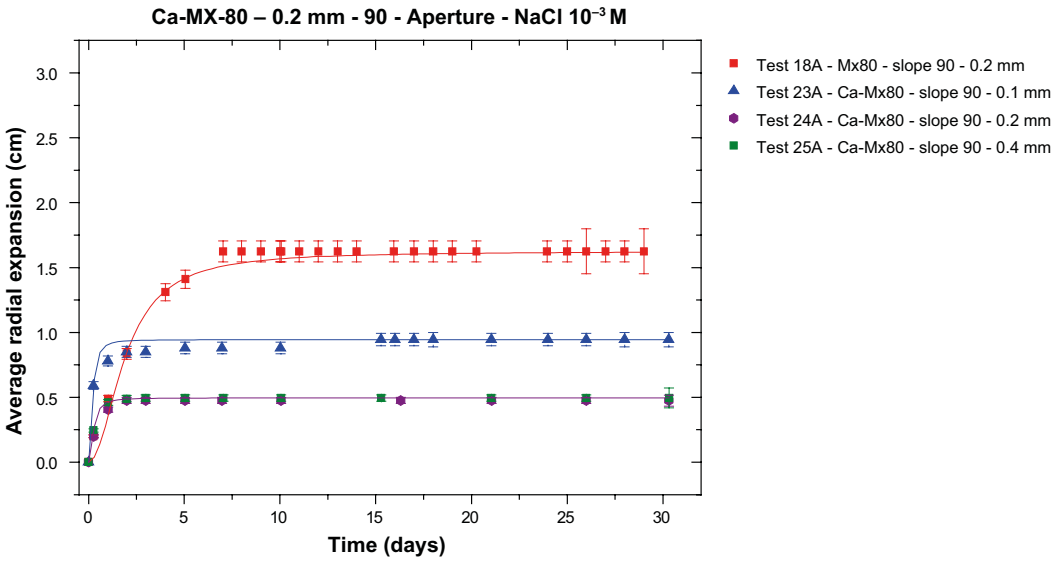

Figure 5-27. *Average radial expansion (in cm) measured for Ca-MX-80 compacted at 1.4 g·cm^{-3}, within smooth narrow fractures filled with NaCl 10^{-3} M at vertical slope (90°). Fracture apertures were 0.1, 0.2 and 0.4 mm. Test carried out with raw MX-80 at vertical slope within a smooth fracture of 0.2 mm is included for comparison.*

5.4.4 Sedimentation tests on sloped smooth fractures with 1 mm aperture

Sedimentation tests were carried out with Nanocor clay compacted at 1.4 $g \cdot cm^{-3}$ in smooth fractures of 1 mm aperture, filled with NaCl 10^{-3} M, respectively placed at different slopes: 0° (Test 52A), 45° (Test 53A) and 90° (Test 54A).

As mentioned, these tests were proposed to be compared with previous studies carried out by Schatz and Akhanoba (2016), which were carried out as well erosion experiments in sloped fractures. In those tests, which were mainly carried out in fractures with apertures of 1 mm, and applying different flow rates (mainly 6×10^{-6} $m \cdot s^{-1}$ and going up to around 2×10^{-4} $m \cdot s^{-1}$).

In Appendix 1, the extrusion and sedimentation behaviour of Tests Test 52A, 53A and 54A (pages 128–130) can be followed. It has to be noted that, when appreciable particle sedimentation was appreciated, the photographs were taken including a black sheet, placed underneath the fracture methacrylate. In those cases were particle sedimentation was observed, not only the extruded are is shown, the shown regions are extended to the fracture limit, to appreciate sedimentation streams and particle accumulation at the bottom of the sloped fracture.

Extrusion in the sloped fractures was fairly similar than in the horizontal experiments: clay starts to gradually extrude in the fracture, exhibiting a homogenous circular pattern. However, in the experiments carried out at 45° and 90° slope, particle fall along fracture slope was appreciated almost form the beginning (after 1 day in the 45° slope) and particles started to be accumulated in the bottom of the fracture.

Figure 5-28 shows the final state of Nanocor® clay after sedimentation in smooth fractures of 1 mm aperture placed at different slope: 0° (Test 52A), 45° (Test 53A) and 90° (Test 54A).

Figure 5-29 shows the average radial expansions experienced by Nanocor® clay in sloped smooth fractures of 1 mm. The average values presented considered the average length of the circular extruded pattern, and do not considered that along fracture slope; the particles fall down, and therefore travelled a longer distance (up to 4.2 cm).

The extrusion distances measured in 1 mm fractures were, in all cases, longer than those previously measured within smaller apertures.

Moreover, and according to wider fracture volume, the mass of clay extruded in the fracture is as well higher than within narrow apertures: 0.6 grams in 0.2 mm (15 % of the initial mass) and up to 1.3 grams (30 % of initial mass), within 1 mm aperture.

The fraction of clay deposited in this test was a 3.4 % of the initial mass at 45° and it was doubled (75 of the initial mass) at 90°. However, despite the evident particle sedimentation stream along fracture direction, the extrusion pattern continues being rather homogenous (Figure 5-28).

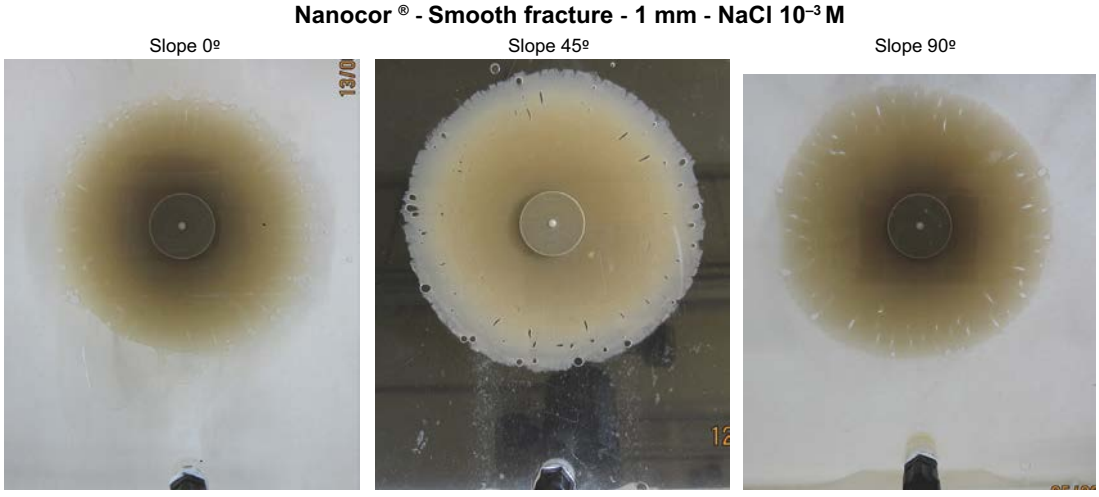

Figure 5-28. *Final state of sedimentation experiments carried out with Nanocor® clay in smooth fractures of 1 mm aperture filled with NaCl 10^{-3} M. Fractures were placed at different slope: 0° (Test 52A), 45° (Test 53A) and 90° (Test 54A). Clay pellet diameter is 19 mm.*

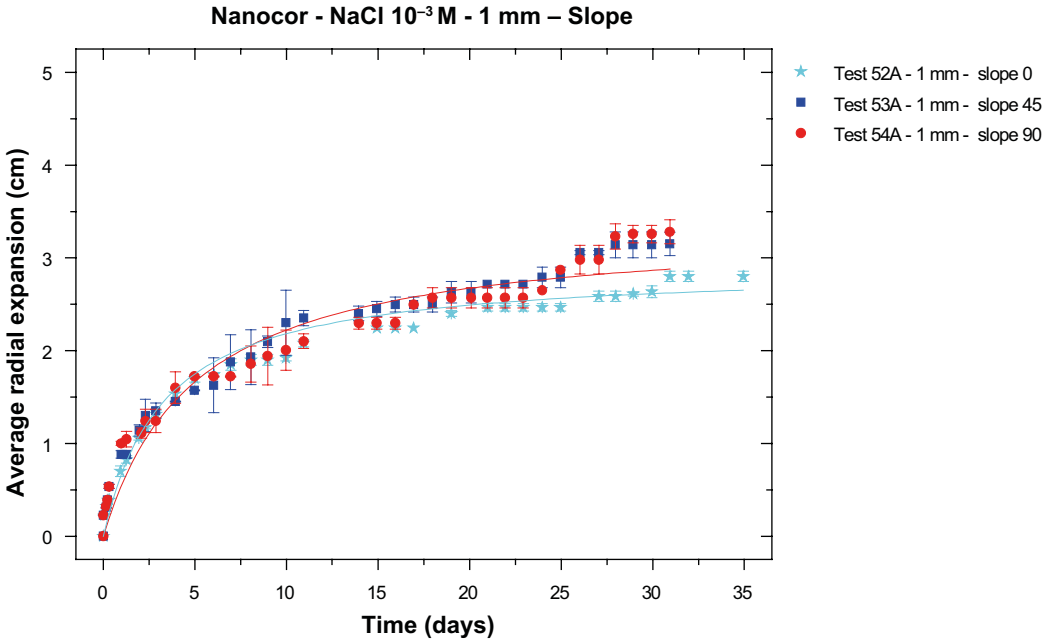

Figure 5-29. *Average radial expansion (in cm) measured for Nanocor® compacted at 1.4 g·cm^{-3}, within smooth fractures of 1 mm aperture filled with NaCl 10^{-3} M, placed at different slope: Test 52 (0°), 53 (45°) and 54 (90°).*

5.5 Sedimentation tests in sloped rough fractures

Sedimentation tests were carried out in fractures with *roughness 1,* placed at different slope (0°, 45° and 90°). In these rough fractures one surface is smooth and the other surface is rough.

For these experiments, sedimentation behaviour of raw MX-80 was compared to that of homoionic Na-MX-80 and Ca-MX-80.

5.5.1 Sedimentation of raw MX-80 in rough sloped fractures

Figure 5-30 shows the final state of the sedimentation experiments carried out with MX-80 clay in rough fractures at different slope: 0° (Test 37A), 45° (Test 42A) and 90° (Test 43A) and

Figure 5-31 shows the average radial expansions experienced. In the figure, open symbols refers to test where sedimentation was appreciated and, in these tests, the average values do not considered that along fracture slope, because the particles fall down.

It can be seen that the expanded ring was very similar at the three slopes analysed, and measured average distances were equivalent. In the test carried out at horizontal slope, the formation of a darker outer ring can be appreciated, which is not so noticeable in the experiments carried out at 45 or 90°.

In fact, at 45° and 90° slope, after 1 day of expansion the clay started to fall down and to sediment along the rough fracture slope (Figure 5-30). Sedimentation was as well observed within smooth fractures of 1 mm aperture, which have equivalent fracture volume than rough fractures (Table 3-1).

All experiments were stopped after 30 days for comparison and the sediment mass was lower than a 7 % of the initial mass, in the worst situation. Higher sedimentation at longer times cannot be discarded.

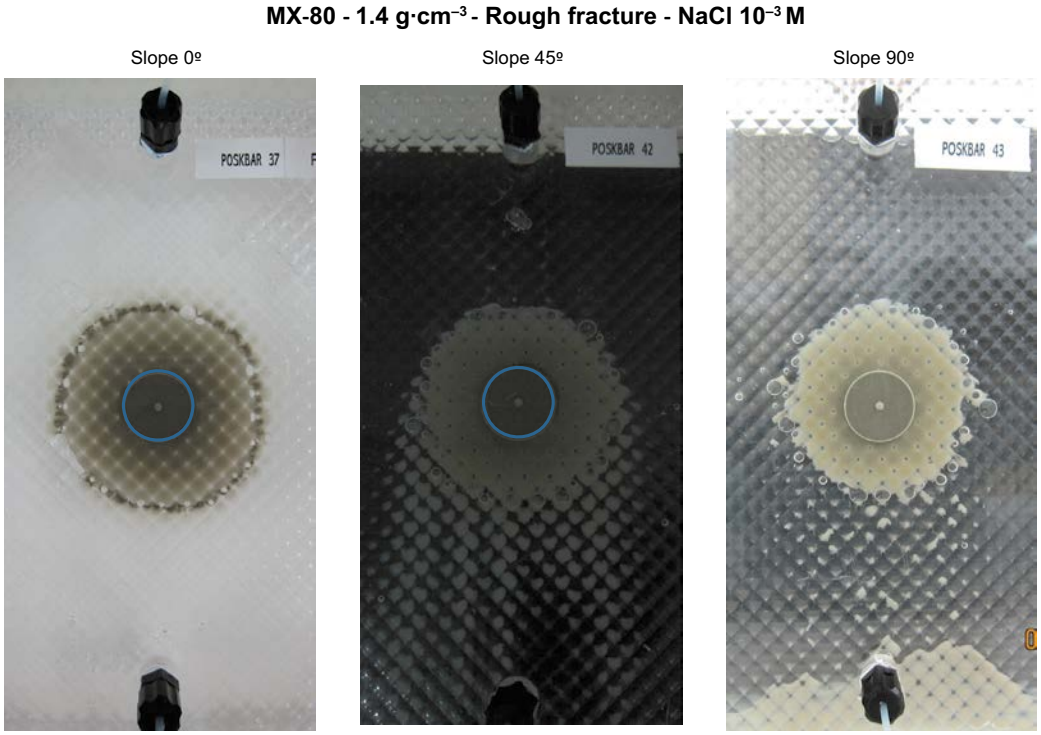

Figure 5-30. *Final state of sedimentation experiments carried out with MX-80 clay in rough fractures filled with NaCl 10^{-3} M. Fractures were placed at different slope: 0° (Test 37A), 45° (Test 42A) and 90° (Test 43A). Clay pellet diameter is 19 mm.*

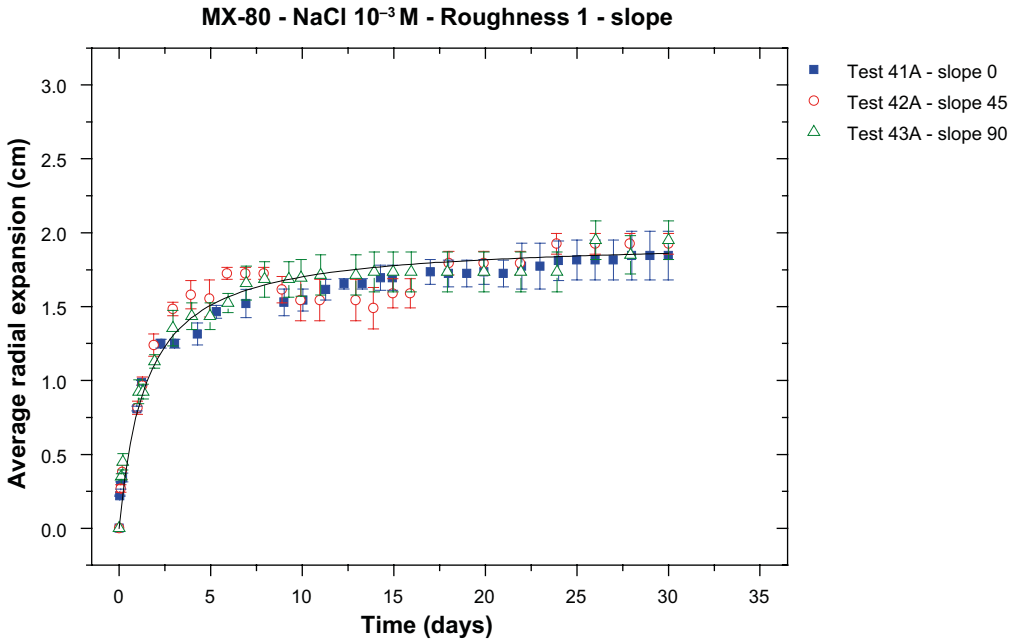

Figure 5-31. *Average radial expansion (in cm) measured for raw MX-80 compacted at 1.4 g·cm^{-3}, within fractures with Roughness 1, filled with NaCl 10^{-3} M. The fractures were placed at different slope: Test 41A (0°), Test 42A (45°) and Test43A (90°). *Open symbols refers to tests where sedimentation along fracture sloped was appreciated, where the average values are calculated excluding the slope direction.*

Total eroded mass fraction was 13 % at 0° or 45° slope and up to a 17 % of the initial clay mass at vertical slope (90°), as can be seen in Table 5-8.

Table 5-8. Total eroded mass and deposited mass experienced by different clays (MX-80, Na-MX-80 and Ca-MX-80) within rough artificial fractures placed at different slopes (0°, 45° and 90°).

Test	Clay	Slope	Initial dry mass (g)	Pellet final mass (g)	Deposited (g)	Eroded mass	Eroded mass (%)
41A	MX-80	0°	3.9778	3.4623	0	0.5155	13.0
42A	MX-80	45°	3.9778	3.4601	0.2715	0.5177	13.0
43A	MX-80	90°	3.9778	3.2801	0.0570	0.6977	17.5
44A	Na-MX-80	0°	4.0053	2.4861	0	1.5192	37.9
45A	Na-MX-80	45°	4.0053	2.4673	0.1255	1.5380	38.4
46A	Na-MX-80	90°	4.0053	2.3551	0.1369	1.6502	41.2
47A	Ca-MX-80	0°	3.9533	3.8558	0	0.0975	2.5
48A	Ca-MX-80	45°	3.9533	3.8120	0	0.1413	3.6
49A	Ca-MX-80	90°	3.9533	3.6204	0	0.3329	8.4

5.5.2 Sedimentation of Na-MX-80 in rough sloped fractures

Figure 5-32 shows the images of the final state of the sedimentation experiments carried out with Na-MX-80 clay in rough at different slope: 0° (Test 44A), 45° (Test 45A) and 90° (Test 46A) and Figure 5-33 includes the average radial expansions experienced. It is evident that Na-MX-80 extrusion is higher than that of raw MX-80, in all conditions analysed.

Looking to the behaviour at different slopes, Na-MX-80 extrusion is significantly higher at horizontal slope, as well as the eroded mass (Table 5-8), in comparison to the case of sloped fractures. This is probably due to the fact that within these sloped fractures, clay particles continuously fall down and sediment. Comparatively, at the end of the experiment the amount of clay that remains extruded in the fracture was smaller in sloped fractures than in horizontal ones. In fact, in these experiments with Na-exchanged clay, the eroded mass fraction was around a 40 % of the initial mass (Table 5-1 and Table 5-2), which is comparatively the highest erosion measured in these experiments. In these sloped experiments sediment mass was lower than a 4 % of the initial clay mass.

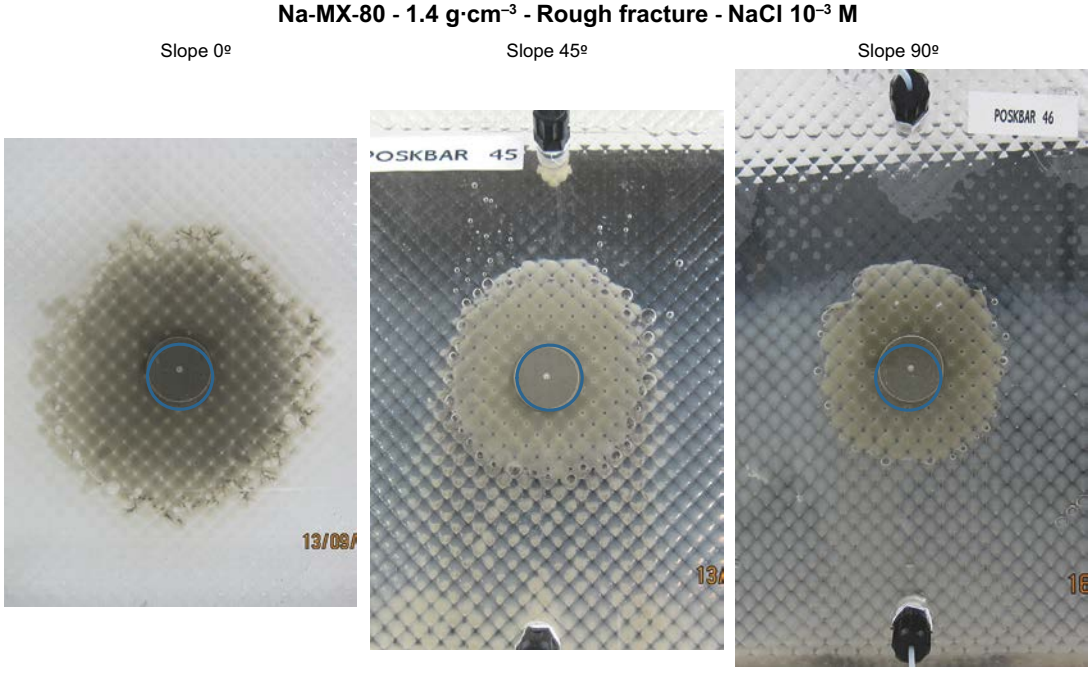

Figure 5-32. *Final state of sedimentation experiments carried out with Na-MX-80 clay in rough fractures filled with NaCl 10^{-3} M. Fractures were placed at different slope: 0° (Test 44A), 45° (Test 45A) and 90° (Test 46A). Clay pellet diameter is 19 mm.*

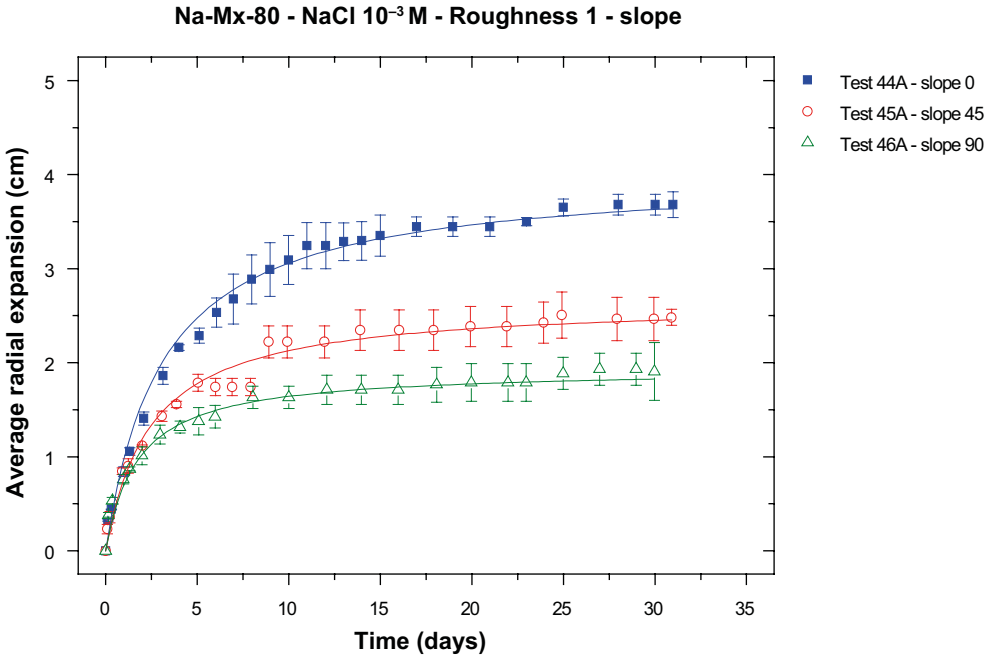

Figure 5-33. *Average radial expansion (in cm) measured for Na-MX-80 compacted at 1.4 g·cm^{-3}, within fractures with Roughness 1, filled with NaCl 10^{-3} M, placed at different slopes: Test 44A (0)°, Test 45A (45°) and Test 46A (90°). Open symbols refers to tests where sedimentation along fracture sloped was appreciated, where the average values are calculated excluding the slope direction.*

5.5.3 Sedimentation of Ca-MX-80 in rough sloped fractures

Figure 5-34 shows the photographs taken at the end of sedimentation experiments carried out with Ca-MX-80 clay in rough at different slope: 0° (Test 47A), 45° (Test 48A) and 90° (Test 49A) and Figure 5-35 shows the average diameters.

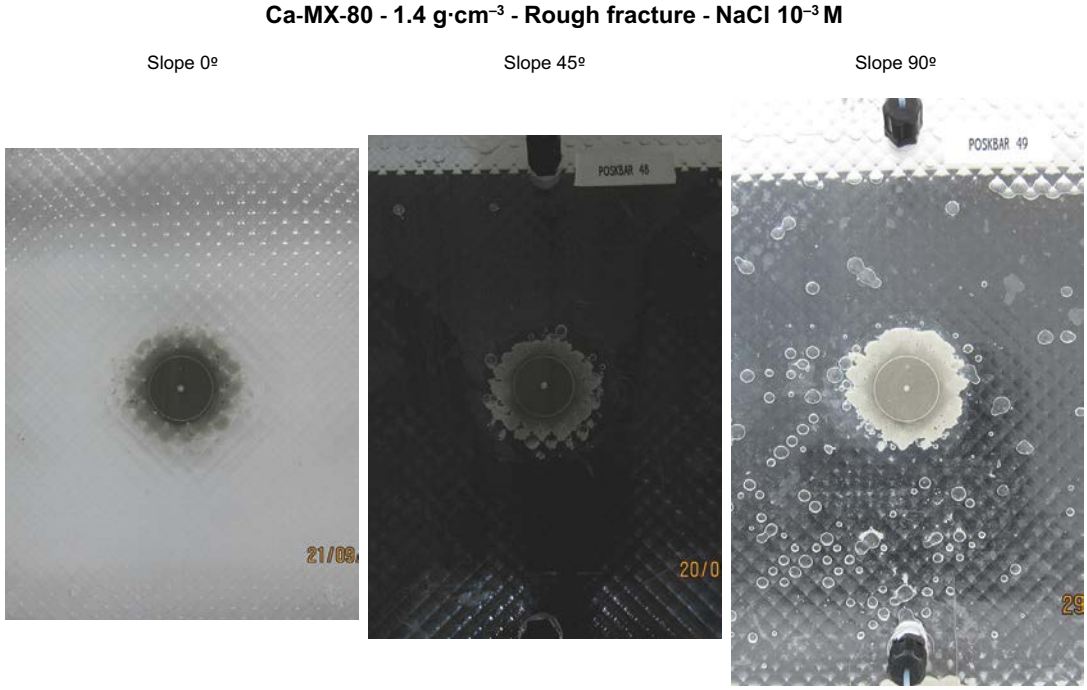

Figure 5-34. *Final state of sedimentation experiments carried out with Ca-MX-80 clay in rough fracture filled with NaCl 10^{-3} M. Fractures were placed at different slope: 0° (Test 47A), 45° (Test 48A) and 90° (Test 49A). Clay pellet initial diameter is 19 mm.*

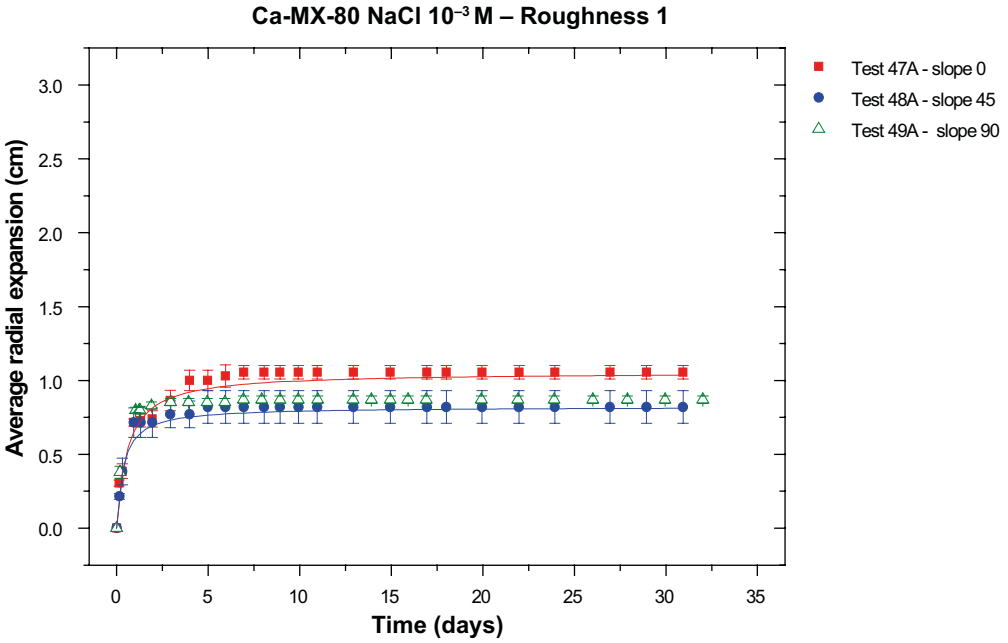

Figure 5-35. *Average radial expansion (in cm) measured for Ca-MX-80 compacted at 1.4 g·cm^{-3}, within fractures with Roughness 1, filled with NaCl 10^{-3} M, placed at different slopes: Test 47A (0°), Test 48A (45°) and Test49A (90°). Open symbols refers to tests where sedimentation along fracture sloped was appreciated, where the average values are calculated excluding the slope direction.*

By comparison with experiments performed with raw MX-80 and Na-exchanged MX-80, three main conclusions are drawn: 1. Extrusion distances of Ca-rich clays within fractures are clearly shorter than that of Na-rich clays; 2. No particle fall down, or sedimentation, was observed in experiments carried out with Ca-clay; 3. Erosion experienced by Ca-clays is not negligible, and measured expanded masses were around an 8–9 % of the initial installed masses (Table 5-1 and Table 5-2).

5.6 Erosion by flow tests in smooth narrow fractures

Flow experiments were always carried out after previous expansion period, during 30 days, under stagnant conditions, (results presented in Section 5.1). Continuing, water flow was applied to the six tests carried out in narrow fractures with 0.2 mm aperture, placed at horizontal slope (0°) with Nanocor® clay (Test 4–5A, 6–7B and 8–9B) and MX-80 clay (Test 10–11A, 12–13A and 14–15A). All tests were carried out with NaCl at 10^{-3} M.

Experimental conditions are presented in Table 5-9. Flow velocities were calculated considering the flow rate (2 mL/day = 2.08×10^{-11} m^3·s^{-1}) and the cross-section (S), which depends on the fracture aperture (0.1 mm: S = 1.7×10^{-5} m^2; 0.2 mm: S = 3.4×10^{-5} m^2; 0.4 mm: S = 6.8×10^{-5} m^2). Flow velocities are inversely proportional to the aperture (0.1 mm: v = 1.36×10^{-6} m·s^{-1}; 0.2 mm: v = 6.1×10^{-7} m·s^{-1}; 0.4 mm: v = 3.4×10^{-7} m·s^{-1}).

Table 5-9. Erosion by flow experiments. Experimental conditions, aperture, flow rate (mL/day) and flow velocity, average radial expansion at the end of expansion test (beginning of flow experiment) and final expansion (in cm) at the end of flow experiment, eluted mass and total eroded mass (in g and %).

Reference	Clay	Fracture aperture (mm)	Flow (mL/day)	Flow velocity ($m \cdot s^{-1}$)	Average radial expansion (cm)	Average radial expansion at the end of flow experiment (cm)	Eluted mass (g)	Eroded mass (g)	Eroded mass (%)
Test 4B–5B	Nanocor®	0.1	2.1 ± 0.5	1.5×10^{-6}	1.43 ± 0.12	1.81 ± 0.04	6.2×10^{-4}	0.3379	8.5
Test 6B–7B	Nanocor®	0.2	1.8 ± 0.2	6.1×10^{-7}	2.48 ± 0.12	3.97 ± 0.08	6×10^{-3}	0.7137	18.0
Test 8A–9A	Nanocor®	0.4	2.0 ± 0.2	1.4×10^{-7}	2.26 ± 0.17	2.59 ± 0.12	9.9×10^{-3}	0.9307	23.5
Test 29A–30A	Nanocor®	0.2	2.0 ± 0.6	1.35×10^{-6}	1.35 ± 0.20	2.24 ± 0.15	2×10^{-4}	0.0205	2.0
Test 31A–32A	Nanocor®	Rough 1//1 mm	0.9 ± 0.3	5.6×10^{-8}	2.26 ± 0.10	3.16 ± 0.17	4.5×10^{-4}	1.2509	31.6
Test 33A–34A	Nanocor®	Rough 2 // 1.7 mm	1.6 ± 1	6.3×10^{-8}	1.60 ± 0.20	2.91 ± 0.20	1.5×10^{-3}	0.9700	24.5
Test 10A–11A	MX-80	0.1	2.0 ± 0.6	1.35×10^{-6}	0.49 ± 0.05	0.51 ± 0.07	2×10^{-4}	0.0205	0.5
Test 12A–13A	MX-80	0.2	2.0 ± 0.4	6.7×10^{-7}	0.82 ± 0.08	0.88 ± 0.07	5×10^{-4}	0.0662	1.7
Test 14A–15A	MX-80	0.4	2.0 ± 0.2	3.6×10^{-7}	0.85 ± 0.07	1.80 ± 0.11	5×10^{-3}	0.1700	4.3
Test 35A–36A	MX-80	0.4	1.6 ± 0.2	5.53×10^{-7}	1.14 ± 0.05	2.29 ± 0.06	1.3×10^{-4}	0.0810	2.0
Test 37A–38A	MX-80	Rough 1//1 mm	1.44 ± 0.6	9.8×10^{-8}	1.56 ± 0.8	1.19 ± 0.12	3.8×10^{-4}	0.6929	17.4
Test 39A–40A	MX-80	Rough 2 // 1.7 mm	1.48 ± 0.7	5.92×10^{-8}	1.48 ± 0.12	2.43 ± 0.09	1.18×10^{-3}	0.4062	10.2

During flow period, a gradual diameter increase was measured as well, but the expansion was fairly homogeneous along all directions, Figure 5-36 presents the additional clay extrusion experienced by Nanocor® (Test 4–5A, 6–7B and 8–9B) during flow period within different fracture apertures.

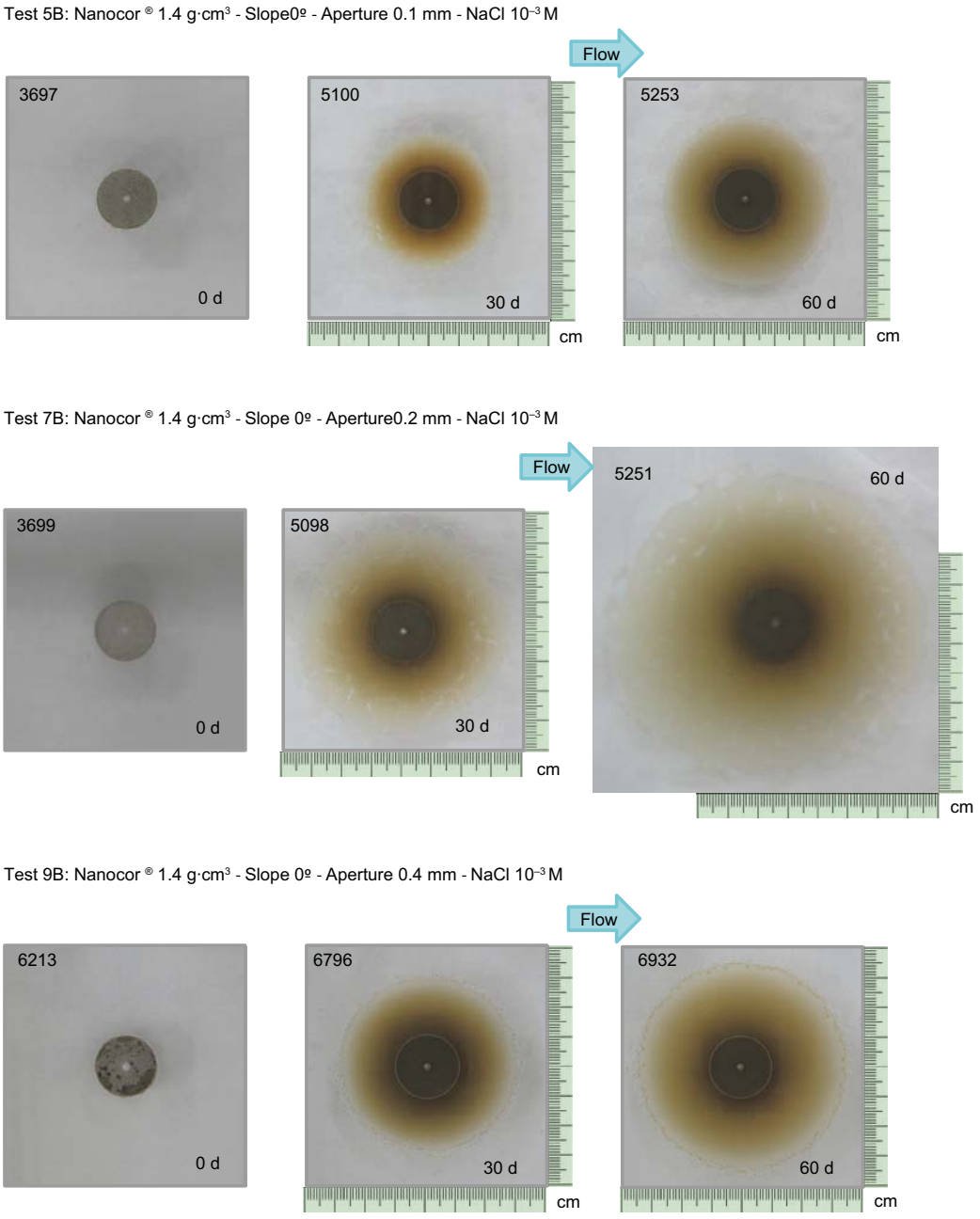

Figure 5-36. *Average radial expansion experienced by Nanocor® clay compacted at 1.4 g·cm^{-3} during expansion (30 days) and subsequent flow period, in an artificial fracture placed horizontally, with different fracture apertures: Tests Test 4B–5B (0.1 mm), Test 6B–7B (0.2 mm) and Test 8B–9B (0.4 mm). Flow direction is indicated.*

Figure 5-37 presents the results for MX-80 (Test 10–11A, 12–13A and 14–15A). In Table 5-9 , the values of average radial expansion at the end of expansion test (beginning of flow experiment) and average radial expansion at the end of flow experiment.

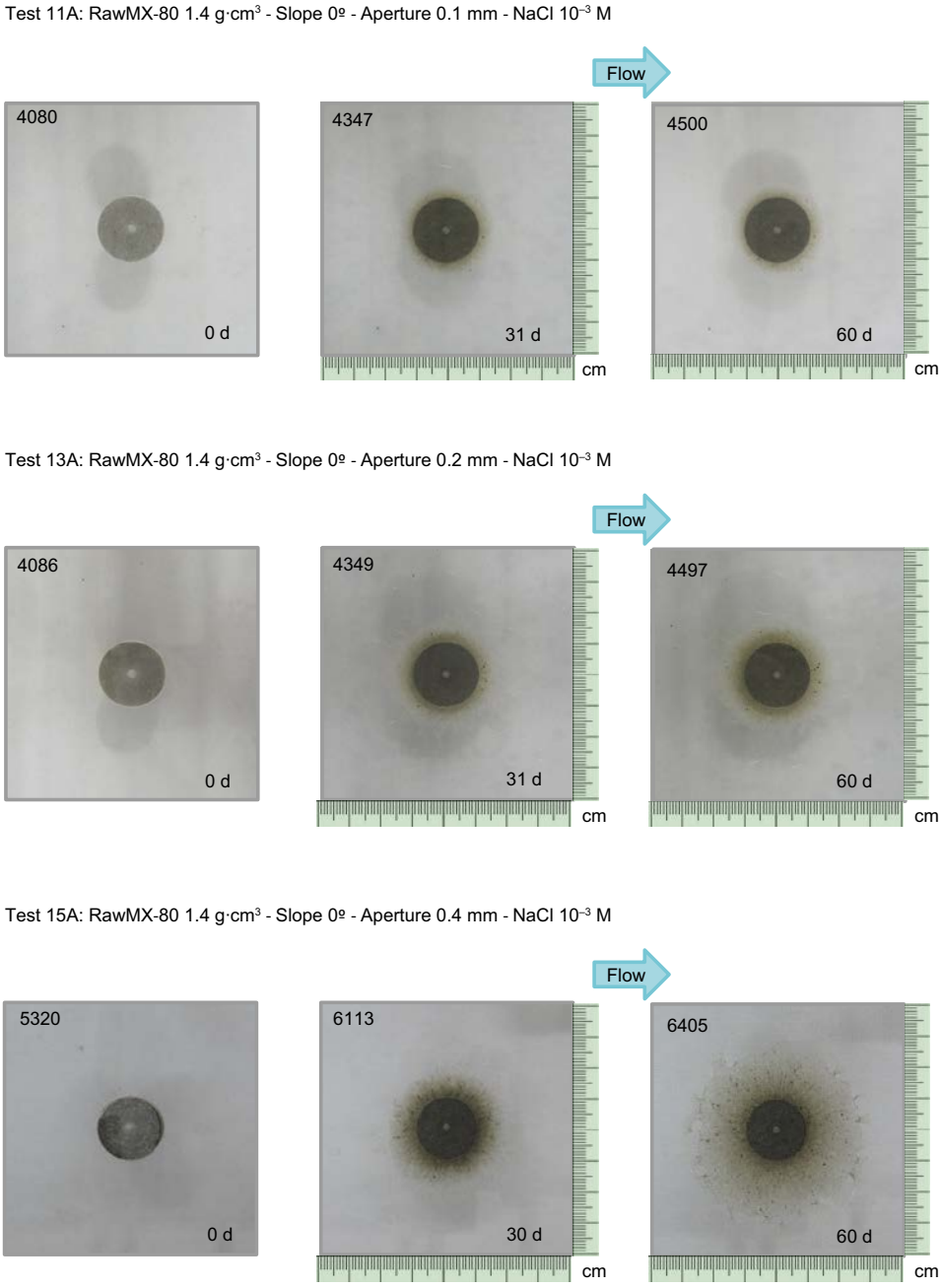

Figure 5-37. *Average radial expansion experienced by MX-80 clay compacted at 1.4 g·cm^{-3} during expansion (30 days) and subsequent flow period, in an artificial fracture placed horizontally, with different fracture apertures: Tests Test 10–11 (0.1 mm), Test 12–13 (0.2 mm) and Test 14–15 (0.4 mm). Flow direction is indicated.*

It is noteworthy that in these flow experiments solid swept away along flow direction was not observed at sight. This may be due to the flow conditions used ($v = 10^{-6}$ m·s^{-1}), which are lower than previous cases. This contrast with the results of the former Benchmark Experiment carried out in EC-BELBAR project (shown in Figure 5-38), which would be comparable to tests Test 6 (Nanocor clay, 0° slope and 0.1 mm aperture). In the BELBAR benchmark, two flows were subsequently applied for 15 days. At the lower flow (comparable to Test velocity of 1.2×10^{-6} m·s^{-1}), no solid movement along flow direction was observed. However, solid movement was clearly observed at higher flow ($v = 9.5 \times 10^{-5}$ m·s^{-1}), as can be seen in Figure 5-38. To remove lower clay masses at lower flow rates seems reasonable.

Some tests carried out under flow conditions were replicated, to be compared to flow experiments within rough fractures, both with Nanocor® (tests Test 29–30A) and MX-80 clays (Test 35–36A) and, as can be seen results were fully comparable (Figure 5-39).

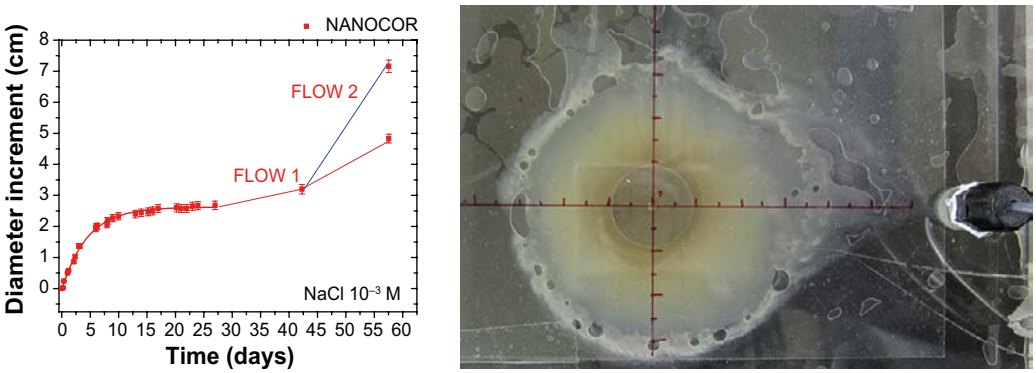

Figure 5-38. *Benchmark test experiment: (Left) Average radial expansion experienced by a Nanocor® pellet 1.4 g·cm^{-3} against NaCl 10^{-3} M: stagnant (30 days) and at two different flows (flow 1 $v_1 = 1.2 \times 10^{-6}$ m·s^{-1}; flow 2 $v_2 = 9.5 \times 10^{-5}$ m·s^{-1}. (Right) Final picture of benchmark test performed in the EC-BELBAR, project, where solid movement along flow direction can be appreciated.*

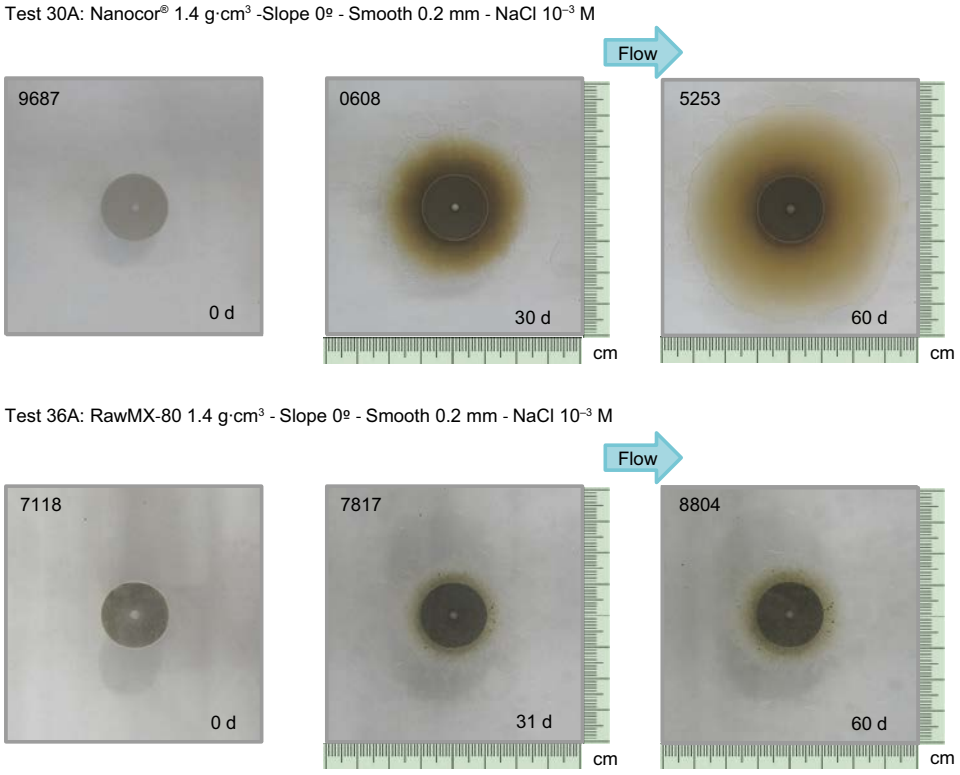

Figure 5-39. *Average radial expansion experienced by Nanocor® clay (Test 30A) and MX-80 clay (Test 36A compacted at 1.4 g·cm^{-3}, during expansion (30 days) and subsequent flow period, in an artificial fracture placed horizontally. Flow direction is indicated.*

In all cases, the average diameter extruded within the fracture increases during flow period. The greatest effect was observed for test Test 9B, carried out with Nanocor® clay, within 0.2 mm fracture aperture.

In all cases the average radial expansion was fairly homogeneous, and not significant differences are at sight measured along flow direction. This is probably due to the fact that flow velocities are not very high.

In these erosion by flow tests, eluted fractions are collected (Figure 3-1) and samples are analysed by PCS.

Figure 5-40 and Figure 5-41 present the particle concentration (in mg) measured in eluted fractions, as a function of time, respectively for Nanocor® and MX-80 clay, within different fracture apertures. Water flow was around 2 mL/day in all cases (Table 5-9). Water supply was equivalent in all tests, but flow velocities differ because of the different fracture aperture.

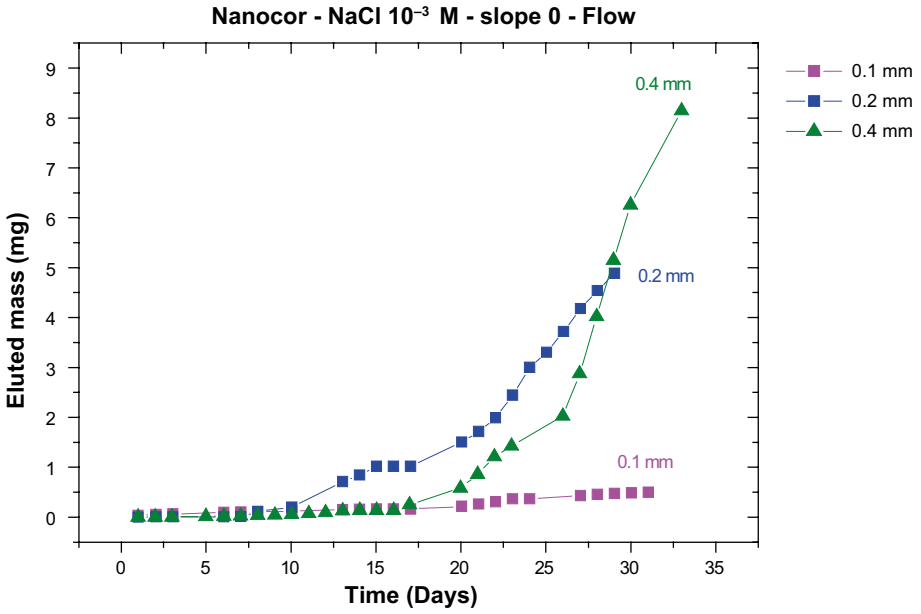

Figure 5-40. *Mass eluted (accumulated) as a function of time from Nanocor® clay compacted at 1.4 g·cm^{-3}, subjected to a water flow of NaCl 10^{-3} M of 2 mL/day, within different fracture apertures (0.1 , 0.2, 0.4 mm).*

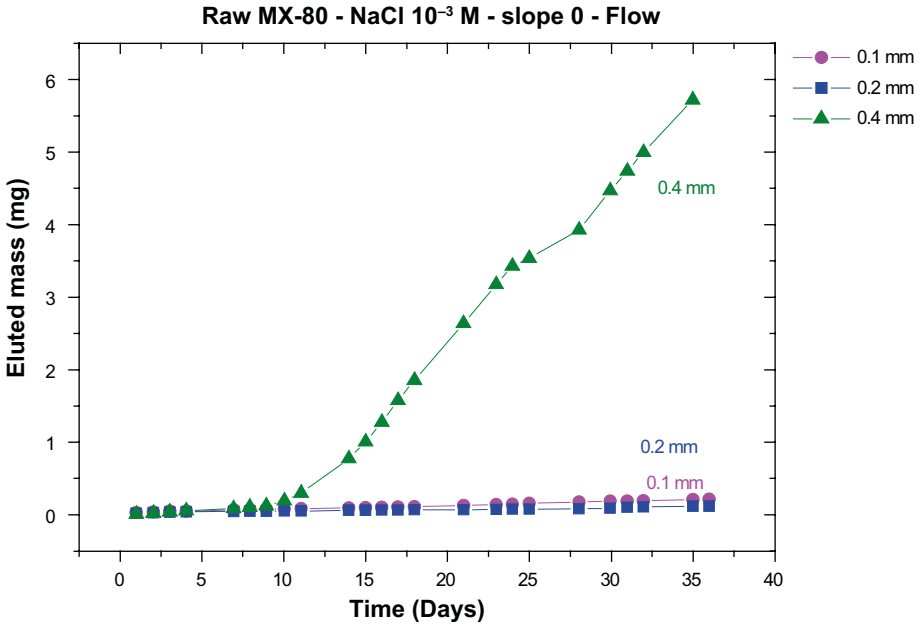

Figure 5-41. *Mass eluted (accumulated) as a function of time from MX-80 clay compacted at 1.4 g·cm^{-3}, subjected to a water flow of NaCl 10^{-3} M of 2 mL/day, within different fracture apertures (0.1, 0.2, 0.4 mm).*

Results showed that eluted fraction depended on fracture aperture, being lower at smaller apertures, and lower for Mx80 (Figure 5-41) than for Nanocor® (Figure 5-40), in agreement to its highest Na content (Table 3-3).

Figure 5-42 presents the particle diameter measured by PCS on eluted samples from Nanocor® (Figure 5-42a) and MX-80 clay (Figure 5-42b) flow tests within different apertures. In the case of Nanocor, eluted particles are in the colloid range, with diameters < 1 mm. Eluted particles form MX-80 are in general bigger, and only within the west fracture (0.4 mm) eluted particles are in the colloidal range. In general, smaller particles are eluted within wider apertures (0.4 mm).

Figure 5-43 presents the evolution of the pH on eluted samples from Nanocor® and MX-80 flow tests within different apertures. Figure 5-44 presents the electrical conductivity measured on the same samples. The initial values of NaCl 10^{-3} M are pH = 5.3 ± 0.5 and electrical conductivity (EC) of 125 ± 2 $\mu S \cdot cm^{-1}$.

At the beginning of "erosion by flow" experiment, the fracture was already filled with water in equilibrium with the clay during 30 days of previous expansion test (initiated with NaCl 10^{-3} M). According to fracture aperture dimensions, the fracture volumes were respectively 2.89×10^{-6} m^3 (0.1 mm), 5.78×10^{-6} m^3 (0.2 mm) and 1.16×10^{-5} m^3 (0.4 mm).

It was shown that eluted particles from the 0.1 mm fracture are much larger, about 2 times, than from the 0.2 and 0.4 mm fractures. This could be caused by a faster flocculation in the narrower fracture induced by the larger velocity gradient. However, concerning the size, two other factors can also explain the differences. On one side, at the beginning of the flow period initial water conductivities were higher at lower apertures, as can be seen in Figure 5-44. On the other hand, the drag forces required to remove smaller particles are higher at lower flow rates, so we can expect to remove bigger particles first. Pusch (1999) concluded that the critical flow rate to remove particles smaller than 0.5 µm is 10^{-4} $m \cdot s^{-1}$.

These small volumes lead to high solid to liquid ratios, which induced chemical changes (pH, conductivity and composition evolution), which may affect erosion process.

In fact, at the beginning of flow experiments, water conductivities were high (Figure 5-44), up to 6 000 µS/cm in the case of Nanocor® in the thinner aperture and 4 000 $\mu S \cdot cm^{-1}$ for MX-80. Once additional NaCl is continuously provided to the experiment, water conductivity started to decrease. The high conductivities measured at the beginning indicate that dissolution of soluble salts present in the clay, halite (NaCl), gypsum ($CaSO_4 \cdot 2H_2O$) and calcite ($CaCO_3$), occurred. Moreover, cation exchange processes most probably took place, varying the initial content of cations in exchangeable positions.

The rather high conductivities measured, explain low mobilisation of eroded masses (Table 5-1 and Table 5-2), because the lower the ionic strength the higher the erosion.

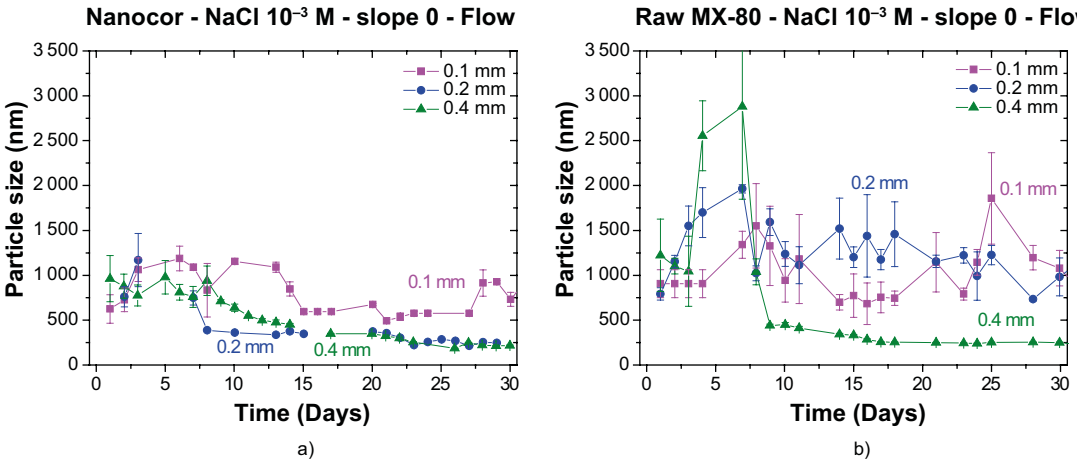

Figure 5-42. *Average hydrodynamic diameter (nm) measured by PCS, as a function of time, on samples eluted from a) Nanocor® or b) MX-80 clay, compacted at 1.4 $g \cdot cm^{-3}$, subjected to a water flow of NaCl 10^{-3} M of 2 mL/day, within different fracture apertures (0.1 , 0.2, 0.4 mm).*

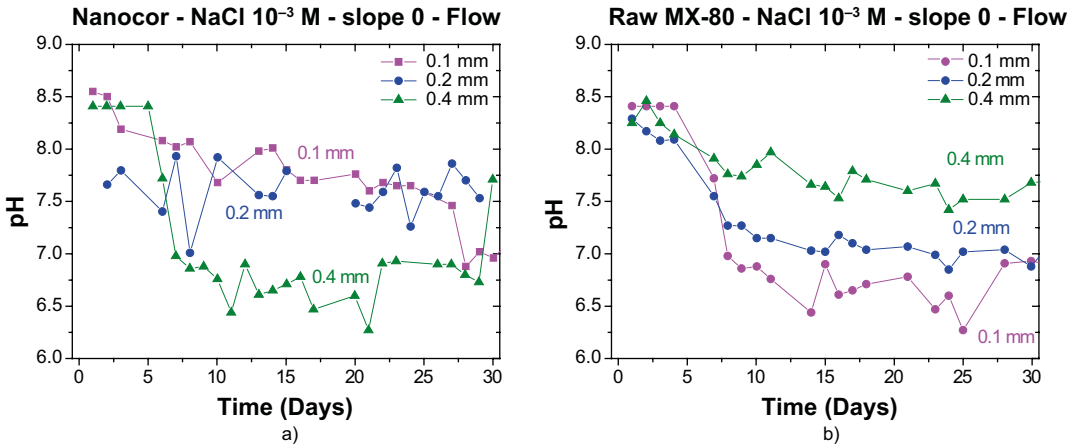

Figure 5-43. *pH measured as a function of time on samples eluted from a) Nanocor® or b) MX-80 clay, compacted at 1.4 g·cm^{-3}, subjected to a water flow of NaCl 10^{-3} M of 2 mL/day, within different fracture apertures (0.1 , 0.2, 0.4 mm).*

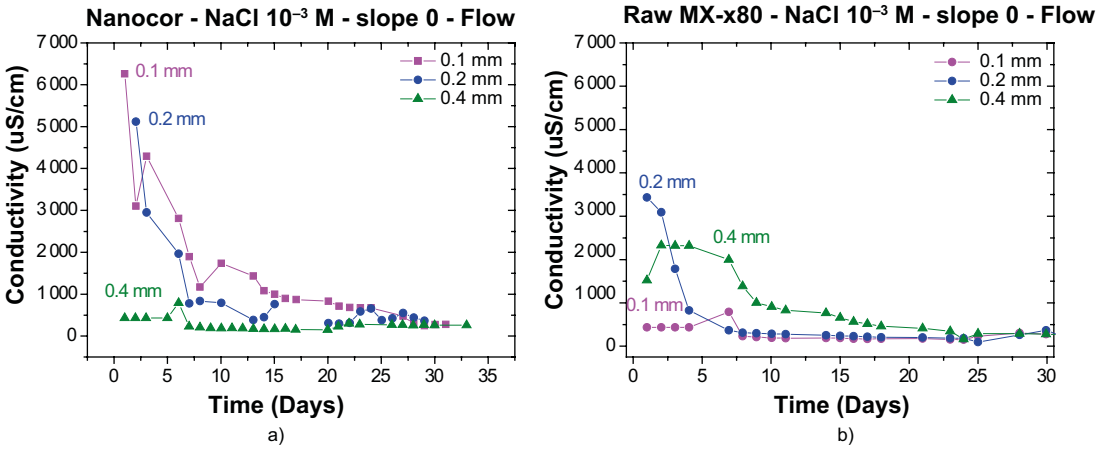

Figure 5-44. *Electrical conductivity (µS·cm^{-1}) measured as a function of time on samples eluted from a) Nanocor® or b) Raw MX-80 clay, compacted at 1.4 g·cm^{-3}, subjected to a water flow of NaCl 10^{-3} M of 2 mL/day, within different fracture apertures (0.1 , 0.2, 0.4 mm).*

5.7 Erosion by flow tests in rough fractures

Flow experiments within rough fractures were performed after a previous expansion period, during 30 days under stagnant conditions.

Flow conditions were applied to Nanocor® clay, considering two different roughness: Test 31–32 (*Roughness 1*) and Test 33–34 (*Roughness 2*). Equivalent flow tests were carried out with MX-80 clay: Tests Test 37–38 (*Roughness 1*) and Test 39–40 (*Roughness 2*). In all cases the fractures were horizontal and their corresponding volumes were indicated in Table 3-1.

All tests were carried out with NaCl at 10^{-3} M and the water caudal and flow velocities applied are indicated in Table 5-9. In the rough fractures, the flow velocities were estimated from the measured caudal and considering the fracture volume and assuming the equivalent cross-sections of a smooth fracture with the same volume. The water supplied per day was the same as in flow experiments carried out in smooth fractures (around 2 mL/day) but flow velocities are slower in this case, because fracture volumes are higher.

During flow period, a gradual diameter increase was measured as well as within smooth fractures. In Table 5-9 , the values of average radial expansion at the end of expansion test (beginning of flow experiment) and average radial expansion at the end of flow experiment.

Figure 5-45 shows the additional clay extrusion experienced by Nanocor® (Test 32–33 and 33–34 during flow period within fractures with different roughness. In the figure, the shown area is enlarged, but scale is maintained to facilitate comparison. Diameter increased upon flow, but following the same shape acquired by the extruded fraction during the previous expansion period. Despite their different shape, clay expansion was quite similar within the two roughness analysed. The same behaviour was observed for the MX-80 clay. Solid swept away along flow direction was neither observed at sight, which is again attributed to the low flow velocities applied ($v = 10^{-7}$ m·s^{-1}). However, preferential expansion along roughness pattern is appreciated.

Figure 5-46 presents the particle concentration (in mg) measured in eluted fractions, as a function of time, respectively for Nanocor® and MX-80 clay, within rough fractures. Eluted fraction measured within smooth fractures with 0.4, 0.2 and 0.1 mm apertures, are included. It can be seen that eluted fractions in rough fractures was always very low, and similar to those measured within smooth fractures with 0.1 mm, what actually have clear smaller volumes (Table 3-1). This indicates that fracture roughness hindered particle mobilisation.

Figure 5-47 presents the particle diameter measured by PCS on eluted samples from flow tests within rough fractures. It is noteworthy that eluted particles were as well in the colloid range, with diameters < 1 mm. Released particles diameters where slightly bigger in fracture with higher roughness, but for Nanocor® and MX-80, most probably because the fracture volume is higher as well.

Figure 5-48 presents the electrical conductivity measured on the same samples. Figure 5-49 presents the evolution of the pH on eluted samples from Nanocor® and MX-80 flow tests within different fractures.

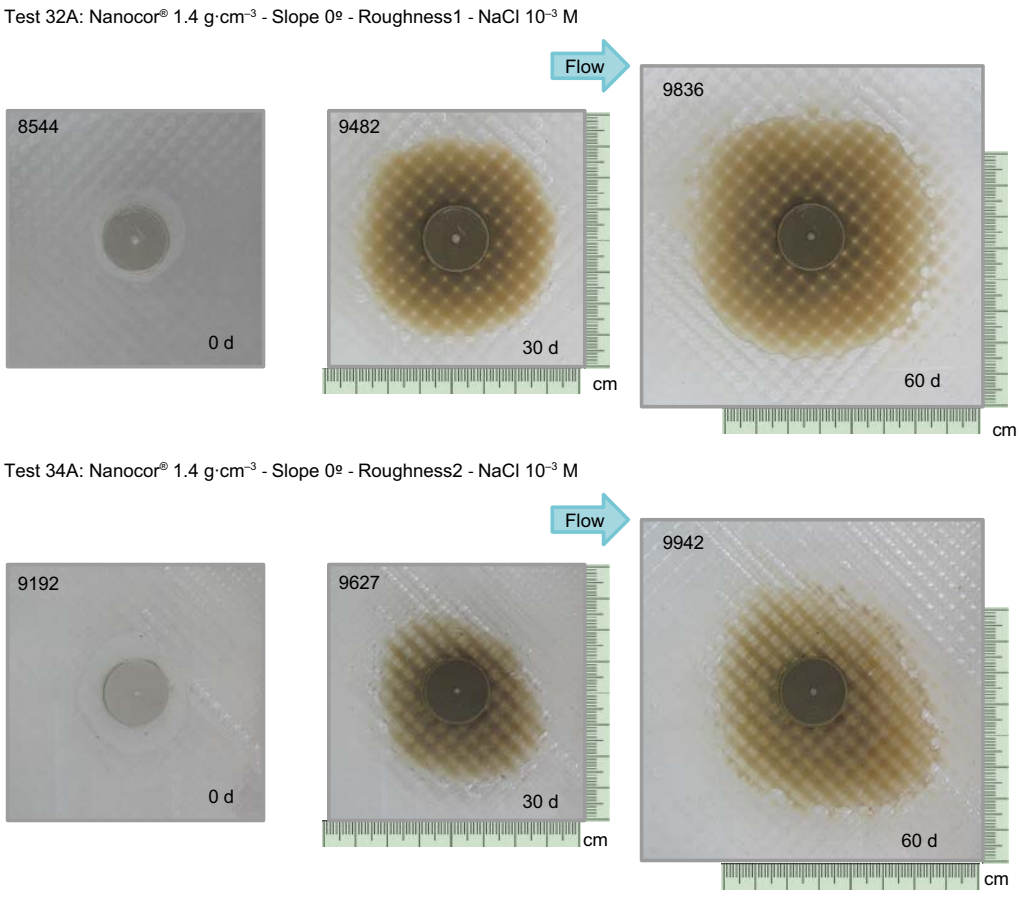

Figure 5-45. *Average radial expansion experienced by Nanocor® clay compacted at 1.4 g·cm^{-3} during expansion (30 days) and subsequent flow period, in fractures placed horizontally, with different roughness. Test 31–32A (Rougness 1), Test 33–34A (Roughness 2).*

At the beginning of "erosion by flow" experiment, the fracture was already filled with water in equilibrium with the clay during 30 days of previous expansion test (initiated with NaCl 10^{-3} M with pH = 5.3 ± 0.5 and electrical conductivity (EC) of 125 ± 2 µS·cm^{-1}.). The electrical conductivities at the beginning of flow phases where in general smaller in the rough fractures than in the smooth ones, because of their bigger volumes. During flow period, electrical conductivity and pH measured on eluted fractions form rough fractures did not change significantly, while the arrival of fresh water had a significant dilution effect within smooth fractures.

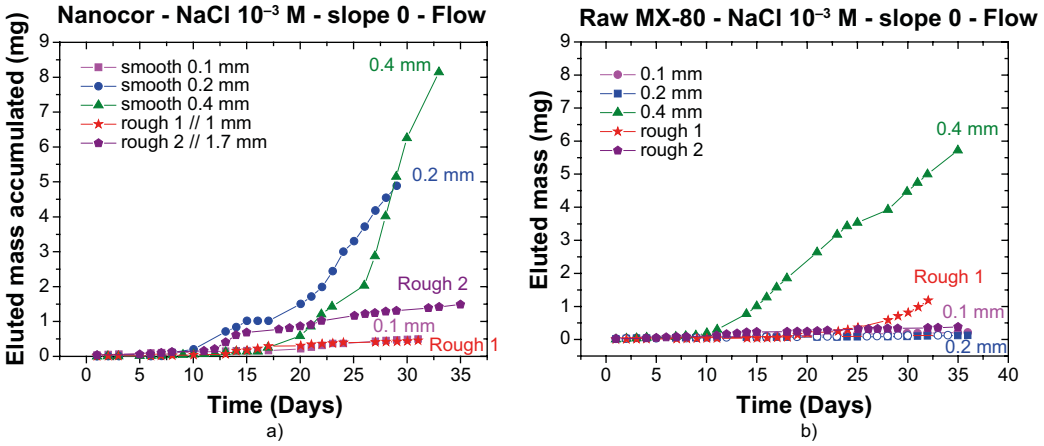

Figure 5-46. *Mass eluted (accumulated) as a function of time from Nanocor® and raw MX-80 clay compacted at 1.4 g·cm^{-3}, subjected to a water flow of NaCl 10^{-3} M of 2 mL/day, within fractures with different roughness (Rough 1 and Rough 2). The eluted fractions measured within smooth fractures of 0.1, 0.2 and 0.4 mm are included for comparison.*

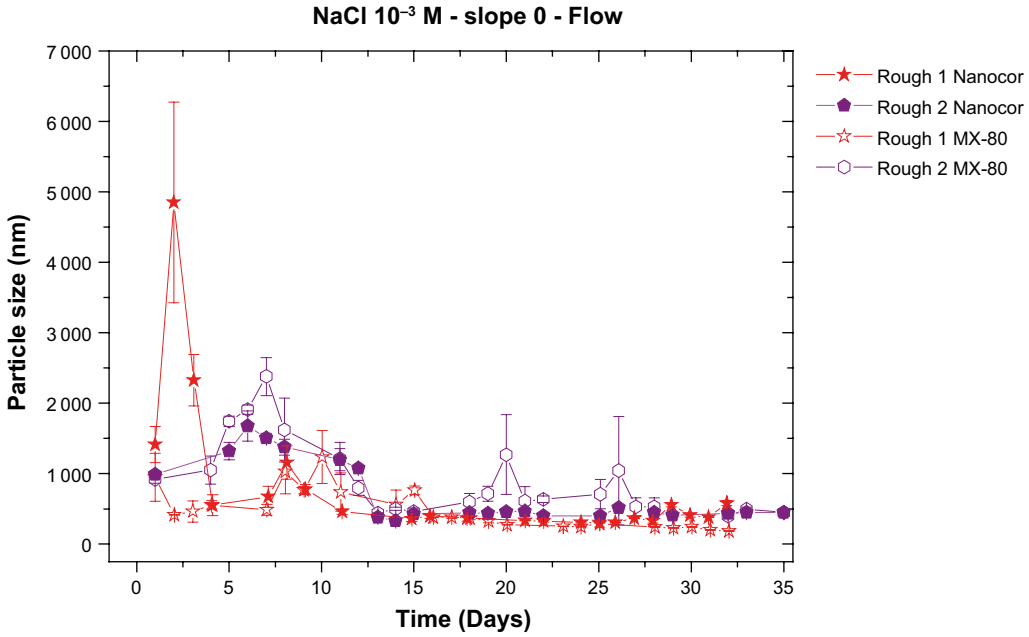

Figure 5-47. *Average hydrodynamic diameter (measured by PCS, as a function of time, on samples eluted from raw Nanocor® and raw MX-80 clays, compacted at 1.4 g·cm^{-3}, subjected to a water flow of NaCl 10^{-3} M of 2 mL/day, within different rough fractures.*

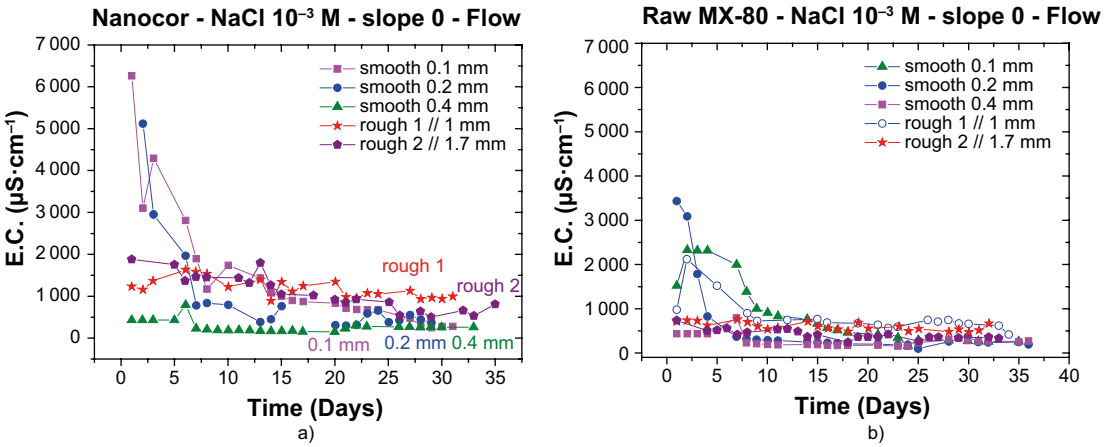

Figure 5-48. *Electrical conductivity (E.C.) measured as a function of time on samples eluted from a) Nanocor® or b) RawMX-80 clay, compacted at 1.4 g·cm^{-3}, subjected to a water flow of NaCl 10^{-3} M of 2 mL/day, within different rough or smooth fractures.*

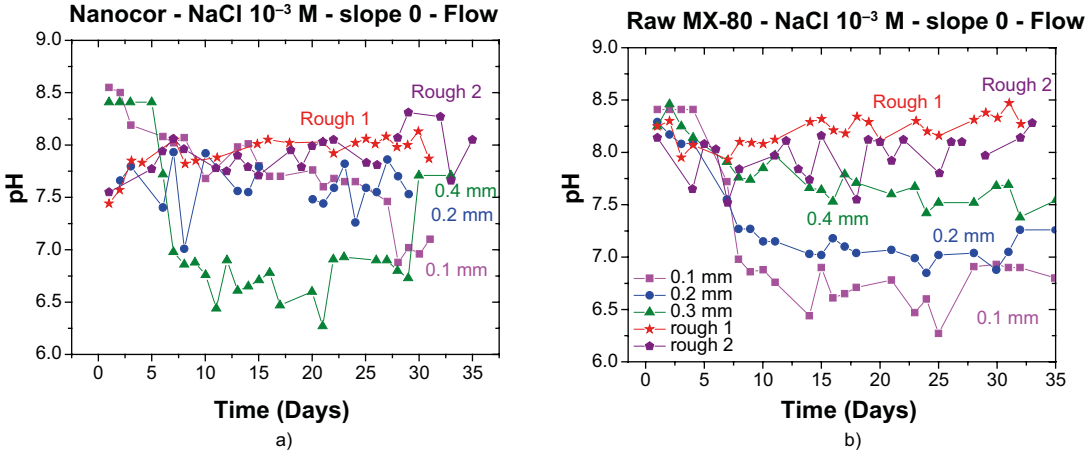

Figure 5-49. *pH measured as a function of time on samples eluted from from a) Nanocor® or b) MX-80 clay, compacted at 1.4 g·cm^{-3}, subjected to a water flow of NaCl 10^{-3} M of 2 mL/day, within different rough or smooth fractures.*

6 Discussion

Clay erosion tests were carried out in artificial fractures under different experimental conditions. The aims were to analyse clay expansion in horizontal fractures, erosion promoted by water flow and sedimentation in sloped fractures.

All experiments were carried out in artificial fractures with clay pellets compacted at 1.4 $g \cdot cm^{-3}$. Different clays were analysed: Nanocor®, MX-80, Ibeco, MCA-C saponite and homoionic Na- and Ca-clays. Different fracture conditions were analysed: smooth or rough surfaces, fracture apertures from 0.1 to 1.7 mm and fracture slopes (0°, 45° and 90°). The reference electrolyte was NaCl at 10^{-3} M ionic strength, but higher initial ionic strengths were also analysed (10^{-2} M or 10^{-1} M).

In all experiments, the clay was allowed to freely expand in the fracture without any inference. Some tests were carried out in duplicate or under experimental conditions previously analysed to verify reproducibility, as shown in Figure 5-3.

All tests have been carried out with compacted samples; therefore, initial expansion is promoted by clay swelling (Norrish 1954). The evolution of expansion within the fracture was followed during 30 days, as shown in Appendix 1 (pages 81–135).

Many factors have been observed to control the clay expansion.

The **chemistry of the equilibrium water** in the fractures has been identifies as first relevant actor. In all experiments, the chemical conditions evolved during the experiment, as indicated the significant increase of electrical conductivities. This increase is attributed to the dissolution of the soluble salts present in the clay. As chemical conditions were not really fixed in any experiment and they acted as an additional variable. This affects experiment comparison, somehow masks the relevance of one parameter with respect to another and difficult quantitative parameterization. In spite of this, a great amount of results are available and the comparison of experiments allowed extracting sound conclusions. In future, the fixation of the chemical conditions from the beginning would be of special interest.

Expansion behaviour in all tests was equivalent, in the sense that once the fracture was filled, the clay gradually (linearly) extruded in the fracture, until stopping after a certain time.

Expansion stopped in all experiments, with the only exception of tests 56A and 57A, carried out with Nanocor® and MX-80 clays in smooth fractures with the widest aperture (1.7 mm). The duration of experiments was 30 days, to facilitate test comparison. At this time, clay expansion was clearly slowed down (Figure 5-1 and Figure 5-2) but not stopped. Longer experimental times are needed to verify if they will stop as well. Erosion steady state was observed as well in other erosion experiments (Alonso et al. 2018). Therefore, some mechanisms are hindering continuous clay expansion in fractures.

In **smooth fractures**, wall friction is not a dominant mechanism slowing down or restricting particle expansion. The **fracture aperture** was demonstrated to be a relevant parameter on clay expansion, as revealed from the comparison of the expansion behaviour of Nanocor®, MX-80 and Ca-MX-80 within smooth fractures of different apertures.

Figure 6-1 shows the average radial expansion, the expanded mass experienced and the final electric conductivity (E.C.) of the equilibrium water measured on different tests, as a function of the fracture aperture . Initial water solution was in all cases NaCl 10^{-3} M (E.C. ≈ 100 $\mu S \cdot cm^{-1}$). It can be seen that both the distance and the expanded mass increased fairly linearly with the fracture aperture. In this case, measured E.C. were higher at smaller apertures, as expected considering a higher solid to liquid ratio (s:l). It is also noteworthy that the expansion experienced by Nanocor® clay was higher (in distance and in expanded mass) at all apertures analysed.

In **rough fractures,** the aperture concept does not apply and comparison must be done with equivalent fracture volumes. In these experiments the analysed roughness compared to smooth fractures with wider apertures (1 mm and 1.7 mm). It was again verified that Nanocor® experienced higher expansion than raw MX-80, most probably due to the fact that it is Na-rich clay (Table 3-3). Expansion was hindered within the fracture with tow rough surfaces compared to the case in which only one surface was rough, but the differences were not very pronounced, especially for MX-80 (Figure 5-19 and Figure 5-20).

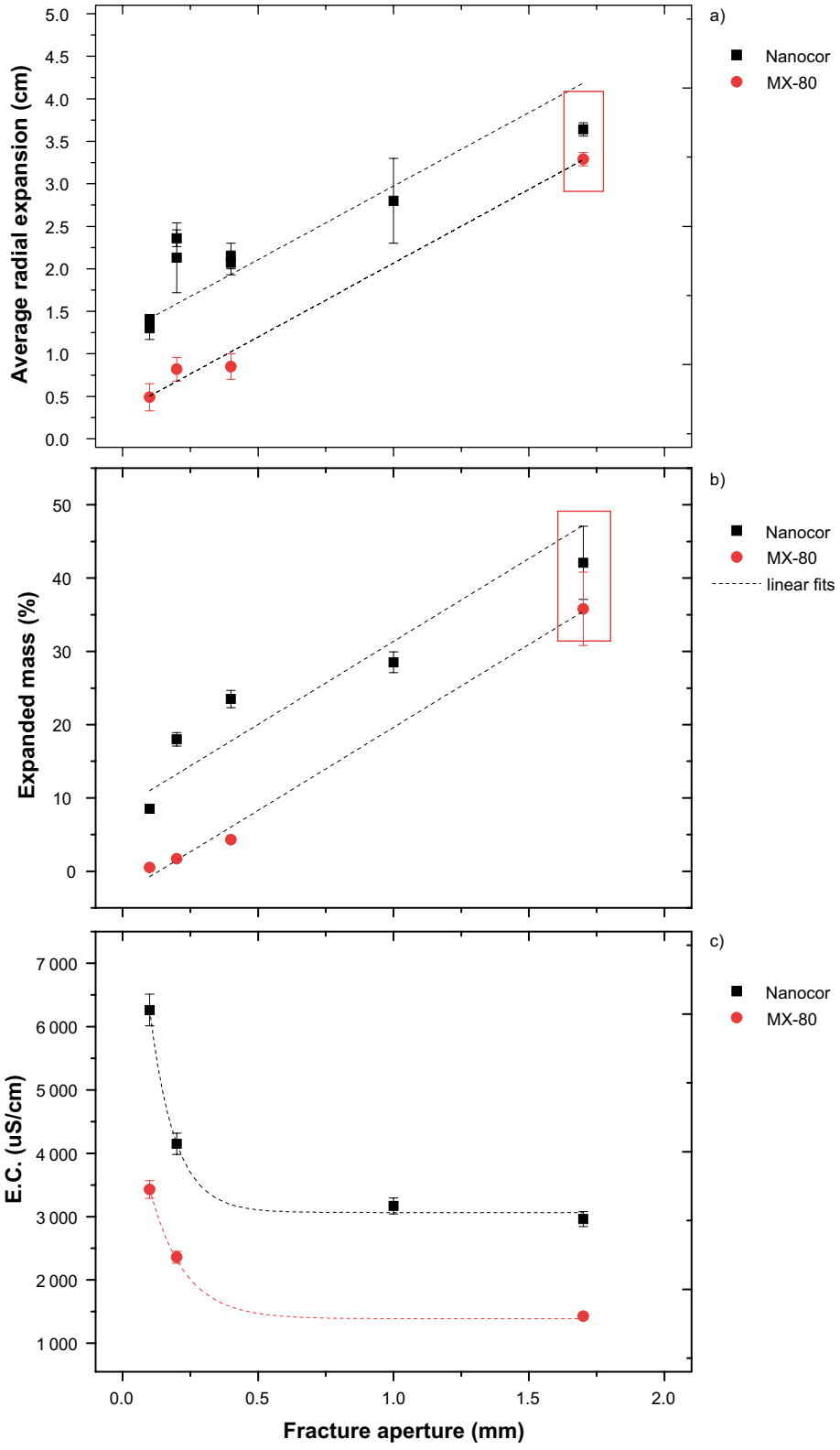

Figure 6-1. *a) Average radial expansion and b) expanded mass (in %) experienced by Nanocor® and MX-80 clays within smooth fractures of different apertures. The red square indicates the two tests where steady state was not fully reached in 30 days.*

Sedimentation experiments were carried out within smooth and rough fractures with different bentonites. Under the experimental conditions analysed, expanded patterns and expanded masses did not vary at different slopes (Figure 5-23 and Figure 5-29), but only in certain cases particle fall down streams along fracture slope were observed.

Sedimentation along fracture slope was only observed within wider fracture apertures (smooth fractures > 0.4 mm) or wider fracture volumes, i.e. in rough fractures.

Fracture aperture was demonstrated to be a relevant parameter on sedimentation process. In experiments carried out within **smooth fractures with small apertures** (0.2 mm) with MX-80, Nanocor®, at different initial ionic strengths, sediment along fracture slope was not observed.

However, **clay sedimentation along fracture slope** was clearly observed in the tests carried out with Nanocor® within fractures of 1 mm aperture (Figure 5-28 and Figure 5-29).

In previous sedimentation experiments reported in Schatz and Akhanoba (2016), carried out within an sloped fracture of 0.1 mm aperture under flow conditions (Test 48 in Schatz and Akhanoba 2016), some solid material lost along slope direction was observed. It was pointed out that "the released mass" seemingly begins to adhere/deposit and spread/collect along the fracture surfaces, without producing significant clay deposition at the bottom of the fractures". However, in experiments carried out with Na-montmorillonite, within fractures of 1 mm aperture (Schatz and Akhanoba 2016), particle sedimentation along fracture sloped was always observed, as well as in our case. Differences can be attributed to diverse experimental conditions.

In our experiments, even when significant deposition was appreciated, the fraction of clay deposited during 30 days was only a 3.4 % of the initial mass at 45° slope and 7.5 % at 90 °. In fact, despite the particle sedimentation stream along fracture direction, the extrusion pattern continued being rather homogenous (Figure 5-28).

Present sedimentation tests were carried out at lower compaction density than in Schatz and Akhanoba (2016), so that lower swelling pressures may be expected. This comparison suggests that applied conditions favour the cohesion of clay particles and their resistance to fall down.

Sedimentation was not observed with Ca-MX-80 within narrow fracture apertures (0.1, 0.2 and 0.4 mm) (Figure 5-27). In Schatz and Akhanoba (2016) Ca-rich clays sediment within wider apertures (1 mm). Overall results indicate that the fracture aperture is a very relevant parameter on sedimentation.

In rough fractures, sedimentation along fracture slope was clearly appreciated for MX-80 and Na-MX-80 both at 45° and at 90° slope. However, no sedimentation as appreciated for Ca-MX-80 (Figure 5-34). With MX-80 deposited fraction varied, being a 1.4 % at 90° to 6.8 % at 45 %. However, with Na-MX-80 clay deposited fraction was, at both slopes analysed, around a 3 % of the initial mass installed (Table 5-8). In general, clay sedimentation behaviour was equivalent at 45° or 90° fracture slope. However, results showed that the clay nature is also playing a role in sedimentation behaviour.

The effect of **clay type** on erosion process was analysed in detail within smooth horizontal fractures of 0.2 mm aperture (Figure 5-5) with different raw clays (Nanocor, MX-80, Ibeco, MCA-C saponite and Ca-MX-80), which all have an smectite content higher than a 75 %. Figure 6-2 presents the average expansion experienced by the different clays, as a function of their Na^+ content in exchangeable positions. It is noteworthy that a clear relationship between the expansion and the Na^+ content is not a appreciated, and it is most probably related to the different water conditions. The final electric conductivity (E.C. in $\mu S \cdot cm^{-1}$) measured on each test is indicated in the figure.

In Missana et al. (2018b), free dispersion of different natural bentonites was analysed in deionised water (solid to liquid ratio, s:L = 1 $g \cdot L^{-1}$), quantification of their colloidal fraction (particles with diameters < 1 mm) as an indication of their maximum erodibility. Colloid releases were higher from those clays with higher smectite and higher Na^+ content. Maximum colloid release was measured for Nanocor® clay, followed by MX-80 and, by far, for Ibeco or MCA-C clay, being ordered by their smectite content and by their Na concentration in exchangeable positions.

In contrast, under confined conditions (Alonso et al. 2018), where the solid to liquid ratio was higher (s:l ~ 20 $g \cdot L^{-1}$) than under dispersed conditions, comparable erosion was measured for Nanocor®, MX-80 or Ibeco, but it was negligible for MCA-C. This behaviour was related to the chemical conditions stablished at equilibrium. In the present experiments solid to liquid ratio is higher than 700 $g \cdot L^{-1}$ (considering an aperture of 0.2 mm) so that salt dissolution causes an effect on water chemistry, more pronounced than in previous studied cases.

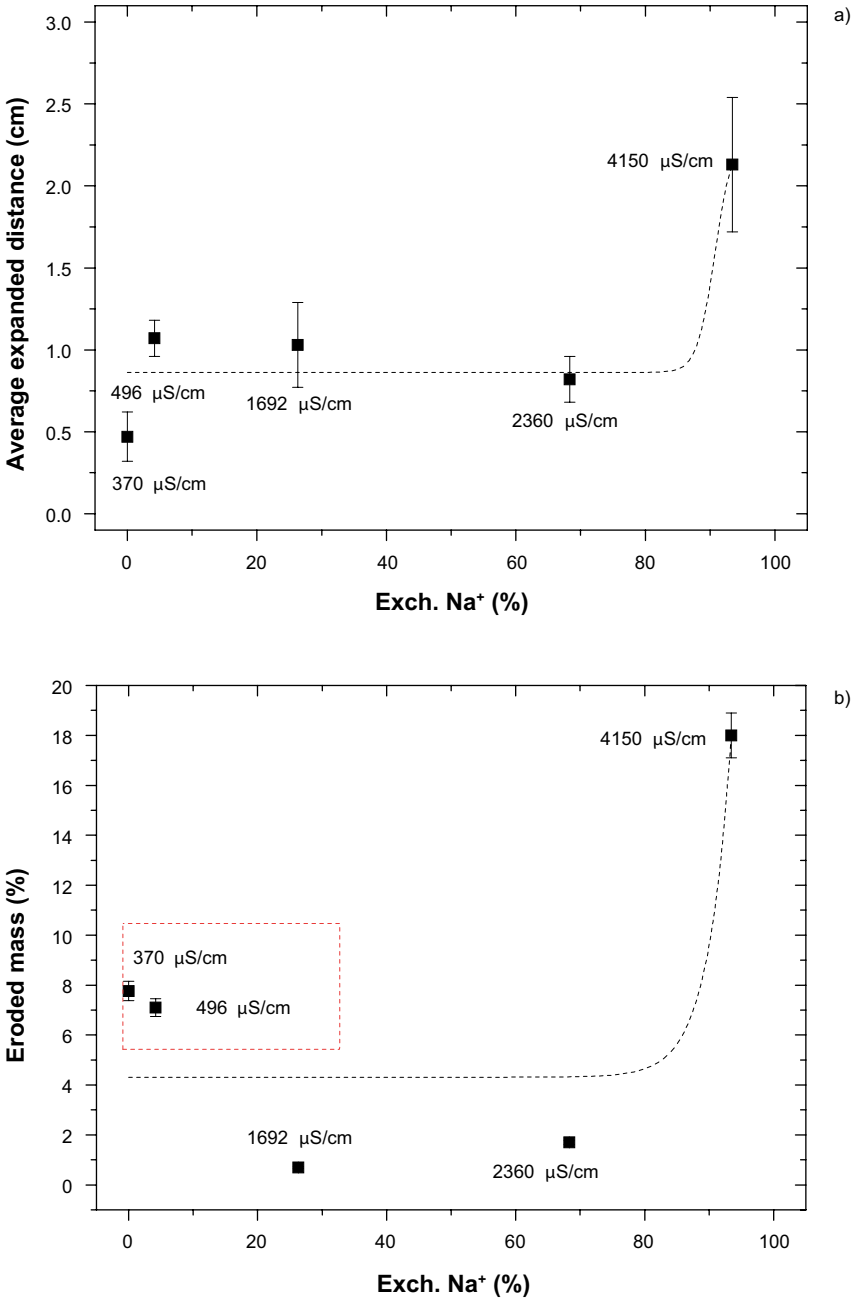

Figure 6-2. *Average radial expansion experienced by different clays within smooth fractures of 0.2 mm, as a function of the exchangeable Na^+ content (%). The final electric conductivity of each test is indicated in the figure (in $\mu S \cdot cm^{-1}$). Line is plotted to guide the eye.*

The **relevance of accessory minerals and of soluble salts** on erosion process was also pointed out by the comparison of the erosion behaviour of raw MX-80, salt-free and minerals-salt free-MX-80 fractions (Figure 5-10 and Figure 5-12). In previous experiments (Reid et al. 2015) the presence of this dark outer ring was attributed to the accumulation of accessory minerals, acting as clay filters which could stop clay expansion. In our studies, an enriched region of accessory minerals at the edge of expanded clay was not appreciated in any case (Section 5.2.3) and results suggested that the outer ring is formed by a clay cake. When particles are far enough from the pellet surface, the compaction density is reduced contributing to slow down or stop the expansion. Moreover, considering that bentonite is a plastic material, at some point, inter-particle forces may be favoured promoting the particles growing and increasing the resistance to movement. The fact that chemical conditions established at equilibrium, were generally of high ionic strength, can definitely additionally contribute to favour particle aggregation (Missana et al. 2018a).

Results showed that, not only the equilibrium water, but also the **initial water chemical conditions** were playing a role. Figure 6-3a shows the average expansion experienced by Nanocor®, as a function of the initial ionic strength (NaCl in M), within smooth fractures of 0.2 mm aperture at two different slopes 0° and 45° slope, corresponding to tests shown in Figure 5-4.

Figure 6-3b presents the expanded masses. In can be seen that, at both fracture slopes, results are comparable and that both the average extrusion distance and the expanded masses decreased exponentially (logarithmic scale) with the initial ionic strength, pointing out the relevance of initial water conditions on erosion process. it has to be noted that final ionic strength increased in comparison to initial values, so that soluble salts dissolution took place in any case.

Results obtained from several erosion experiments carried out under different experimental conditions led to the conclusion that a salinity higher than $1–2 \times 10^{-2}$ M (in Na) inhibits the erosion process (Missana 2016, Schatz and Akhanoba 2016).

According to (Birgersson et al. 2009), montmorillonites do not suffer erosion when the external ionic strength is higher than 4×10^{-3} M, for Na-bentonites, or higher than 2.5×10^{-3} M for mixed Na/Ca montmorillonites ($Ca^{2+} > 20$ %).

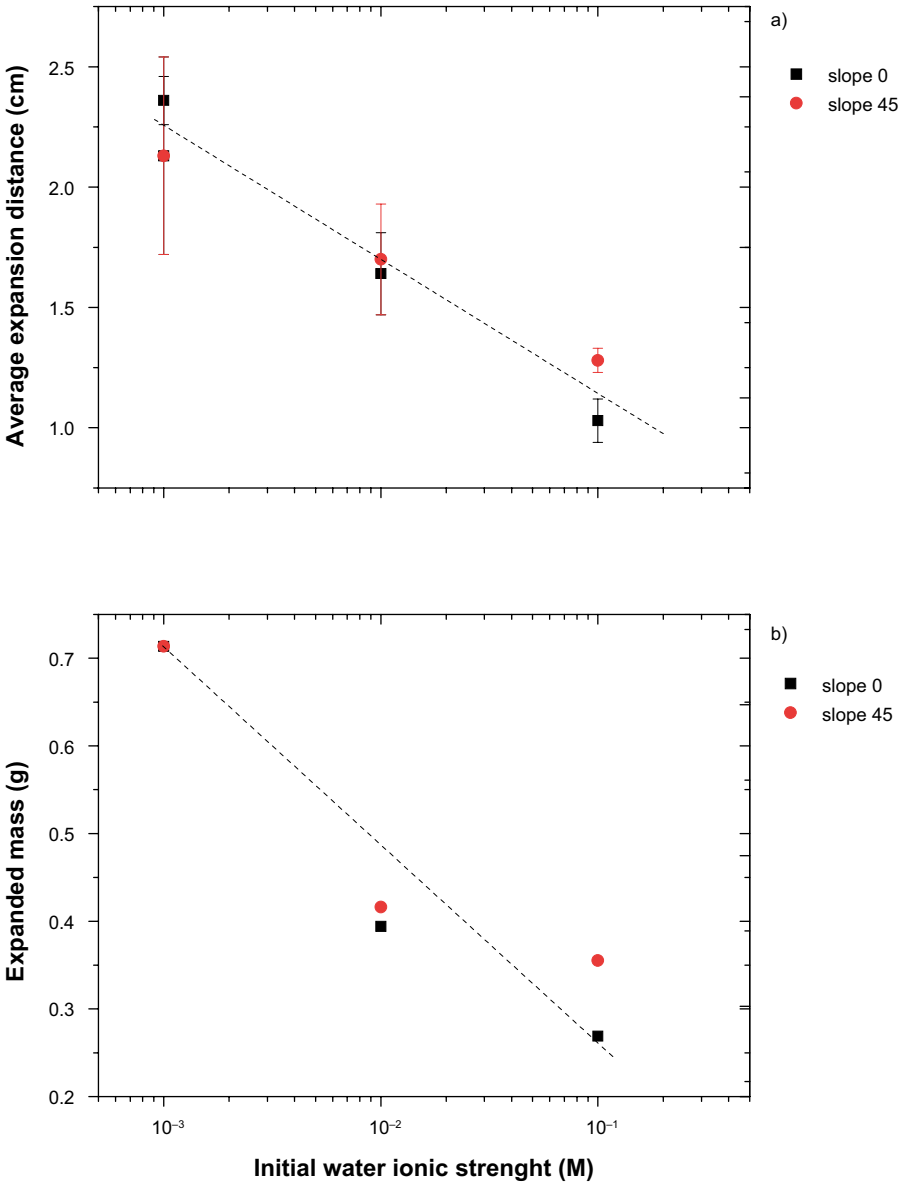

Figure 6-3. *Erosion experienced by Nanocor® within smooth fractures of 0.2 mm aperture at 0° and 45° slope: a) Average radial expansion and b) expanded mass as a function of the initial water ionic strength.*

The possibility that initial water conditions evolved, from higher to lower ionic strengths, was implicitly analysed in **flow experiments** carried out both in smooth (Section 5.6) and rough fractures (Section 5.7). In all cases, flow conditions were applied after a previous expansion period under stagnant conditions. This implied that at the beginning of flow experiments ionic strength were in all cases high (Figure 5-44 and Figure 5-48). In all cases the arrival of fresh water, and the subsequent decrease in ionic strength, promoted longer clay expansion. However, the mobilisation of particles with the water flow was very limited, and clay eluted fraction was in all cases very low (lower than a 0.02 % of the initial mass installed.

7 Conclusions

The erosion behaviour of compacted bentonite was experimentally studied under different physico-chemical conditions.

The main physical variables analysed were: fracture roughness (smooth or rough), aperture (from 0.1 to 1.7 mm) and slope (horizontal to vertical). The erosion behaviour of Na-rich bentonites (Nanocor® and Wyoming MX-80) was mainly analysed, and compared to that of Na- or Ca-exchanged MX-80. Some experiments were also carried out with a Ca–Mg bentonite (Ibeco) and a Spanish saponite (MCA-C). Most of the experiments were carried out with 1 mM NaCl as initial electrolyte, but higher onic strengths were analysed as well.

In the experiments, the clay extrusion in the fracture was followed during 30 days, periodical photographs were taken to measure extrusion distances. Eroded masses and physico-chemical evolution were evaluated by post-mortem analyses.

All erosion experiments carried out within narrow fractures with apertures smaller than 1 mm, showed that clay extrusion in the facture was stopped at some time. Clay expansion was favoured within fractures of wider apertures.

In general, Na-rich bentonites (Nanocor® or Na-exchanged MX-80) exhibited longer extrusion distances than raw MX-80 or Ibeco. Extrusion distances measured for Ca- exchanged bentonites, or other clays as saponite, were clearly shorter, but not null. As suggested by previous studies, which related clay erosion capability to its intrinsic characteristics, the relevance of clay properties is again pointed out.

Each clay established particular chemical conditions, mainly induced by soluble salt dissolution, which generally led to significant increases of water ionic strengths. The water chemistry established at equilibrium plays a major role on erosion.

Particle sedimentation along fracture slope was not detected in smooth fractures with apertures thinner than 0.4 mm, but particle sedimentation streams were observed within smooth fractures of 1 mm aperture and within rough sloped fractures, whose equivalent apertures were wider than 1 mm. Sedimentation behaviour within smooth and rough fractures was dependent on the clay nature: Na-rich bentonites sediment along fracture slope almost from the beginning. In contrast, sedimentation of Ca-rich bentonites was not detected under experimental conditions. In any case, the deposited fraction, under experimental conditions, was always lower than a 6 % of the initial mass.

The effect that accessory minerals and soluble salts have on clay erosion processes was analysed in detail by comparing the expansion behaviour of raw MX-80, salt-free MX-80 and minerals&salt-free MX-80,. Physico-chemical analyses of their corresponding extruded rings within the fracture was conclusive. Coarse mineral fractions can effectively restrict clay extrusion in narrow fractures; however, an enriched region with accessory minerals was not identified in the edge of the extruded clay. Instead, the smectite particles themselves accumulate and form a filter, which is able to stop further particle expansion.

Erosion by flow was analysed after a previous expansion period of 30 days under stagnant conditions, so that the clay had previously extruded in the fractures. Applying flow velocities in the range of 10^{-7}–10^{-6} $m \cdot s^{-1}$, fresh water is provided and the ionic strength decreased, an additional clay expansion was measured. The mass of eluted particles was lower than a 0.02 % of the initial mass, indicating that particle mobilization in the water flow, under studied conditions, was clearly restricted, even though additional expansion was measured.

In all the tests, the major role of water chemistry established at the equilibrium was evidenced.

References

SKB's (Svensk Kärnbränslehantering AB) publications can be found at www.skb.com/publications.

Albarran N, Degueldre C, Missana T, Alonso U, García-Gutiérrez M, López T, 2014. Size distribution analysis of colloid generated from compacted bentonite in low ionic strength aqueous solutions. Applied Clay Science 95, 284–293.

Alonso U, Missana T, García-Gutiérrez M, 2007. Experimental approach to study the colloid generation from the bentonite barrier to quantify the source term and to assess its relevance on the radionuclide migration. MRS Online Proceedings Library 985: Scientific Basis for Nuclear Waste Management XXX, 605–610.

Alonso U, Missana T, Fernandez A M, García-Gutiérrez M, 2018. Erosion behaviour of raw bentonites under compacted and confined conditions: relevance of smectite content and chemical equilibrium. Applied Geochemistry 94, 11–20.

Ammann L, Bergaya F, Lagaly G, 2005. Determination of the cation exchange capacity of clays with copper complexes revisited. Clay Minerals 40, 441–453.

Bessho K, Degueldre C, 2009. Generation and sedimentation of colloidal bentonite particles in water. Applied Clay Science 43, 253–259.

Baik M-H, Cho W-J, Hahn P-S, 2007. Erosion of bentonite particles at the interface of a compacted bentonite and a fractured granite. Engineering Geology 91, 229–239.

Bradbury M H, Baeyens B, 2009. Experimental and modelling studies on the pH buffering of MX-80 bentonite porewater. Applied Geochemistry 24, 419–425.

Birgersson M, Börgesson L, Hedström M, Karnland O, Nilsson U, 2009. Bentonite erosion. Final report. SKB TR-09-34, Svensk Kärnbränslehantering AB.

Birgersson M, Hedström M, Karnland O, 2011. Sol formation ability of Ca/Na-montmorillonite at low ionic strength. Physics and Chemistry of Earth 36, 1572–1579.

Cuevas J, Pelayo M, Rivas P, Leguey S, 1993. Characterization of Mg-clays from the Neogene of the Madrid Basin and their potential as backfilling and sealing material in high level radioactive waste disposal. Applied Clay Science 7, 383–406.

Degueldre C, Benedicto A, 2012. Colloid generation during water flow transients. Applied Geochemistry 27, 1220–1225.

Fernández A M, Baeyens B, Bradbury M, Rivas P, 2004. Analysis of porewater chemical composition of a Spanish compacted bentonite used in engineered barrier. Physics and Chemistry of the Earth 29, 105–118.

Fernández A M, Missana T, Alonso U, Rey J J, Sánchez-Ledesma D M, Melón A, Robredo L M, 2017. Characterisation of different bentonites in the context of BELBaR Project (Bentonite erosion: effects on the long term performance of the engineered barrier and radionuclide transport). CIEMAT Technical Report, Spain.

García-García S, Degueldre C, Wold S, Frick S, 2009. Determining pseudo-equilibrium of montmorillonite colloids in generation and sedimentation experiments as a function of ionic strength, cationic form, and elevation. Journal of Colloids and Interface Science 335, 54–61.

Grissinger E H, 1966. Resistance of selected clay systems to erosion by water. Water Resources Research 2, 131–138.

Hedstrom M, Birgersson M, Nilsson U, Karnland O, 2011. Role of cation mixing in the sol formation of Ca/Na-montmorillonite. Physics and Chemistry of Earth 36, 1564–1571.

Hedström M, Ekvy Hansen E, Nilsson U, 2016. Montmorillonite phase behaviour: Relevance for buffer erosion in dilute groundwater. SKB TR-15-07, Svensk Kärnbränslehantering AB.

Holthoff H, Egelhaaf S U, Borkovec M, Schurtenberger P, Sticher H, 1996. Coagulation rate measurements of colloidal particles by simultaneous static and dynamic light scattering. Langmuir 12, 5541–5549.

Kallay N, Barouch E, Matijevic E, 1987. Diffusional detachment of colloidal particles from solid/solution interfaces. Advances in Colloid and Interface Science 27, 1–42.

Karnland O, 2010. Chemical and mineralogical characterization of the bentonite buffer for the acceptance control procedure in a KBS-3 repository. SKB TR-10-60, Svensk Kärnbränslehantering AB.

Karnland O, Birgersson M, Hedström M, 2011. Selectivity coefficient for Ca/Na ion exchange in highly compacted bentonite. Physics and Chemistry of Earth 36, 1554–1558.

Kaufhold S, Dohrmann R, 2008. Detachment of colloidal particles from bentonites in water. Applied Clay Science 39, 50–59.

Kaufhold S, Dohrmann R, 2016. Distinguishing between more and less suitable bentonites for storage of high-level radioactive waste. Clay Minerals 51, 89–302.

Koch D, 2002. Bentonites as a basic material for technical base liners and site encapsulation cut-off walls. Applied Clay Science 21, 1–11.

Koch D, 2008. European bentonites as alternatives to MX-80. Science & Technology Series 334, 23–30.

Ledin A, Karlsson S, Düker A, Allard B, 1993. Applicability of photon correlation spectroscopy for measurement of concentration and size distribution of colloids in natural waters. Analytica Chimica Acta 281, 421–428.

Liu L, 2010. Permeability and expansibility of sodium bentonite in dilute solutions. Colloids and Surfaces A: Physicochemical and Engineering Aspects 358, 68–78.

Liu J, Neretnieks I, 2006. Physical and chemical stability of the bentonite buffer. SKB R-06-103, Svensk Kärnbränslehantering AB.

Liu L, Moreno L, Neretnieks I, 2009. A dynamic force balance model for colloidal expansion and its DLVO-based application. Langmuir 25, 679–687.

Luckham P F, Rossi S, 1999. The colloidal and rheological properties of bentonite suspensions. Advances in colloid and Interface Science 82, 43–92.

Mackenzie R C (ed), 1957. The differential thermal investigation of clays. London: Mineralogical Society.

Missana T, 2016. Evaluation of experimental results on bentonite erosion. BELBaR Project (UE-FP7 295487). Deliverable D2.11. European Commission.

Missana T, Alonso U, Turrero M J, 2003. Generation and stability of bentonite colloids at the bentonite/granite interface of a deep geological radioactive waste repository. Journal of Contaminant Hydrology 61, 17–31.

Missana T, Alonso U, García-Gutiérrez M, Mingarro M, 2008. Role of bentonite colloids on europium and plutonium migration in a granite fracture. Applied Geochemistry 23, 1484–1497.

Missana T, Alonso U, Albarran N, García-Gutiérrez M, Cormenzana J-L, 2011. Analysis of colloids erosion from the bentonite barrier of a high level radioactive waste repository and implications in safety assessment. Physics and Chemistry of the Earth 36, 1607–1615.

Missana T, Alonso U, Fernández A M, García-Gutiérrez M, 2018a. Colloidal properties of different smectitic clays: significance for the bentonite barrier erosion and radionuclide transport in radioactive waste repositories. Applied Geochemistry 97, 157–166.

Missana T, Alonso U, Fernández A M, Lopez T, García-Gutiérrez M, 2018b. Analysis of stability behavior of colloids obtained from different raw bentonites for its implications on erosion processes in the frame of high-level waste repositories. Applied Geochemistry 92, 180–187.

Müller-Vonmoss M, Kahr G, 1983. Mineralogische Untersuchungen von Wyoming Bentonite MX-80 und Montigel. Nagra NTB 83-13, Nagra, Switzerland.

Neretnieks I, Liu L, Moreno L, 2009. Mechanisms and models for bentonite erosion. SKB TR-09-35, Svensk Kärnbränslehantering AB.

Neretnieks I, Moreno L, Liu L, 2017. Clay erosion – impact of flocculation and gravitation. SKB TR-16-11, Svensk Kärnbränslehantering AB.

Norrish K, 1954. The swelling of montmorillonite. Discussions of the Faraday Society 18, 120–134.

Pertsov A V, 2005. Quasi-spontaneous dispersion of solids. Colloid Journal 67, 459–468.

Pusch R, 1999. Clay colloid formation and release from MX-80 buffer. SKB TR-99-31, Svensk Kärnbränslehantering AB.

Pusch R, 2008. Geological storage of radioactive waste: current concepts and plans for radioactive waste disposal. Berlin: Springer.

Pusch R, Karnland O, Sanden T, 1996. Final report of Physical Test program concerning spanish clays (saponites and bentonites). ENRESA Report 02/96, Spain.

Reid C, Lunn R, El Mountassir G, Tarantino A, 2015. A mechanism for bentonite buffer erosion in a fracture with a naturally varying aperture. Mineralogical Magazine 79, 1485–1494.

Richards T, 2010. Particle clogging in porous media. Filtration of a smectite solution. SKB TR-10-22, Svensk Kärnbränslehantering AB.

Richards T, Neretnieks I, 2010. Filtering of clay colloids in bentonite detritus material. Chemical. Engineering Technology 33, 1303–1310.

Rinderknecht F R, 2017. Bentonite erosion and colloid mediated transport of radionuclides in advection controlled systems. PhD thesis. KIT, Germany.

Sawhney B L, 1970. Potassium and cesium ions selectivity in relation to clay mineral structure. Clays and Clay Minerals 18, 47–52.

Schaefer T, Huber F, Seher H, Missana T, Alonso U, Kumke M, Eidner S, Claret F, Enzmann F, 2012. Nanoparticles and their influence on radionuclide mobility in deep geological formations. Applied Geochemistry 27, 390–403.

Schatz T, Akhanoba N, 2016. Buffer erosion in sloped fracture environments. Posiva 2016-13, Posiva Oy, Finland.

Schatz T, Kanerva N, Martikainen J, Sane P, Olin M, Seppälä A, Koskinen K, 2013. Buffer erosion in dilute groundwater. Posiva 2012-44, Posiva Oy, Finland.

Schatz T, Eriksson R, Ekvy Hansen E, Hedström M, Missana T, Alonso U, Mayordomo N, Fernández A M, Bouby M, Heck S, Geyer F, Schäfer T, 2015. WP2 partners final report on bentonite erosion. BELBaR Project (UE-FP7 295487). Deliverable D2.12. European Commission.

Seher H, Albarran N, Hauser W, Götz R, Missana T, Geckeis H, Fanghänel T, Schäfer T, 2009. Colloid generation by erosion of compacted bentonite under different geochemical conditions. In 4th FUNMIG Annual Workshop Proceedings, FZK Report FZKA 7461, Karlsruhe, Germany.

Sellin P, Leupin O X, 2013. The use of clays as an engineered barrier in radioactive-waste management: A review. Clays and Clay Minerals 61, 477–498.

Wersin P, Kiczka M, Koskinen K, 2016. Porewater chemistry in compacted bentonite: Application to the engineered buffer barrier at the Olkiluoto site. Applied Geochemistry 74, 165–175.

Appendix 1

Periodical photographs of all erosion tests (Table 4-1 and Table 4-2) during expansion period

To facilitate the comparison of different tests, the following criteria were generally followed for the presentation of the expansion photographs,

1. A fracture region that covers an area of 7.4 x 7.4 cm^2 is shown when no sedimentation was observed. With this selection it is intended to show a sufficient number of periodic photographs to adequately follow the expansion over time (from 0 to 30 days). The pellet diameter is 1.9 cm in all cases and the scale is indicated with a small ruler.
2. In those cases where the expansion surpassed the region of above mentioned region, the photos are shown expanded to enlarge the area (9.6 x 9.6 cm^2), and the corresponding scale is indicated. In those tests fewer periodic photographs are presented.
3. In those experiments where clay sedimentation was observed, in any direction (i.e. along fracture slope), the photographs were taken including a black sheet, placed underneath the fracture methacrylate. In those cases, not only the extruded area is shown, but the shown regions are extended to the fracture limit, to appreciate sedimentation streams and particle accumulation at the bottom of the sloped fracture.

Test 1A: Nanocor® 1.4 g·cm^{-3} - Slope 0 - Aperture 0.2 mm - NaCl 10^{-3} M

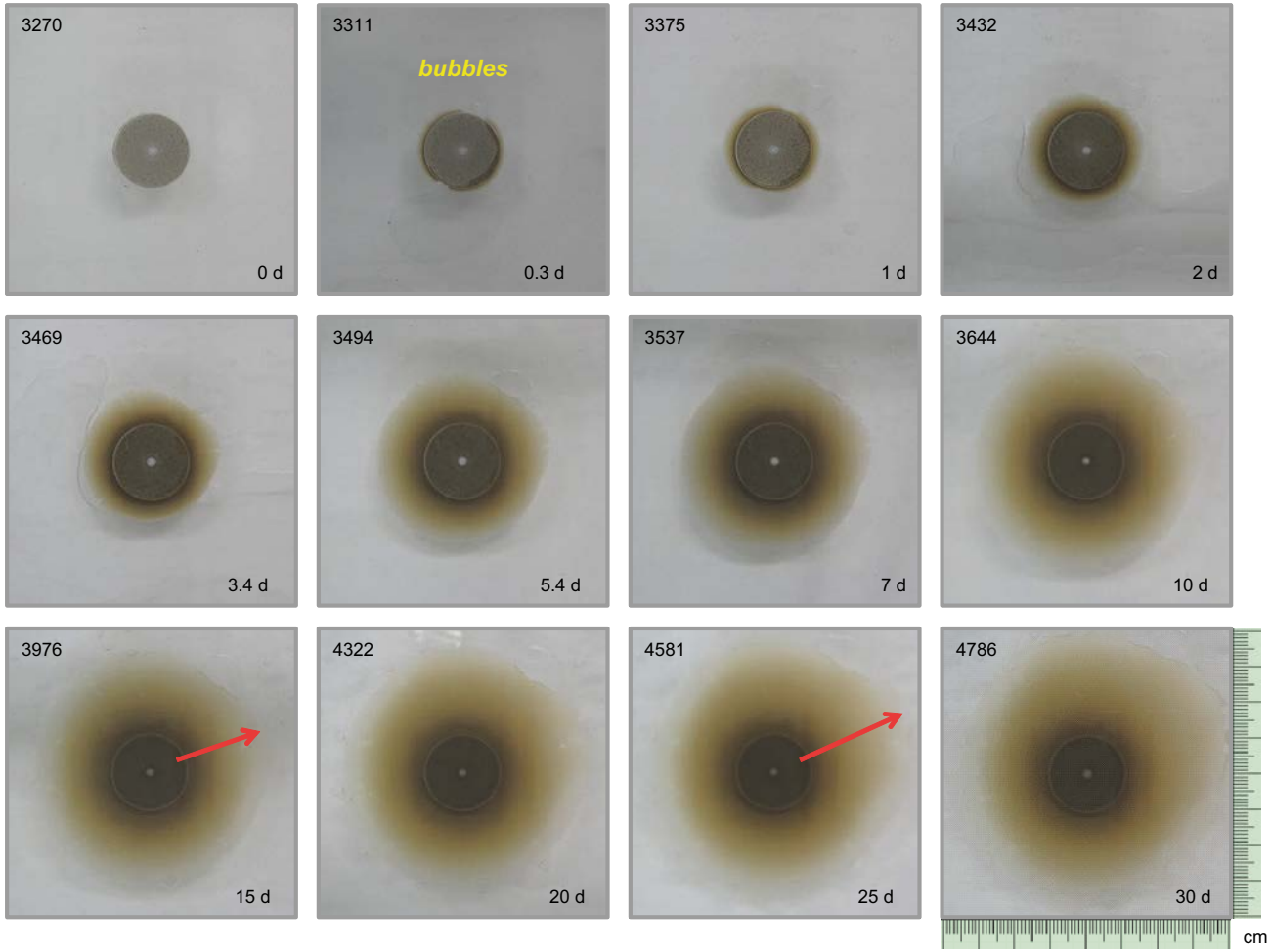

Test 2A: Nanocor® 1.4 g·cm^{-3} - Slope 45º - Aperture 0.2 mm - NaCl 10^{-3} M

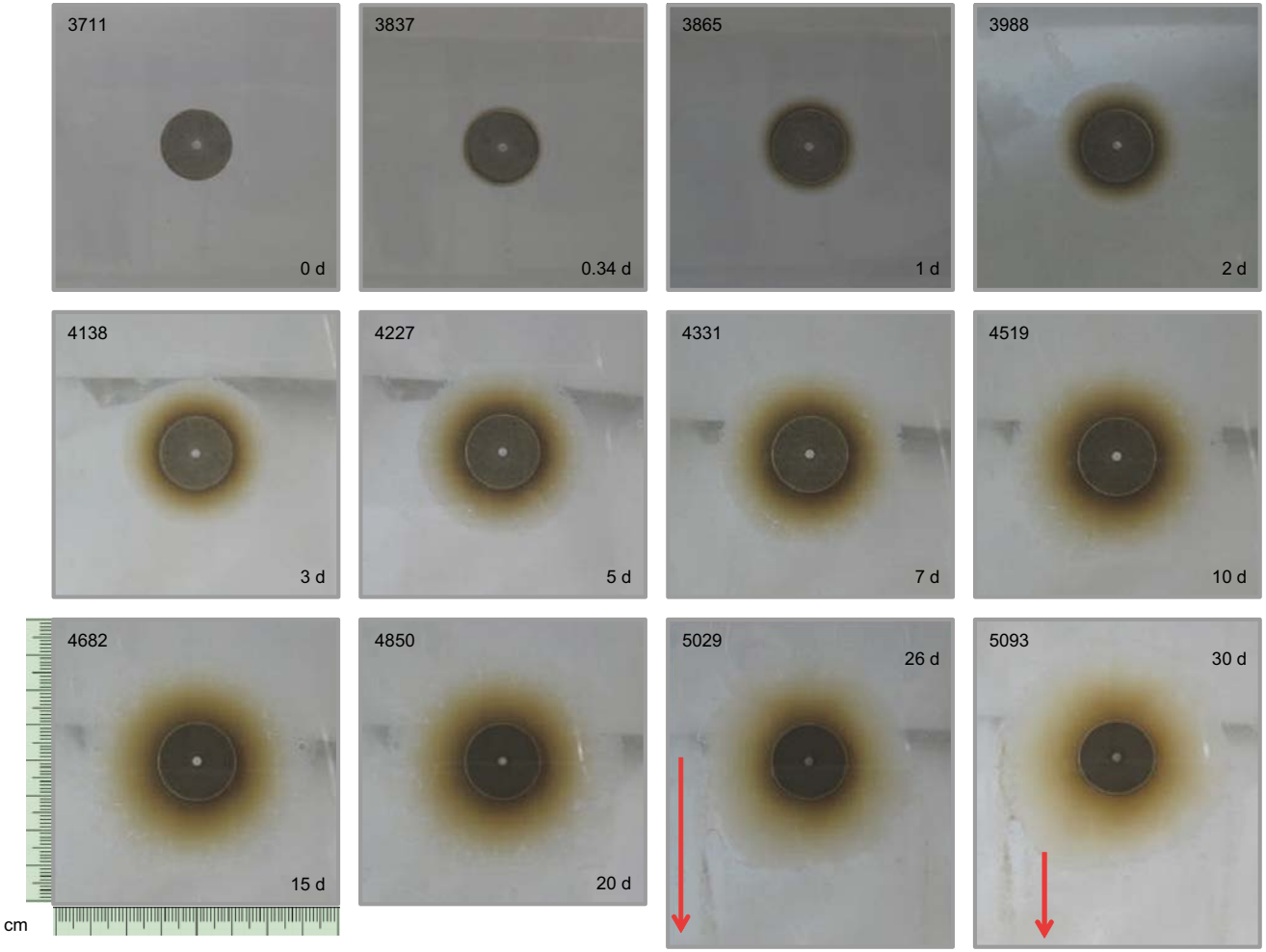

Test 3A: Nanocor 1.4 g·cm^{-3} - Slope 90º - Aperture 0.2 mm - NaCl 10^{-3} M

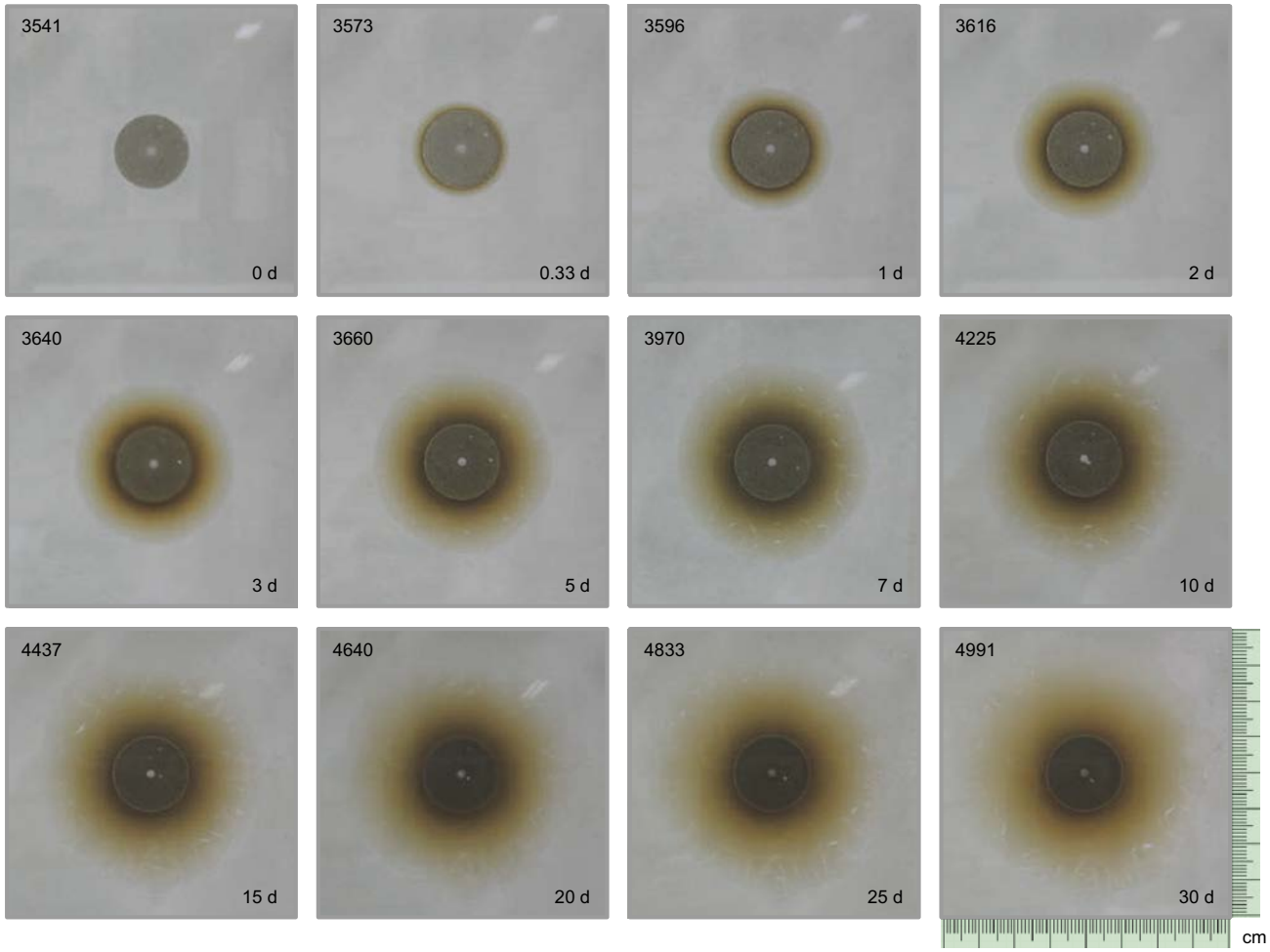

Test 4A: Nanocor® 1.4 g·cm^{-3} - Slope 0º - Aperture 0.1 mm - NaCl 10^{-3} M

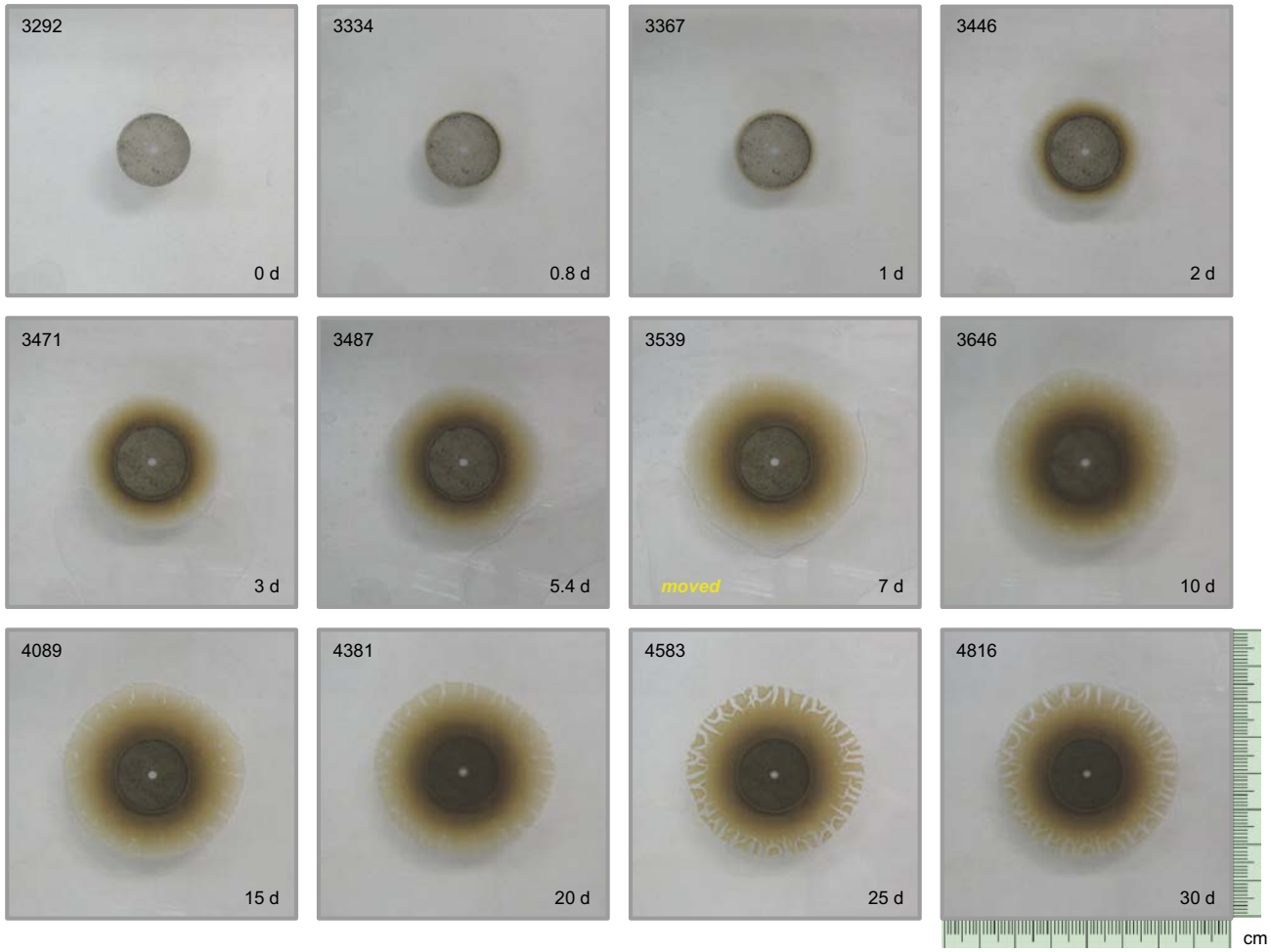

Test 4B: Nanocor® 1.4 g·cm^{-3} - Slope 0º - Aperture 0.1 mm - NaCl 10^{-3} M

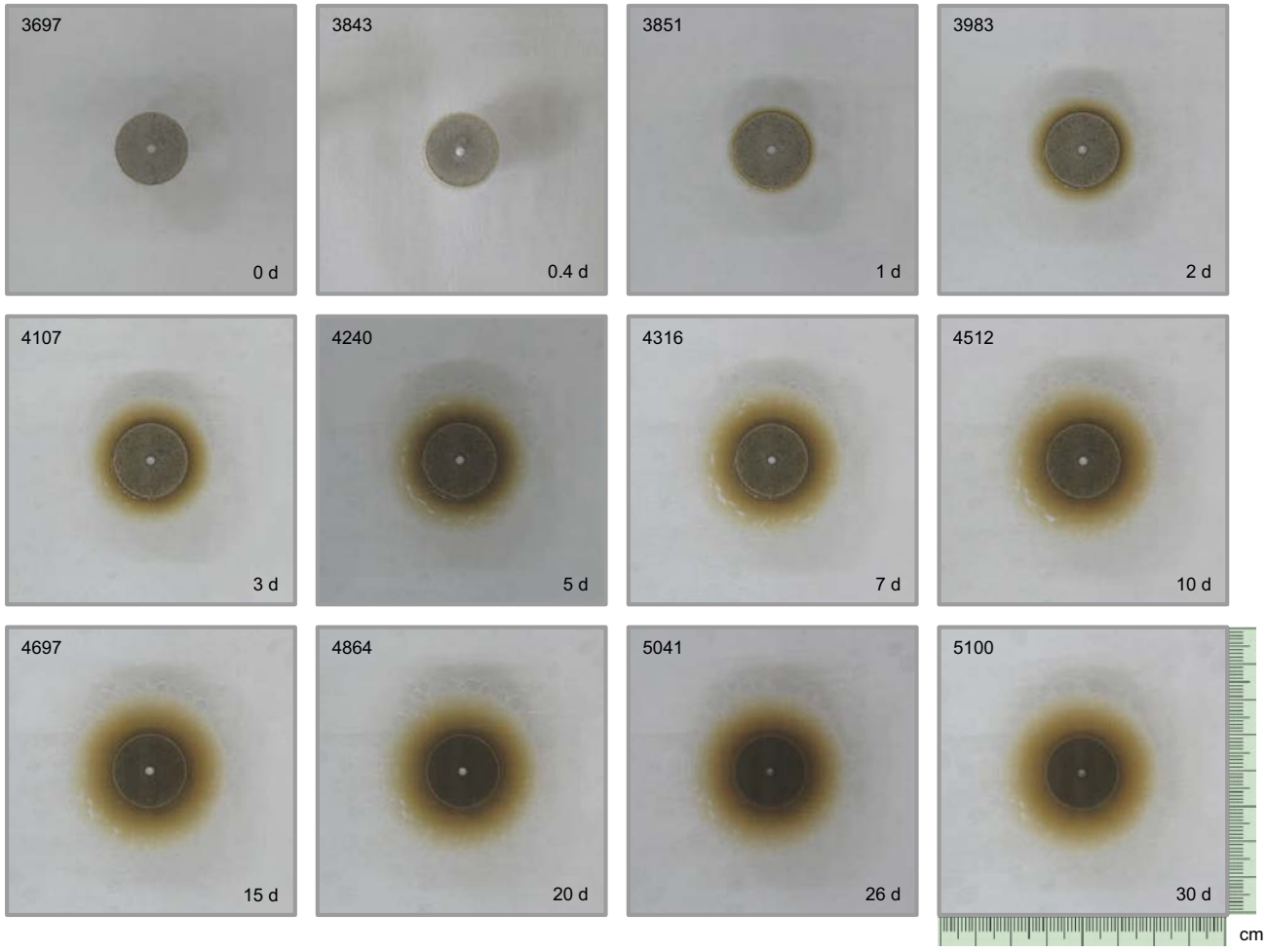

Test 6A: Nanocor® 1.4 g·cm^{-3} - Slope 0º - Aperture 0.2 mm - NaCl 10^{-3} M

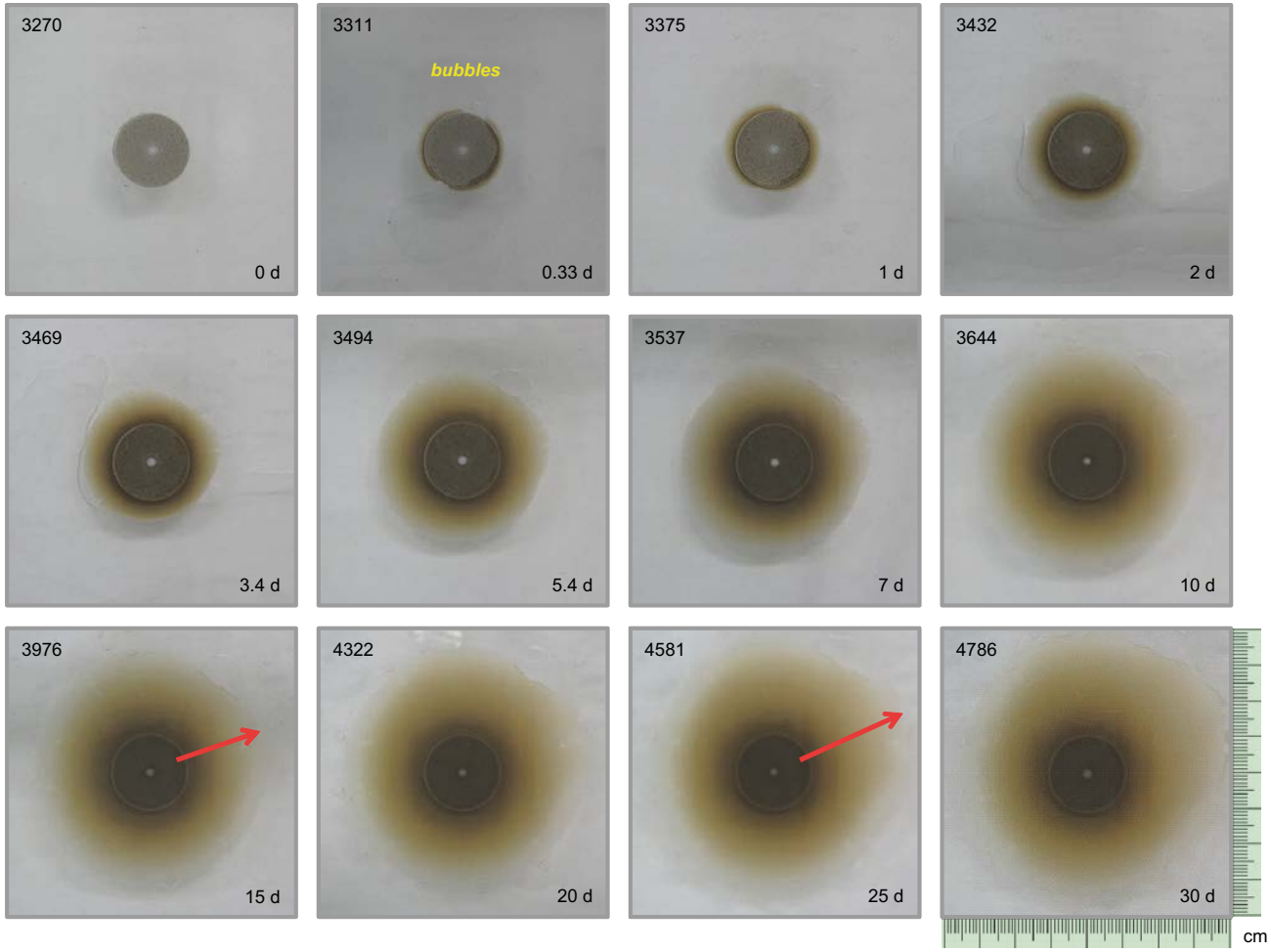

Test 6B: Nanocor® 1.4 g·cm^{-3} - Slope 0º - Aperture 0.2 mm - NaCl 10^{-3} M

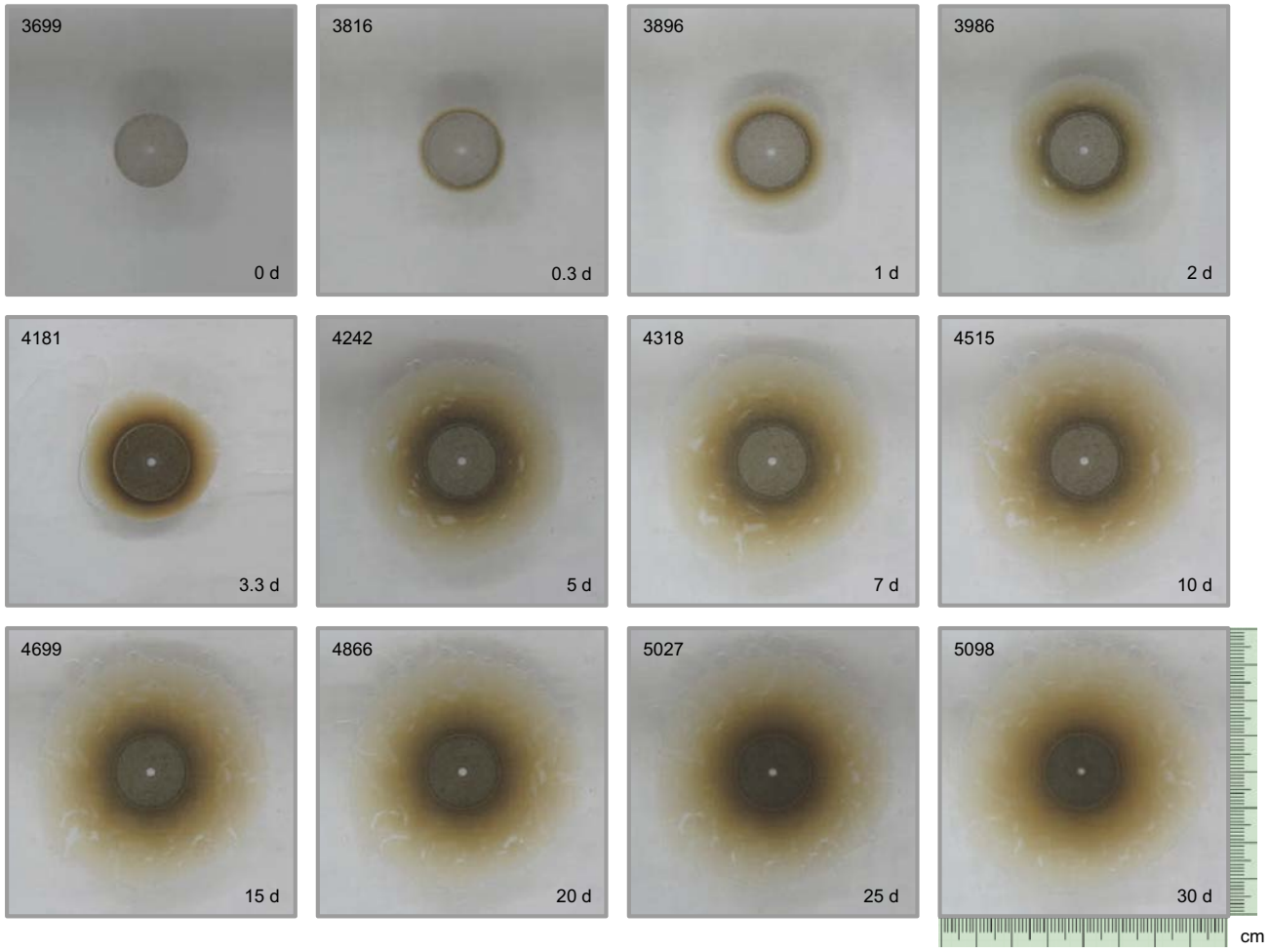

Test 8A: Nanocor® 1.4 g·cm^{-3} - Slope 0º - Aperture 0.4 mm - NaCl 10^{-3} M

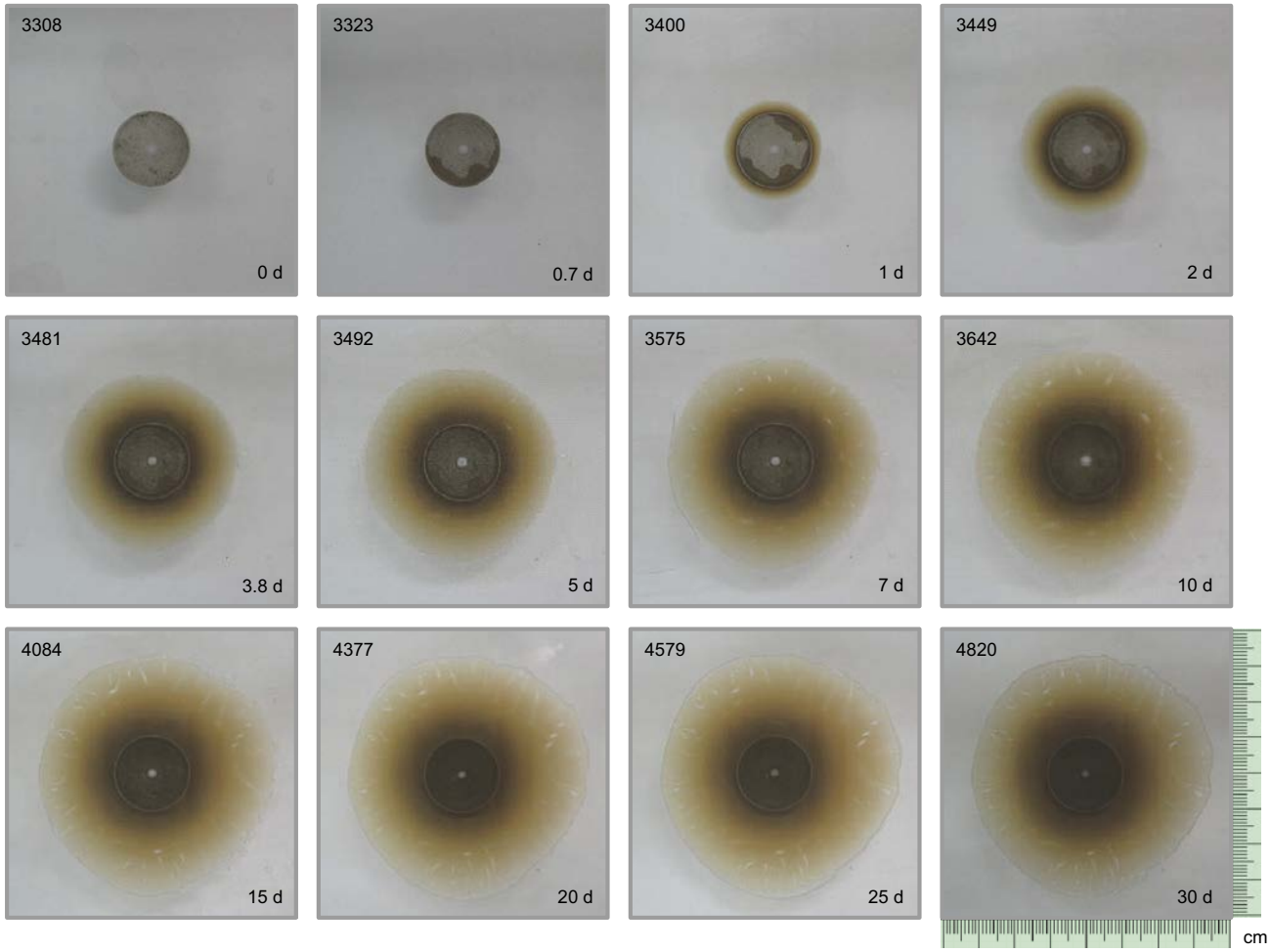

Test 8B: Nanocor® 1.4 g·cm^{-3} - Slope 0º - Aperture 0.4 mm - NaCl 10^{-3} M

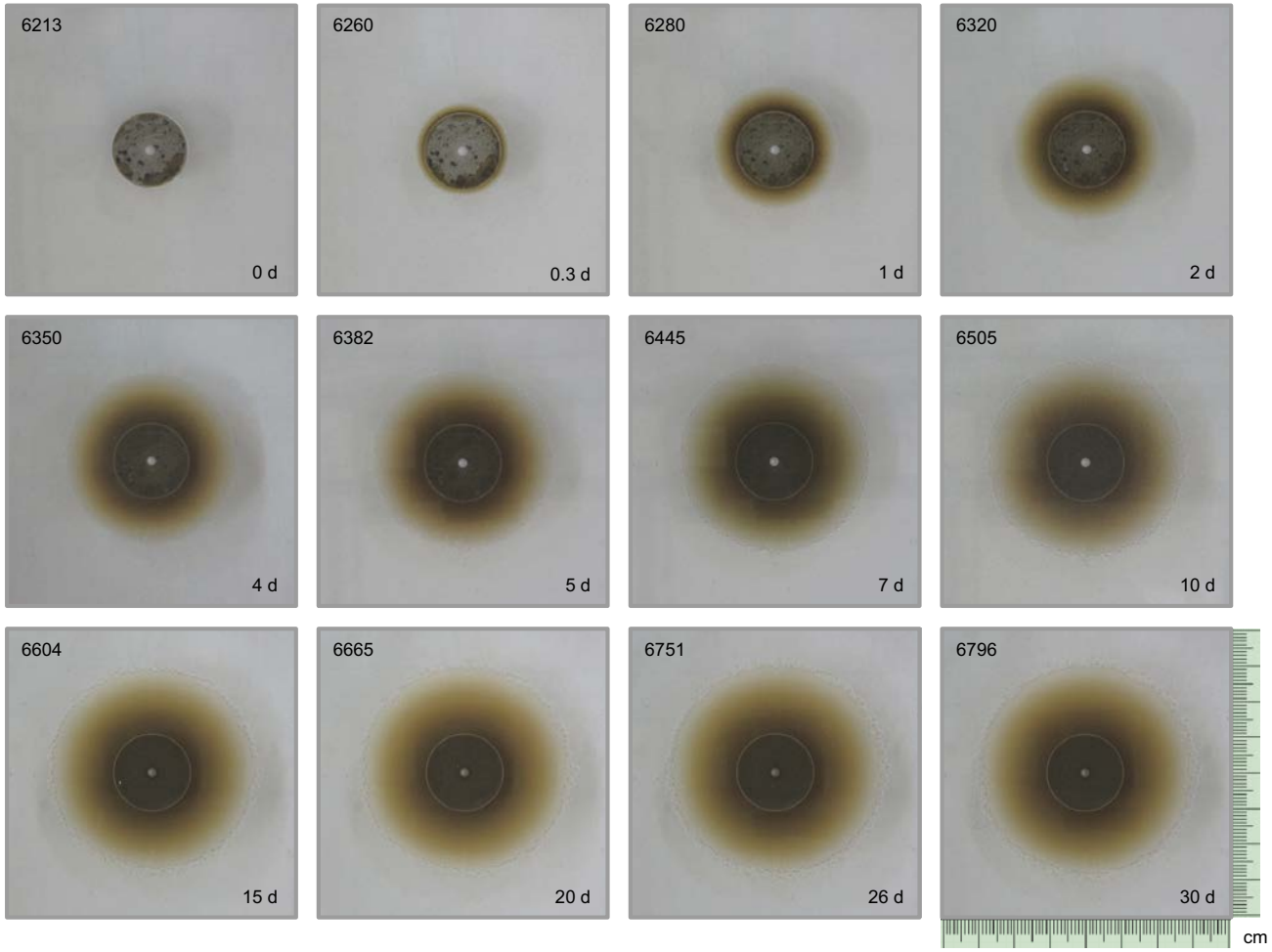

Test 10A: Raw MX-80 1.4 g·cm^{-3} - Slope 0º - Aperture 0.1 mm - NaCl 10^{-3} M

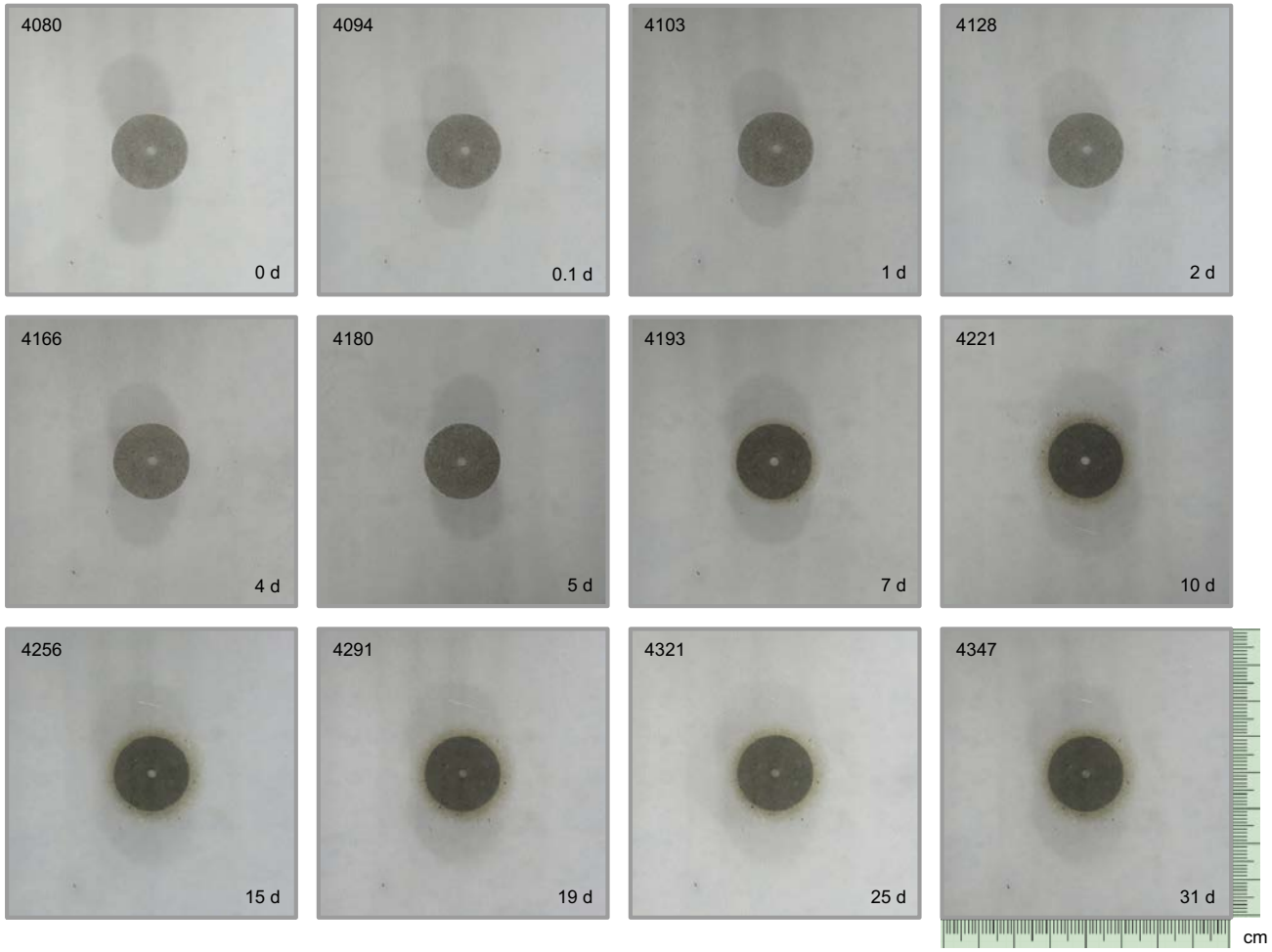

Test 12A: Raw MX-80 1.4 g·cm^{-3} - Slope 0º - Aperture 0.2 mm - NaCl 10^{-3} M

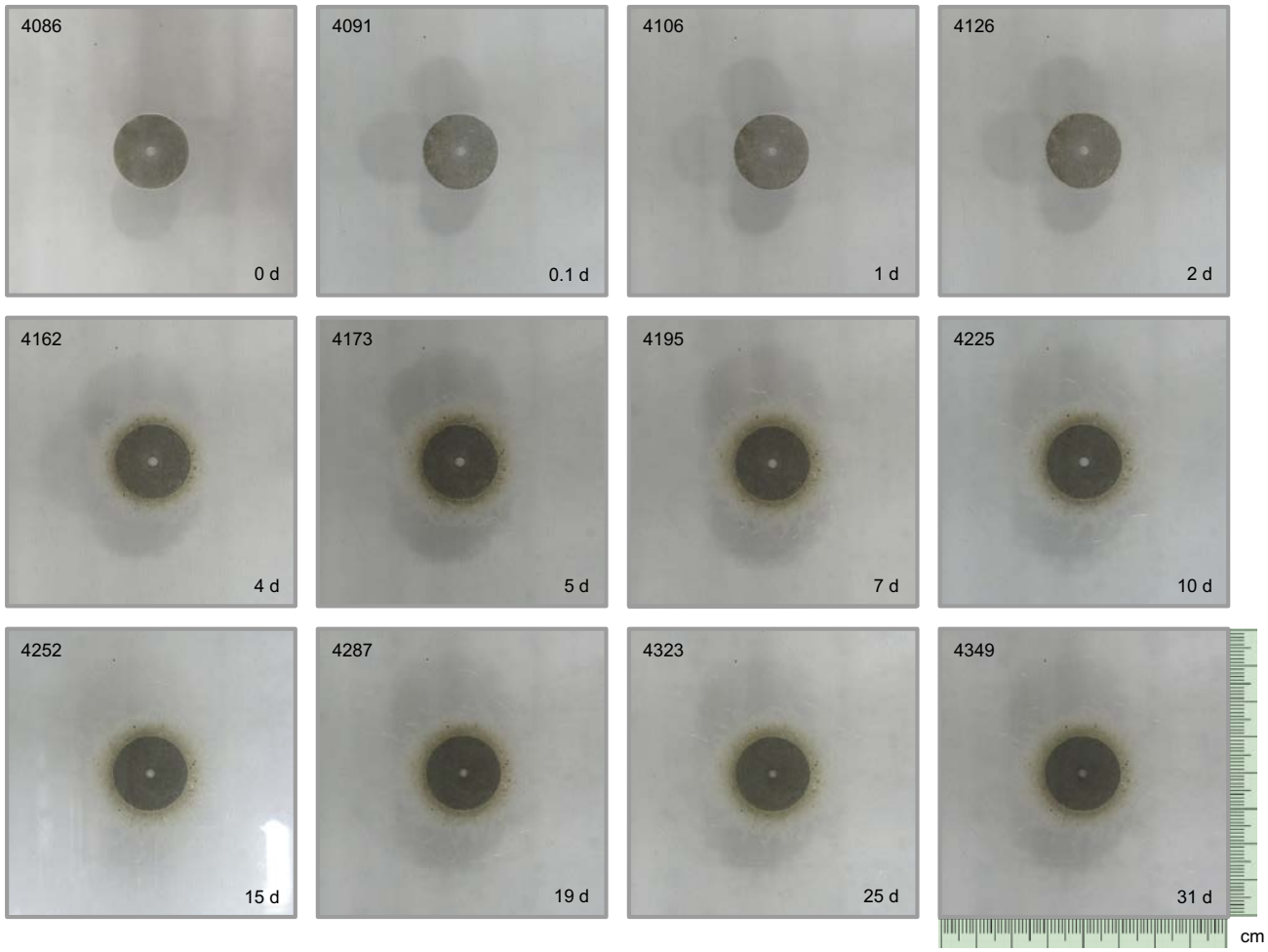

Test 14A: Raw MX-80 1.4 g·cm^{-3} - Slope 0º - Aperture 0.4 mm - NaCl 10^{-3} M

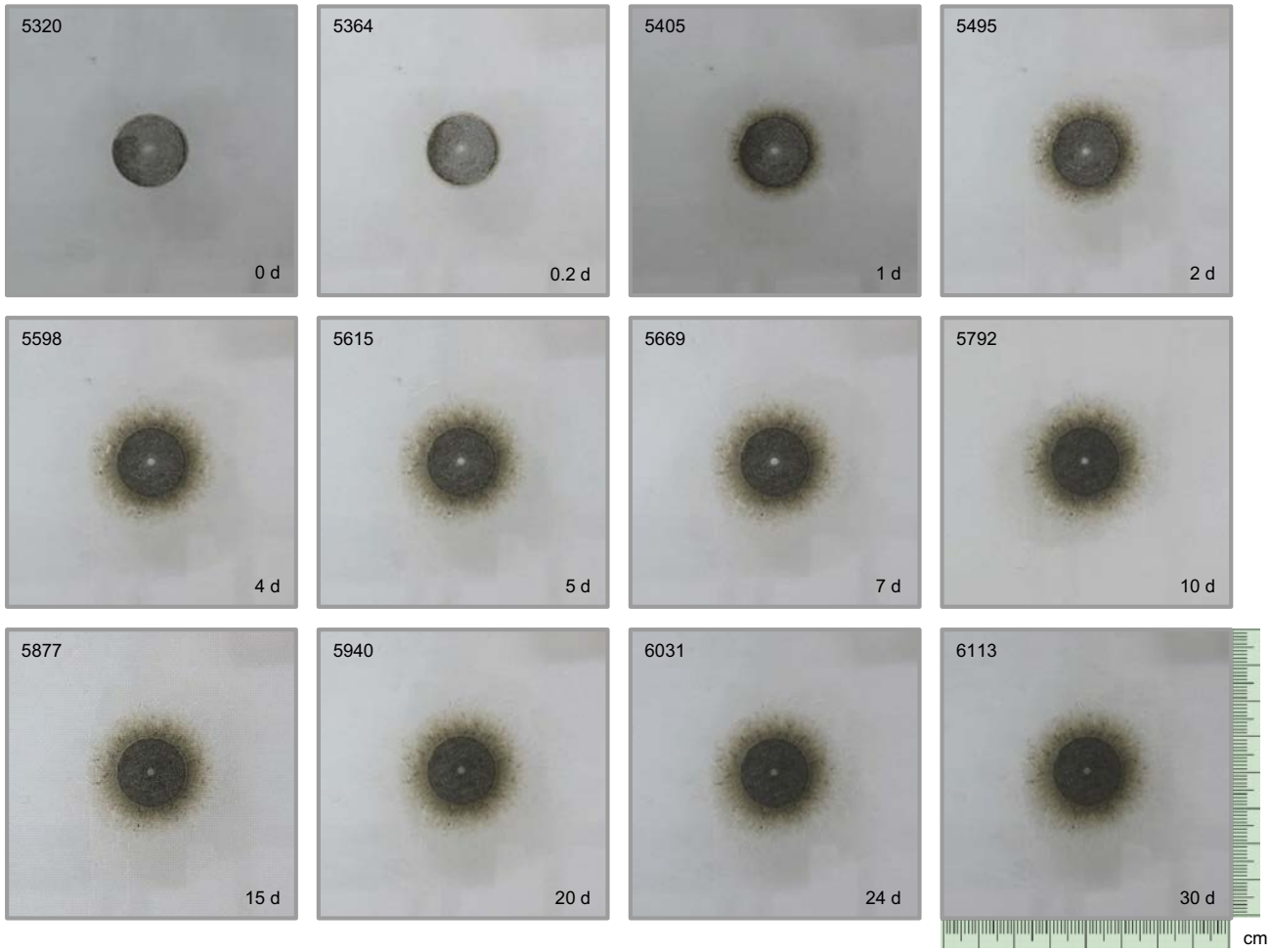

Test 16A: Raw MX-80 1.4 g·cm^{-3} - Slope 0º - Aperture 0.2 mm - NaCl 10^{-3} M

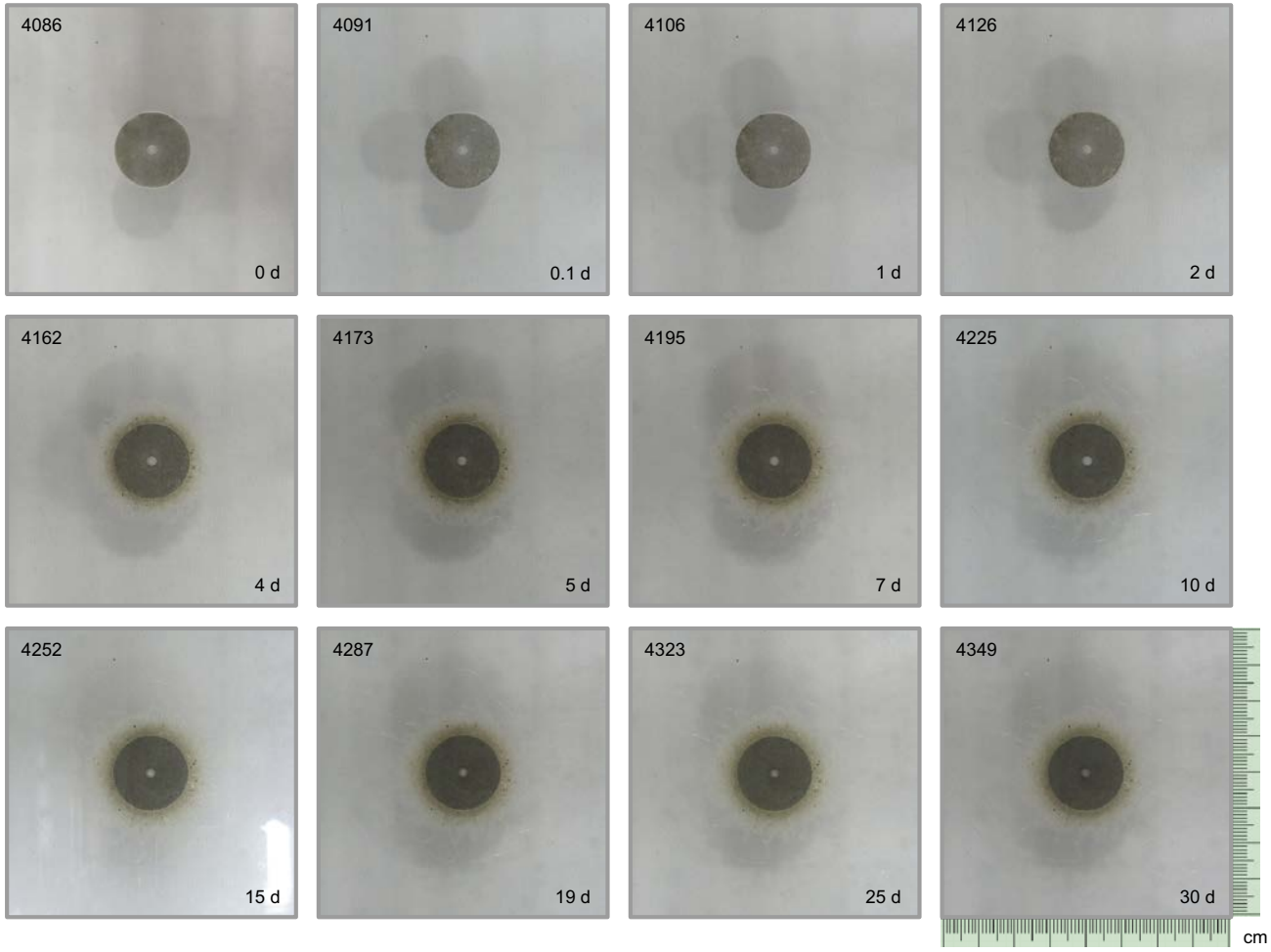

Test 17A: Raw MX-80 1.4 g·cm^{-3} - Slope 45º - Aperture 0.2 mm - NaCl 10^{-3} M

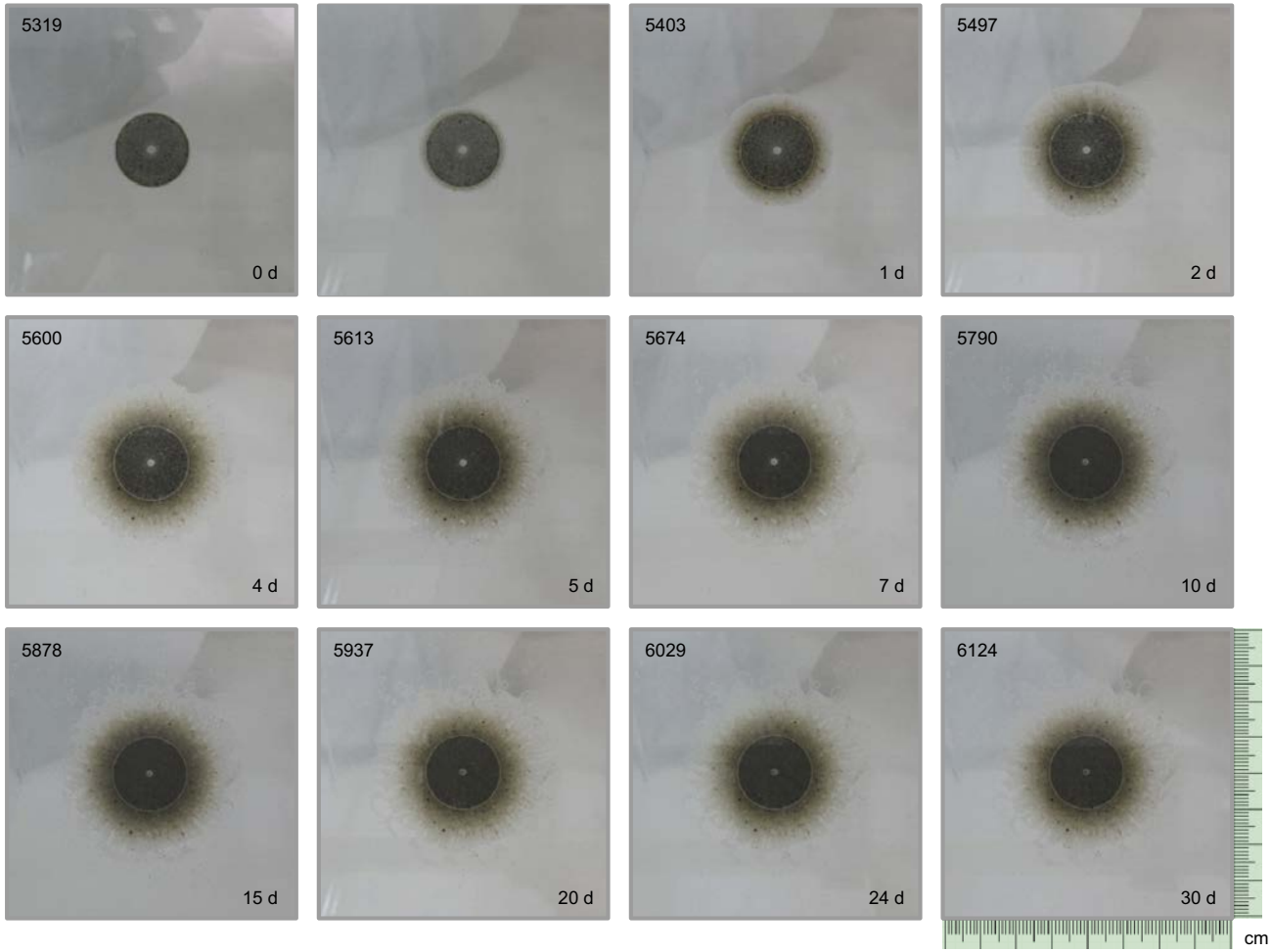

Test 18A: Raw MX-80 1.4 g·cm^{-3} - Slope 90º - Aperture 0.2 mm - NaCl 10^{-3} M

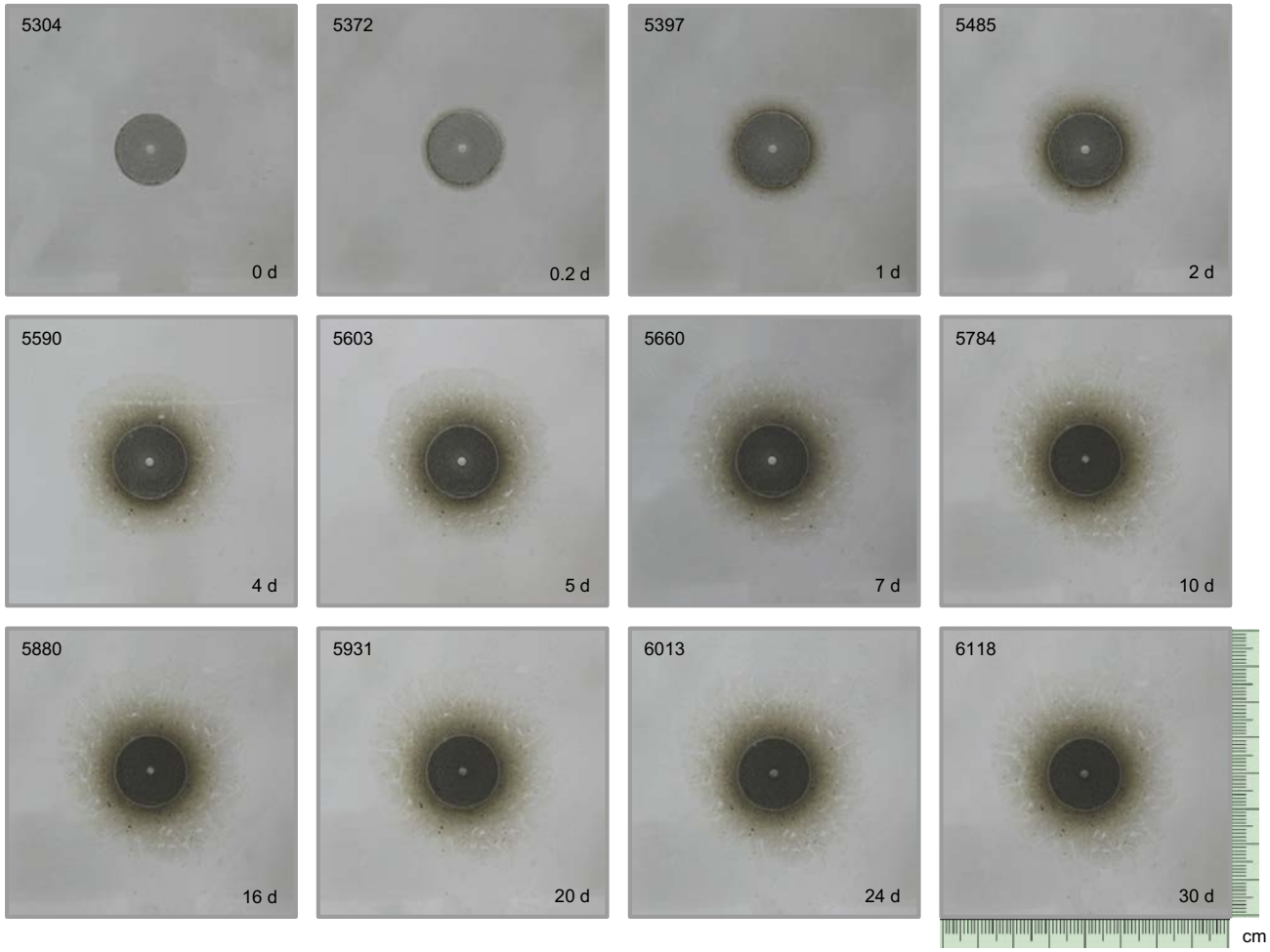

Test 19A: Nanocor® 1.4 g·cm^{-3} - Slope 0º - Aperture 0.2 mm - NaCl 10^{-2} M

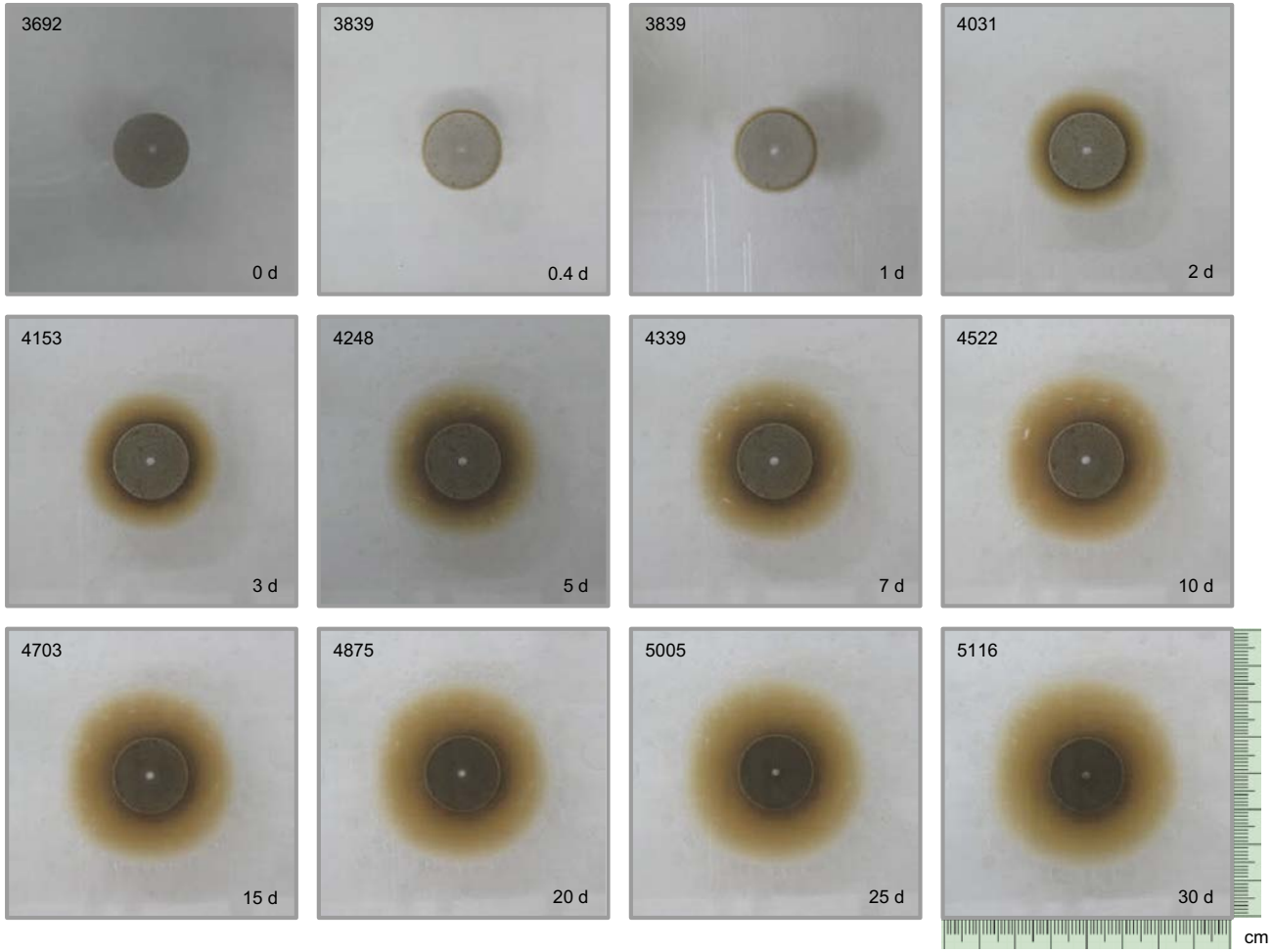

Test 20A: Nanocor® 1.4 g·cm^{-3} - Slope 0º - Aperture 0.2 mm - NaCl 10^{-1} M

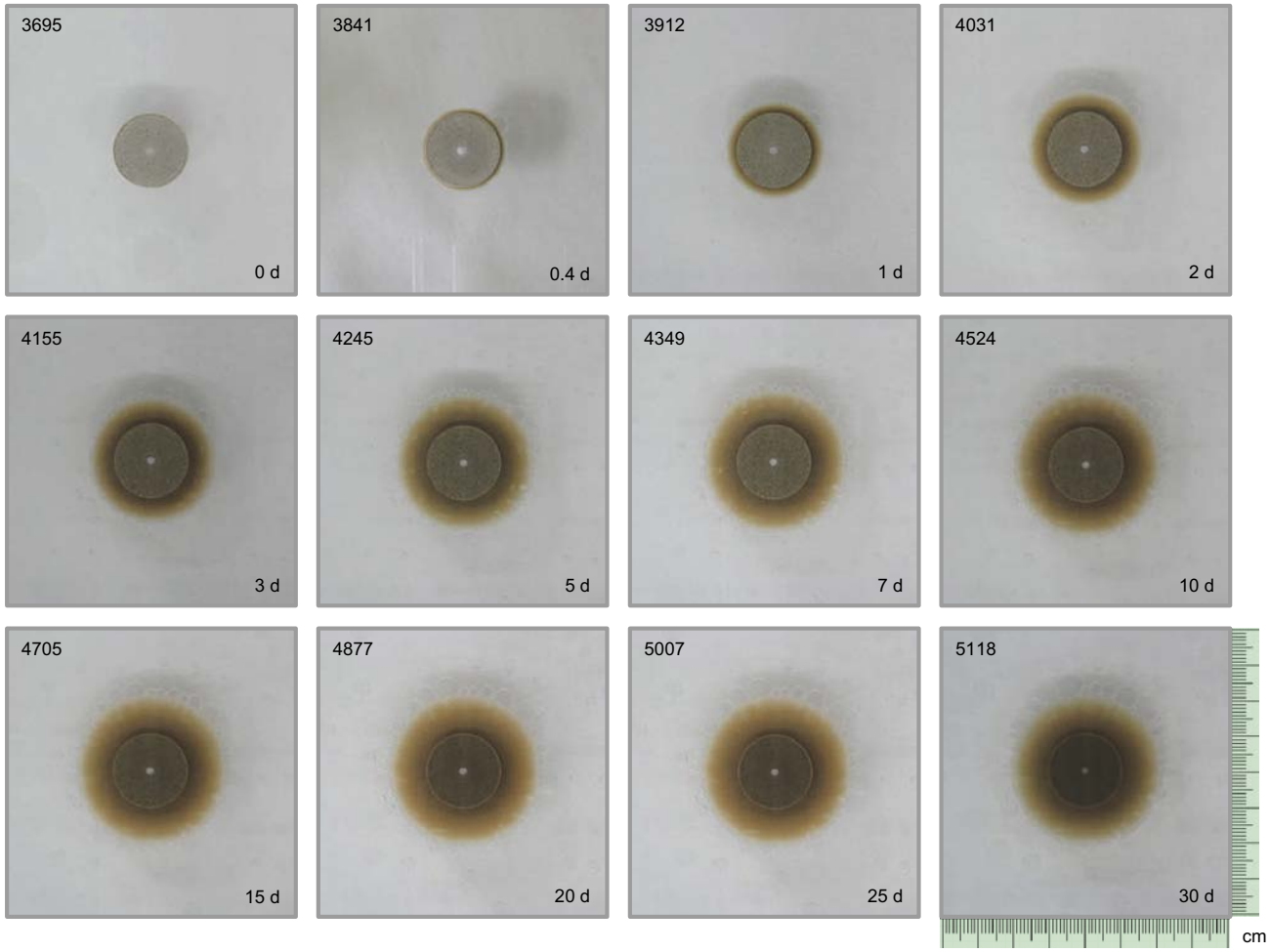

Test 21A: MCA-C 1.4 g·cm^{-3} - Slope 0º - Aperture 0.2 mm - NaCl 10^{-3} M

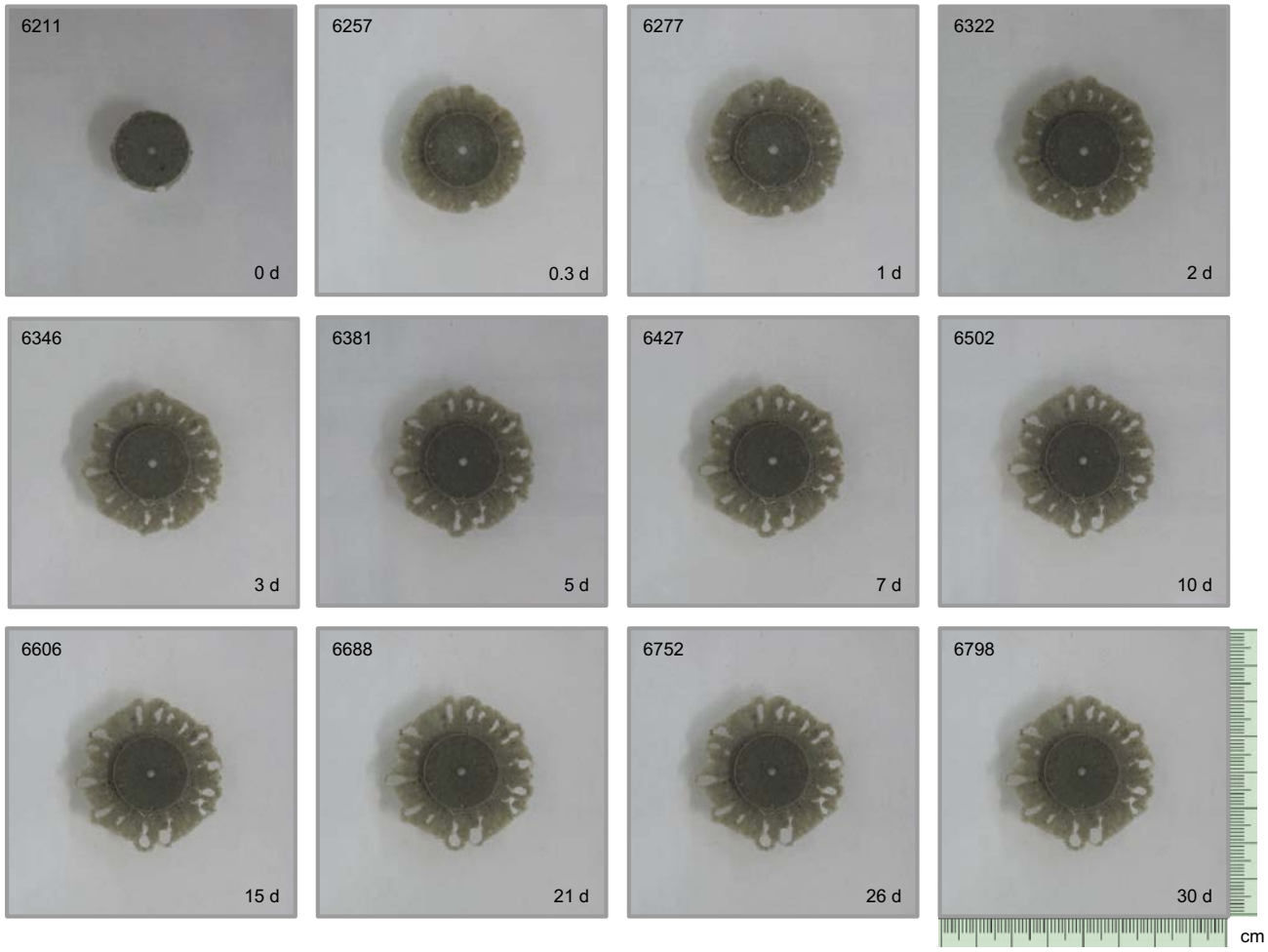

Test 22A: Ibeco1.4 g·cm^{-3} - Slope 0º - Aperture 0.2 mm - NaCl 10^{-3} M

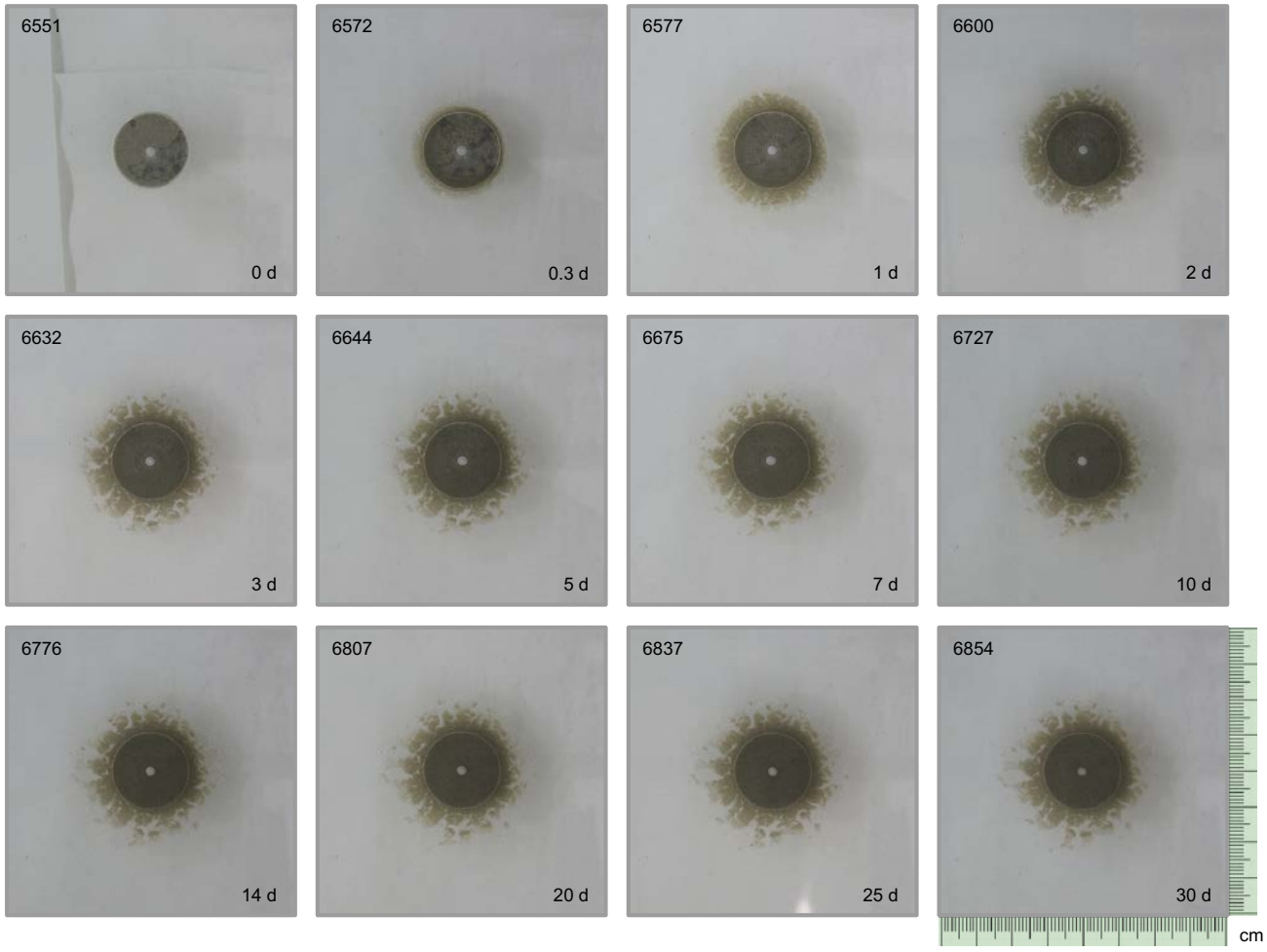

Test 23A: Ca-MX-80 1.4 g·cm^{-3} - Slope 90º - Aperture 0.1 mm - NaCl 10^{-3} M

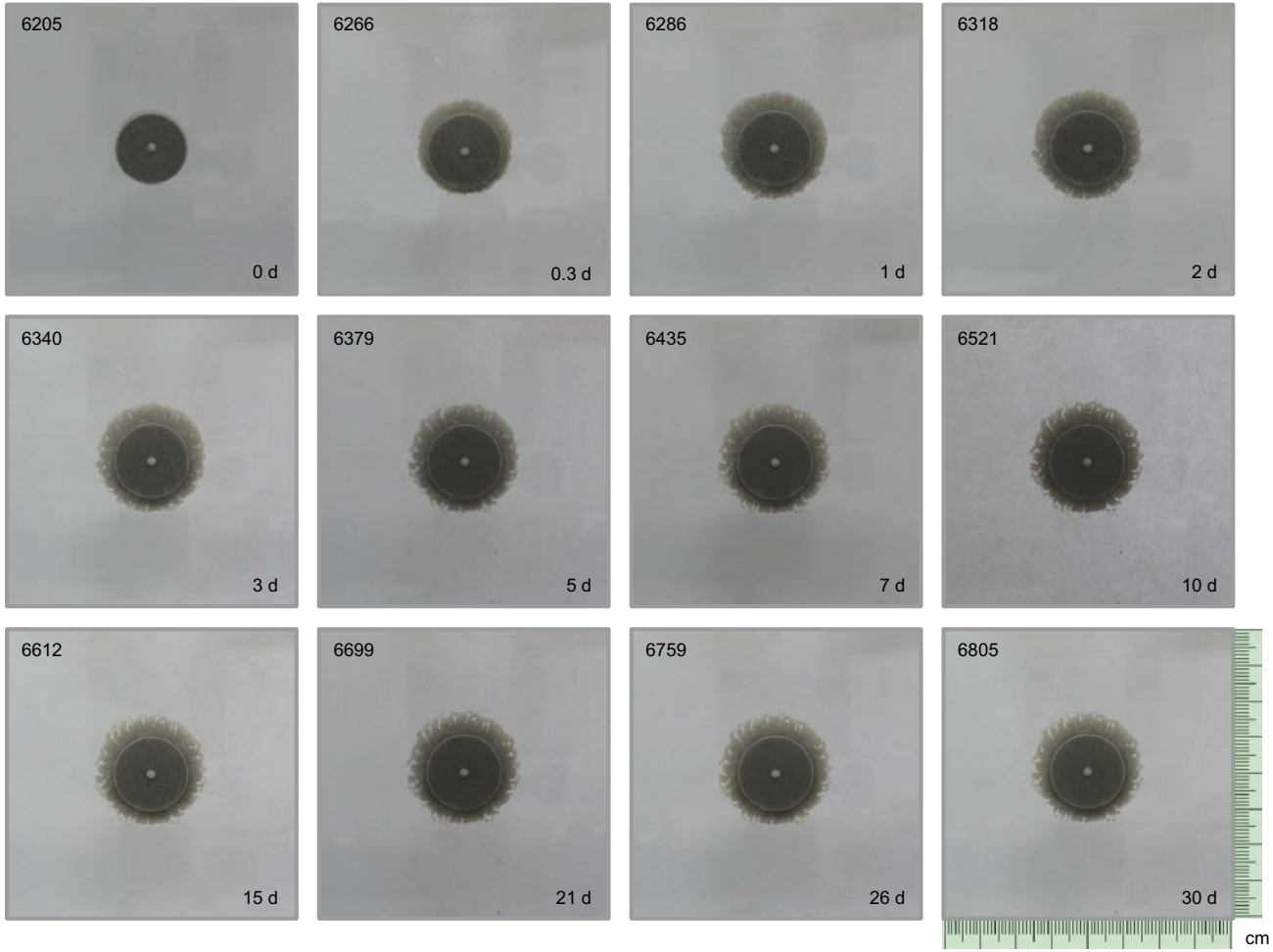

Test 24A: Ca-MX-80 1.4 g·cm^{-3} - Slope 90º - Aperture 0.2 mm - NaCl 10^{-3} M

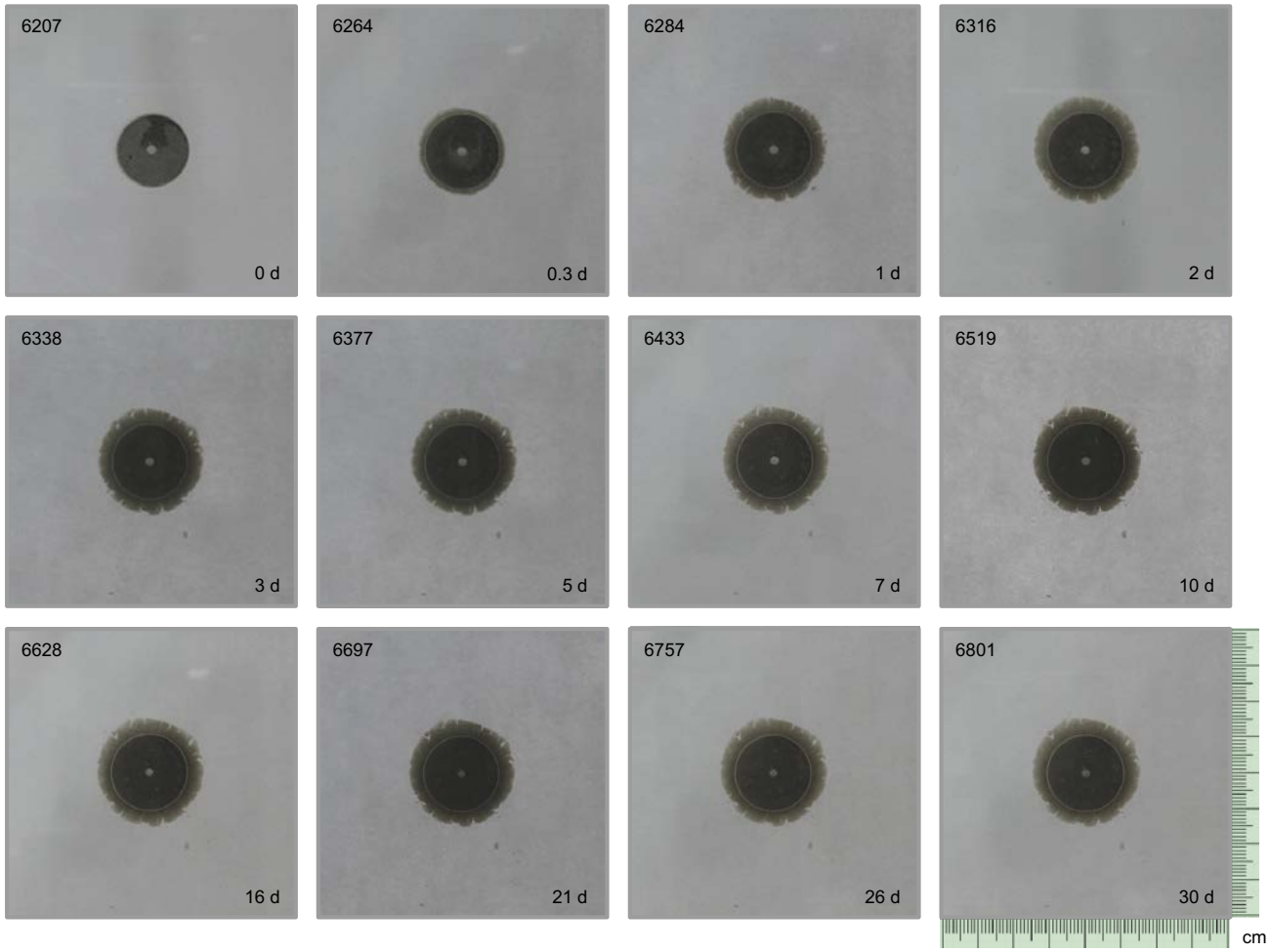

Test 25A: Ca-MX-80 1.4 g·cm^{-3} - Slope 90º - Aperture 0.4 mm - NaCl 10^{-3} M

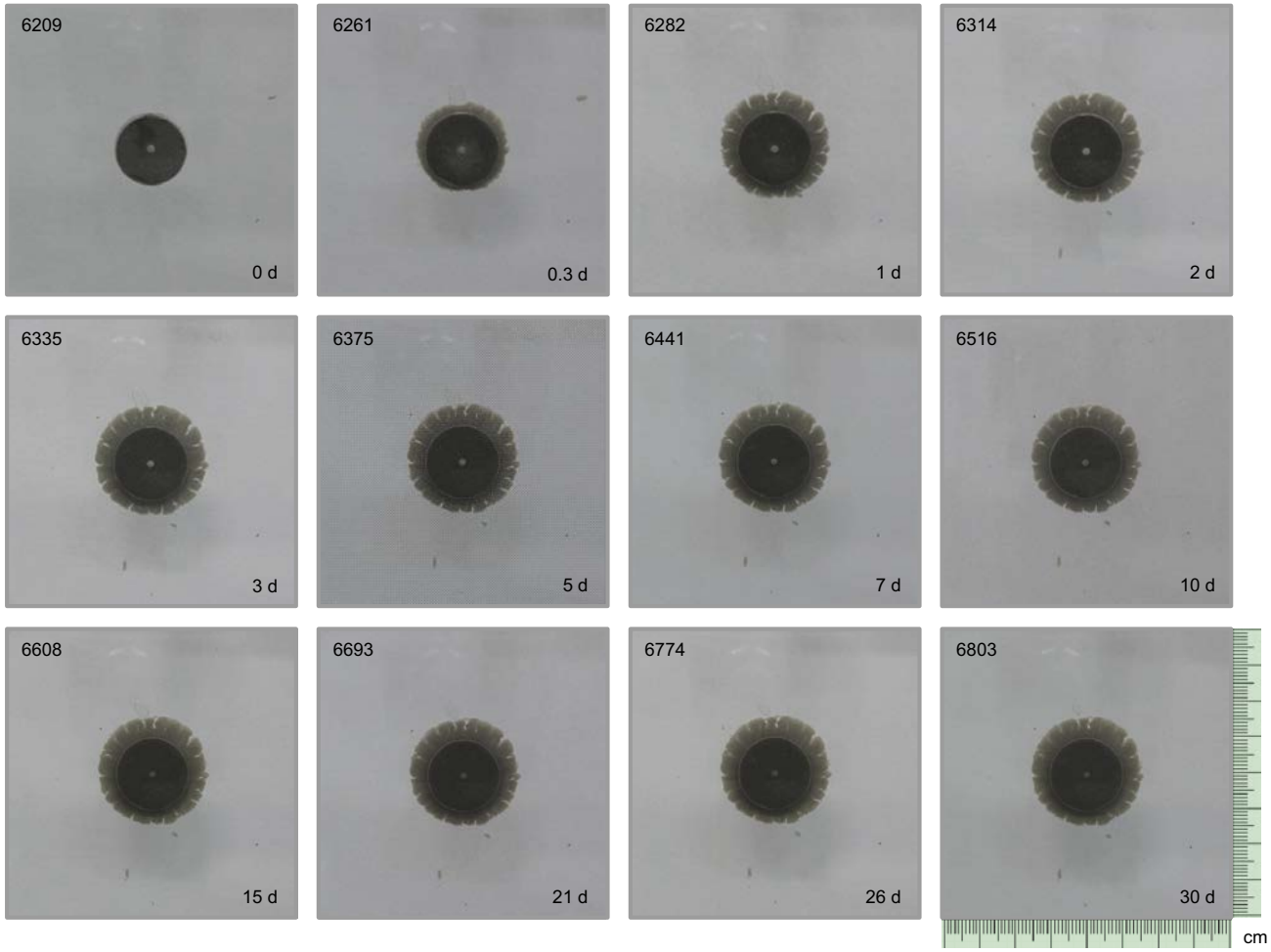

Test 26A: Nanocor® 1.4 g·cm^{-3} - Slope 45º - Aperture 0.2 mm - NaCl 10^{-2} M

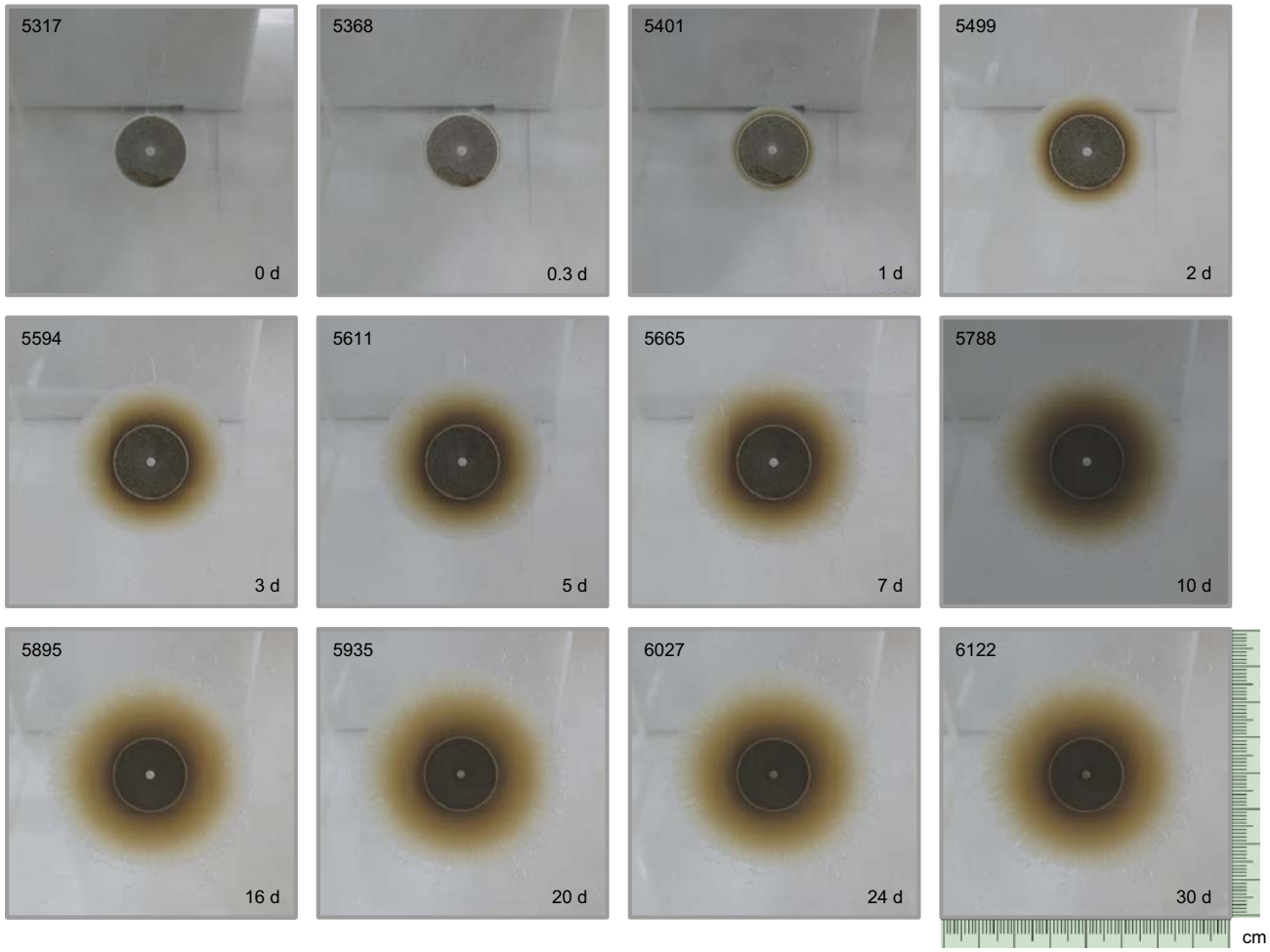

Test 27A: Nanocor® 1.4 g·cm^{-3} - Slope 45º - Aperture 0.2 mm - NaCl 10^{-1} M

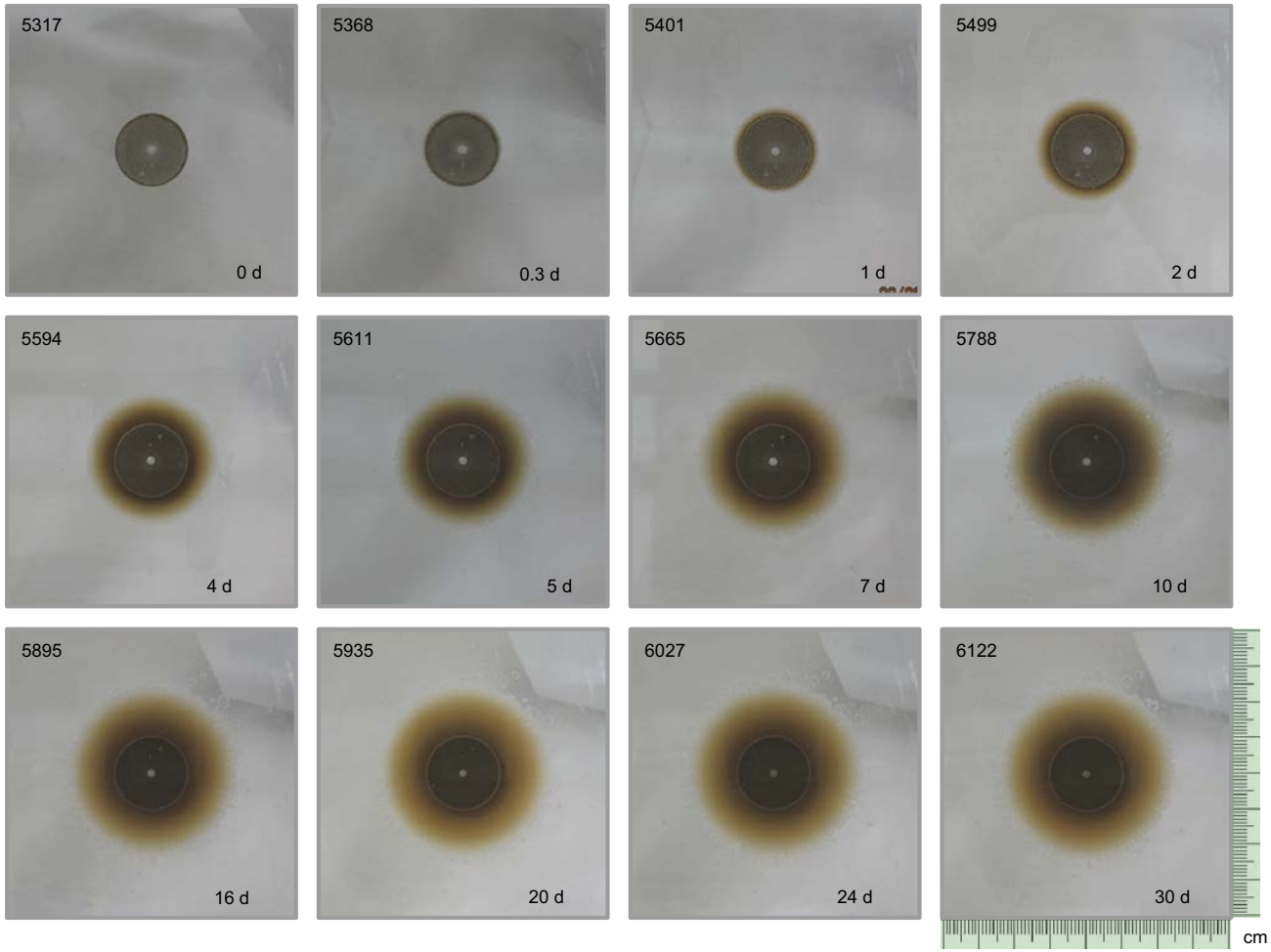

Test 28A: Nanocor® 1.4 g·cm^{-3} - Slope 45º - Aperture 0.2 mm - NaCl 10^{-3} M

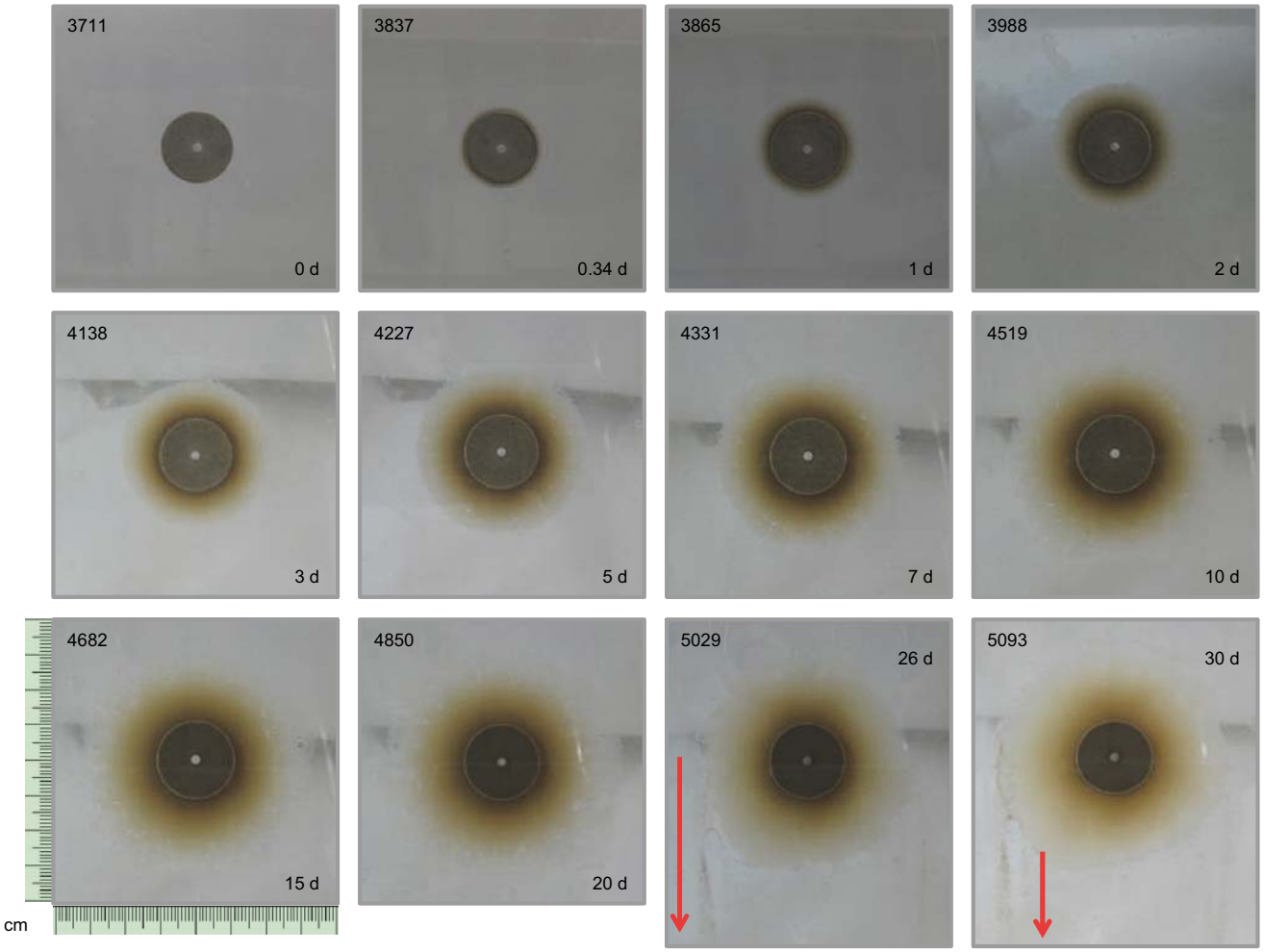

Test 29A: Nanocor® 1.4 g·cm^{-3} - Slope 0 – smooth 0.1 mm - NaCl 10^{-3} M

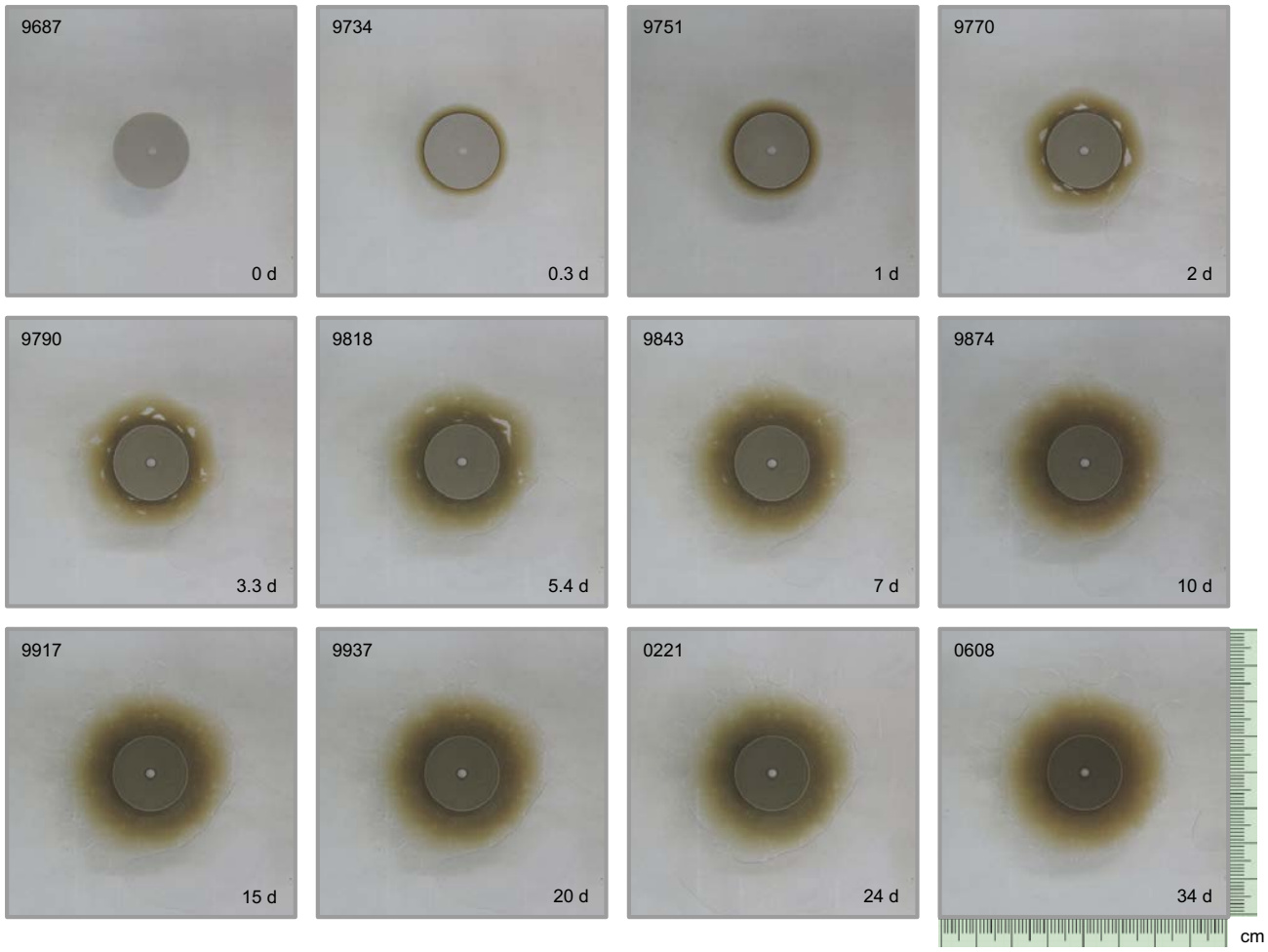

Test 31A: Nanocor® 1.4 g·cm^{-3} - Slope 0 – Roughness 1 - NaCl 10^{-3} M

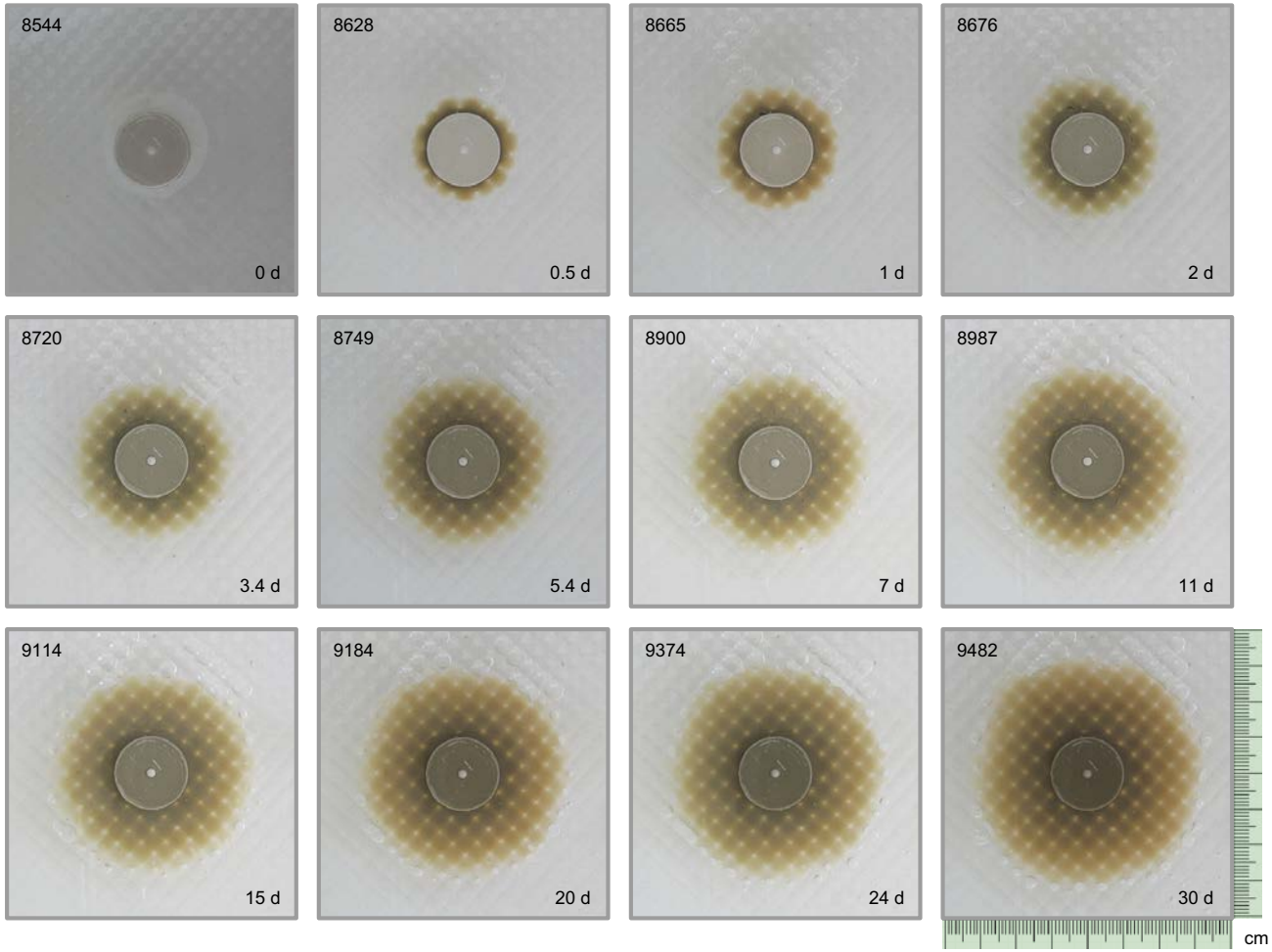

Test 33A: Nanocor® 1.4 g·cm^{-3} - Slope 0º – Roughness 2 - NaCl 10^{-3} M

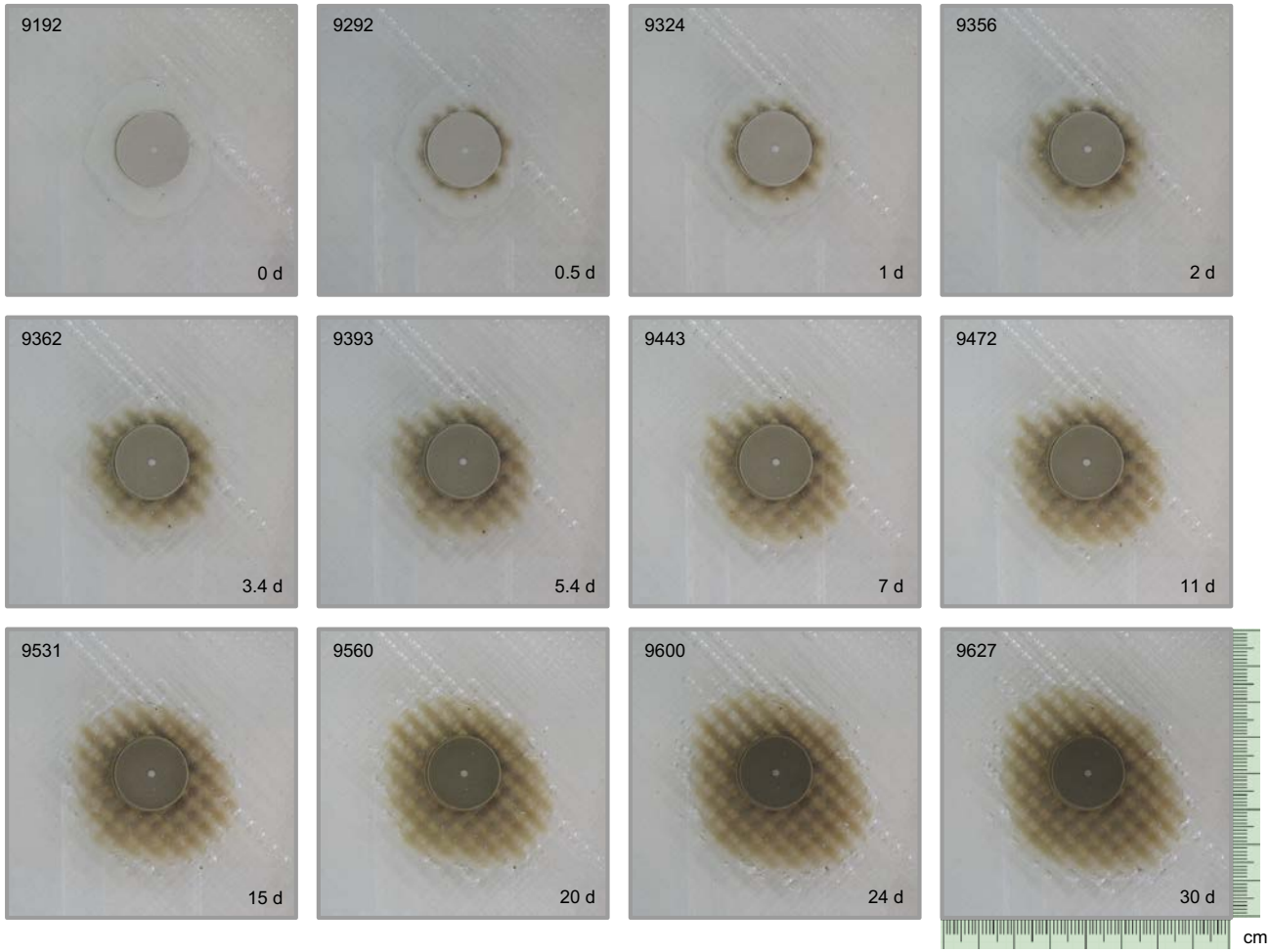

Test 35A: Raw MX-80 1.4 g·cm^{-3} - Slope 0 - smooth 0.2 mm - NaCl 10^{-3} M

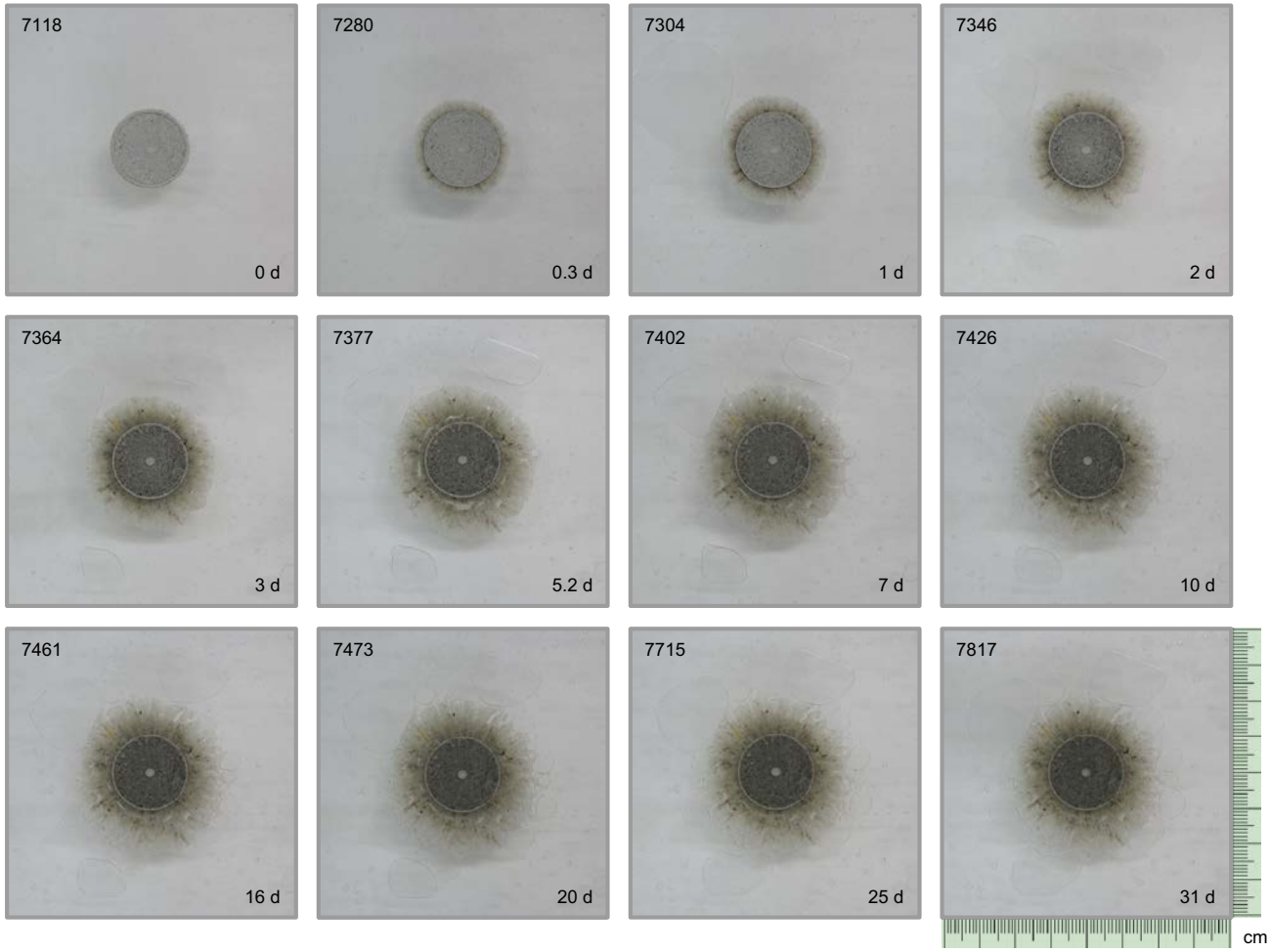

Test 37A: Raw MX-80 1.4 g·cm^{-3} - Slope 0 – Roughness 1 - NaCl 10^{-3} M

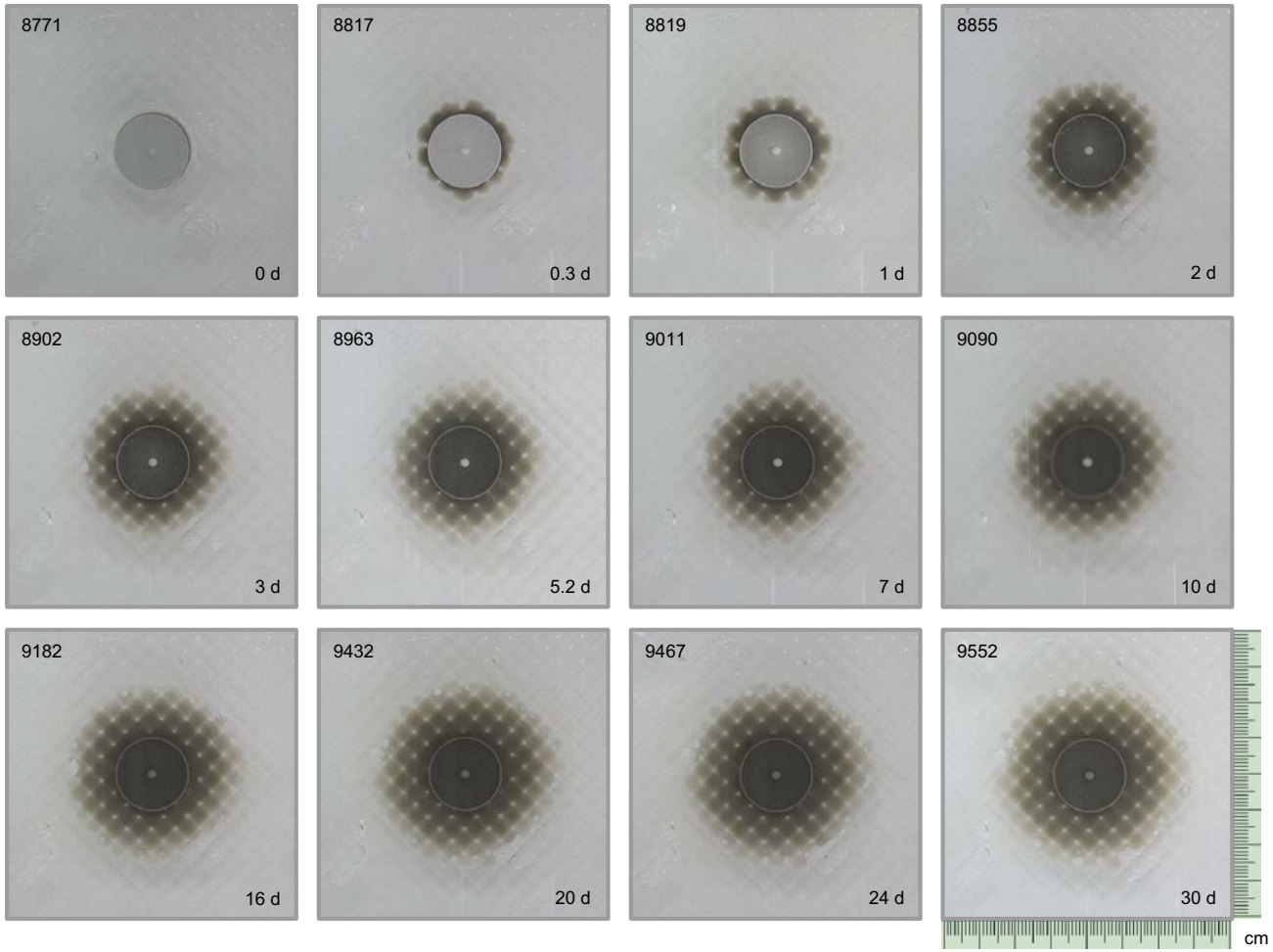

Test 39A: Raw MX-80 1.4 g·cm^{-3} - Slope 0 – Roughness 2 - NaCl 10^{-3} M

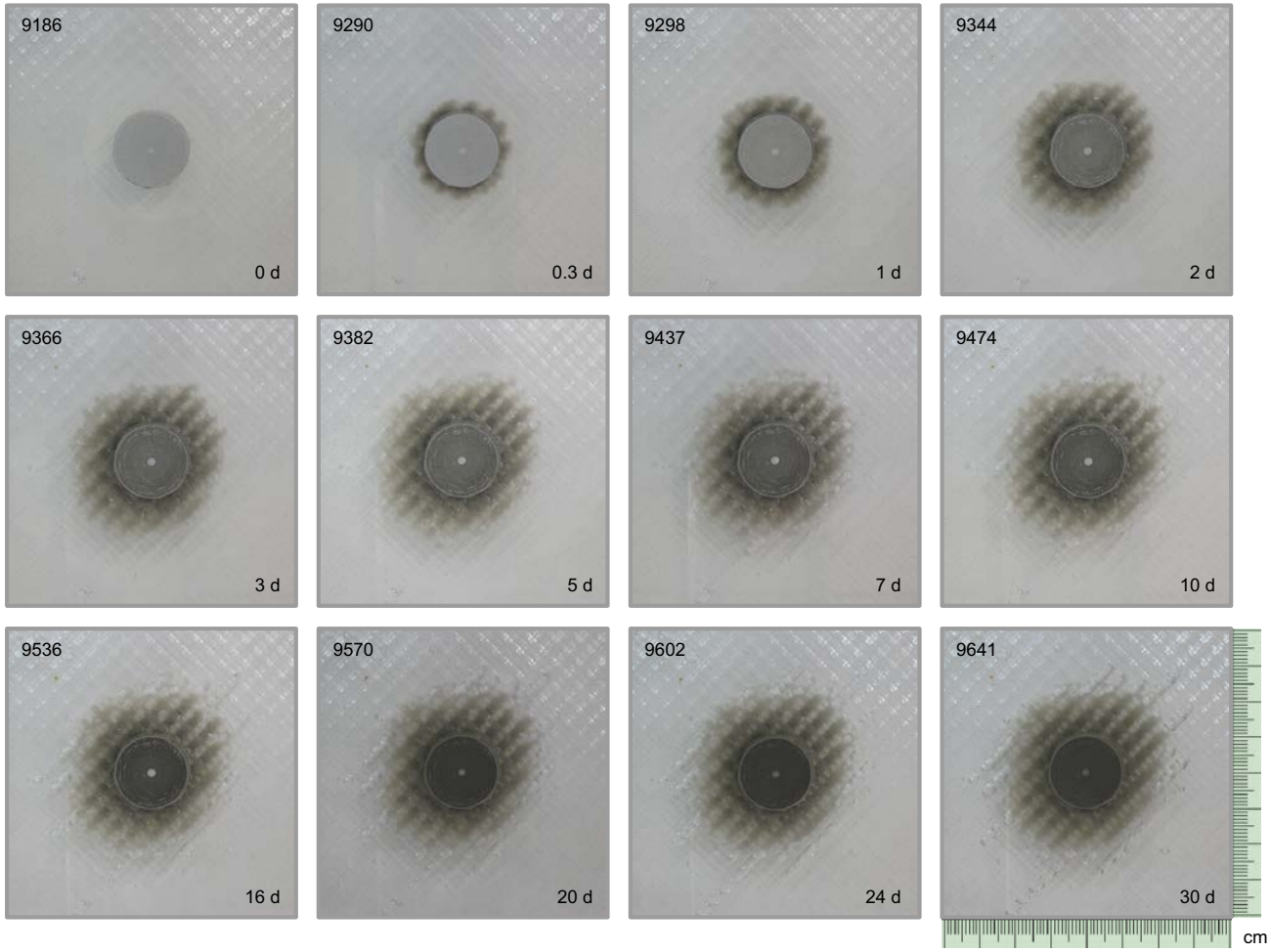

Test 41A: Raw MX-80 1.4 g·cm^{-3} - Slope 0º – Roughness 1 - NaCl 10^{-3} M

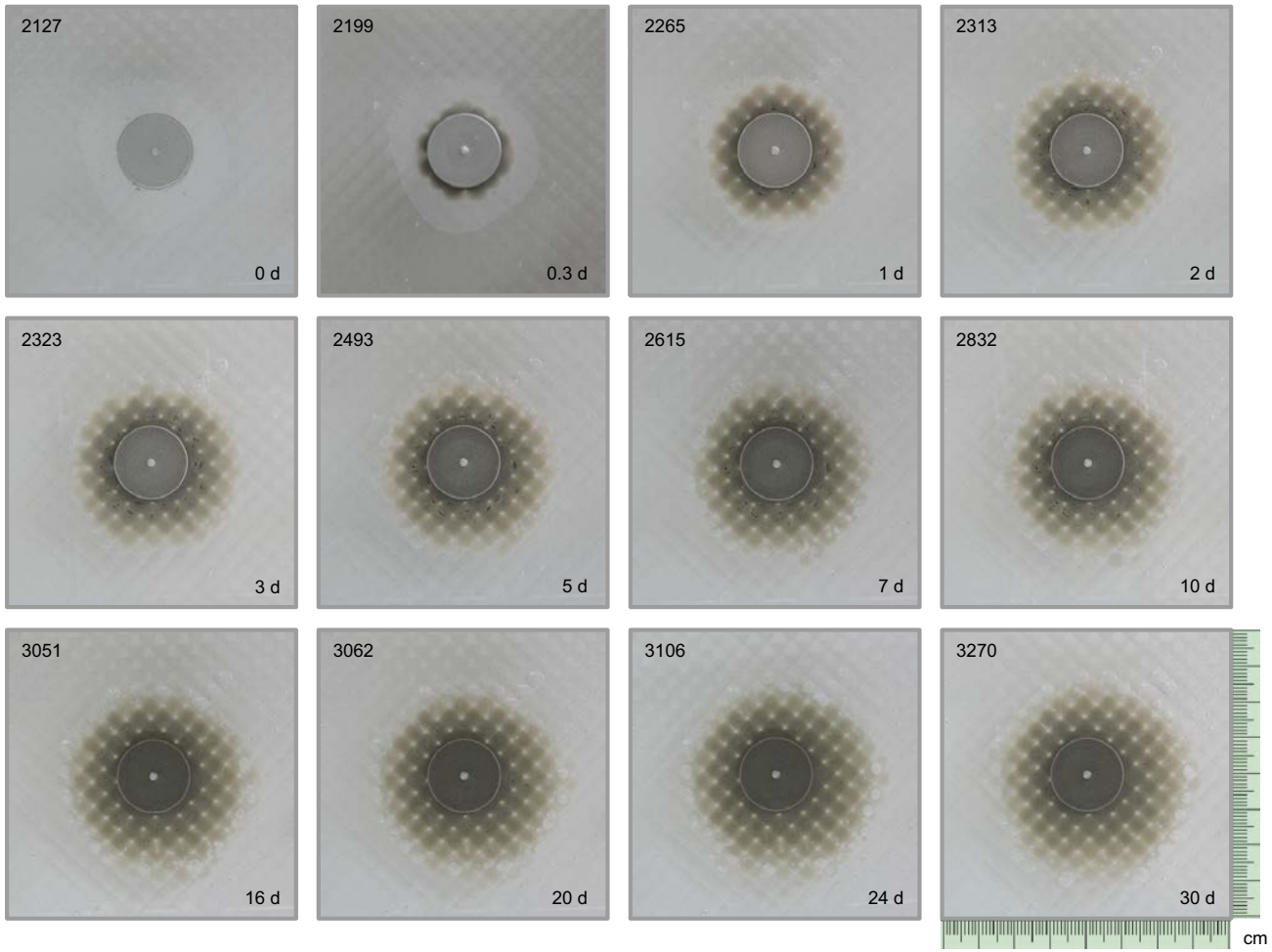

Test 42A: Raw MX-80 1.4 g·cm^{-3} - Slope 45º – Roughness 1 - NaCl 10^{-3} M

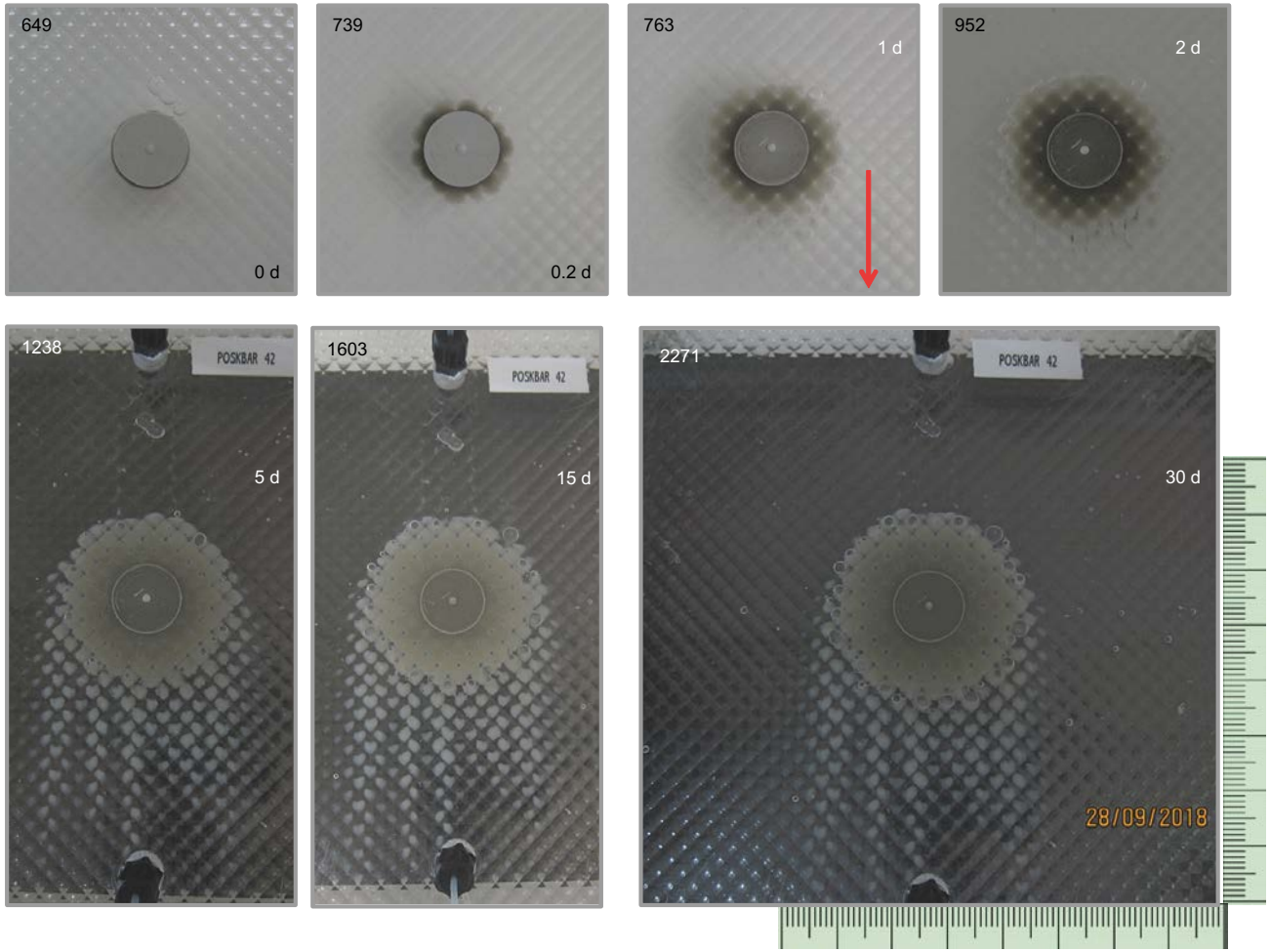

Test 43A: Raw MX-80 1.4 g·cm^{-3} - Slope 90º – Roughness 1 - NaCl 10^{-3} M

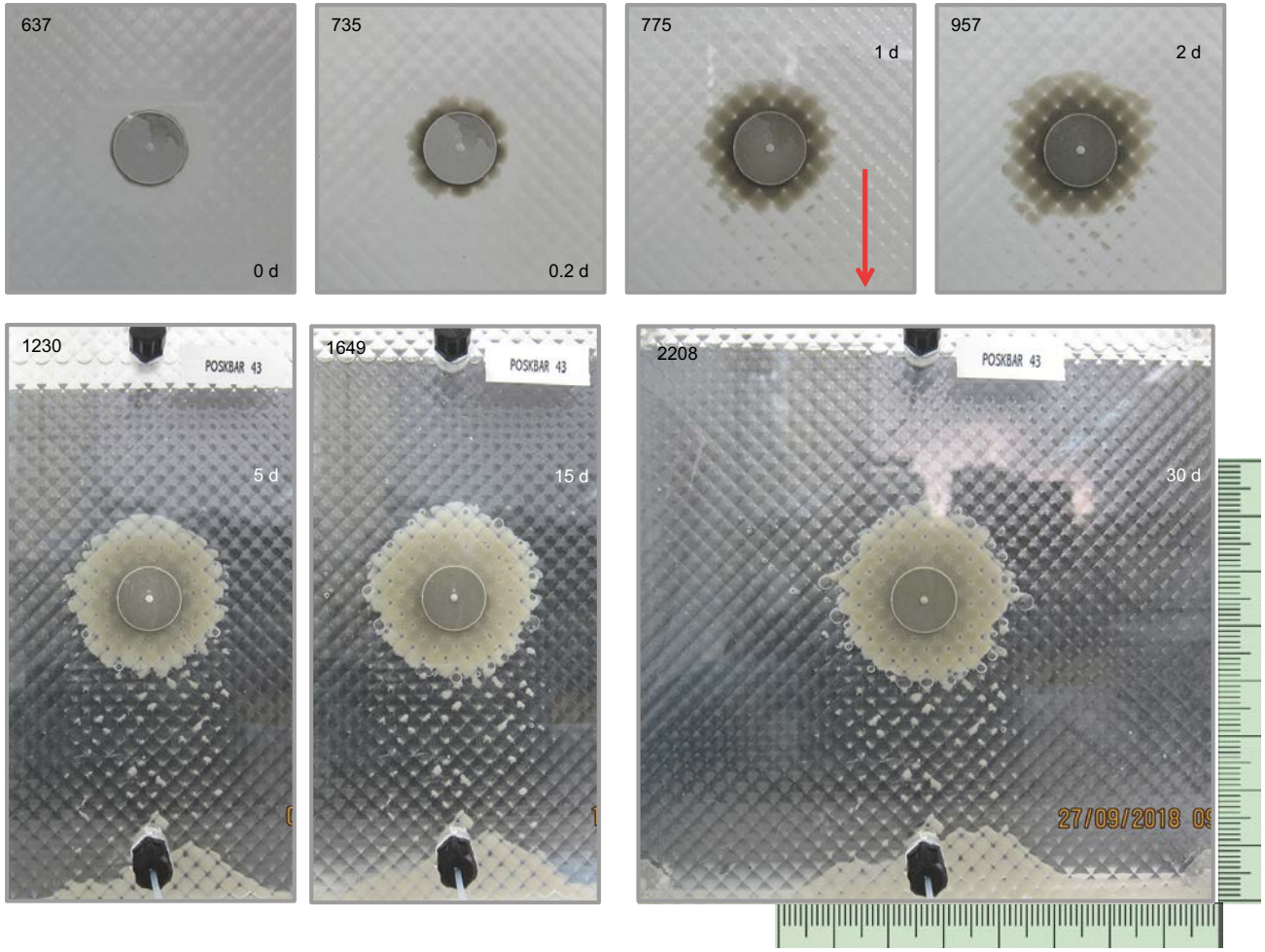

Test 44A: Na-MX-80 1.4 g·cm^{-3} - Slope 0º – Roughness 1 - NaCl 10^{-3} M

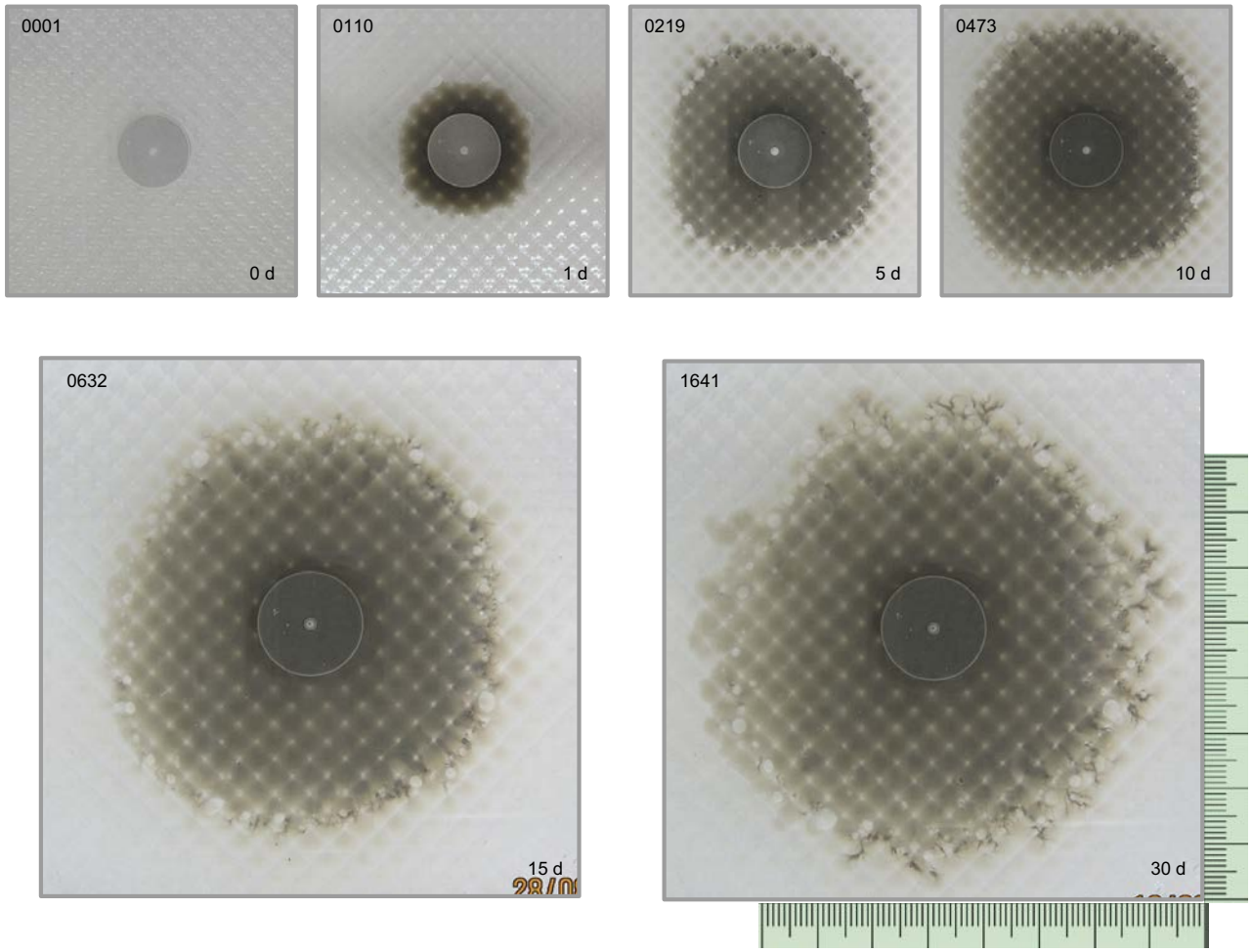

Test 45A: Na-MX-80 1.4 g·cm^{-3} - Slope 45º – Roughness 1 - NaCl 10^{-3} M

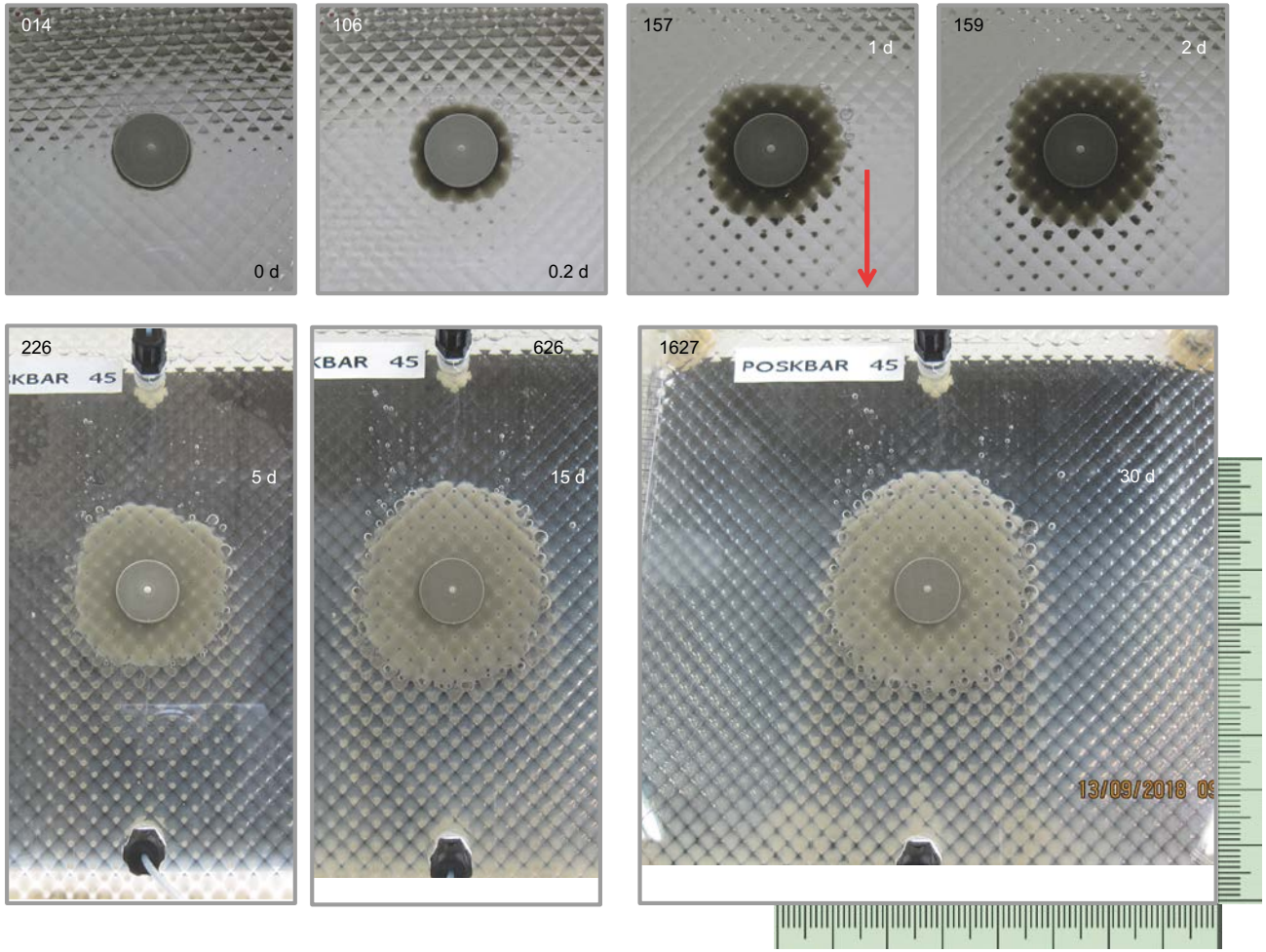

Test 46A: Na-MX-80 1.4 g·cm^{-3} - Slope 90º – Roughness 1 - NaCl 10^{-3} M

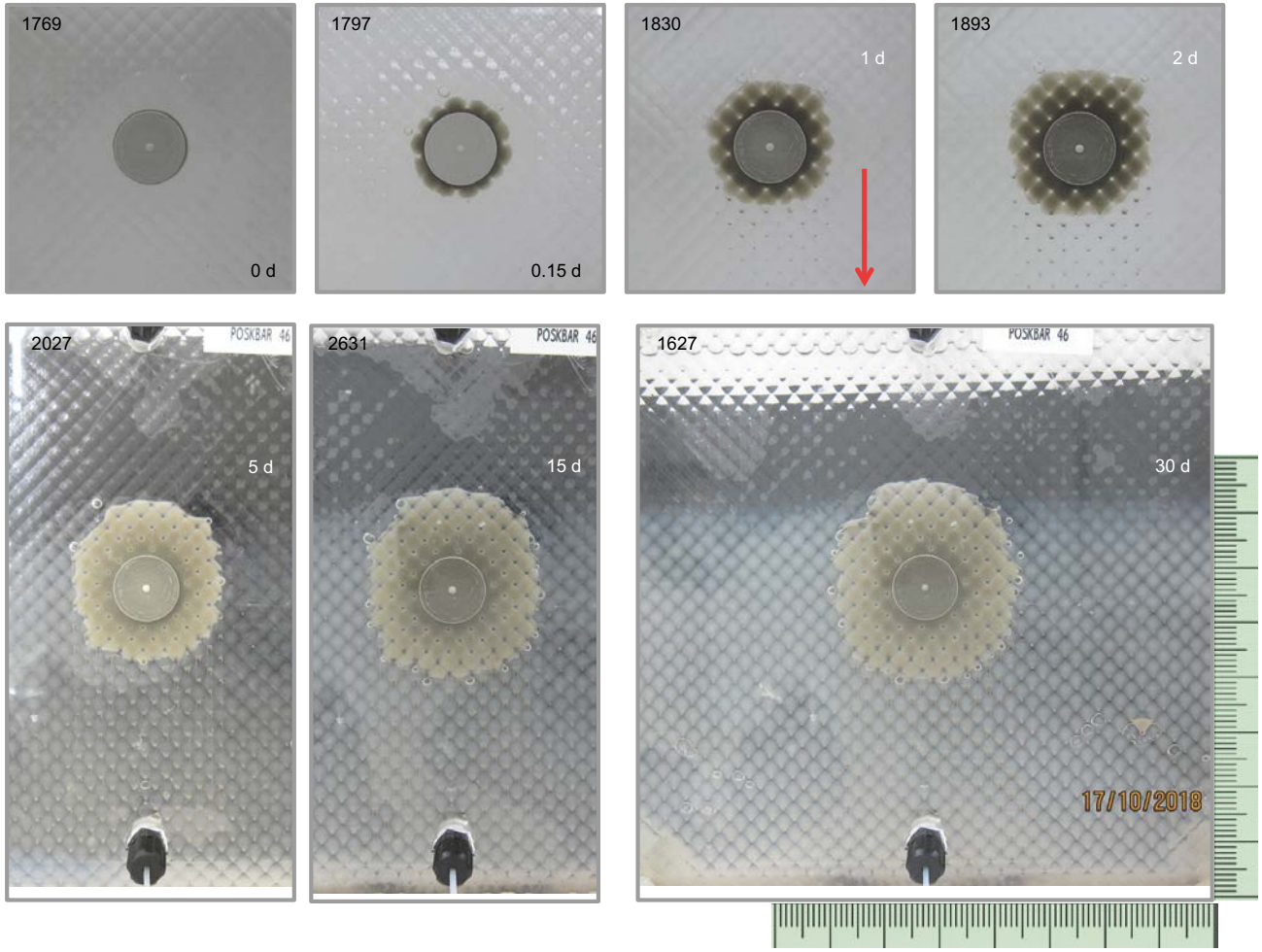

Test 47A: Ca-MX-80 1.4 g·cm^{-3} - Slope 0º – Roughness 1 - NaCl 10^{-3} M

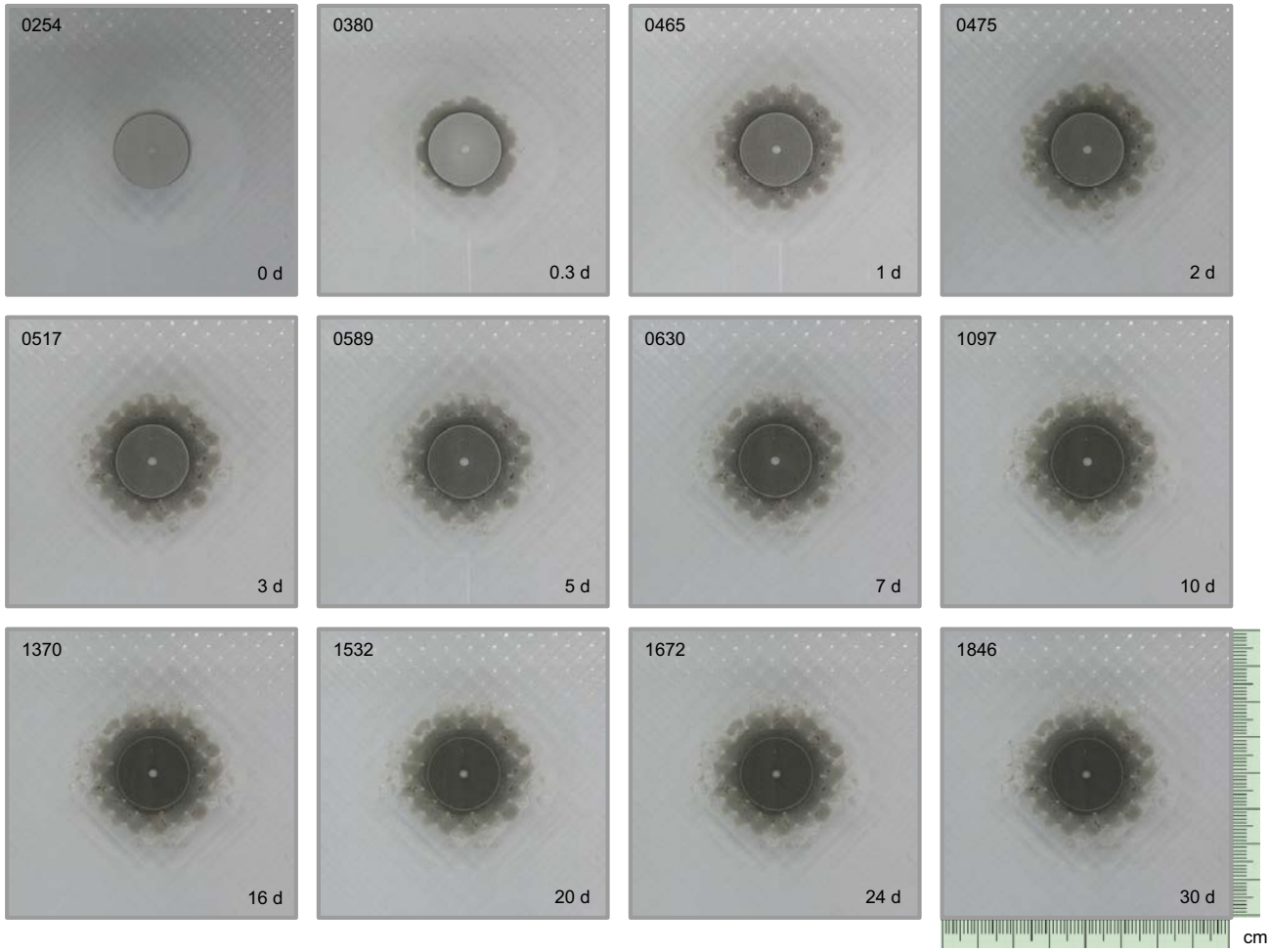

Test 48A: Ca-MX-80 1.4 g·cm^{-3} - Slope 45º – Roughness 1 - NaCl 10^{-3} M

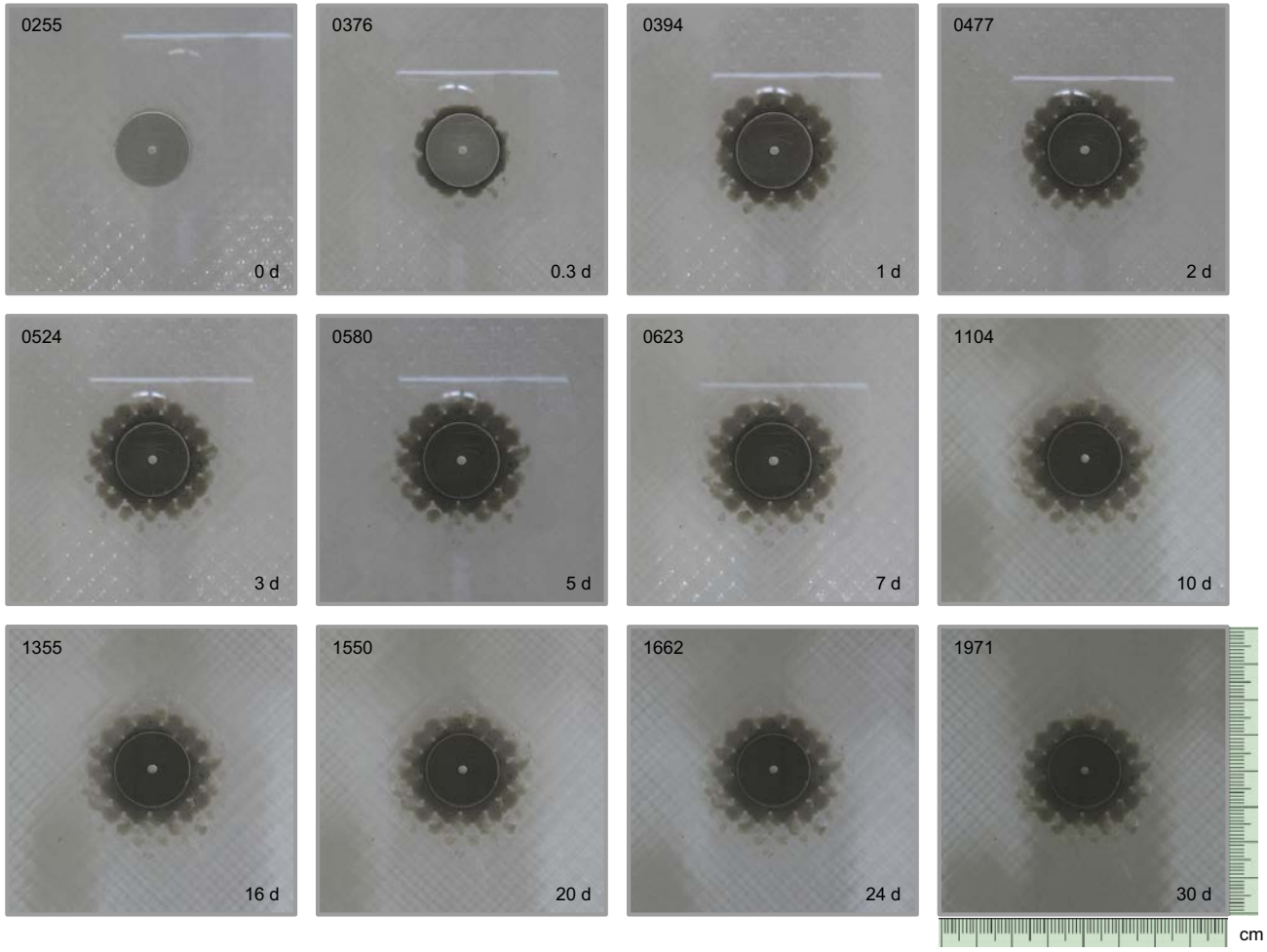

Test 49A: Ca-MX-80 1.4 g·cm^{-3} - Slope 90º – Roughness 1 - NaCl 10^{-3} M

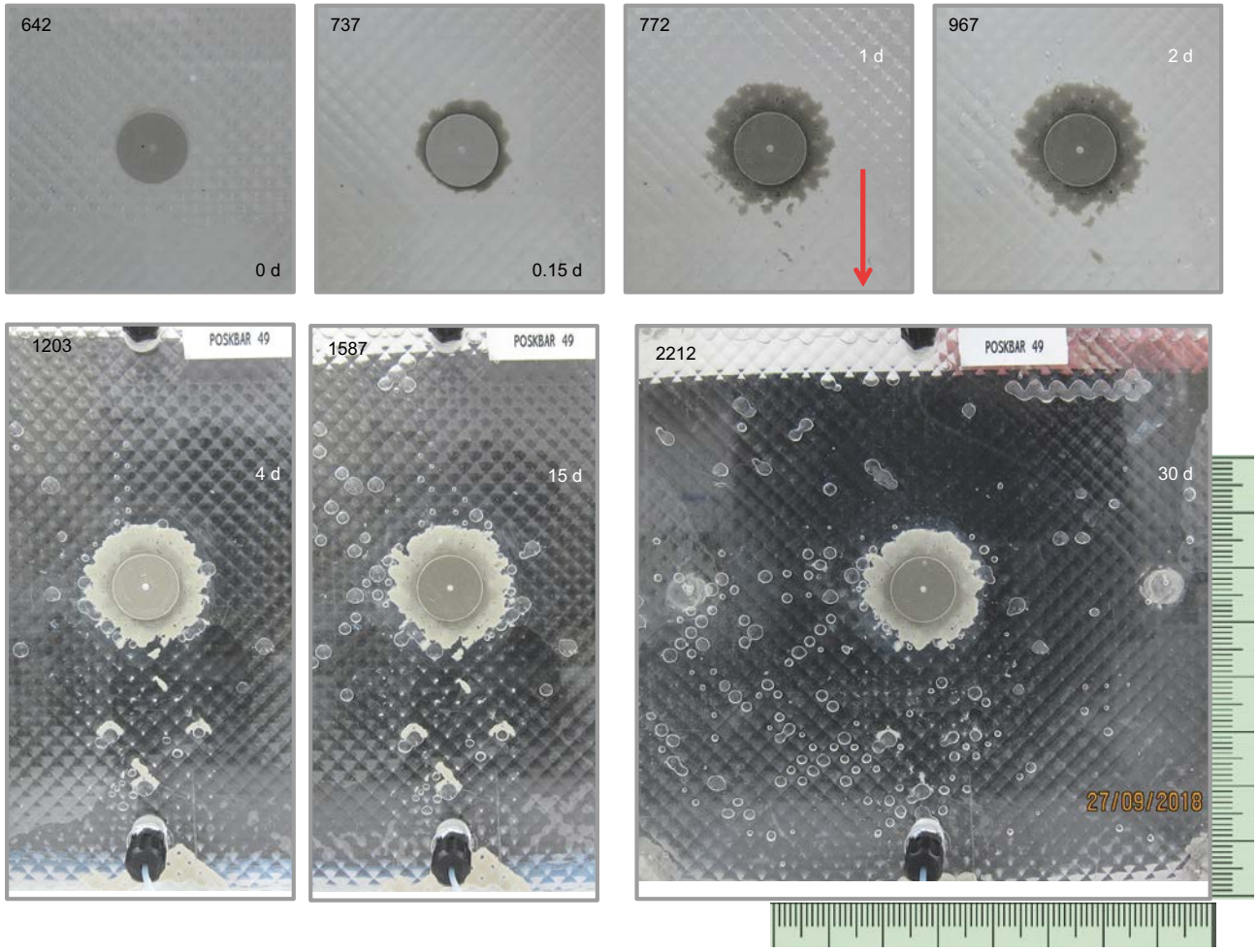

Test 50A: Raw MX-80 1.4 g·cm^{-3} - Slope 0º - 0.2 mm - NaCl 10^{-3} M

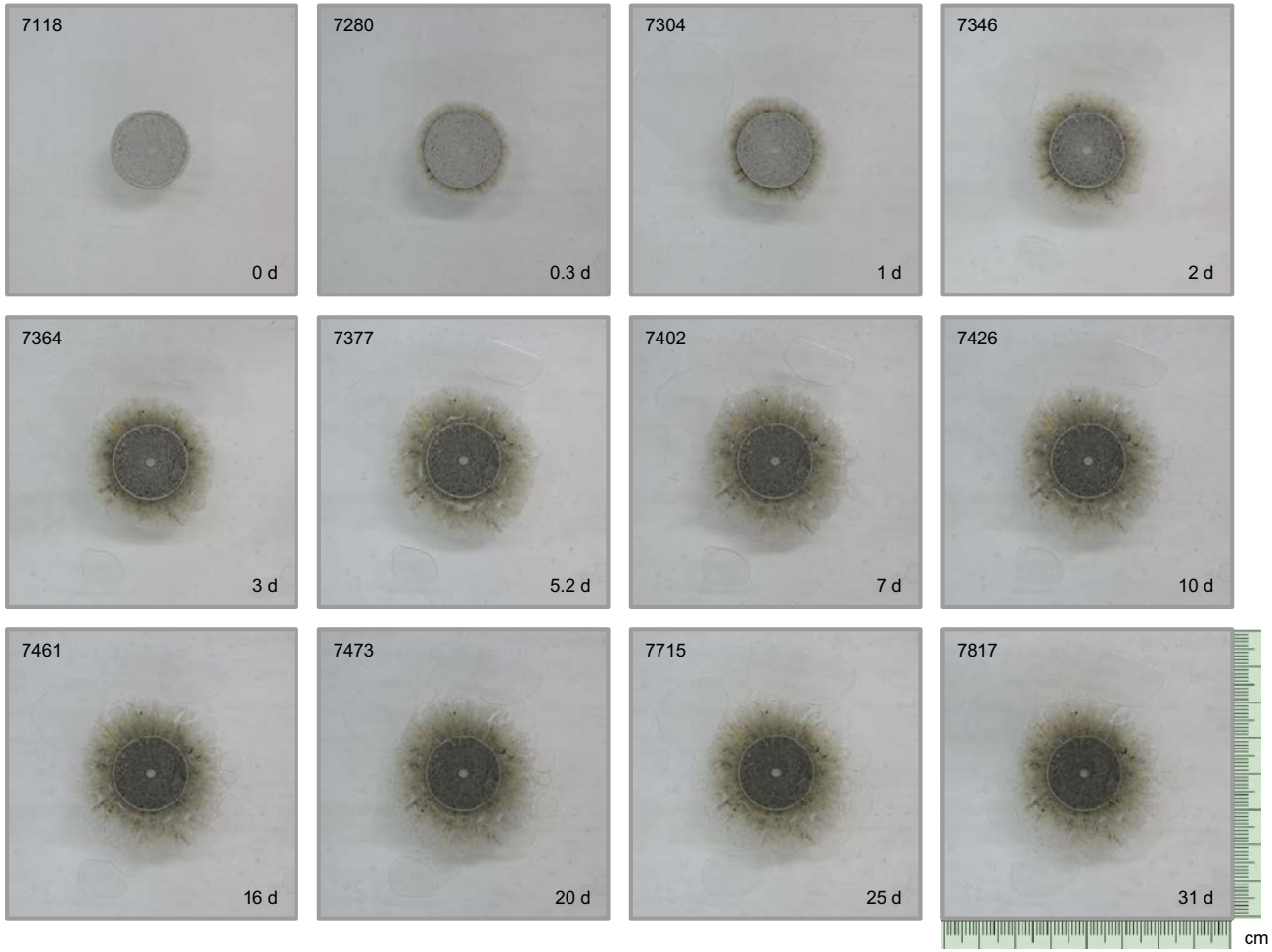

Test 50B: Raw MX-80 1.4 g·cm^{-3} - Slope 0º - 0.2 mm - NaCl 10^{-3} M

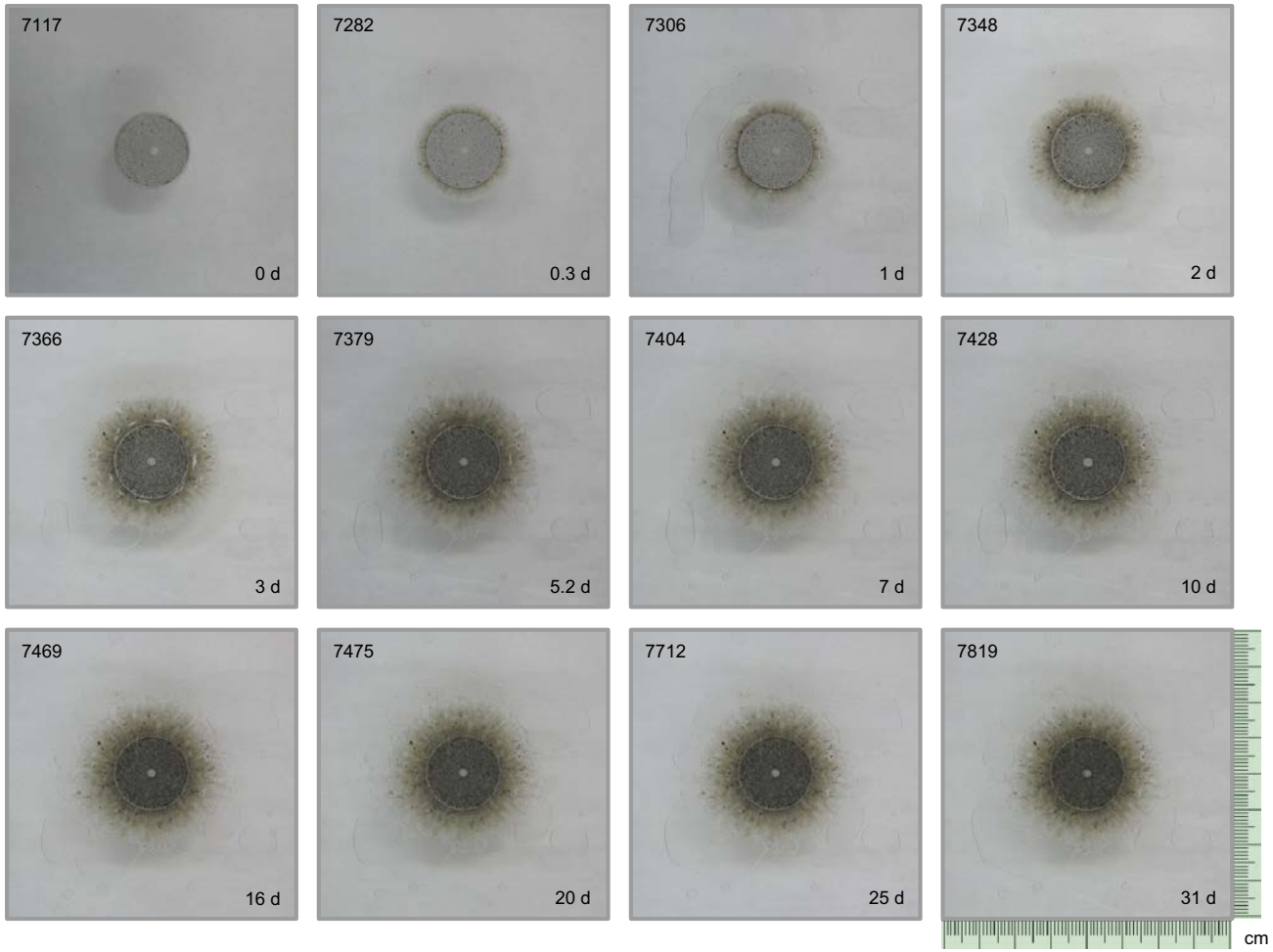

Test 50C: Raw MX-80 1.4 g·cm^{-3} - Slope 0º - 0.2 mm - NaCl 10^{-3} M

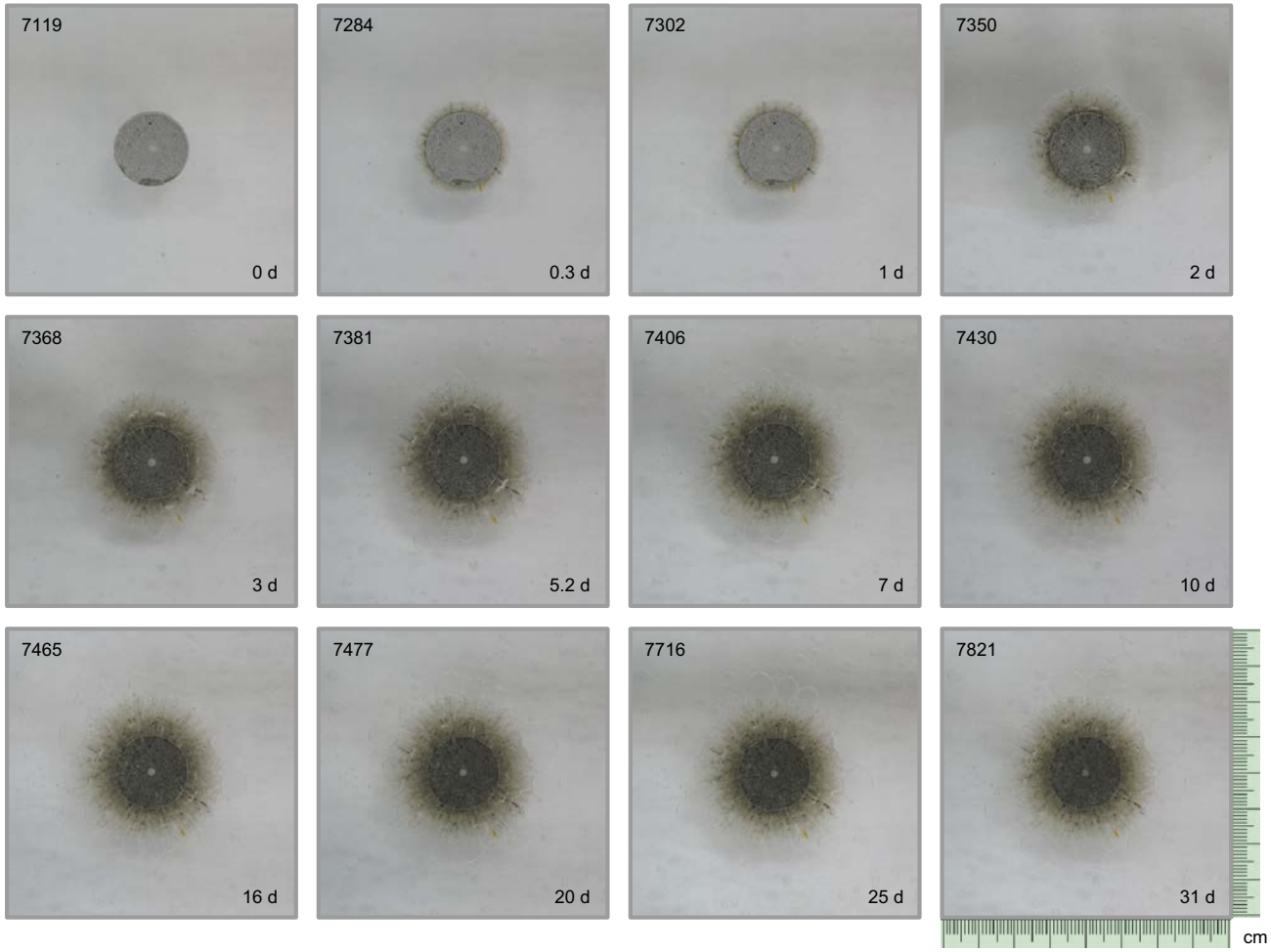

Test 51A: Minerals&salt-free MX-80 1.4 g·cm^{-3} - Slope 0º - 0.2 mm - NaCl 10^{-3} M

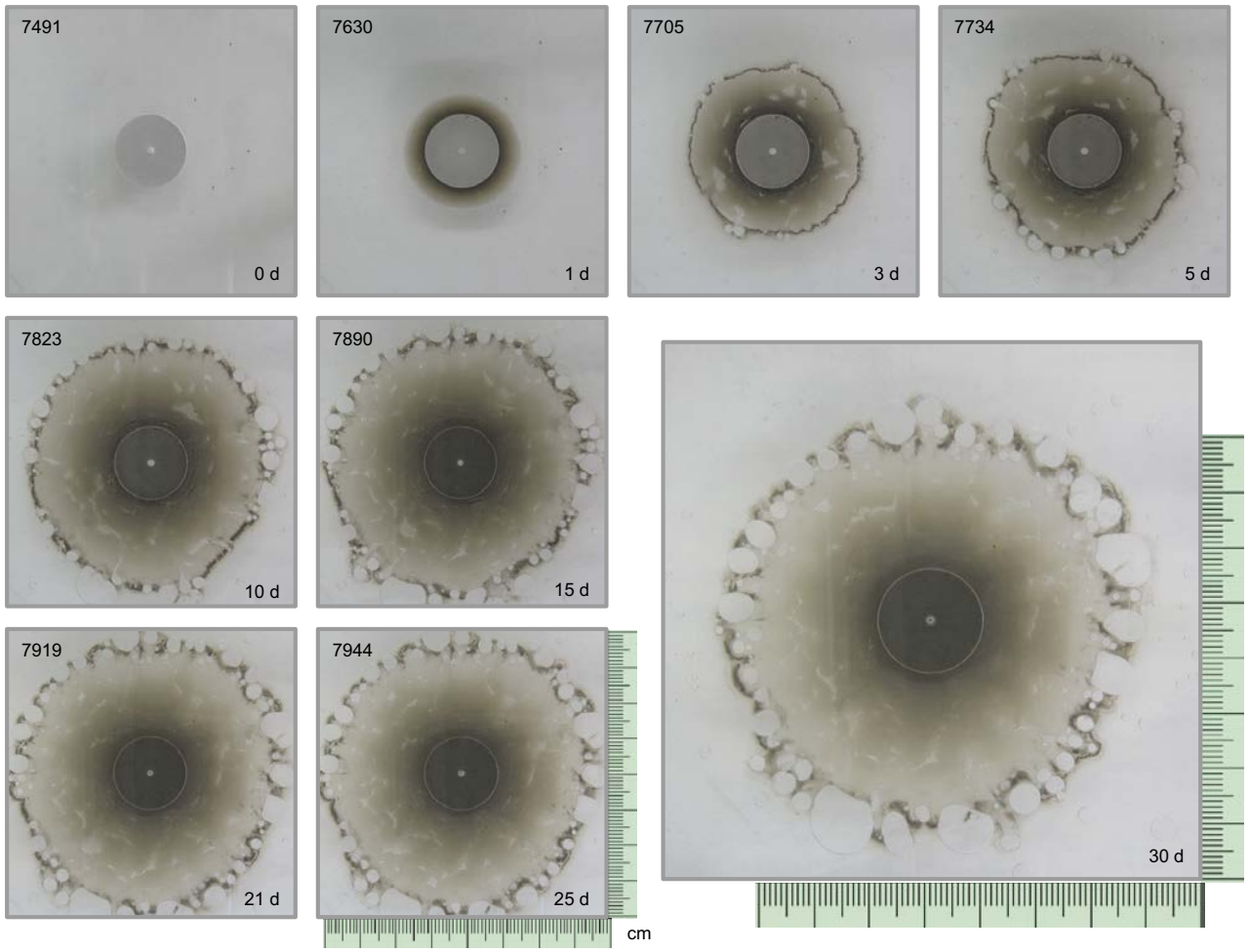

Test 51B: Minerals&salt-free MX-80 1.4 g·cm^{-3} - Slope 0º - 0.2 mm - NaCl 10^{-3} M

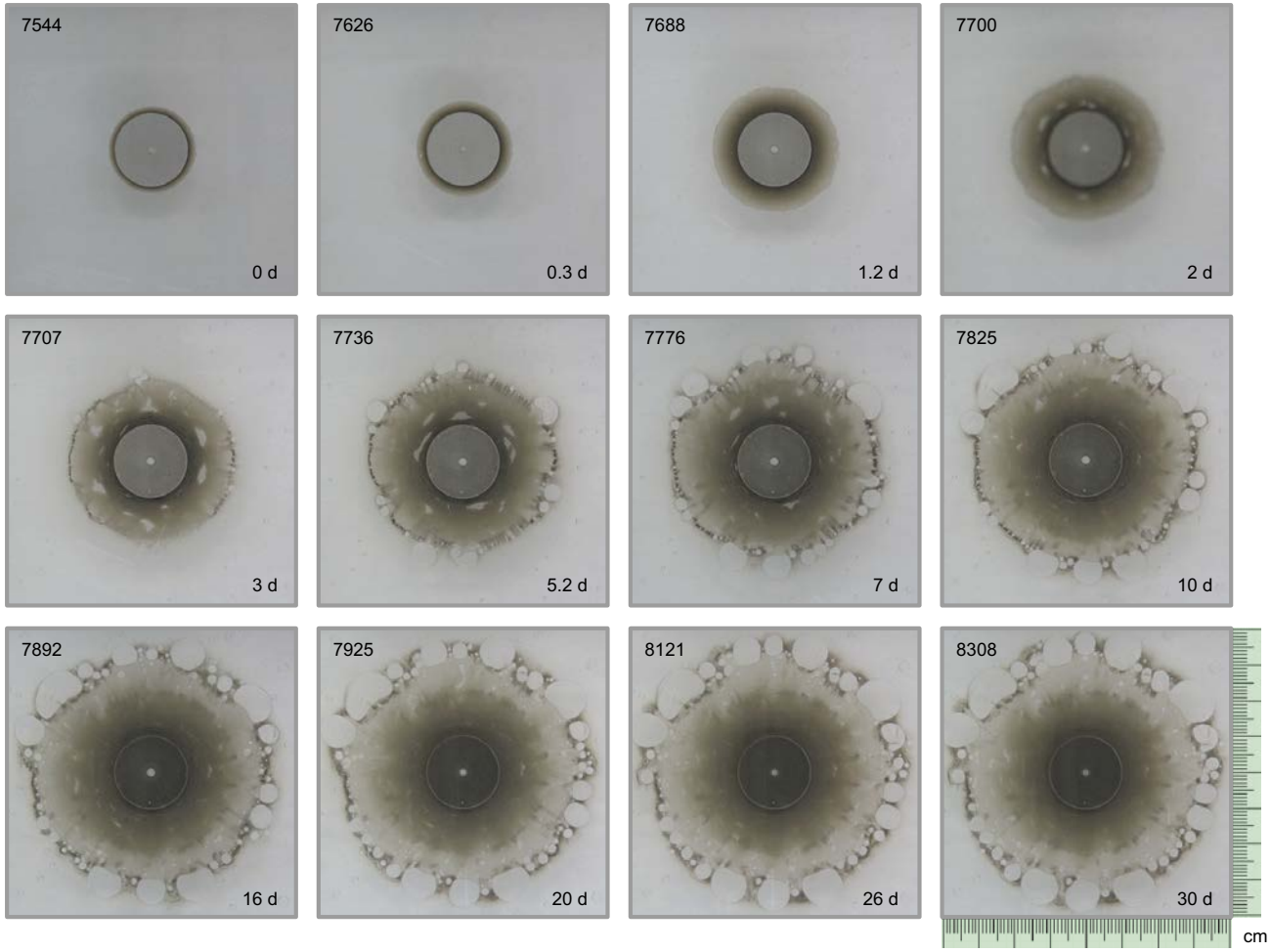

Test 51C: Minerals&salt-free MX-80 1.4 g·cm^{-3} - Slope 0º - 0.2 mm - NaCl 10^{-3} M

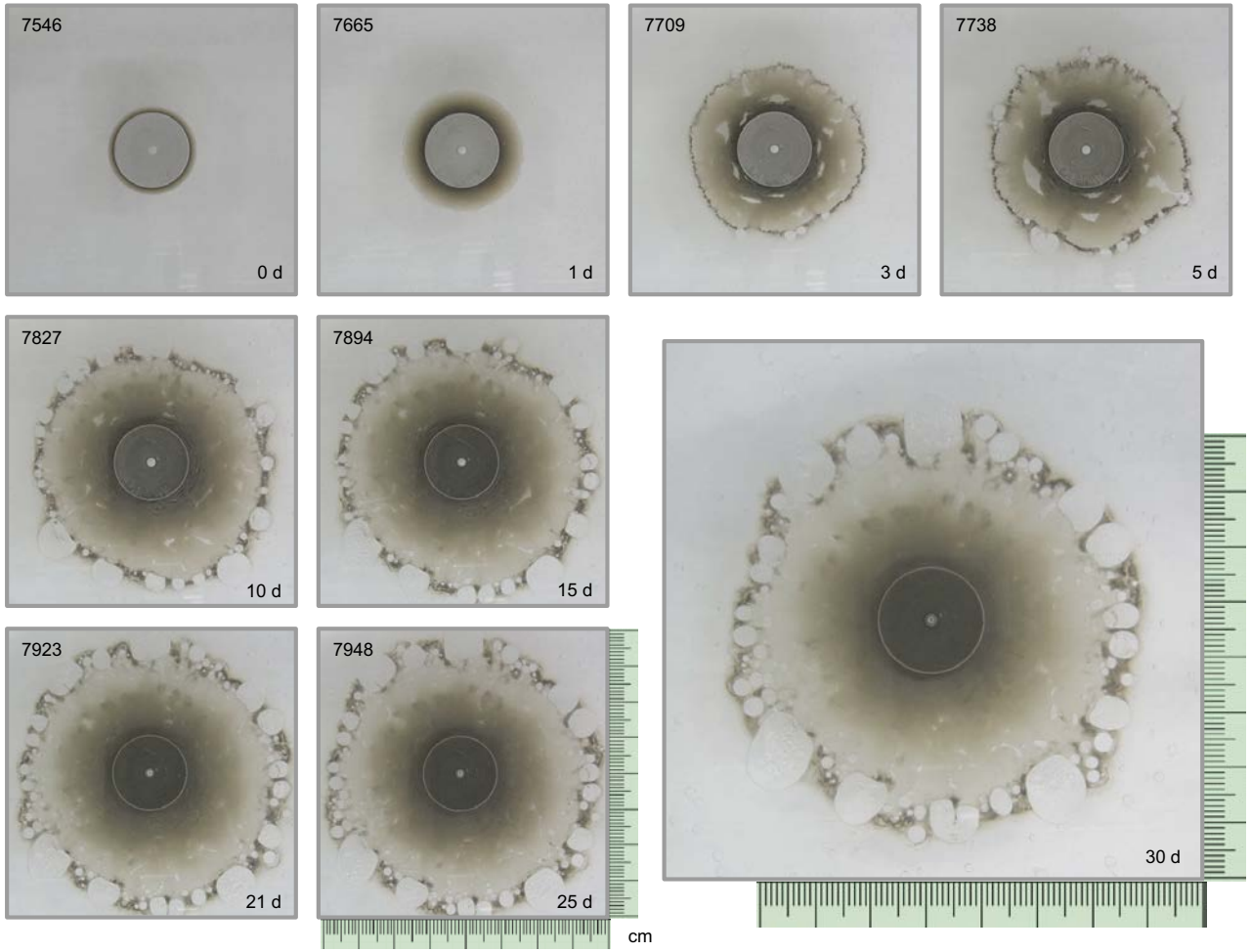

Test 52A: Nanocor® 1.4 g·cm^{-3} - Slope 0º – Aperture 1 mm - NaCl 10^{-3} M

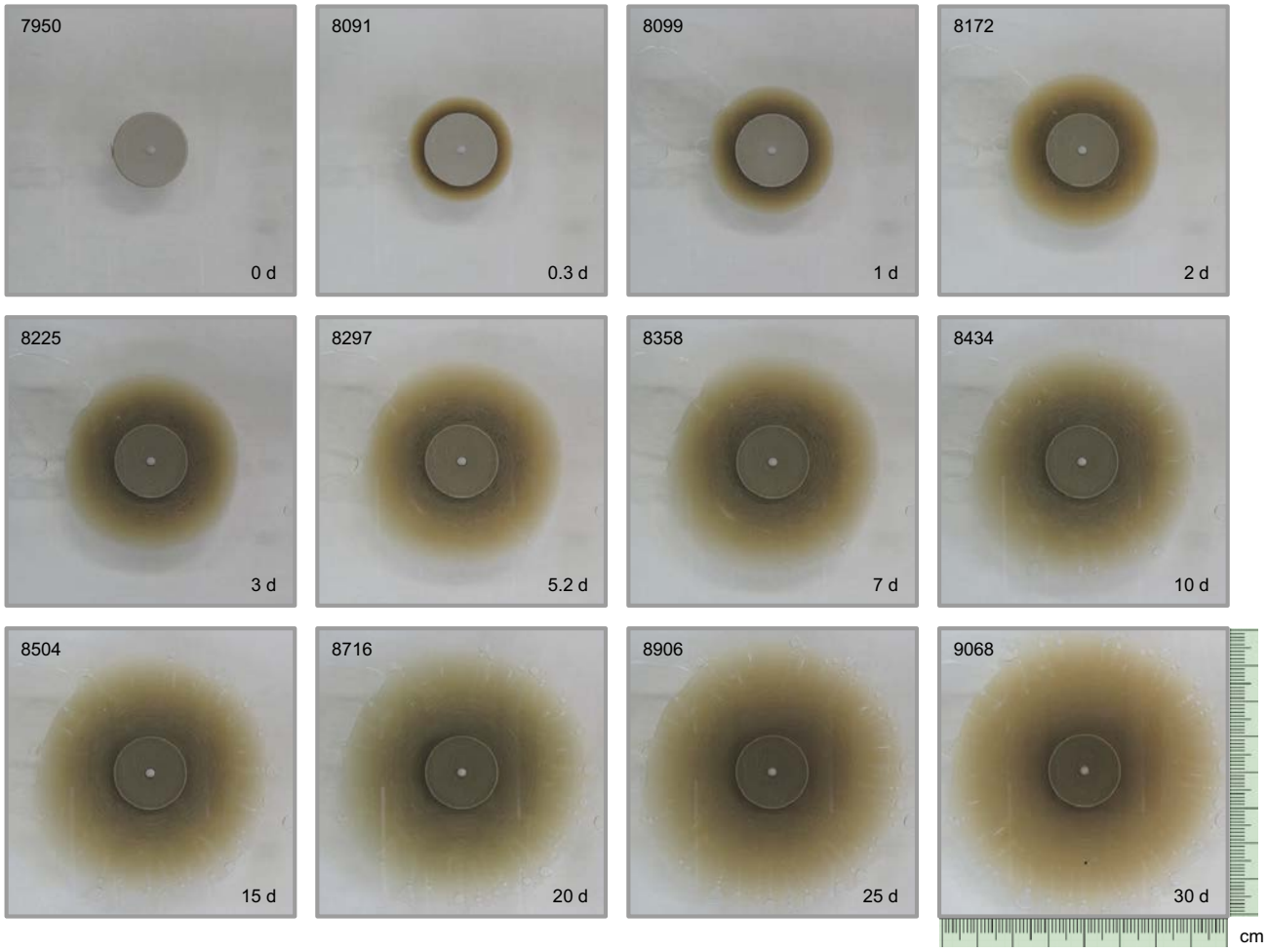

Test 53A: Nanocor® 1.4 g·cm^{-3} - Slope 45º – Aperture 1 mm - NaCl 10^{-3} M

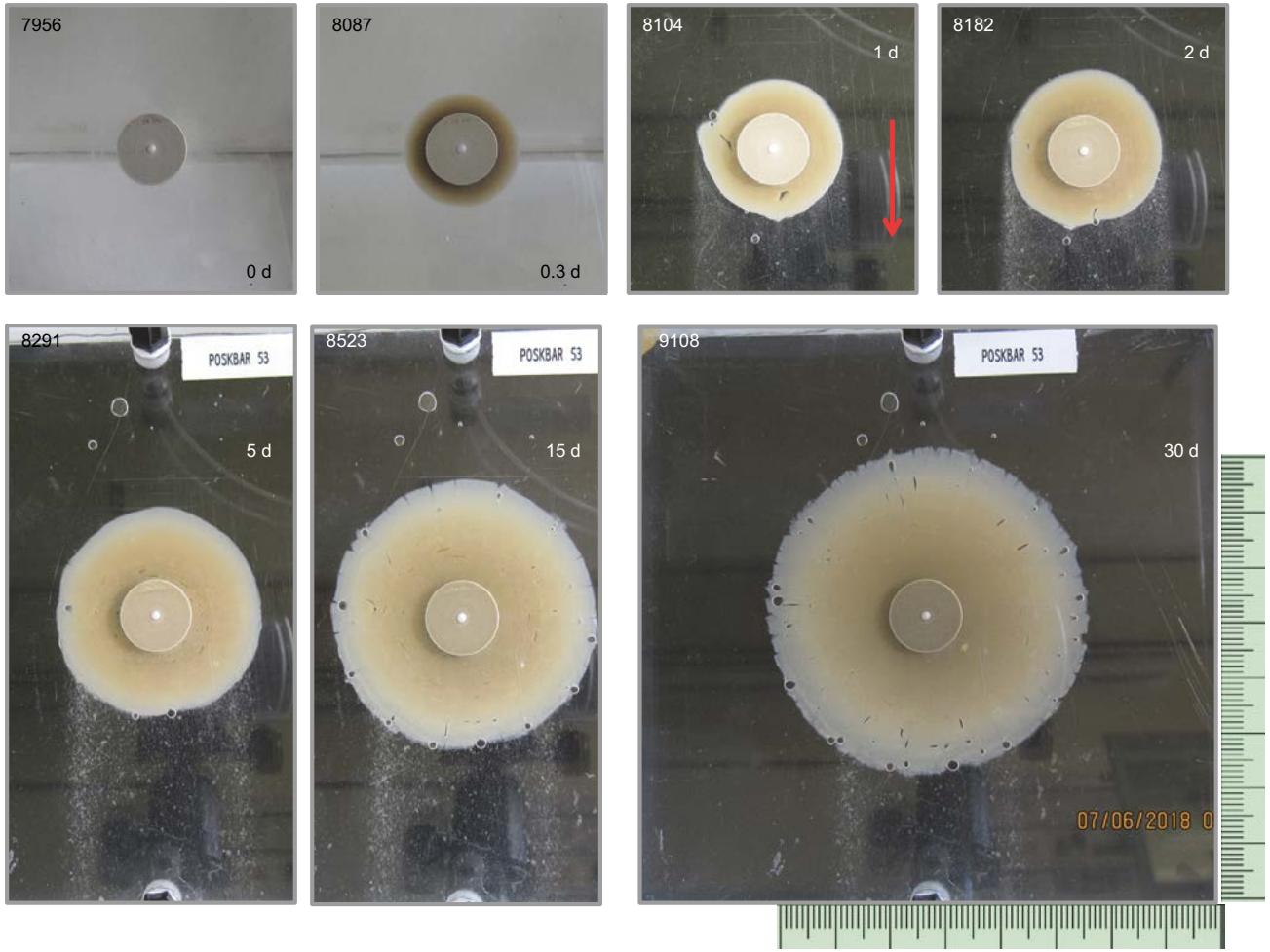

Test 54A: Nanocor® 1.4 g·cm^{-3} - Slope 90º – Aperture 1 mm - NaCl 10^{-3} M

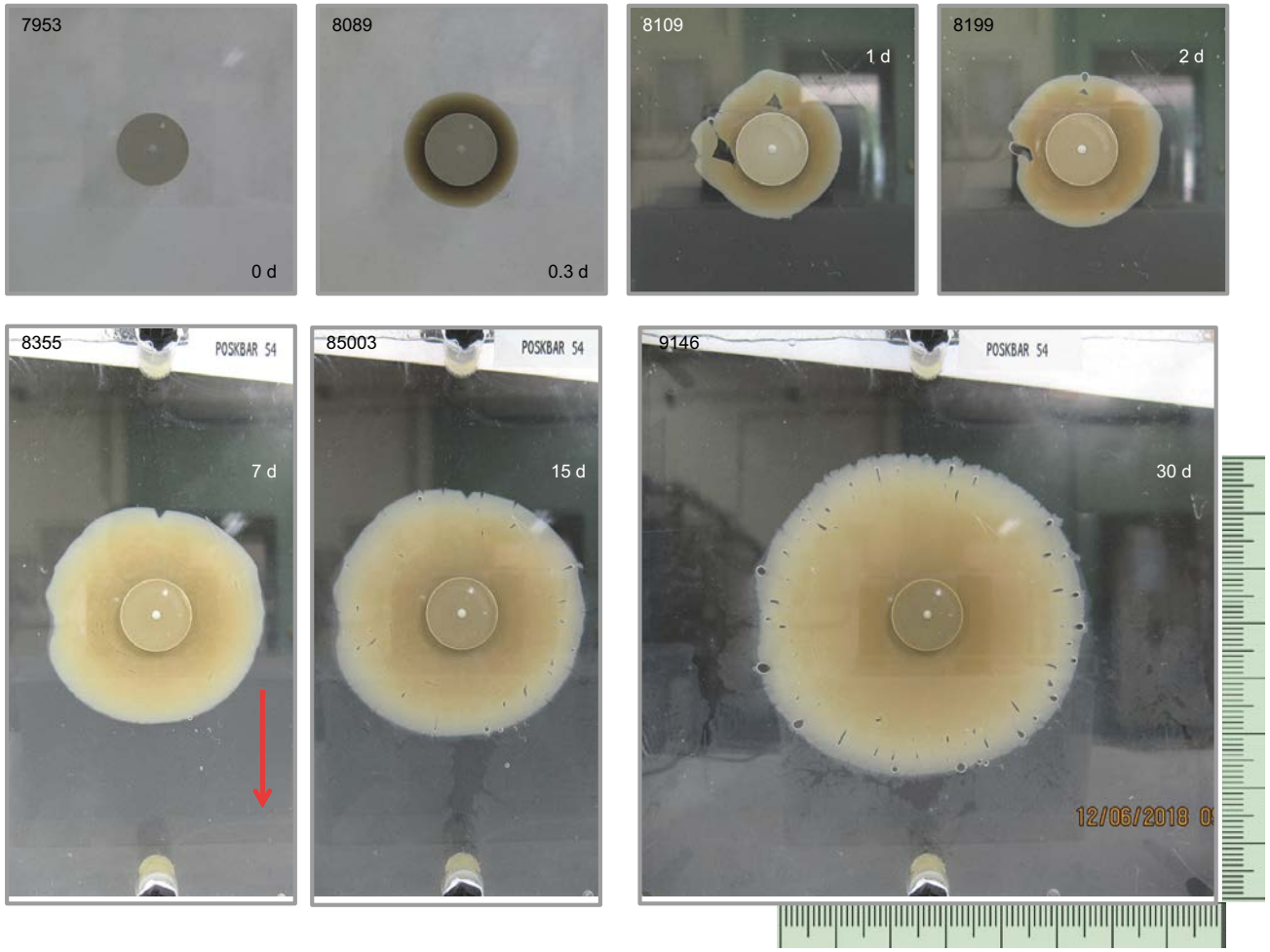

Test 55A: Salt-free MX-80 1.4 g·cm^{-3} - Slope 0º - 0.2 mm - NaCl 10^{-3} M

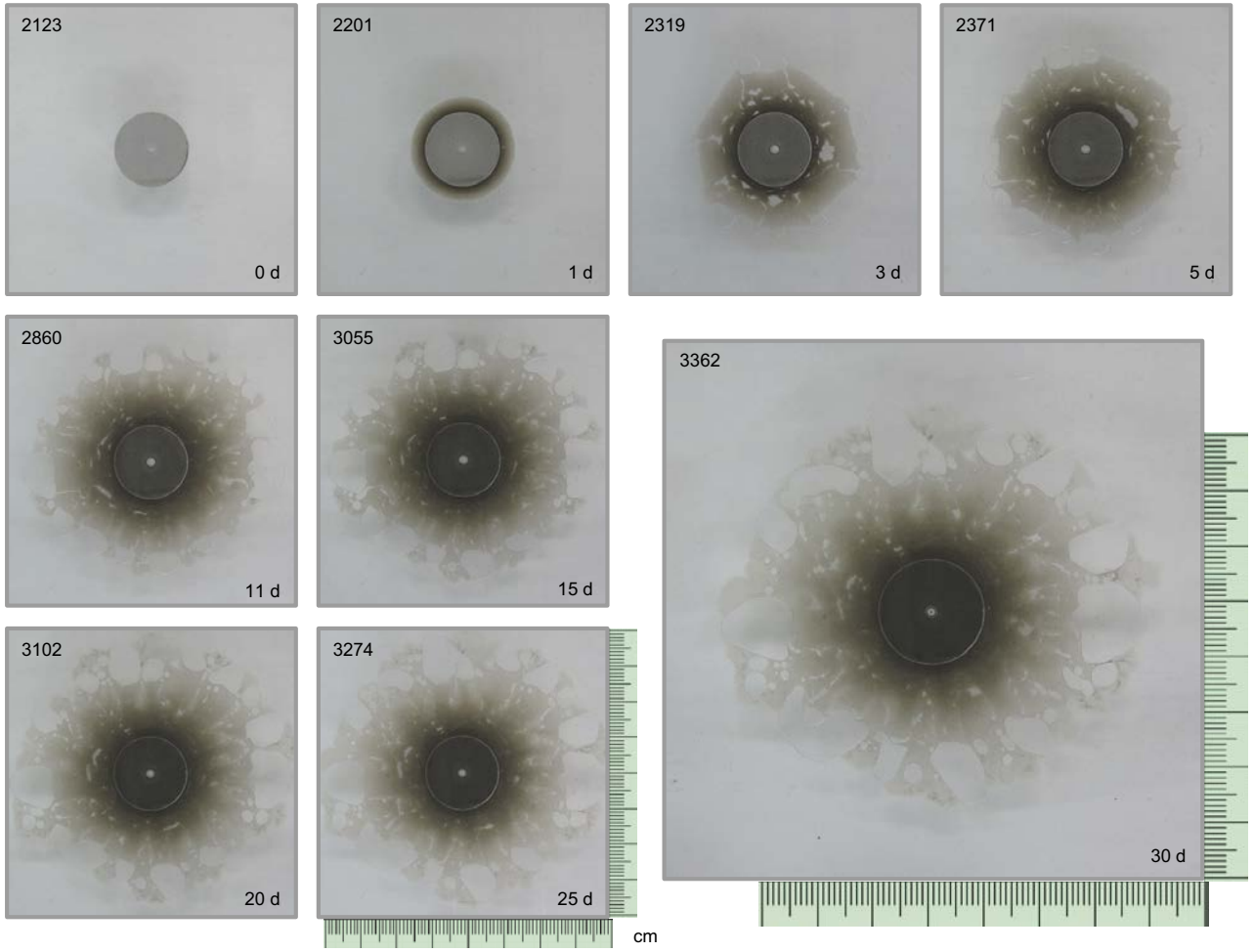

Test 55B: Salt-free MX-80 1.4 g·cm^{-3} - Slope 0º - 0.2 mm - NaCl 10^{-3} M

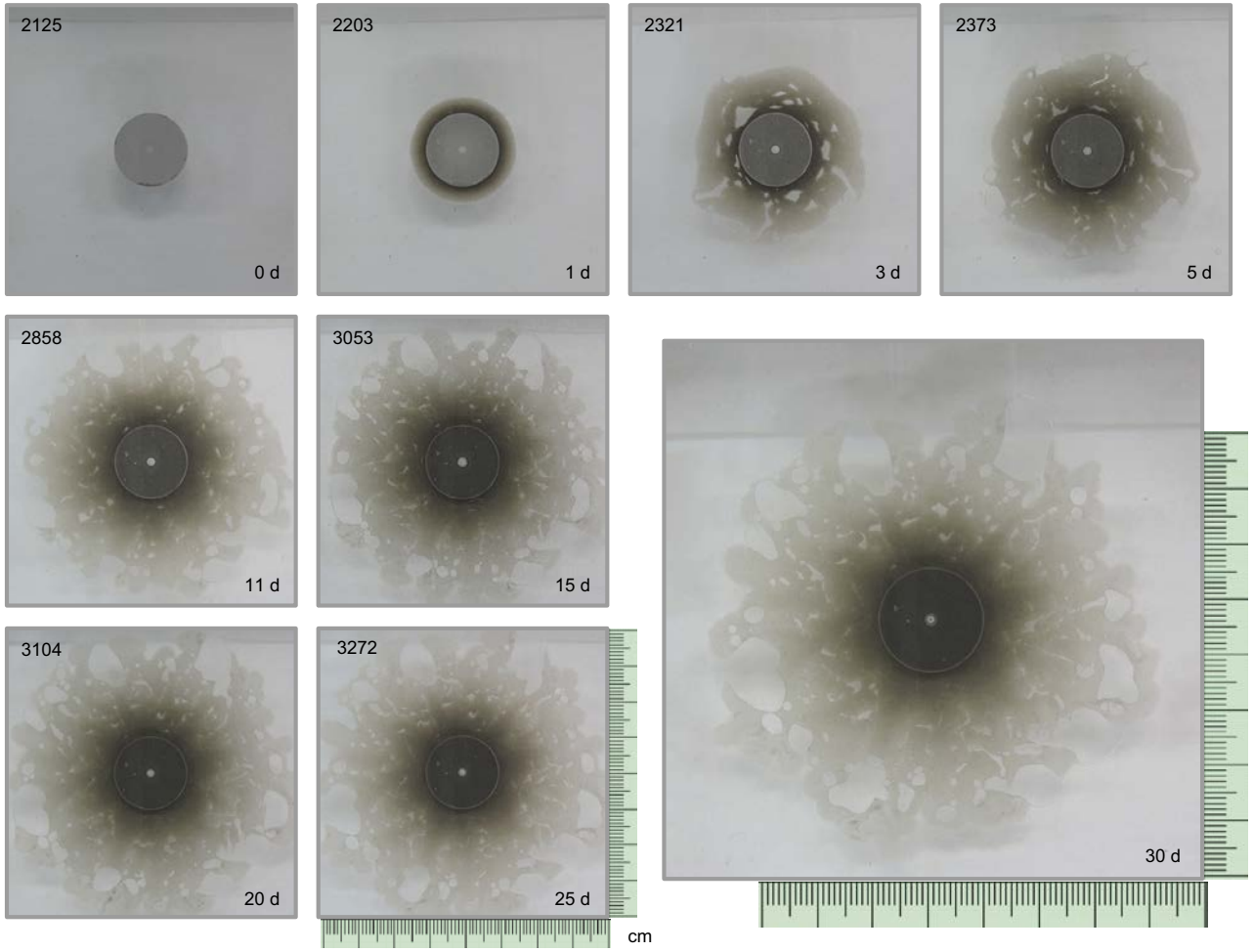

Test 55C: Salt-free MX-80 1.4 g·cm^{-3} - Slope 0º - 0.2 mm - NaCl 10^{-3} M

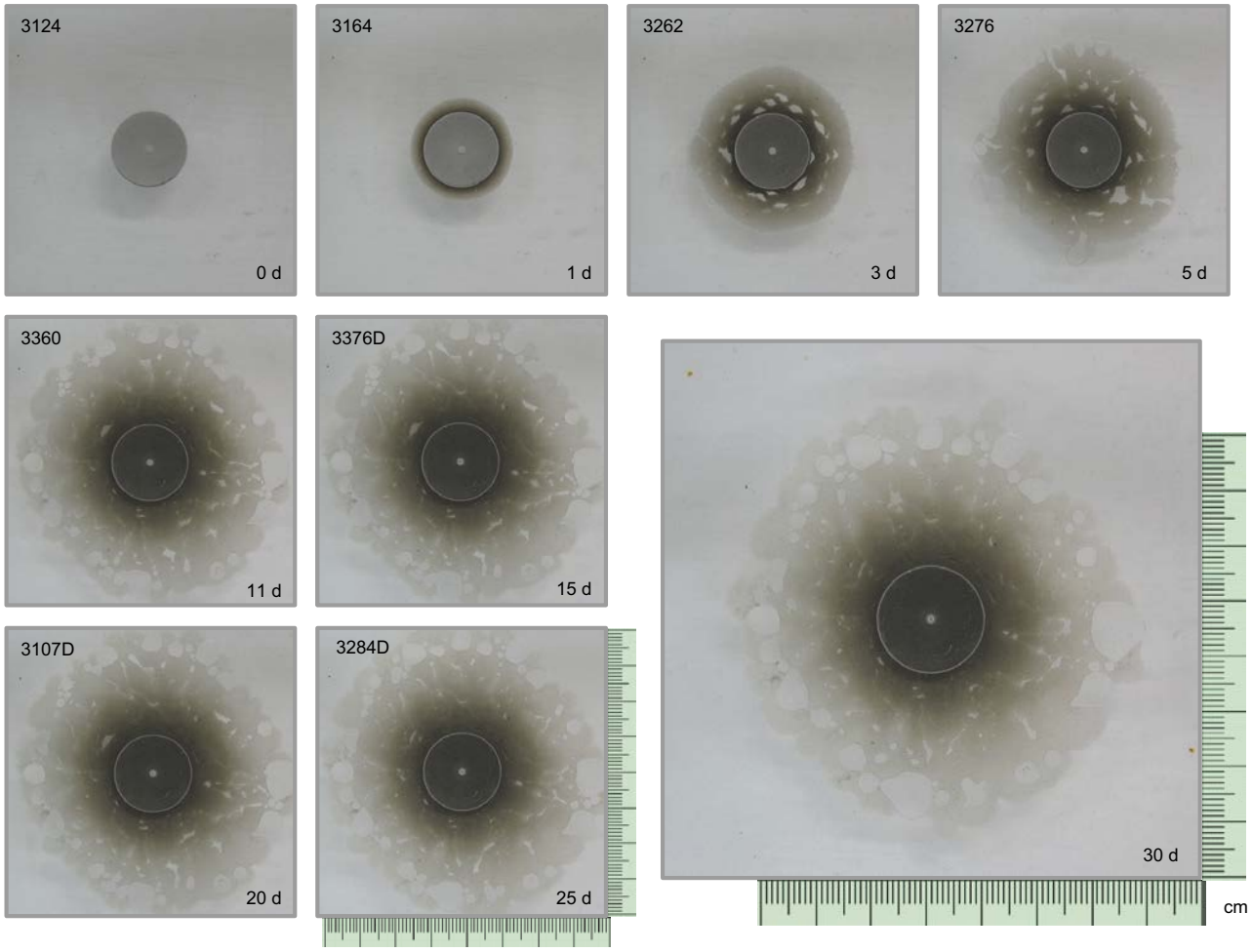

Test 56A: Nanocor® 1.4 g·cm^{-3} - Slope 0º – Aperture 1.7 mm - NaCl 10^{-3} M

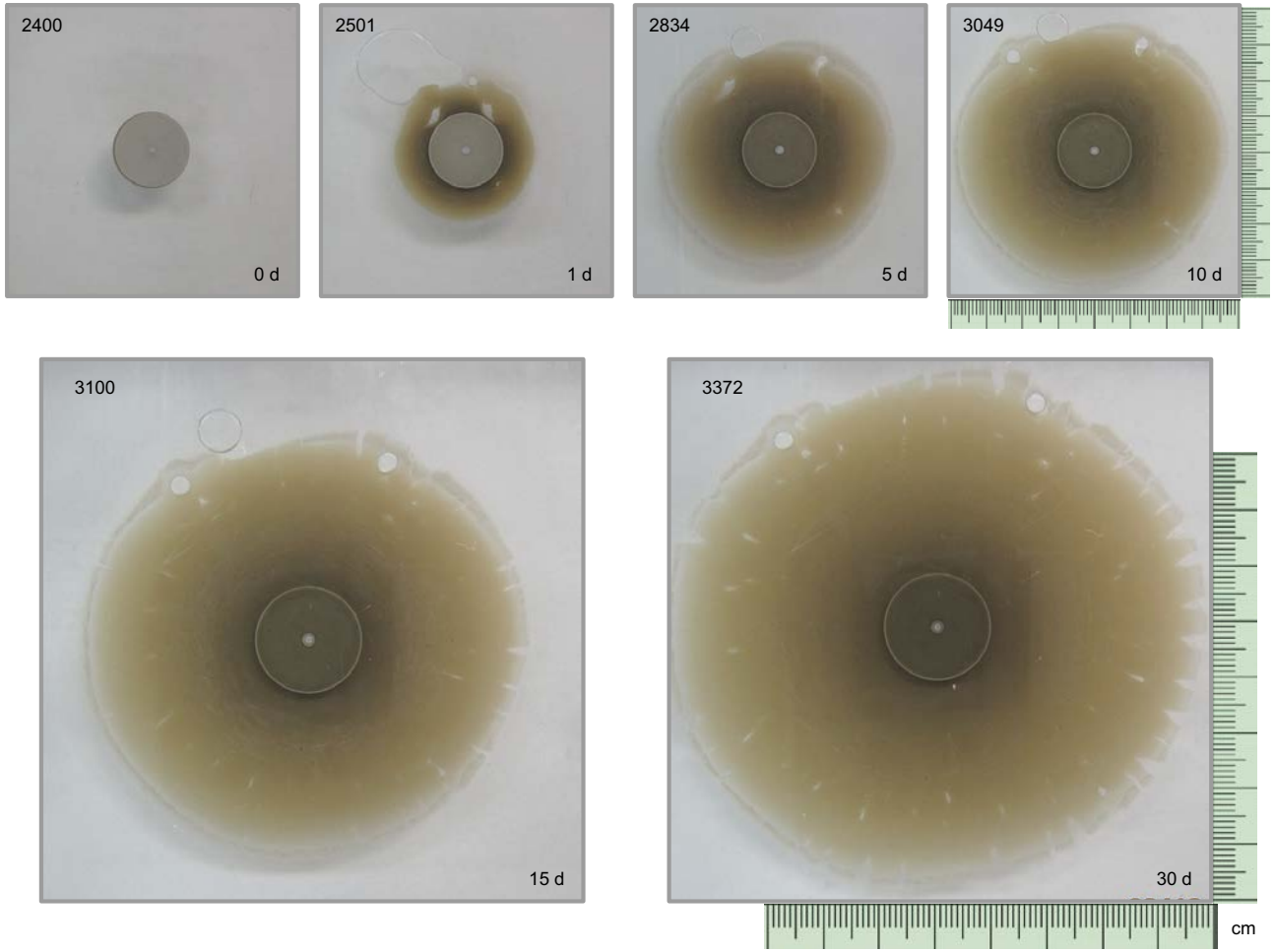

Test 57A: Raw MX-80 1.4 g·cm^{-3} - Slope 0º – Aperture 1.7 mm - NaCl 10^{-3} M

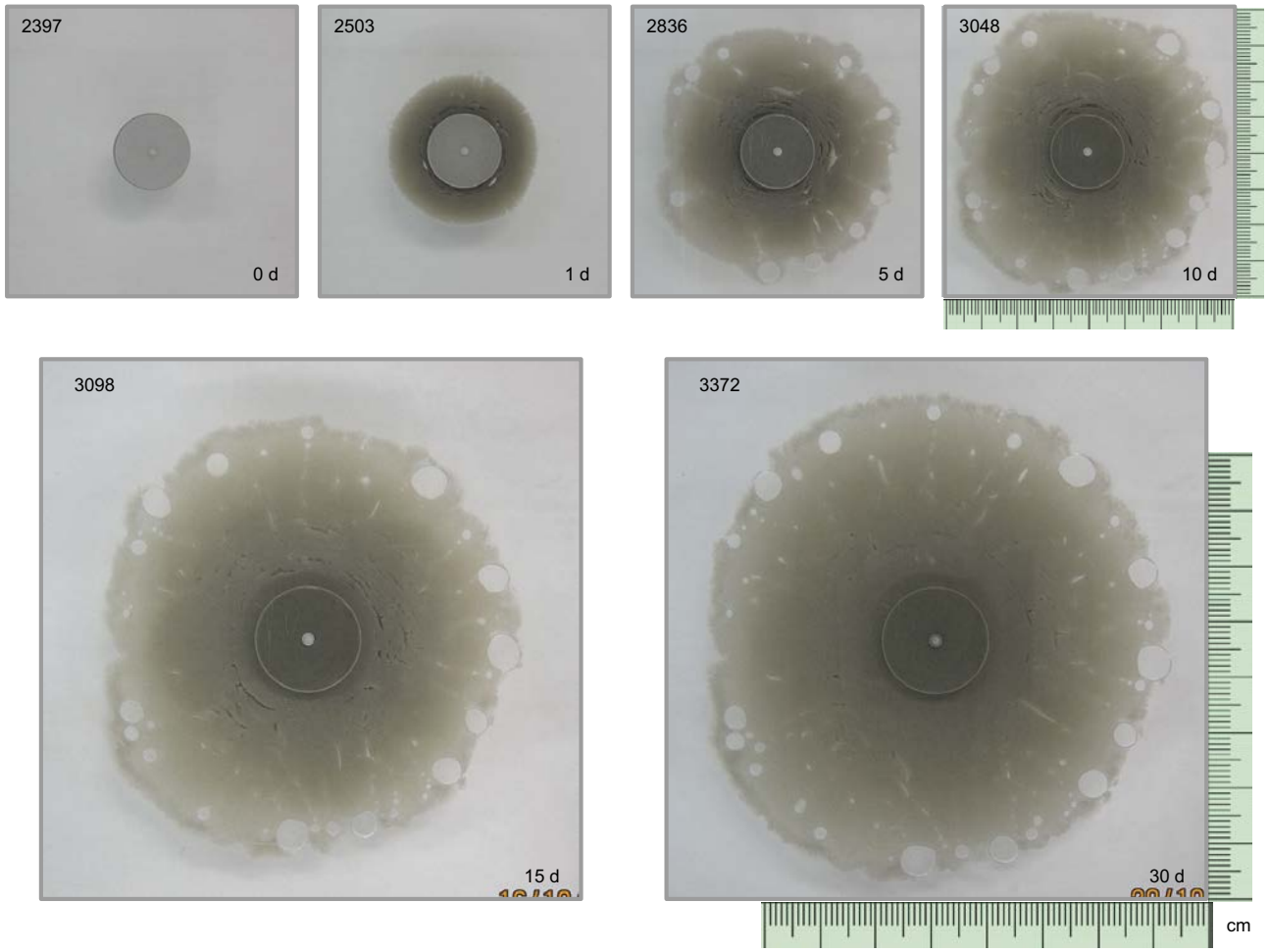

Arkitektkopia AB, Bromma, 2019

SKB is responsible for managing spent nuclear fuel and radioactive waste produced by the Swedish nuclear power plants such that man and the environment are protected in the near and distant future.

skb.se